Single and multi-junction thin film silicon solar cells for flexible photovoltaics

Thèse présentée à la Faculté des Sciences
Institut de Microtechnique
Université de Neuchâtel

Pour l'obtention du grade de docteur ès sciences

Par

Thomas Söderström

Acceptée sur proposition du jury :
Prof. C. Ballif, directeur de thèse
Dr. F.-J. Haug, rapporteur
Dr. V. Terrazzoni-Daudrix, rapporteur
Dr. W. Soppe, rapporteur
Dr. D. Fischer, rapporteur
Prof. H. Stoekli-Evans, rapporteur

Soutenue le 20 mars 2009
Université de Neuchâtel
2009

Université de Neuchâtel

FACULTE DES SCIENCES
Secrétariat-Décanat de la faculté
- Rue Emile-Argand 11
- CP 158
- CH-2009 Neuchâtel

IMPRIMATUR POUR LA THESE

Single and multi-junction thin film silicon solar cells for flexible photovoltaics

Thomas SÖDERSTRÖM

UNIVERSITE DE NEUCHATEL

FACULTE DES SCIENCES

La Faculté des sciences de l'Université de Neuchâtel,
sur le rapport des membres du jury

Mmes H. Stoeckli-Evans, V. Terrazzoni-Daudrix,
MM. C. Ballif (directeur de thèse), F.-J. Haug,
D. Fischer (VHF-Technologies SA, Yverdon-les-Bains)
Et W. Soppe (Petten, NL)

autorise l'impression de la présente thèse.

Neuchâtel, le 31 mars 2009

Le doyen :
F. Kessler

UNIVERSITE DE NEUCHATEL
FACULTE DES SCIENCES
Secrétariat - décanat de la faculté
Rue Emile-Argand 11 - CP 158
CH-2009 Neuchâtel

Felix Kessler

Téléphone : +41 32 718 21 00 E-mail : secretariat.sciences@unine.ch www.unine.ch/sciences

Mots clés

Cellules solaires en couches minces, silicium amorphe, silicium microcristallin, cellule micromorph tandem, piégeage de la lumière, cracks, substrats flexibles

Keywords

Solar cells, thin film silicon, amorphous, microcrystalline, micromorph tandem cells, light trapping, cracks, flexible substrates

Abstract

This thesis investigates amorphous (a-Si:H) and microcrystalline (μc-Si:H) solar cells deposited by very high frequency plasma enhanced chemical vapor deposition (VHF-PECVD) in the substrate (n-i-p) configuration. It focuses on processes that allow the use of non transparent and flexible substrates such as plastic foil with $T_g < 180°C$ like poly-ethylene-naphtalate (PEN).

In the first part of the work, we concentrate on the light trapping properties of a variety of device configurations. One original test structure consists of n-i-p solar cells deposited directly on glass covered with low pressure chemical vapor deposition (LP-CVD) ZnO. For this device, silver is deposited below the LP-CVD ZnO or white paint is applied at the back of the glass as back reflector. This avoids the parasitic plasmonic absorptions in the back reflectors, which are observed for conventional rough metallic back contacts. Furthermore, the size and morphology of the LP-CVD ZnO are varied. The relation between the substrate morphology and the short circuit current density (J_{sc}) is experimentally explored. As a result, the J_{sc} can be increased by 23% for a-Si:H and 28% for μc-Si:H solar cells compared to the case of flat substrate and the role of the size and shape can be clearly separated. We also explore the optical behavior of single and multi-junction devices prepared with different back and front contacts. The back contact consists either of a 2D periodic grid with moderate slope, or of LP-CVD ZnO with random pyramids of various sizes. The front contacts are either a 70 nm thick, nominally flat ITO or a rough 2 μm thick LP-CVD ZnO. We observe that, for a-Si:H, the cell performance is critically dependent on the combination of thin flat or thick rough front TCOs and the back contact. Indeed, for a-Si:H, a thick LP-CVD ZnO front contact provides more light trapping on the 2D periodic substrate. The J_{sc} relatively increases by 7 % with LP-CVD ZnO compared to ITO. Then, we study the influence of the thick and thin TCOs in conjunction with thick absorbers like triple junction or μc-Si:H solar cells. Because of the different nature of the optical systems, thick (> 1μm) against thin (<0.3 μm) absorber layer, the antireflection effect of ITO becomes more effective and the structure with the flat TCO provides as much light trapping as the rough LP-CVD ZnO. Finally, the conformality of the layers is investigated and guidelines are given to understand the effectiveness of the light trapping in devices deposited on periodic gratings.

In the second part, we quantitatively describe the effect of continually varying the substrate morphology on open-circuit voltage (V_{oc}) and fill factor (FF) for the device in the n-i-p configuration. Transmission electron microscope (TEM) observations show that V shape morphology creates nano-cracks and reduces the V_{oc} and FF of the solar cells. Hence, we investigate cell designs and processes that avoid V_{oc} and FF losses. For a-Si:H solar cells, we introduce an amorphous silicon carbide n-layer (n-SiC), a buffer layer at the n/i interface, and show that the new cell design yields high V_{oc} and FF on both flat and textured substrates, contrary to the usual microcrystalline silicon n-doped layer. Finally, the beneficial effect of our optical and electrical findings is used to fabricate a-Si:H solar cell with an initial efficiency of 8.8 % and stabilized efficiency of 7% on plastic foil. We find that for our reduced temperature processes windows, the light-induced degradation of a-Si:H solar cells depends strongly on the thickness of the absorber layer. Indeed, the relative efficiency degradation is reduced from 27% to 17% for 400 nm and 200 thick cells, respectively. This degradation can be further lowered to 15 % in a-Si/a-Si tandem structure, and still using a total 300 nm thick absorber layer. For μc-Si:H solar cells, we introduce a buffer layer with a higher amorphous fraction between the n-doped and intrinsic layer. Our study reveals that the buffer layer limits the formation of voids and porous areas (nano-cracks), which promotes oxygen diffusion in the μc-Si:H material. Therefore, this layer mitigates the V_{oc} and FF losses which enhances the performance of the μc-Si:H solar cell. By applying our findings, we make μc-Si:H solar cells with an efficiency of 8.7% on plastic foil for an only 1.2 μm absorber layer thickness.

The micromorph solar cell (stack of amorphous and microcrystalline cells) concept is the key for achieving high efficiency stabilized thin film silicon solar cells. We present results with and without an intermediate reflector. In particular, we introduce an original device structure that allows a better control of the layer growth and of the light in-coupling into the two sub-cell components. It is based on an asymmetric intermediate reflector (AIR), which increases the effective thickness of the a-Si:H by a factor of more than three. Hence, the a-Si:H thickness reduction diminishes the light-induced degradation, and micromorph tandem cells with 11.2 % initial and 9.8% stabilized efficiencies (1000h, 50°C, 100mW/cm^2) are achieved on plastic foil. The stabilized J_{sc} of the n-i-p tandem solar cells is close to 12 mA/cm^2, which offers the possibility for the low T_g flexible substrate technology to compete with state of the art stabilized thin film silicon devices.

Based on the results obtained here, the use of ITO front contact, a further optimisation of the ITO/p and p-i interfaces, should allow it to be possible to exceed 12.5 % stabilized efficiency on low Tg plastic substrate for micromorph tandems cells.

Abbreviations

AM1.5g	Air mass 1.5 global (standard solar spectrum on the earth)
a-Si:H	Amorphous silicon
AIR	Asymmetric intermediate reflector
Ag	Silver
Al	Aluminum
AFM	Atomic force microscopy
BL	Buffer layer
c-Si	Crystalline silicon
CH_4	Methane
C_R	Raman crystallinity
Dilution	H_2/ SiH_4
EQE	External quantum efficiency
E_g	Energy band gap
η	Efficiency
FTPS	Fourier transform photocurrent spectroscopy
FF	Fill factor
FIB	Focused ion beam
Ge	Germanium
H_2	Hydrogen
ITO	Indium tin oxide
IR	Intermediate reflector
JV	J(V) or current voltage curve
J_{sc}	Short circuit current density
k	Extinction coefficient
LP-CVD	Low pressure chemical vapor deposition
LID	Light induced degradation
λ_n	Light wavelength in media with refractive index n
μc-Si:H	Microcrystalline silicon
n	Refractive index
n-μc	Microcrystalline n-layer
n-SiC	Amorphous silicon carbide n-layer
RF	Radio frequency
PECVD	Plasma enhanced chemical vapor deposition
PH_3	Phosphine
SiH_4	Silane
SIR	Symmetric intermediate reflector
SOIR	Silicon oxide intermediate reflector
SIMS	Secondary ion mass spectroscopy
SC	Silane concentration: $SiH_4/ (H_2+SiH_4)$
SEM	Scanning electron microscope
TCO	Transparent conductive oxyde

TZIR	Textured zinc oxide intermediate reflector
T_g	Glass transition temperature
TMB	Trimethylboron
TEM	Transmission electron microscope
V_{oc}	open circuit voltage
VHF	Very high frequency
VIM	Variable illumination measurement
ZnO	Zinc oxide
ZIR	Zinc oxide intermediate reflector

TABLE OF CONTENTS

Chapter 1: Introduction

Energy needs and thin film silicon solutions

1.1 Introduction

1.1.1 Energy Issues

The need for energy resources is becoming one of the critical issues of this century. Indeed, the heating of the homes and workplaces, the industry needs, transportation and our modern lifestyle demand a tremendous quantity of energy, almost 40 thousand kWh per capita per year in Switzerland. This is equivalent to almost 4 tons of oil. However, the price of oil started an upward rally from 15 $/b in 1999 to 150 $/b in 2008. Even though the oil price is decreasing in 2009, one thing is clear: the era of easy oil is over. Hence, it forces everyone to create new energy paradigm based on energy efficiency and renewable energy.

Historically, a massive growth in energy consumption, as shown for Switzerland in Figure 1-1, started in the fifties during industrialization and it is still growing today. An interesting phenomenon is that the ratio between electricity over the total energy consumption also follows an increasing trend. In 2007 in Switzerland, the electricity consumption represented 24 % of the total energy. In addition, this ratio will certainly increase because of the awareness of finite oil resources, the use of heat pumps, electronic products and need for air conditioning. Even the US car companies like General Motors plan to base their novel strategy on cars running with electric power.

Hence, there is no doubt that the electricity markets will be challenged by consumers demand in the coming years. For the durability of the mankind, the reasons are obvious why the resources have to be sustainable. However in 2007, 55 % of electricity produced in Switzerland came from hydropower plants, 40 % came from nuclear power plants and 5 % came from thermal plants and others [1]. Although, almost half of the electricity is provided by nuclear power, it should ideally be avoided because the resources are finite, there is no proven solution for nuclear waste disposals and no insurance company wants to take on the risk of a nuclear accident. In fact, the possibility of a nuclear accident persuades many leading countries (Germany, Sweden, etc.) to look for alternative electricity sources.

This work focuses on photovoltaic (PV) energy. The photovoltaic effect, i.e. the conversion of solar light energy into electricity, was discovered by A. E. Becquerel in 1839 [2]. One of the advantages of this energy is that it has an immense potential for electricity production and it is based on a renewable source. In fact, the solar irradiation on earth in 1 hour exceeds the total energy consumption of the world during 1 year [3]. It is estimated that if only 4 % of the deserts on earth were covered with PV modules, the energy needs of the world would be satisfied [4]. In Switzerland, it is estimated that 35 % of the electricity needs would be met if the existing suitably oriented roofs could be covered with solar PV modules [5].

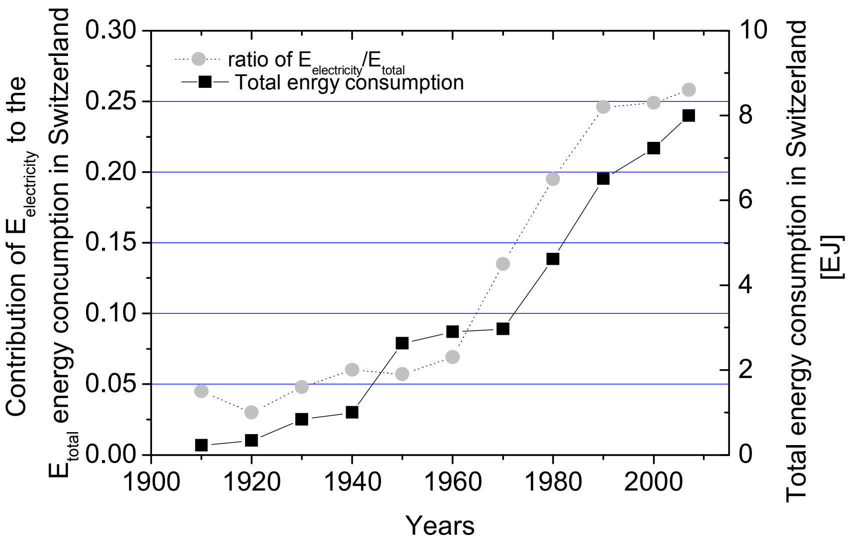

Figure 1-1: Energy consumption and ratio between electricity over energy consumption in Switzerland. Energy statistic in Switzerland from the OFEN [1].

1.1.2 Photovoltaics energy (PV)

PV energy is not yet fully competitive within the electricity market. In fact, it is only recently that strong efforts from the industry and research laboratories have focused on decreasing the cost per Watt peak (W_p) of the solar panels (modules). The incentives that changed the world of PV started in Japan and in Germany, the latter introducing a nationwide feed-in-tariff in 2000, which resulted in a boom of the solar module demand. This law encourages the installation of solar modules by buying back the renewable electricity. The program is based on the obligation of the electricity utilities to buy renewable electricity at a fixed price, which is guaranteed for 20 years. For PV it is currently around twice the grid market price or 32-42 euro cts per kWh (as of 2009). Because of this incentive, the cost of renewable energy decreases and therefore the price for every new installed system decreases yearly, with the aim to converge quickly to grid parity. The result of the German law is clearly shown by the strong increase of module installation and production after 2000 as shown in Figure 1-2 and Figure 1-3. It stimulates companies from all over the world to start production or increase production capacities. Therefore, mass production has started, with a production volume of 6 GW_p in 2008 and estimation of 20 GW_p by 2012, which represents 200 million square meters built per year (assuming modules at 10% efficiency) [6]. Many technologies (c-Si, CdTe, CIGS, thin film silicon, CSG, Dye-sensitized, polymer) are in competition both in terms of cost/watt or watt/sqm, depending on the applications.

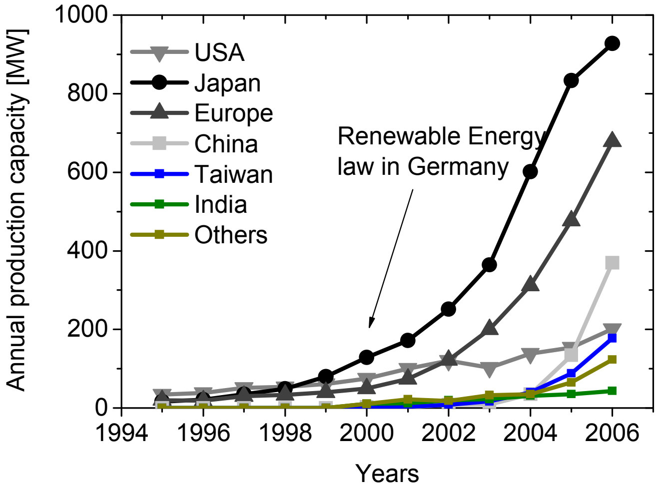

Figure 1-2: Annual production capacity in the world from 1995 to 2006

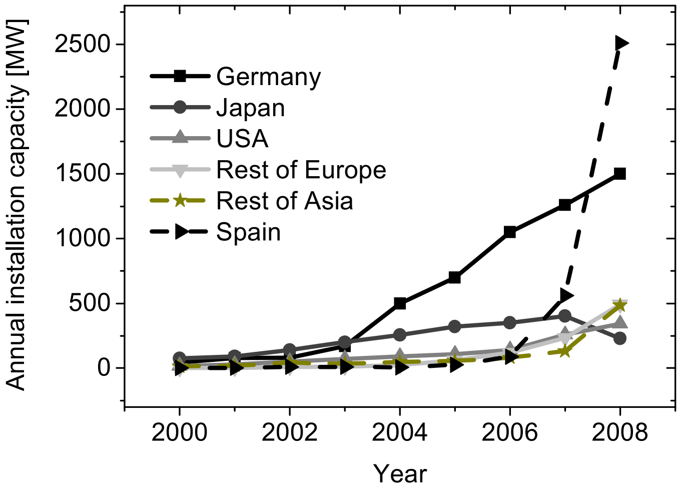

Figure 1-3: Installed capacity of solar panels in the world from 2000 to 2008

So far, crystalline silicon (c-Si) dominates this market with a 90% share in 2007 [6]. Si has an inherent advantage since it is the second most abundant element on earth (after oxygen). Nevertheless, the standard wafer-based crystalline silicon solar cell (c-Si) has suffered from a feed stock problem in the last three years [7]. This feed stock issue coupled with strong demand for modules by the German and Spanish markets prevented further price reduction of solar modules, even though strong cost reduction by large economy of scale has been achieved. This is shown in Figure 1-4 where the price per module did not decrease in 2008, even though the production grew strongly. The lower dependence on feed stock of thin film silicon solar cells, which uses more than hundred times less material than c-Si cells, is one of the reasons why more than 70 companies announced that they would start the production soon. Due to the inherent properties of thin film (low material costs, few process steps), these companies also expect to be able to make great advances in terms of cost reductions, e.g. United Solar expects modules costs of 1 $/W_p$ in 2012 [8], the company First Solar announced on their website that modules cost are below 1 $/W_p$ or the fourth quarter of 2008 . In 2009, module price has already decreased sharply because of change in feed-in-tariff in Germany and in Spain, financial crisis and strong supply. Crystalline sells for 2.1 €/W_p and thin film modules for 1.7 €/W_p (~ 2.2 $/W_p$). Therefore, complete PV system could be installed at 3.5 €/W_p (2 € for the module, 0.5 € for inverter and 1.5 € for installation). As a result, the price of solar energy per kWh is close to 16 €cts in Switzerland and 8 €cts in south of Spain (assuming 25 years of module life time, no module degradation and no rent for the initial investment).

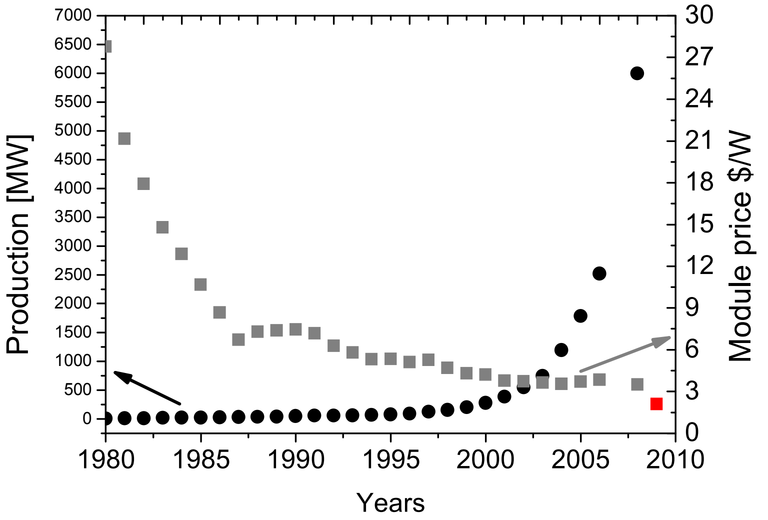

Figure 1-4: Production capacity (solid line) of solar panels in the world from 1980 to 2008 and module cost per W_p (dashed line).

Data given in Figure 1-2, Figure 1-3, Figure 1-4 are compiled by Earth Policy Institute from Worldwatch Institute [9].

1.1.3 Thin film silicon technology

The materials used in thin film silicon solar cells are hydrogenated amorphous silicon (a-Si:H) and microcrystalline silicon (μc-Si:H). The typical cell thickness is limited to 0.2 to 2 μm for a-Si:H and μc-Si:H thin film silicon solar cells , respectively, because of the poor charge transport of these materials. Hence, light trapping is needed in order to absorb equivalent light in the infra red part of the spectrum compared to 200 to 400 μm thick c-Si wafers.

Thin film silicon solar cells have had a poor reputation in the past decade, especially the a-Si:H cells. The reason comes from the decrease of conversion efficiency after light exposure. This effect is called the Staebler-Wronski effect first described in 1977 [10]. Nonetheless, the degradation reaches a quasi-steady state after a given light exposure time. The cells are said to be in the stabilized state after 1000h in light soaking conditions. The typical degradation is between 15% to 25% for a-Si:H cells, 0 to 10% for microcrystalline cells and 5% to 20% for tandem micromorph devices (consisting of a stack of a-Si:H and μc-Si:H). In this thesis, we present initial and stable efficiencies of cells and not for modules. Note that module efficiencies tend to be 10% to 20% lower than cell efficiencies. The principal reasons for this difference are the interconnections losses (dead areas) between the cells in the module, the homogeneity challenges for the large area film deposition and the edge area loss in modules.

The a-Si:H and μc-Si:H materials are usually deposited by plasma enhanced chemical vapor deposition (PECVD) on various substrates (glass, aluminum, steel, plastics, etc.). The deposition technique is similar to the one used in flat panel displays. Incidentally, because of shrinking margins, the flat panel industry currently looks for diversification and new applications. In 2000, the industry started focusing on implementing their plants for solar panel production. Today companies like Oerlikon, Applied Material and Ulvac are setting up complete “turnkey” factories for thin film silicon solar cells on glass substrates. Part of the technological know-how for designing thin film silicon solar cells is not completely public knowledge yet. This know-how is shared by laboratories (Neuchâtel, Jülich, AIST, ECN, Utrecht, Toledo, Delft, etc.) and companies (Kaneka, Fuji, United Solar, Oerlikon, Mitsubishi, Flexcell, Nuon, etc.), some of them listed in Table 1-1. The world leader in terms of efficiencies is the company Kaneka with the certified world record stabilized efficiency of 11.7 % for a micromorph tandem cell, 10.1 % for single junction μc-Si:H solar cell and the laboratory in Neuchâtel with a 9.5 % stabilized single junction a-Si:H cell. Note that, initial efficiencies are not always relevant because of light-induced degradation and uncertified result may not always be accurate.

Table 1-1: Initial efficiencies of small area (between 0.25 cm^2 and 1 cm^2) solar cells from different companies and laboratories. The efficiencies in brackets are stabilized efficiencies and those in bold are certified results by an external laboratory.

[%]	Country	a-Si	μc-Si	micromorph	comments
Kaneka	Japan		**10.1**	13.1 (12) (**11.7**)	[11, 12])
USCC	USA	10.7		14.6 (13)	Triple junction with Ge ([11, 13])
Oerlikon	CH	10.7% (9.1)	--	11.2 (10.6)	[14-16]
Jülich (Lab)	Germany		9.8	12.5 (11.2)(**10.8**)	[17, 18]
Neuchâtel pin	CH	11.2 (**9.5**)	9.9	13.3 (11.1)	[19, 20]
Neuchâtel nip	CH	9.2 (7.4)	9.0	10.3 (10.1)	This thesis on glass substrate

1.2 Thin Film Materials

1.2.1 Amorphous silicon (a-Si:H)

Silicon (Si) is a member of the IV group and thus prefers chemical bonding in a four-fold coordination. In its crystalline form it is normally bonded to four neighboring silicon atoms in the tetrahedral structure of the diamond lattice shown schematically on the left side of Figure 1-5. The hydrogenated amorphous silicon, shown on the right side of Figure 1-5, deviates from the crystalline diamond-like structure. The coordination number, bond lengths, bond angles and dihedral angles fluctuate and lead to a disordered material. This disorder is the main feature that distinguishes amorphous silicon from to its crystalline counterpart. Note that the crystalline form of Si is the ground state (or global minimum energy) for the silicon material. In fact the amorphous material is not in a stable equilibrium but in a metastable state. One property of every semiconductor is the energy band gap, which separates the valence band from the conduction band. In crystals, the energy band gap is a consequence of the periodicity of the lattice and the conservation rules between photons and phonons. The disorder of a-Si:H silicon requires an approach other than the standard Bloch theorem, which is central to the description of crystalline semiconductor [21]. Nonetheless, the disorder in amorphous silicon is not total, but only in the long range and therefore the description of this material focuses more on short range interaction (chemical bonding). In fact, the band can also be described by bonding states, short range order being the most influential [22]. The defects in crystalline lattices refer to atoms that are not correctly positioned in the crystal (vacancies, interstitials, and dislocations). For amorphous silicon, this definition loses its meaning because the atoms have partially lost their order and do not have a precise location. In fact, the defects in amorphous silicon are often related to the coordination defects, which are not allowed in a perfect crystal.

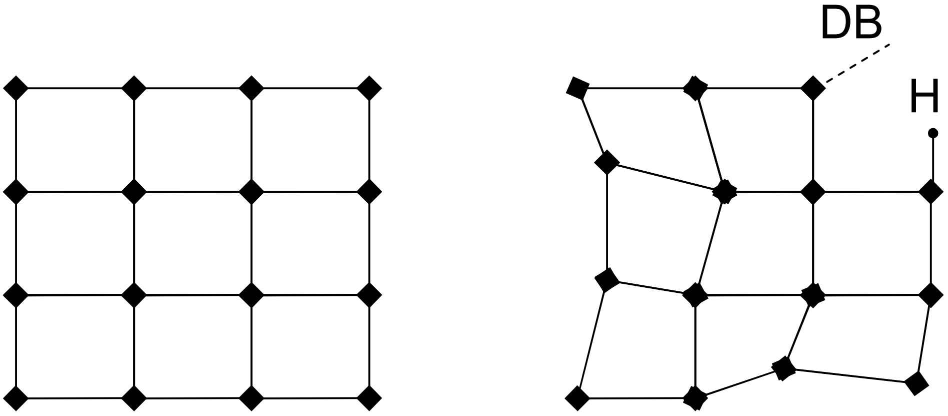

Figure 1-5: Schematic lattice in 2-dimensions of crystalline silicon (left), lattice of hydrogenated amorphous silicon (right). Coordination defects or dangling bonds (DB) are created to relax the system and then hydrogen atoms are bound to some of the unoccupied Si bonds. This is a schematic 2 D representation, whereas the real structure has a tetrahedral 3 D diamond-like structure.

The disorder structure influences the electronic properties in different ways. The covalent bonding in a-Si:H is similar to that of c-Si, resulting in similarities in the overall electronic structure with an energy band gap. The density of states of the energy structure of a-Si:H is usually represented as in Figure 1-6. Structural defects such as breaking of Si-Si bonds create localized states. These states are called dangling bonds and lie in the energy band gap and create defective states in the mobility gap of a-Si:H. These states are recombination centers for the electron-hole charge carriers. For electric applications this process should be minimized in order to diminish recombination losses in the photovoltaic material.

Electronic grade a-Si:H material is deposited by a PECVD process from the decomposition of silane (SiH_4) mixed with hydrogen (H_2). The hydrogen has an important role in the material because it passivates the dangling bonds and thus reduces the defect density by several orders of magnitude. The typical dangling bond density of a device quality a-Si:H material is 10^{16} cm^3 which remains still elevated compared to typical semiconductors! The second consequence of the bonding disorder (lengths, angles) in the material is the band tails, shown in Figure 1-6, which are localized states near the band edge. These tails are induced by the lack of periodicity as demonstrated by the model of Anderson [23]. One important fact is the asymmetry of the conduction and valence band tails. In fact, the valence band tail is much larger than the conduction band tail, leading to reduced hole band mobility (electron mobility is 100 to 1000 time higher than hole mobility) and reduced p-type doping efficiency compared to n-type. This reduced hole mobility for a-Si:H compels the light illumination through the p-layer, which limits the hole path in the device. Therefore, the n-i-p configuration is used in the case of an opaque substrate.

In fact, it was not trivial that a-Si:H could be doped because the coordination disorder would in principle relax the coordination of the substitution dopant. Nevertheless, it was found that substitutional doping occurs in a-Si:H but with limitations in the doping process [24]. In addition, every dopant that is incorporated in the material also creates more defects because more mis-coordination opportunities are offered in the lattice. These defect states partially compensate the doping, such that the carrier density increases only as $N^{1/2}$, where N is the dopant density. Hence, the asymmetry of the band tails explains why the doping efficiency is more effective for n-doped layers than for p-doped layers.

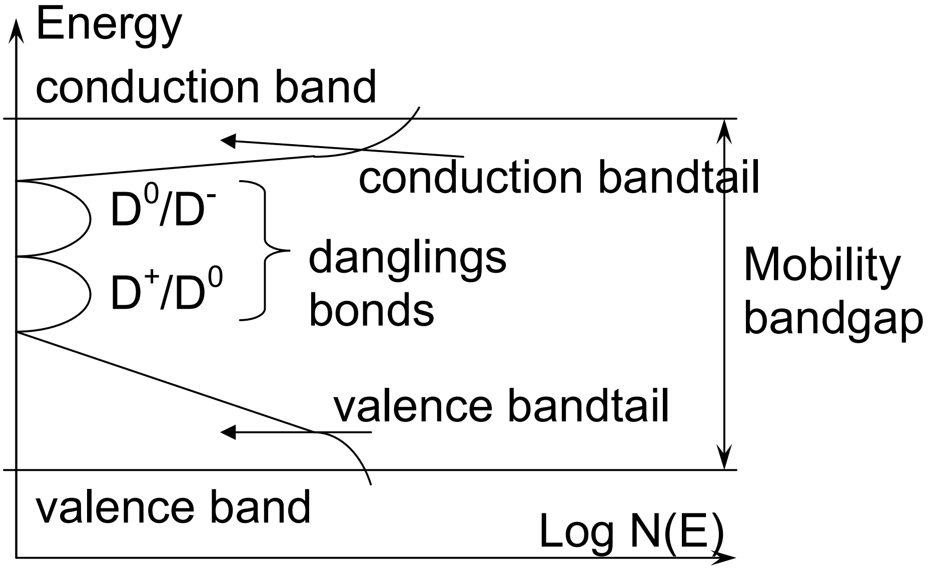

Figure 1-6: Density distribution of states in the mobility gap of hydrogenated amorphous silicon.

The amorphous silicon is subject to light-induced degradation or the so-called Staebler-Wronski effect [10]. The mechanism is not yet fully understood but it is clear that the defect density increases when recombination occurs in the a-Si:H material, which is the case when the device is operated in forward or when light illuminates the device [25]. In fact, when the solar cell is illuminated, the light generates electron-hole pairs and a portion of them recombine, inducing the creation of defects [26] (dangling bonds by breaking weak Si-Si bounds), which are therefore new recombination centers. A “steady state” is reached after a prolonged illumination [27-29]. Note that this process is in principle fully reversible by annealing the samples at higher temperatures (between 70°C – 200°C). The annealing mechanism is partly responsible for the improved performances of the a-Si:H module during summertime. More details about hydrogenated amorphous silicon and on the nature of the light induced degradation can be found elsewhere [22, 30-33].

1.2.2 Microcrystalline silicon (μc-Si:H)

Microcrystalline silicon (μc-Si:H) is a mixed phase material, which contains crystalline grains between 5 to 100 nm in an amorphous matrix. The μc-Si:H material grows in the form of cones, which consist of smaller grains. Grain boundaries appear where the cones collide with each other. The grain boundaries are important because they are sources of defects where recombination occurs [34]. Transmission electron microscope (TEM) observation show that the grain boundaries are nuclei for cracks or voids, which create contamination and shunting paths in the solar cells [35]. One possibility to obtain μc-Si:H is to increase the hydrogen content in a standard a-Si:H PECVD deposition process. As shown in Figure 1-8, µc-Si:H material appears as the dilution gas flux ratio (H_2/SiH_4) is increased, i.e. the hydrogen content in the deposition chamber is increased. Note that the µc-Si:H can also be grown by changing the power, pressure and not only the dilution [36, 37].

Different models like surface diffusion [38], selective etching [39], and chemical annealing [40, 41] have been used to explain the transition from amorphous material to microcrystalline material with the dilution of hydrogen. In the surface diffusion model, the hydrogen assists the nucleation of the crystalline phase and facilitates the diffusion of the species, which can then relax to the energy minimum. In the etching model, both a-Si:H and µc-Si are deposited simultaneously but the hydrogen etches only the a-Si:H which favors µc-Si:H growth. In the chemical annealing model, the chemical reaction of hydrogen with the layer surface mediates the crystallisation of the film. The reality is probably a combination of these mechanisms. Further details on µc-Si:H material and solar cells can be found in, e.g. the PhD thesis of F. Meillaud [42], C. Droz [34] and T. Dylla [43].

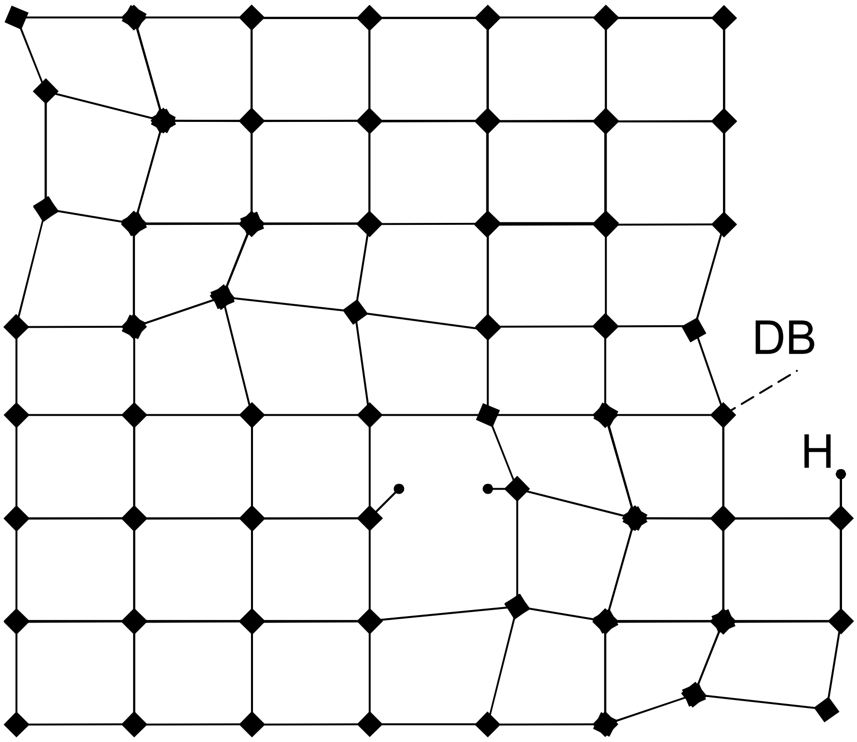

Figure 1-7: Schematic lattice in 2-dimensions of a lattice of hydrogenated microcrystalline silicon. The well ordered crystalline lattice is surrounded by an amorphous phase.

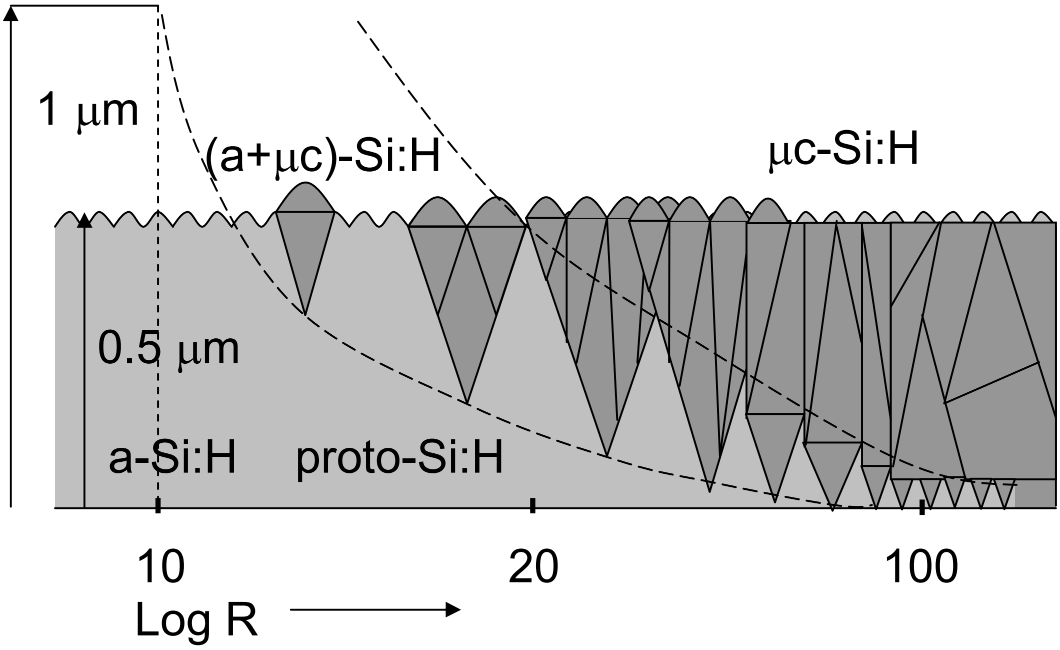

Figure 1-8 : From a-Si :H to μc-Si:H growth with increasing hydrogen content during deposition. Redrawn from R.W Collins et al. [44]

1.3 Solar cells

1.3.1 Solar cells in the substrate configuration (n-i-p solar cells)

The charge carriers in high quality c-Si have high diffusion lengths of more than 100 μm. Hence, the standard design for such a device is a p-n junction, which works mainly by diffusion of the carriers in the bulk part and a comparatively small contribution by drift in the field across the junction. For a-Si:H and μc-Si:H silicon materials, the situation is more complex. Both materials are defective, which implies a decrease in "diffusion length" of the charge carrier in the range 1 μm or even less for a-Si:H material. Hence, the extraction of the carrier is assisted by drift with an external electric field. This can be achieved with the p-i-n or n-i-p design where an undoped absorber material is sandwiched between the negatively (n-layer) doped and positively (p-layer) doped layers creating an electric field in between. The absorber material has to be intrinsic (i layer) in order to minimize the defect density. The doped layers are eventually electrically dead and no photovoltaic current can be extracted from them. Hence, they serve only to create the electrical field. In all devices the interface defect density will also play a role and usually "buffer" layers are introduced to reduce these defects. Figure 1-9 illustrates the generation of an electron hole pair with an incoming photon. The electrons drift into the electric field to the n layer and the holes to the p layer. The generation profile in the absorber layer is asymmetric. It is higher at the front interface because most of the high energy photons (400nm - 500nm) are absorbed within the first 50-100 nm. For all devices, the light will come through the p layer because in the a-Si:H case, the holes have a mobility 3 times lower than the electrons. In fact, the p-i-n or n-i-p configurations differ by the sequence of deposition. In p-i-n, the p doped layer is deposited first, then the intrinsic layer and then the n layer, and vice and versa for the n-i-p (e.g. p-i or i-n). In this thesis, we focus on solar cells deposited on flexible substrates covered with a metallic back contact and, therefore, the n-i-p structure is preferred.

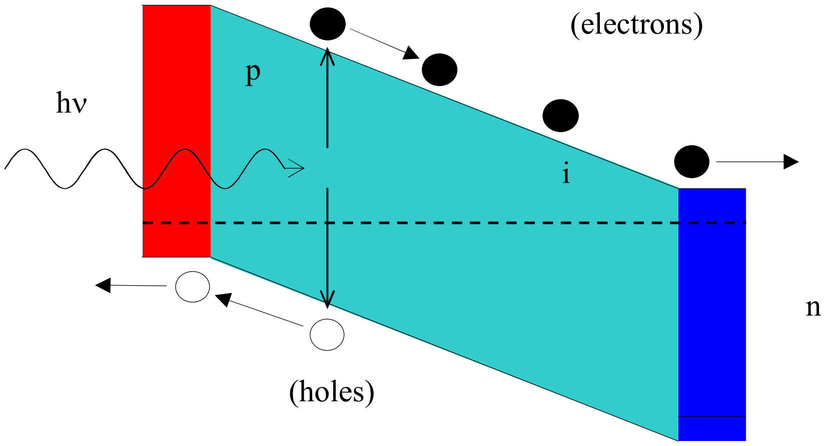

Figure 1-9: Schematic illustration of a n-i-p device under illumination in short circuit conditions.

1.3.2 Light trapping

The optical energy band gap of the semiconductor is defined as the minimum energy to create an electron hole pair, i.e. to excite an electron from the valence band to the conduction band. The material is then transparent for wavelengths below the energy band gap and only defect states in the energy band gap yield a remaining level of light absorption. The drop of the absorption curves in Figure 1-10 shows this effect. In this graph the optical band gaps for c-Si, a-Si:H and μc-Si:H, are 1.1eV, 1.7eV and 1.1eV, respectively. The absorption coefficient of a-Si:H and μc-Si:H is higher compared to c-Si for wavelengths between 400 nm to 750 nm. The reason is the disorder of the a-Si:H material, which relaxes the selection rules of the indirect band gap of the c-Si. Nevertheless, the low deposition rate and low electronic properties of a-Si:H and μc-Si:H require the use of thin films with thicknesses below 300 nm and 5 μm, respectively. Therefore, the optical path in the device needs to be enhanced. This is achieved with textured interfaces, which creates light scattering and light trapping in the device.

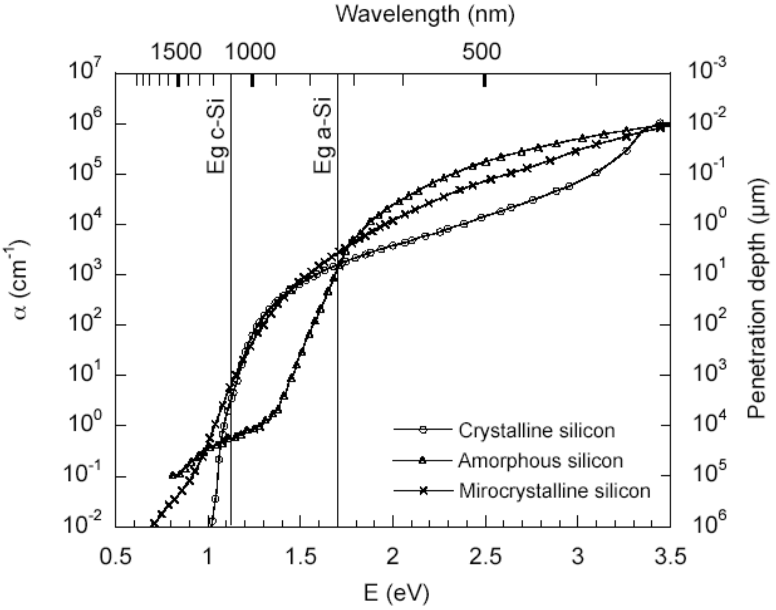

Figure 1-10: The absorption coefficient of a-Si:H, µc-Si:H, and crystalline silicon from ref. [45].

The structure of an n-i-p thin film silicon device is presented in Figure 1-11. The first deposited layers are the back reflector on the substrate, then the silicon layers n-i-p and finally the top contact, which is a front transparent conductive oxide (TCO) like ZnO or ITO. The role of the top contact in the n-i-p solar cells will be discussed in detail in Chapter 5. The back reflector is usually 100 nm of a metal, like silver or aluminum, and a thin 60 nm TCO like ZnO. The metallic layer acts also as back contact for the solar cell. The thin TCO acts as a barrier that protects the active layers (silicon layers) from diffusion of the metallic atoms and as optical matching between the silicon layers and the metallic layers [46]. The back reflector (BR) is often textured in order to promote rough interfaces in the entire device. The effect of the rough interfaces compared to a flat substrate is shown in Figure 1-11. On the flat substrate the blue part of the light (400nm-550nm) is totally absorbed before hitting the BR, the red part of the light (550nm-1100nm) is specularly reflected by the BR and the effective absorption thickness will be twice the intrinsic layer thickness. On the textured substrates, the light is scattered at the TCO/Si interfaces. Hence, the light path is enhanced in the absorber and for elevated scattering angles the light can even be trapped in the absorber thanks to total internal reflection at the front Si/TCO interface. Thus the red part of the spectrum can make several passes in the solar cells.

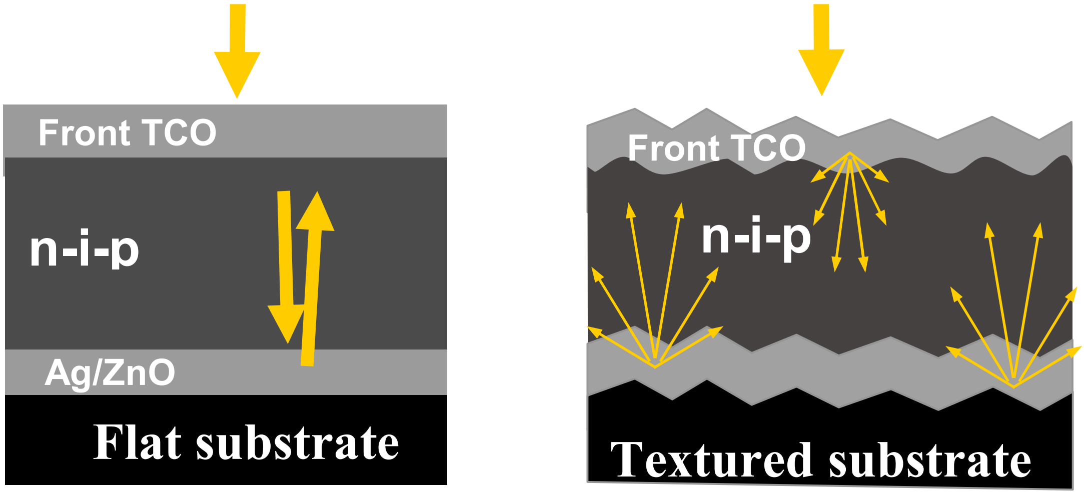

Figure 1-11: Structure of a thin film silicon solar cell with flat (left) and textured substrates (right). The thicknesses of the layers are 100 nm of Ag, 60 nm of ZnO, 200 nm to 300 nm of a-Si:H or 1 µm to 3.5 µm of µc-Si:H, and 80 nm of ITO or 2 µm LP-CVD ZnO.

1.3.3 Micromorph tandem concept

The inherent correlation between voltage and light absorption limits the efficiency of single junction solar cells. For ideal single junction the limit is close to 30 % [47, 48]. Multi-junction devices offer the opportunity to efficiently convert the high energy photons into high voltage while still absorbing a wide spectral range. In fact for the ideal case of four junctions, the limits is close to 50 % [47].

Hence, the micromorph tandem cell consisting of a stack of a-Si:H and µc-Si.H solar cells was proposed by J. Meier et al. [49] in order to further improve the efficiency of single a-Si:H cells. By adding a µc-Si:H cell below the a-Si:H cell, the tandem is capable of absorbing a wider range of the solar spectrum. The solar spectrum AM 1.5g is shown in Figure 1-12 with the typical region of absorption for a-Si:H material (between 400 nm to 750 nm) and for µc-Si:H (between 400 nm to 1100 nm). The main advantage of this tandem structure is that both cells can be deposited in the same PECVD reactor.

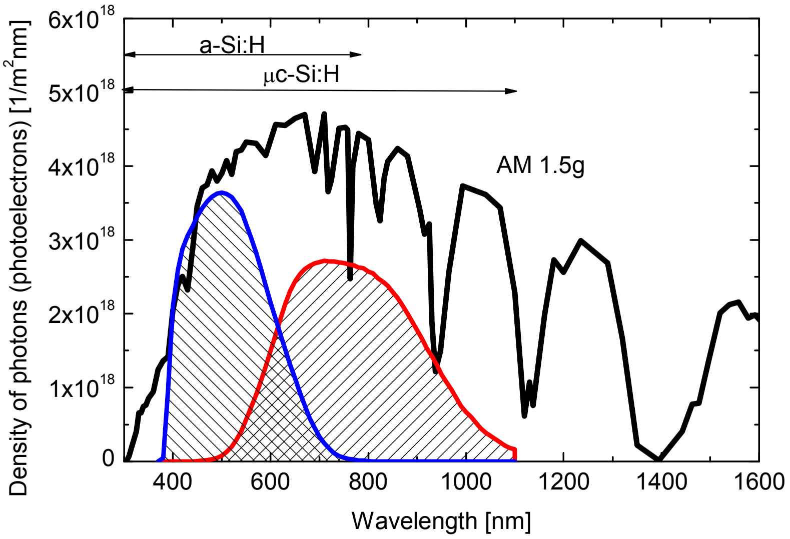

Figure 1-12: The AM 1.5g light intensity spectrum and the absorption spectrum of an a-Si:H and μc-Si:H in the micromorph tandem cell.

1.4 Content of the thesis

1.4.1 Status of the research field

This work focuses on the development of thin film silicon solar cells for flexible applications. The advantages of flexible sheets are the possible lower substrate cost per square meter compared to iron free glass, the possibility to use roll to roll processes that allow deposition of hundreds of meters of solar cells in one run, and most importantly the light weight, reduced fragility and flexibility of the modules which reduce the storage, breakage and transportation costs. This strategy is followed in production or R&D by different companies such as Flexcell, Powerfilm, Fuji Electric, Canon, Sanyo, Nuon and United Solar. Several research institutes are also working on flexible cells; Utrecht, Toledo, AIST, ECN, Stuttgart and Neuchâtel. Some companies have reported high initial efficiency at cell level, between 13% and 15%, by using multi junction devices deposited at high temperature on polyimide sheets or metallic foils [50, 51]. But so far, these efficiencies are often neither confirmed nor translated into high stabilized module efficiency. Nevertheless, there are various strategies to make thin film silicon on a flexible substrate. Here, we summarize the activities and research units that make contributions to the domain of thin film silicon solar cells deposited on flexible substrates.

Silicon layers can be deposited by various techniques such as PECVD, Hot Wire CVD or Micro Wave PECVD. Pioneer work at IMT Neuchâtel [52] showed that the very high frequency (VHF) glow discharge yields increased deposition rate and reduced ion bombardment compared to RF-PECVD (13.56 MHz). Higher deposition rate with VHF has also recently been reported by the company United Solar [53]. Fuji Electric has recently showed that higher deposition rate with RF-PECVD for a-Si:H cannot be achieved without degrading the stabilized cell performances [54]. Indeed, their best stabilized a-Si:H solar cells deposited at 1 A/s has a stabilized efficiency of 8%, whereas the cell deposited at 5 A/s has a stabilized efficiency of 7% only. At the Energy Center of Netherlands (ECN), the current work focuses on developing roll to roll processes with MW-CVD deposition [55]. This technique is well established by their technology partner Roth and Rau (Germany) for large area deposition of silicon nitride passivation layers in c-Si cells. Because of high ionization, MW-CVD is expected to yield high deposition rates for μc-Si:H layers [56]. At Utrecht University, the HW-CVD process is used by Schropp et al. [57] for making n-i-p devices. The absence of ion bombardment increases the material quality and should (in principle) also increase the device performances. Microcrystalline n-i-p cell with an efficiency of 8.8 % is made on stainless steel covered with a hot silver textured back reflector.

The choice of process temperature is important for making high efficiency devices. Indeed for both μc-Si:H and a-Si:H layers, the minimum defect density observed for temperature is between 200 and 300°C, as reported by A. Matsuda [58]. Nevertheless, devices with very low deposition temperature (100°C) are investigated at the AIST Research Institute in Japan where they produced a n-i-p μc-Si:H solar cell with 6% efficiency on a polymer substrate (without texture) [59]. The University of Stuttgart also developed a low temperature process and demonstrated an efficiency of 6% (without texture) [60, 61]. Nippon Synthetic Chemical Industry investigates the p-i-n strategy with devices deposited on plastic foil with light impinging through the plastic sheet. Initial 8% efficiency with a-Si:H compared to 9.4% obtained on glass substrates [62]. At Utrecht University PECVD deposition processes are also used to make n-i-p cells on plastic foils. Rath et al. [63] have achieved an initial efficiency of 6.2 % for a single a-Si:H cell on flat substrate. In Neuchâtel, the pioneer work on solar cell deposited on plastic foils was performed by P. Pernet and al. [64], then continued by V. Terrazzoni [65] and J. Bailat [66]. The work focused on optimization of deposition temperature and preliminary textured foils for a-Si:H solar cells. The work showed that temperatures between 150 and 200°C are possible for the growth of Si and that texturation of the plastic foils is improving the J_{sc} by 16 % compared to flat substrate.

Strong efforts were made on the texturation of the back reflector for n-i-p solar cells. Banerjee and Guha (United Solar) [46] or Suzuki et al. (Tijin) [67] showed that the light absorption is enhanced by incorporating texture back reflectors in the device. Nevertheless, the optimum morphology of the back texture is still unknown and it is not yet known whether the best substrate should have a periodic or random structure. Sai et al. [68] have explored the influence of grating period for back reflectors in microcrystalline n-i-p solar cells on stainless steel. He showed that the current density is increasing with the period of the lattice and saturates for a lattice constant over 1 μm. J_{sc} of 24.3 mA/cm^2 is achieved for the best grating period of 0.9 μm and a 1 μm thick layer. Furthermore, Heine and Morf [69] suggest blazed gratings as the ideal substrate because the reduced symmetry of the system prevents outcoupling into a zero order beam. Also, there is a trade off between the suitable texture for the light scattering and the losses in the back reflector, which come from surface plasmon absorptions in the rough metallic layer [70]. J. Bailat et al. [66] have shown that the increase of J_{sc} (15 %) with textured substrate in a-Si:H cell is coupled with a loss of V_{oc} and FF for the a-Si:H. This leads to equivalent efficiency (7.6%) for a-Si:H on flat and on textured substrates.

However, the detailed relation between the substrate surface morphology and the performance parameters of μc-Si:H solar cells has only recently been addressed by Nasuno et al. [71]. In addition, Bailat et al. [72] have shown that, in the p-i-n configuration, the substrate morphology significantly influences the quality of the μc-Si:H solar cells. Furthermore, TEM observation made by M. Python et al. [73] have showed the apparition of nano-cracks in the layer and how these defective regions are quantitatively correlated with the V shape substrate morphology. Recently, Li et al. [74] have also reported crack formation in layers grown by HW-CVD, which demonstrate that there is no direct correlation between the cracks and the ion bombardment.

The light induced degradation of a-Si:H requires the use of thin cells. For high efficiency devices, the company United Solar (USA) has, so far, the most successful concept with stabilized efficiency of 13 % as shown in Table 1-2. They used three n-i-p thin cells deposited by PECVD with different gradings of Ge [51]. Alloying silicon with Ge reduces the band gap of a-Si:H (from 1.75 to 1.1 eV) and therefore increases the optical region of absorption. The major difficulty comes from the alloying of Ge in the a-Si:H network. In fact, it creates additional defects and makes the cell more sensitive to light-induced degradation. The solution to minimize these effects is to introduce grading profiles that reduce the content of Ge close to the n-i and p-i interfaces [75]. The University of Toledo also develops triple junction devices with Ge deposited by PECVD [76]. Fuji Electric use tandem junction n-i-p cells with SiGe bottom cell to improve the cell efficiency; initial efficiency of 12% on 1 cm^2 has been reported but not certified [77]. In Utrecht, Schropp et al. also use triple junction devices with Ge to achieve an initial efficiency of 10.9% [78]. The research group at Canon have impressive results with 30 mA/cm^2 total current density in triple junction a-Si:H/μc-Si:H/μc-Si:H. Since thick layer (total thickness over 5 μm) is needed to achieve such high J_{sc}, their focus is on high deposition rate. Triple junction solar cells are made with initial 13.1 % efficiency with deposition rate of 3 nm/s. High deposition pressure and small electrode distance is used to make these devices [79].

Many companies are already producing flexible modules. Currently in the beginning of 2009, United Solar produced 120 MW flexible modules (triple junction SiGe deposited stainless steel). The spin-off company from Toledo University Xun-light was created in 2006 and runs a 100 kW production line, however, the cell design is not clear yet. Fuji Electric (Japan) is also a company that develops n-i-p process (tandem a-Si/a-SiGe) but on polyimide foils, which are also resistant to high temperature processes such as hot silver back contact (40 MW capacity in 2009 should be installed). The company Flexcell (Switzerland) is a spin-off of IMT. They are starting mass production in 2009 with a 25 MW production line for single junction n-i-p a-Si:H silicon line on PEN plastic foils covered with metal back contact. They recently successfully increased the width of the foils from 30 cm to 50 cm, while keeping homogenous film quality with the multipass PECVD concept. The modules from their current 40 kWp Pilot production are TÜV certified have 4.5 % to 5.0 % stabilized aperture area efficiency but no light trapping scheme is implemented yet. Founded in 1998, PowerFilm are producing flexible single junction a-Si:H and a-Si:H/a-Si:H tandem modules with 10 MW capacity plant [80]. One very challenging approach is the transfer process used by Nuon Helianthos [81, 82]. They use a temporary aluminum substrate to deposit p-i-n device on aluminum foil covered with SnO_2 deposited at $T > 300°C$ by APCVD. After the PECVD deposition of silicon layers, the cell is transferred onto a plastic foils and the aluminum is wet etched. They achieve stabilized efficiencies of 6% for modules on 30 cm width foils. At the time of writing, the work focused on increasing the width of the foils to 1 m before entering mass production. They also collaborated with Utrecht University and the Jülich group in Germany for making micromorph tandem devices. They produced micromorph tandem modules (5 * 5 cm^2) with initial efficiency of 9.4% together with the Jülich group. Finally, Sanyo offers a-Si flexible OEM modules within their Amorton product range [83].

Table 1-2: Initial and stable efficiency of small area (between 0.25 cm^2 and 1 cm2) solar cells from different companies and laboratories in flexible photovoltaics. The values in parentheses are the best stabilized efficiencies. The confirmed efficiencies are in bold.

	Country	a-Si	μc-Si	Micromorph	Comments
Canon	Japan			13 (11.5)	[50, 79] Triple
USCC	USA	10.7	8.4%	15.1 (13.3)(**12.1**)	Triple junction with Ge [11, 51, 84, 85]
Fujy	Japan	9 (8)		12	[54, 77] Tandem a-Si with Ge
Nuon	NL	7.7 (6)		9.4	PIN [81, 82] Module for a-Si:H
Flexcell	CH	5.5 (5.0)			Module results
Toledo	USA	8.9	7.2	11	[86] [76, 87] Triple with Ge
Utrecht	NL	6.2	8.8	10.9	[57, 63] Triple with Ge
AIST	JAPAN	8.0	6.0		[59] (100°C)
Stuttgart	D	6.0			[60, 61] (100°C)
Teijin	JP	11.3			[67, 88] 500 nm thick absorber layer
IMT	CH	8.8 (7.0)	8.7	11.2 (9.8)	This thesis on PEN

1.4.2 Contribution of this work to the research field

The challenges and contributions of our work are to develop high efficiency devices, with two additional constraints; one is to ensure the compatibility with low T_g substrates such as poly-ethylene-naphtalate (PEN), the second is to concentrate on silicon-based thin film materials like a-Si:H and µc-Si:H without the addition of Ge. Thus, we have to deal with the accessible range of deposition temperature between 150 and 190°C, which is not ideal for the deposition of high quality silicon material, and with the accessible band gaps of a-Si:H and µc-Si:H, which limits the choice for spectrum splitting in the sub-cell component. Nevertheless, we achieve efficiencies well within the range of state of the art devices. In the following, we summarize the main steps that improved the solar cell performances.

The coupling of the light in the device is crucial for high efficiency thin film silicon solar cells. By comparing various optical systems, mainly a thin ITO layer or a thick textured LP-CVD ZnO front contact, we experimentally demonstrated that the effect of the texture at the front of the solar cell is not efficient for the light trapping in the solar cells. However for thin a-Si:H deposited on periodical grating, we show that a thick textured front LP-CVD ZnO increases the J_{sc} by 7% compared to flat ITO. Since the texture is not effective, we demonstrate that the thick ZnO switch off the grating periodicity and therefore allows a better capture of the weakly absorbed light. On this periodic substrate, the best J_{sc} is 14.4 mA/cm^2 for a-Si:H (with 200 nm thick absorber layer) cells and 25 mA/cm^2 (with 3 µm thick absorber layer) for µc-Si:H solar cells on periodic substrate. Furthermore, we demonstrate high potential of periodic substrate, with J_{sc} as high as on random substrates [89].

For a-Si:H solar cells, we explore the influence of the substrate morphology on the J_{sc} but also on the V_{oc} and FF. We show that the growth condition of the n-µc layer is strongly influenced by the morphology of the substrate. In fact, the severe V shape substrate morphology coupled with n-µc layer creates porous area in the absorber layer. For that, we introduce a new amorphous n-SiC layer, which removes the apparition of cracks in the absorber and keeps the V_{oc} stable on textured morphology compared to flat substrate. As a result, the increase of absolute initial efficiency is 1.9% on textured substrate compared to flat substrate whereas only 0.7 % is observed when n-µc is used. The beneficial effect of our optical and electrical findings removes the negative correlation between J_{sc} loss and V_{oc} gain. Hence, this strategy is used to fabricate a-Si:H solar cells on PEN substrate with an initial efficiency of 8.8% for an i-layer thickness of 270 nm [90, 91].

For our low process temperature condition, we show that the light-induced degradation (LID) also depends mainly on the film a-Si:H absorber thickness. The LID decreases from 27% for a 400 nm thick a-Si:H absorber to 10% for a 140 nm thick absorber layer. Hence, we implement tandem a-Si:H cells, which reduces the light induced degradation from 20% for 300 nm single junction solar cells to 15% for tandem a-Si:H with 360 nm total absorber thickness. The best device has a single junction stabilized efficiency of

7.3% on glass substrate and 7% on plastic substrate whereas 8% is achieved with a tandem a-Si/a-Si structure on glass substrate.

For μc-Si:H solar cells, the rough morphology of the substrate also decreases the V_{oc} and FF of the solar cells. As previously shown for p-i-n solar cells, we also find for n-i-p that (nano-)cracks are formed in the absorber material and that oxygen is incorporated in these cracks. Nevertheless as for the p-i-n case, these negative effects are mitigated by rounding the rough morphology. This increases V_{oc} of n-i-p μc-Si:H solar cells from 450 mV to 514 mV, but it also reduces J_{sc} by at least 5% relatively. To remove the trade-off between V_{oc} and J_{sc}, we introduce an amorphous buffer layer during the start of absorber layer growth. This buffer layer reduces the density of cracks and the oxygen content in the absorber layer. With such a buffer layer, we make μc-Si:H solar cells with 9% efficiency on glass and 8.7% on plastic foil with only a 1 μm thick absorber layer [92].

For tandem micromoprh solar cells, we demonstrated the limit of a micromorph cell without an intermediate reflector. In fact, stabilized J_{sc} over 10.5 mA/cm^2 is not feasible without increasing the deposition temperature, which is, in fact, not compatible with our low T_g plastic substrate. Therefore, we implement an asymmetric intermediate reflector concept, which allows us to separate the light in-coupling between the top a-Si:H and bottom μc-Si:H solar cells. It increases, the stabilized J_{sc} over 12 mA/cm^2. With this AIR, we achieve tandem cells with initial efficiency of 11.2 % (9.8% stabilized) on low T_g (PEN) plastic foil. This strategy offers an alternative to triple junction devices with Ge for high stabilized efficiency devices [93].

1.4.3 Outline of the thesis

The first part of this thesis (Chapter 1) intends to provide an overview of the photovoltaic domain and provide knowledge about thin film silicon solar cells. Chapters 2 to 5 are the pillars leading to fabricate the final micromoph tandem cell device that is presented in Chapter 6.

Figure 1-13 is a SEM micrograph of an n-i-p/AIR/n-i-p micromorph tandem device. The thesis is organized according to the growth direction of the deposited layers. First Chapter 2 presents the different textured substrates used in this thesis in order to implement the light trapping scheme needed for our devices (LP-CVD ZnO, Hot Silver, 2-D periodic grating). It also briefly presents the deposition processes and characterization tools. Chapter 3 concentrates on the deposition of μc-Si:H silicon solar cells. The influences of the textured substrates in the μc-Si:H solar cell performances are explored. Chapter 4 focuses on the optimization of a-Si:H solar cells and special attention is paid to the relationship between the substrate texture and the growth of the different layers. After that, Chapter 5 explores the choices of front TCO contact for n-i-p solar cells. It compares the standard ITO front contact usually used in the industry to our in-house thick textured LP-CVD ZnO. Finally, Chapter 6 combines these results for the creation of a micromorph tandem cell. Furthermore, the implementation of an asymmetric intermediate reflector which uncouples the light trapping of the top and bottom cell is presented. The splitting of the light trapping allows direct integration of the single junction solar cells resulting (Chapter 3-5) in the multi-junction devices of Chapter 6.

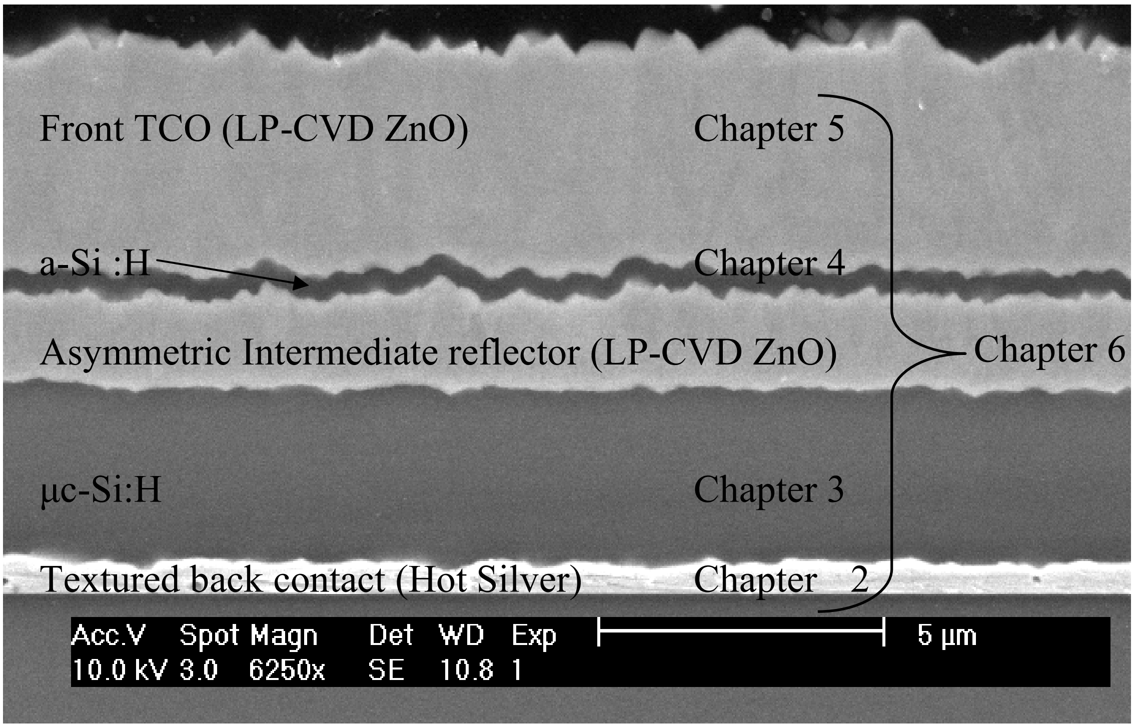

Figure 1-13: Micrograph, obtained from scanning electron microscope (SEM), of a micromorph tandem solar cell deposited on glass covered with a textured hot silver and including an asymmetric intermediate reflector.

Chapter 2: Materials & Methods

Layers, methods and rough substrates

2.1 Introduction

This chapter briefly presents deposition techniques for thin film layers and characterization setups used throughout this work. The main deposition method is plasma enhanced chemical vapor deposition (PECVD) which is used for the deposition of silicon layers. The back contact is usually made by sputtering of a metal (Ag or Al) directly onto the substrate. The front contact is a transparent conductive oxide (TCO) such as sputtered ITO or ZnO deposited by low pressure chemical vapor deposition (LP-CVD ZnO). Structuring of the cells is achieved by lift-off of the front contact and dry etching of the silicon with SF_6 [94]. External quantum efficiency (EQE) and the current voltage measurements (IV) determine the efficiency of the cells. Fourier transform spectroscopy (FTPS) and the Raman crystallinity (C_R) are used to characterize, respectively, the defect density and the crystallinity of the μc-Si:H material. Atomic force microscopy (AFM) and scanning electron microscopy (SEM) are used to probe the surface of the layers. Transmission electron microscopy (TEM) and focused ion beam (FIB) techniques are used to make cross-section micrographs of our films. Secondary Ion mass spectrometry (SIMS) is used to quantify the contamination in our layers. Optical spectrometry (R, T) and ellipsometry (n and k) are used to characterize the optical properties of our layers.

2.2 Silicon layers deposited by PECVD

The deposition of amorphous silicon (a-Si:H) by glow discharge or plasma enhanced chemical vapor deposition (PECVD) from silane gas (SiH_4) was already reported 40 years ago [95]. A typical PECVD process is made in a vacuum reactor at low pressures in the order of 0.1 to 10 mbar. It uses typically capacitive coupling meaning that the plasma is sustained by radio frequency (RF) between two flat electrodes. The plasma itself consists of electrons and ionized atoms (or molecules), which respond collectively to the electromagnetic field. The individual particles in the plasma are electrically charged but on a macroscopic level the plasma is neutral. It is frequently described as an “ionized gas” or a “soup of charged particles”. After ignition of the plasma, the electric field between the two plates accelerates free electrons which collide with the atoms. This creates additional electrons that sustain the plasma. The electrodes consist of two 8 cm by 8 cm parallel plates, described in the thesis of V. Terrazzoni [65]. The RF power is applied on the bottom electrode, which has a shower head for the gas distribution in the plasma. The gases used are SiH_4, H_2, CH_4, TMB for p doped and PH_3 for n doped layers. The typical deposition parameters are a pressure of 0.4 mbar, a power density of 0.08

W/cm^2, a silane flow density of 0.1 sccm/cm^2, a temperature of 200°C, and a very high excitation frequency (VHF) of 70 MHz. The typical deposition rates are 3-5 Å/s for both a-Si:H and μc-Si.H. Note that more sophisticated electrode designs that reduce the bombardment or powder formation in the reactor are investigated by AIST [96] or Mitsubishi [97].

2.3 Substrates and back reflector

The silicon layers are deposited on various substrates, e.g. glass, plastic, stainless steel (SS), etc. The silicon layers can be deposited directly on the substrate if it is conductive (ex: SS), whereas an additional back contact (Ag, Al) has to be deposited before the silicon layers when a non conductive substrates is used (e.g. glass, or plastic). This work focuses on plastic substrates but glass substrates are used for reference or development. Plastic substrates are coated with Cr-Ag-ZnO stacks deposited by a roll-to-roll process in a large area multi-source sputtering system at the Fraunofer Institute für Elektronenstrahl und Plasmatechnik (FEP), Dresden [98]. Glass substrates (Schott AF 45) are coated with Cr-Ag-ZnO deposited using our in-house sputtering system. The chromium is an adhesion layer, the silver serves as back reflector and electrical contact for the solar cell and finally the ZnO protects the silicon layer from diffusion of metallic atoms and it enhances the optical matching between the Si and the back reflector [46].

The substrate texture is compulsory to increase the path of the light in the solar cells. We present various methods to produce rough surfaces adapted for the scattering of visible light wavelengths into silicon. The rough substrates can be achieved by replication of a texture onto the plastic substrate as shown in Figure 2-1 (right) or can be producedby deposition of a rough layer such as LP-CVD ZnO or hot silver as shown in Figure 2-1 (left). The LP-CVD ZnO can be deposited directly on glass or plastic substrates whereas the hot silver can only be deposited on glass because the deposition temperature is too high for low T_g plastic substrates such as poly-ethylene-naphtalate (PEN) or poly-ethylene-teraphtalate (PET), which typically limit the processing temperature to below 200°C. Additionally, we developed new back reflectors, in which flat silver on glass or on PEN is coated with a rough LP-CVD ZnO. However, for ease of handling we carry out most of the development on glass substrates with a transparent back contact. In this case, the back reflector is a white paint applied at the back of the glass. This configuration is very useful for a study of absorption and carrier collection close to the n-side of the cell [99]. For that the white paint is removed and the cell can be illuminated through the n-side (through the glass).

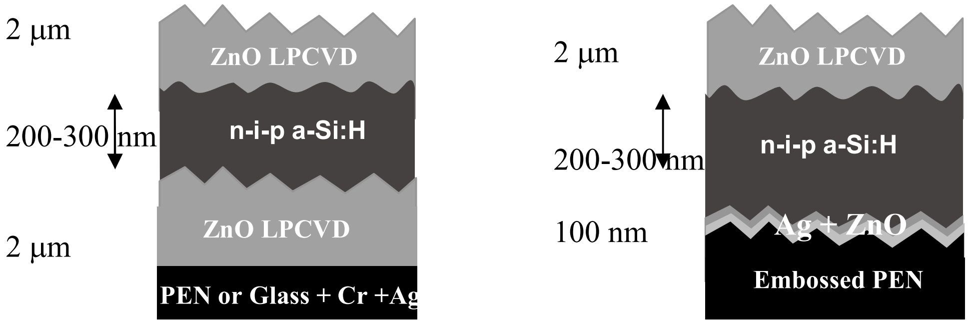

Figure 2-1: Structure of the n-i-p solar cell on substrates coated with silver and LP-CVD ZnO (left) and structure of the n-i-p solar cell deposited on substrates where the texture is replicated on the plastic and coated with a thin Ag/ZnO layer.

2.3.1 LP-CVD ZnO

The highest confirmed stabilized a-Si:H efficiency of 9.5 % is achieved in the p-i-n configuration on glass coated with LP-CVD ZnO at Neuchâtel [20]. Here, we use this ZnO layer in the as substrate for the n-i-p solar cells. This Transparent Conductive Oxide (TCO) consists of boron-doped zinc oxide (ZnO:B) deposited by low pressure chemical vapor deposition (LP-CVD) under conditions that result in a textured surface. The variation of the parameters allows independent variation of the dimensions and the shapes of the surface texture. The surface of LP-CVD ZnO consists of pyramidal structures whose size varies with deposition time and doping [10, 11]. Therefore, the feature size of the LP-CVD ZnO can be tuned for light trapping in a-Si:H or µc-Si:H cells. For µc-Si:H the grain size is increased. In this work, typical Root Mean Square roughness (rms) and lateral dimensions are 70 nm and 350 nm for a-Si:H solar cells and 140 nm and 1 µm for µc-Si:H solar cells, respectively. A subsequent surface plasma treatment of the surface is used to change the morphology. Therefore, two degrees of freedom are available to investigate light trapping. The details of the morphological changes is studied by J. Bailat et al. [70] for the case of µc-Si:H solar cells in p-i-n configuration. It was observed that the plasma treatment transforms the valleys between the pyramids from a V- to a U-shape as illustrated in Figure 2-2. More details about the nature of the LP-CVD ZnO can be found in the thesis of J. Steinhauser [100], further details about the application in the solar cells is discussed by D. Dominé [19] and M. Python [35].

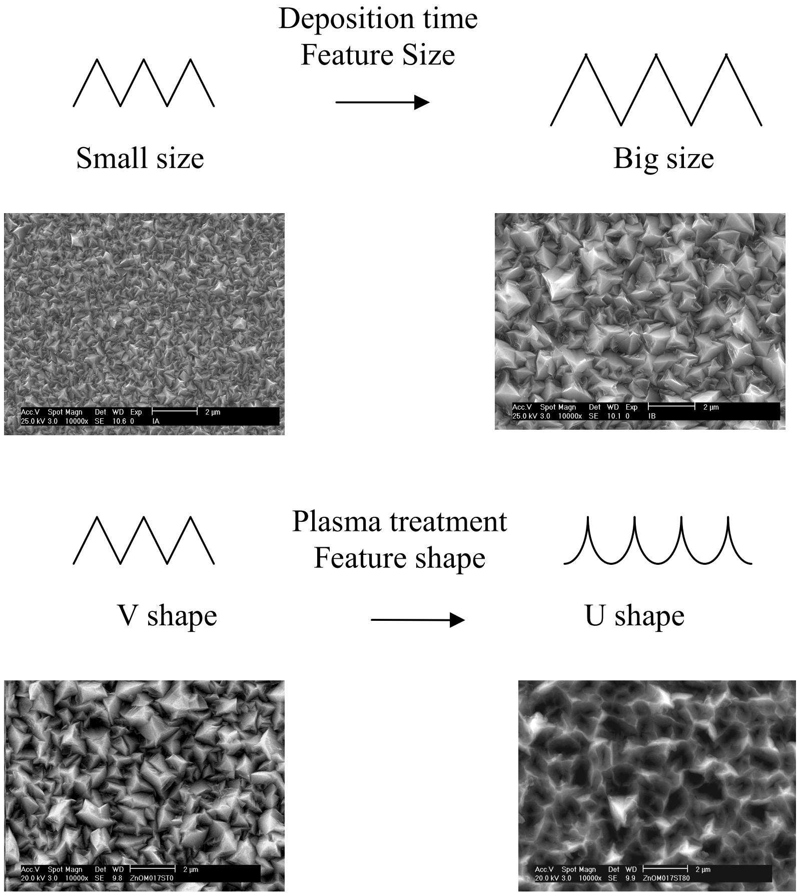

Figure 2-2: SEM micrographs of the LP-CVD ZnO. The size of the pyramids can be controlled with the thickness of the films (small to big size). The morphology can be varied from V- to U-shape with the surface plasma treatment.

2.3.2 Hot silver

The hot silver substrate is used and developed in the industry, e.g. by Fuji Electric, as a back reflector for n-i-p solar cells [46]. This silver layer is deposited by sputtering at high substrate temperatures between 300°C and 400°C, which produces a rough texture as described elsewhere [46, 101]. The roughness can be adjusted with the temperature and the deposition time. The typical dimensions of the silver crystals are in the range of 800-1000 nm with rms roughness of 70 nm as shown.

2.3.3 Plastic films

The final aim is to produce solar modules by roll to roll deposition on plastic substrates such as poly-ethylene-naphtalate (PEN) or poly-ethylene-teraphtalate (PET). The preferable way of texturing is embossing a texture directly into the plastic [102] or into a soft lacquer added and cured on the plastic [103]. Both methods need to be homogeneously reproduced on the substrate, compatible with the cells processing and stable in the long term as the module is exposed to rain, ice and sun during more than 20 years. Figure 2-3 is an example of a roll in which a cross grating texture has been embossed into lacquer by OVD Kinegram [66, 104] and then coated with 80 nm of aluminum and 60 nm of ZnO. Figure 2-4 shows SEM micrographs of the replication of an arbitrary structure on a lacquer. It shows that the pyramids are well reproduced.

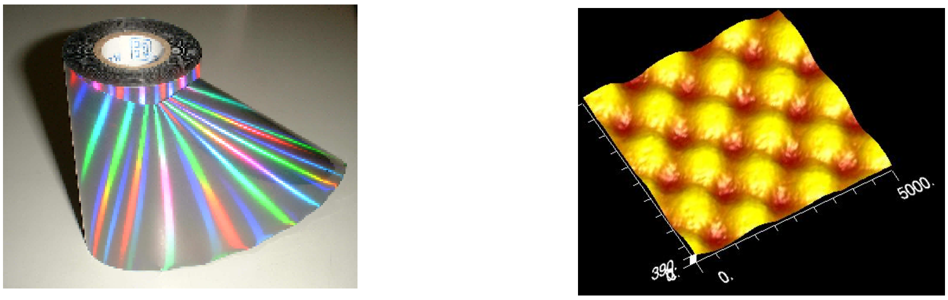

Figure 2-3 Plastic roll with a periodic cross grating coated with aluminum (left) and AFM micrograph of the cross grating.

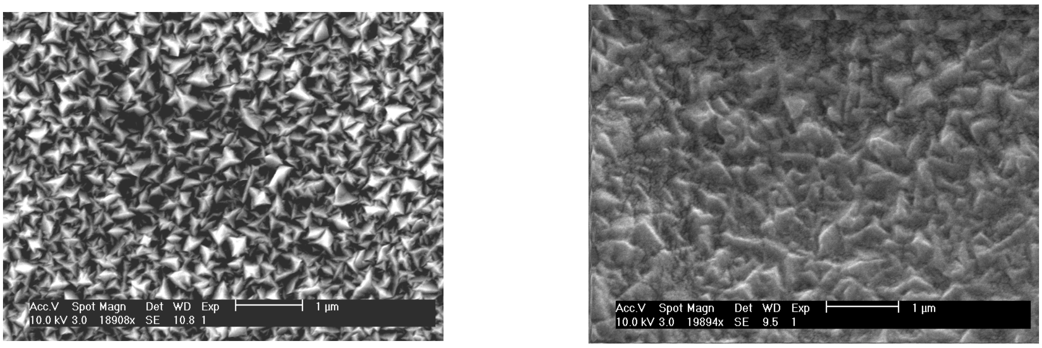

Figure 2-4 SEM micrographs of the LP-CVD ZnO replication (right) covered with 15 nm of gold and the LP-CVD ZnO as grown on glass (left).

2.4 Characterization techniques

2.4.1 External quantum efficiency

The external quantum efficiency (EQE) measures, for every light wavelength impinging on a solar cell, the ratio between the number of electrons collected and the number of photons hitting the cells. Thus, for a given wavelength the number (1 – EQE) gives the portion of photons which are lost by either reflection, absorption in non-active layers (doped layers, TCO, metal) or recombination in the absorber layers. Experimentally, the setup contains a Xe lamp. The light of the Xe is chopped and focused onto a monochromator, which selects the wavelength hitting the cell. The cell is maintained at short circuit condition during the measurement. The EQE can also be measured under different bias voltages conditions, e.g. forward or reverse bias. A negative bias voltage increases the electric field within the cells and diminishes the probability of recombination in the intrinsic layer. Hence, it suppresses the electrical collection problem of the cell.

The spectral response (SR) gives the ratio of current to incident power and is directly calculated from the EQE:

$$SR(\lambda) = EQE(\lambda)\frac{q}{E(\lambda)} = EQE(\lambda)\frac{\lambda[nm]}{1240} \tag{2.1}$$

where $\lambda[nm] = \dfrac{1240}{E(\lambda)[eV]}$ and E(λ) is the photon energy.

The short circuit current (I_{sc}) can be calculated from the convolution of the solar spectrum Spec (λ) with the spectral response in short circuit condition as shown in Equation 2.1. This method to calculate I_{sc} avoids the uncertainties on the solar cells surface area.

$$I_{sc} = J_{sc} = \int_{\lambda_{\min}}^{\lambda_{\max}} Spec(\lambda) SR_{CELL}(\lambda) d\lambda \tag{2.2}$$

For tandem or multi-junction solar cells, the measurement is slightly more complicated. Indeed, the two cells in the tandem are connected in series. Hence, the current from the tandem cell is determined, in a first approximation, by the lowest current of the two sub cells. In the situation for a tandem cell with complementary absorption spectra such as micromorph, at short wavelengths only the top cell is absorbing and generates a current whereas the bottom cell is blocking the charge transport (reverse blocking diode). As a result, the tandem will not generate any current. The same holds at long wavelengths, where the top cell is transparent and only the bottom cell is absorbing. Therefore, the spectral response measurement of the tandem cell shows only a response in the region where both cells generate a current, i.e. in the region where the absorption spectra overlap as shown by the black line of Figure 2-5. In order to overcome this problem, one of the two cells must be selectively illuminated, with an intensity high enough to prevent current limitation by this cell (also called bias light illumination). Then the spectral response of the other cell can be measured. Similarly the spectral response of the first cell can be measured by selectively illuminating the second cell. In our setup the selective illumination is applied by halogen lamps in combination with color filters, or by LED's of the desired wavelength.

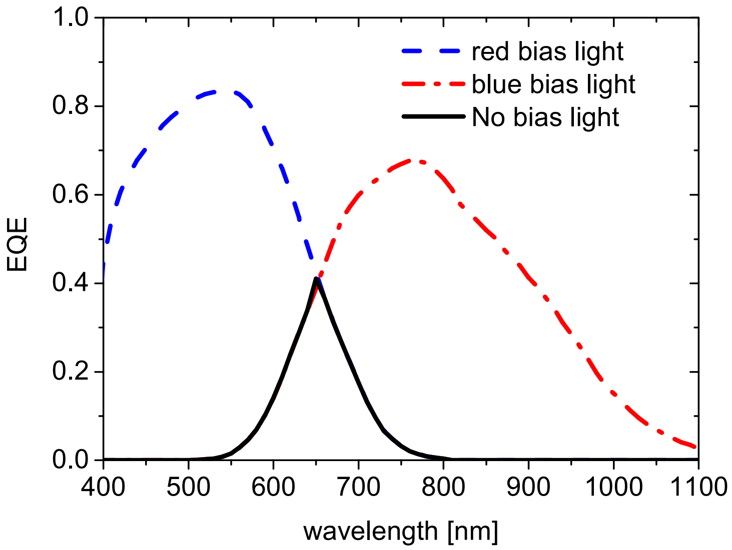

Figure 2-5: EQE of micromorph tandem cells measured with blue bias light (red line), red bias light (blue line) and no bias light (black line).

2.4.2 Current voltage measurements (I(V) or J(V))

The goal is to measure the output power produced by the solar cell at standard test conditions (STC). The cell is illuminated while varying a load resistance contacted to the cell. The STC are AM 1.5g solar spectrum (normalized at 100 mW/cm^2), which approximates noon time solar irradiation in Central Europe and 25°C. The solar spectrum is reproduced with a dual lamp (xenon and halogen lamps) simulator (class A, WACOM). The halogen lamp provides the red part of the spectrum (600 nm -1500nm) and the xenon lamp the blue part (350 nm - 600 nm). By optimizing the intensities between the two lamps, it is almost possible to reproduce the intensity of the AM 1.5g and its spectrum as shown in Figure 2-6.

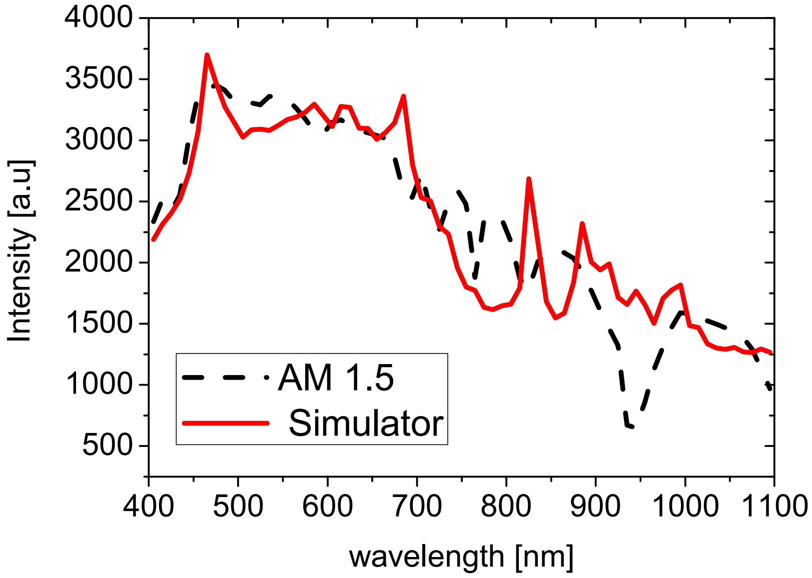

Figure 2-6: Comparison between the solar irradiation AM 1.5g (dashed line) and the solar spectrum of our simulator in Neuchâtel (solid line).

The current voltage curve (I(V)) describes the current for different voltages of the cells under the standard illumination. From the IV measurements in Figure 2-7, the maximum output power from the solar cell is given at V_m and I_m. On this curve, we define the following quantities: short circuit current (I_{sc}), open circuit voltage (V_{oc}) and the fill factor (FF). The FF is ratio between $V_m*I_m/V_{oc}*I_{sc}$. Hence, the efficiency of the cells measured at STC can be expressed as:

$$\eta = \frac{I_m \times V_m}{\text{incident power}} = \frac{I_{sc} \times V_{oc} \times FF}{\text{incident power}} = \frac{I_{sc} \times V_{oc} \times FF}{100\text{mW/cm}^2} \qquad (2.3)$$

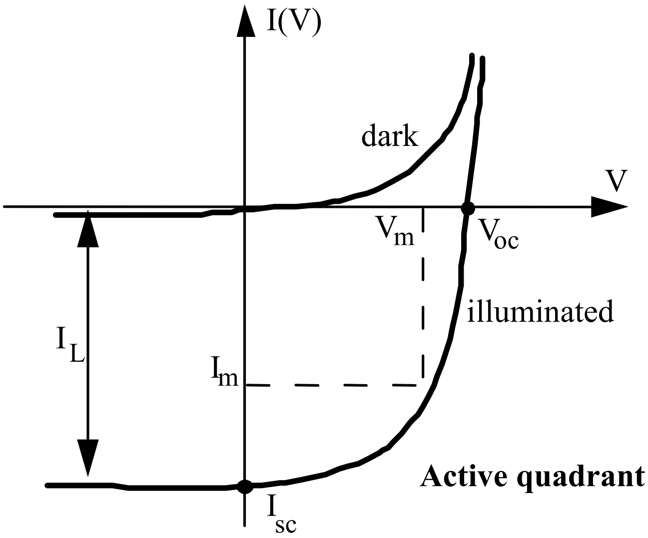

Figure 2-7: I(V) curve of dark and illuminated solar cells.

The I(V) curve can be measured at full illumination, in the dark and at variable intensities (VIM) [42]. Note that for an ideal p-n junction, the curve is the typical diode equation plus the photogenerated current density. In the case of thin film silicon, the superposition principle of the diode equation and a photogenerated current is not valid because the current collection varies with the applied voltage. However, there are different analytical models based on simple assumptions [105] and numerical models [106] which try to describe the behavior of the thin film silicon solar cells. Merten et al. [107] demonstrated the validity of improved analytical equivalent circuit where a recombination current is added in the conventional p-n equivalent circuit as shown in Figure 2-8. R_s is the serie resistance, R_{sh} the shunt resistance, D the ideal diode, I_L the photogenerated current density, I_{rec} the recombination current density. Merten et al. shows that the open circuit resistance $R_{oc} = \left.\frac{\partial V}{\partial I}\right|_{I=0}$ is related to R_s when the cell is working at high illumination (3 sun) and that the short circuit resistance $R_{sc} = \left.\frac{\partial I}{\partial V}\right|_{V=0}$ is related to R_{sh} when the cell is working at low illumination (0.1 sun). Here, the current density I_{rec} is a function of V and I_L and depends on the intrinsic layer quality, whereas the shunt resistance R_{sh} originates from electrical shunts.

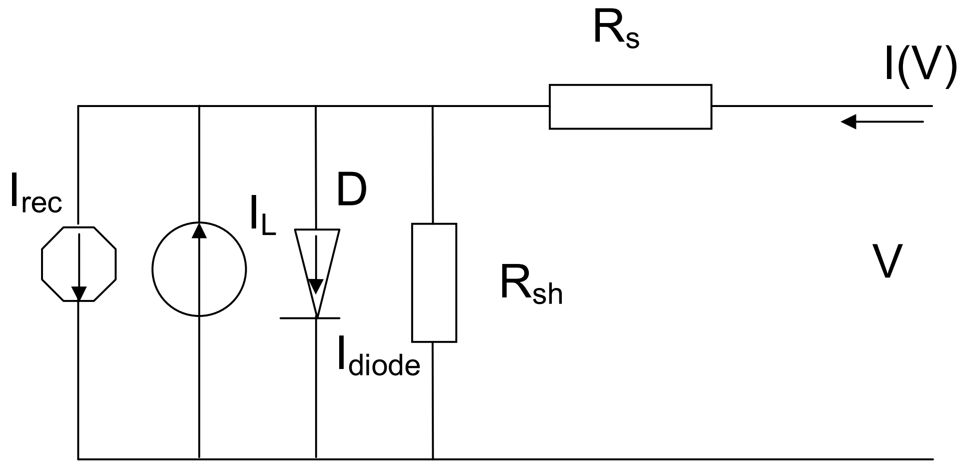

Figure 2-8: Improved equivalent circuit for thin film silicon solar cells [107] with I_L the photogenrated current density, D the ideal diode, Rsh the shunt resistance, Rs the series resistance and, I_{rec} te recombination current density.

2.4.3 Fourier transform spectroscopy

The absorption spectrum of weakly absorbing thin films can be extracted with different techniques such as constant photocurrent method (CPM) [108], photothermal deflection spectroscopy (PDS) [109] or Fourier transform photocurrent spectroscopy (FTPS) [110]. The FTPS method is a fast measurement (a few seconds of data acquisition) that can be used to evaluate the intrinsic material quality on complete µc-Si:H solar cells. The FTPS spectrum is proportional to the absorbance of the sample. The curves are normalized to present the same absorption at 1.4 eV. We assume that the absorption occurs only in the crystalline phase. This suppresses the determination of the sample thickness. The sub band gap absorption coefficient at 0.8eV ($\alpha_{0.8}$) determined by FTPS [42]. The coefficient $\alpha_{0.8}$ is given in absolute units, even though the absolute values should be considered with care, as absorption in the TCO and the light multiplication path are respectively higher and lower at 0.8 eV than at the FTPS curve calibration point. Providing that they change the same way for all samples of a given set, a comparison between samples like the one of Chapter 3 is still valid, though. Figure 2-9 shows two absorption spectra of different µc-Si:H solar cells. The solid (red) curve has $\alpha_{0.8}$ higher than the black curve. This indicates that the absorption from the defects in the gap is lower for the dashed (black) curve, which increases the quality of the material. Further details about the applications of FTPS are described in the thesis of M. Python [35], F. Meillaud [42] and J. Bailat [45] .

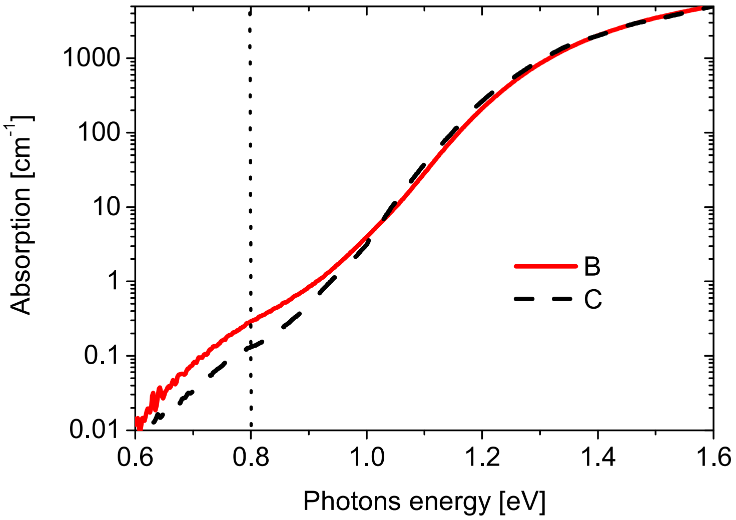

Figure 2-9: Comparison of absorption curves of two μc-Si:H solar cells obtained from FTPS measurements. The absorption at 0.8 eV is lower for the dashed (black) curve indicating lower defect absorption of the material.

2.4.4 Raman crystallinity

Raman spectroscopy measurements [111] are performed in the back scattering configuration with a green Argon laser (514 nm), which has a penetration depth of approximately 150 nm in μc-Si:H material. The Raman spectra is fitted with three Gaussian peak: 480 cm^{-1} for a-Si:H, 510 cm^{-1} for nano-crystal, and 520 cm^{-1} for c-Si. The Raman crystalline volume fraction C_R is obtained by deconvolution of Raman spectra and evaluation of the scattered intensities assigned to amorphous and crystalline parts using:

$$R_c = \frac{I_{510} + I_{520}}{I_{480} + I_{510} + I_{520}} \qquad (2.4)$$

In addition to the measurement of the crystallinity at the front of the cell (p-side), the transparent LP-CVD ZnO substrate also permits the measurement through the back contact, which probes the crystallinity in the nucleation region close to the n-side. The measurement with the green laser from the p or n side probes both the intrinsic layer and the doped layer. The n- or p-doped layer are usually 20-30 nm highly crystalline (more than 70%) for high μc-Si:H device performance. Therefore, the measured C_R is the average between the doped layers and the intrinsic layer. It tends to overestimate the true crystallinity of the absorber layer.

2.4.5 Cells measurements

The results of the cells presented in the thesis are based on the deposition of at least 16 cells. The cells are isolated with lift off of the front contact and dry etching of the silicon layer (SF_6). The area of the cells is typically between 0.25-1 cm^2. The V_{oc} and FF are determined from the IV measurement and the J_{sc} of the IV curve is normalized with the J_{scEQE} obtained from the EQE measurement. This avoids the uncertainties on the exact cell area. The best cell of each data set is presented in the thesis. The typical spread over the 16 cells is in relative 2-3%.

2.4.6 Light soaking

The performances of single and multi-junction amorphous thin film silicon solar cells degrade when exposed to light. After a given time, a steady state is reached and the cells are considered stabilized. The standard conditions of degradation are 1000h at one sun (100mW/cm^2). Nonetheless, most of the degradation measurements in this thesis are made during 1000h at 50 mW/cm^2 because the setup was not fully operational. The results are shown with 50 mW/cm^2 except when something else is specified. The impact of the light intensity on the solar cells performances is reported by Bennett [112] and by Stutzmann and Street [113].

2.4.7 AFM, SEM, TEM, FIB

The surfaces of the thin layer are characterized by a Burleigh, Vista-100 atomic force microscope (AFM). The AFM probes the surface of the layer and gives the surface height for each point. From the AFM data points, we can extract different parameters: the most frequently used here is the root mean square roughness (rms). The rms is the standard deviation of the data points.

The surfaces and cross-sections of the layers are also analyzed by scanning electron microscope (SEM), and transmission electron microscope (TEM). The preparation for TEM is done by focus ion beam (FIB) or tripod technique described elsewhere [114] . All these techniques are describe in detail in the thesis of M. Python [35].

2.4.8 Spectrometer

The spectrometer is used for transmission (T), reflection, diffuse transmission (DT), or diffuse reflection (DR) measurements for the wavelength range 200 nm to 2000 nm. The photo-spectrometer used is a Perkin Elmer lambda 900 with integrating sphere. The T and R of layers deposited on glass substrate are measured with light impinging from the layer side. From this, the absorption (A) is calculated from $A = 1\text{-}T\text{-}R$. The Haze (H) is defined as (DR/T) and represents the ratio of transmitted diffuse light and transmitted specular light. With our setup, the light scattered with an angle over 5° is considered as diffuse light.

The absorption of light in a layer is linked to the absorption coefficient α and the intensity (I) of incident light. The Beer–Lambert laws state that there is a logarithmic dependence between the T, α and the path length l:

$$T = \frac{I}{I_0} = e^{\alpha \cdot l} \text{ where l is the path length} \qquad (2.5)$$

The penetration depth is therefore the inverse of the path length.

The reflection of light on surface is described by the Fresnel coefficient. The reflection depends on the surface angles and refractive index. This is an important fact because our solar cells have rough interfaces and layers with different refractive indices. The Fresnel coefficients predict that a larger difference in refractive index between two layers and a higher angle of incidence result in more reflection. When light is interacting with rough surfaces with a feature size close the light wavelength, then scattering occurs. In this case, the reflection can be predicted by using semi-empirical theories such as the scalar scattering theory proposed by Beckman and Spizzichno [115] and more details can be found in the thesis of V. Terrazzoni [65]. In this case the haze (H) can be calculated as:

$$H(\lambda) = 1 - \exp\left[-\left(4\pi \cdot \frac{\sigma_{rms}}{\lambda} \cdot C \cdot |n_1 - n_2| \right)^{\beta} \right] \qquad (2.6)$$

where λ is the light wavelength, σ_{rms} is the rms of the surface, n_1 and n_2 are the refractive indices of the incident and transmission media, respectively, and C, β are fitting parameters. Experimentally, β is close to 3 as shown by D. Dominé [116].

2.4.9 SIMS

Secondary ion mass spectrometry (SIMS) is a technique that detects the atomic concentration in a layer. For SIMS, the layer is sputtered by a focus primary ion beam. Part of the sputtered atoms are removed and ionized from the sputtered surface. Then, the ions are analyzed with their charge to mass ratio. This process can be continuously monitored and a complete concentration profile can be measured. This technique is used in thin film silicon solar cells to evaluate the contamination of the μc-Si:H and a-Si:H absorber layers [117].

2.4.10 Ellipsometry

The main interest of ellipsometry is to determine the optical properties of layers. These properties are the refractive index n(λ) and extinction coefficient k(λ). These values depend on the wavelength λ as shown in Figure 2-10 for a-Si:H layer deposited in our PECVD system.

The technique is based on the reflection of polarized light on the layer. After reflection, the phase shift and the change in amplitude are measured. The measured samples are often multilayer stacks where thicknesses are unknown. Therefore, the technique needs to fit the data to a model in order to extract the n and k value. This technique is applied with success with μc-Si:H growth in-situ [44] or on complete layers [118].

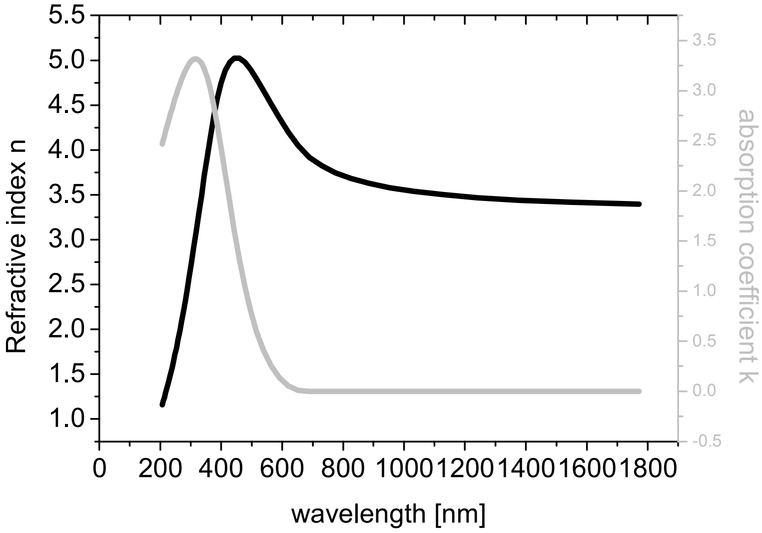

Figure 2-10: Refractive index n (black) and absorption coefficient k (grey) of amorphous silicon deposited at 190°C and with dilution 3. The n and k values are determined by ellipsometry measurement with a Tauc-Lorentz model.

Chapter 3: Microcrystalline Si

Material growth and solar cells

3.1 Introduction

Our final goal is to increase the stabilized efficiency of tandem micromorph solar cells. For this purpose, we optimize single junction microcrystalline (μc-Si:H) n-i-p solar cells on textured plastic substrates with light trapping capabilities. Texturing of the (plastic) surface is the conventional way to achieve high J_{sc} and still keep thin absorber layers, which is compulsory from a production point of view (high efficiency and high throughput).

The complex relationship between the substrate surface morphology and the performance parameters of μc-Si:H solar cells was first addressed by Nasuno et al. [71]. Furthermore, Bailat et al. [119] showed that, in the p-i-n configuration, the substrate morphology significantly influences the quality of the μc-Si:H solar cells. A next step toward a better understanding is provided by Python et al. [73] who shows that the cracks in the μc-Si:H are responsible for the poor solar cell performance on textured substrates. All these reports studied superstrate configuration whereas here we discuss the challenges for the substrate (n-i-p) configuration.

In the first part of this chapter, we use the textured substrates described in Chapter 2 consisting of surface plasma treated LP-CVD ZnO. The surface treatment transforms the sharp valley (V-shape) of the initial ZnO growth into smoother valleys (U-shape). Similarly to the case of the p-i-n structure, by increasing the substrate plasma treatment time (smoothening of the substrate surface), we find significant improvements of open circuit voltage (V_{oc}) and fill factor (FF) in n-i-p μc-Si:H solar cells. However, the morphologies used for high V_{oc} and FF lead to reduced light trapping and thus reduced short circuit current density (J_{sc}). This motivates the need for better μc-Si:H solar cells on V-shape morphology. In other words, the challenge is to increase V_{oc} and FF while keeping the excellent light trapping capabilities of the substrate.

In the second part of this chapter, we find that a buffer layer (BL) at the N/I interface enhances the performance of the n-i-p μc-Si:H cells on rough “unfavorable” substrates. Finally, we compare our results obtained on LP-CVD ZnO substrate with our in-house hot silver substrate. This type of substrate is commonly used in the n-i-p structure, but its direct application is restricted to stainless steel foils and high temperature resistant plastic substrates such as polyimide. Plastic substrates with low temperature resistance and low glass transition temperatures suggest a different approach, e.g. embossing of the light trapping structures like the LP-CVD ZnO morphology directly into the plastic substrate.

In the third part of this chapter, we explore the deposition of thick μc-Si:H (above 2 μm) on textured substrates. A priori, it should be a triviality to increase the thickness of the cell, to absorb more light and thus to increase J_{sc}. Nevertheless, the thickness of the layer tends to reduce the V_{oc} and the FF of the cell, and the J_{sc} (25 mA/cm^2) saturates after 2.5 μm. In addition, these thickening effects are worse for cells deposited on severerly textured substrates.

In c-Si silicon, the grain size is one of the limiting factors of solar cells efficiencies [120] because the grain boundaries are defectives and act as recombination centers. μc-Si:H has small grain size (10-50 nm) as its name indicates. The recombination at these grain boundaries is mitigated by the amorphous matrix, which surrounds the grains and passivates the defects at the surface of the nanocrystal. Nonetheless, the amorphous material or the interface material suffers from the light-induced degradation and therefore we also investigate the possible light-induced degradation in our μc-Si:H material in the device.

3.2 Results

3.2.1 Substrate morphologies

3.2.1.1 Efficiency of μc-Si:H solar cells

We investigate the relationship between substrate morphology and the performance of the n-i-p μc-Si:H solar cell deposited on rough LP-CVD ZnO substrates. This TCO allows for easy control of the feature size, and the surface morphologies can be varied from V-shape to U-shape with a surface plasma treatment such as described in Chapter 2. As shown in Table 3-1, the trend observed for μc-Si cells in the n-i-p configuration corresponds to the one reported in the p-i-n configuration [119], i.e. a substantial improvement in V_{oc} and FF on treated substrates, improving efficiencies from 4.1% to 7.5% as the treatment time is varied from 0 to 40 minutes (40’). Note in Table 3-1 that the μc-Si:H solar cells on the substrate treated for 60 minutes (60’) have peeled off because the substrate is strongly flattened by the long plasma treatment time and only a few cells survived. Hence, this creates a lack of statistics, which might explain why the FF is lower for 60’ than for 40’.

Table 3-1: μc-Si:H solar cell parameters for 0’, 20’, 40’ and 60’ surface treated ZnO LP-CVD.

Treatment time	0’	20’	40’	60’
J_{sc}[mA/cm2]	20.0	22.0	20.8	20.7
V_{oc} [mV]	454	494	514	503
FF [%]	45.5	60.6	70.0	67.7
Efficiency [%]	4.1	6.6	7.5	7.1

3.2.1.2 Cracks in μc-Si:H solar cells

Cross-sectional samples of the μc-Si:H solar cells on various ZnO morphologies are prepared for SEM and TEM experiments. On untreated substrates, TEM and SEM micrographs reveal a large quantity of cracks in the μc-Si:H layer as shown in Figure 3-1 (left) and Figure 3-3. The areas with nano-cracks are indicated by arrows. The micrographs reveal that the cracks disappear with the plasma treatment and correlate well with the increase of solar cell efficiency. This confirms the link between cracks, voids or porous areas and poor cell performance proposed by M. Python et al. [73] for p-i-n devices. The crack formation originates from the valley of the pyramids and pinches. Porous areas appear also at the substrate n doped layer interface as shown in Figure 3-2.

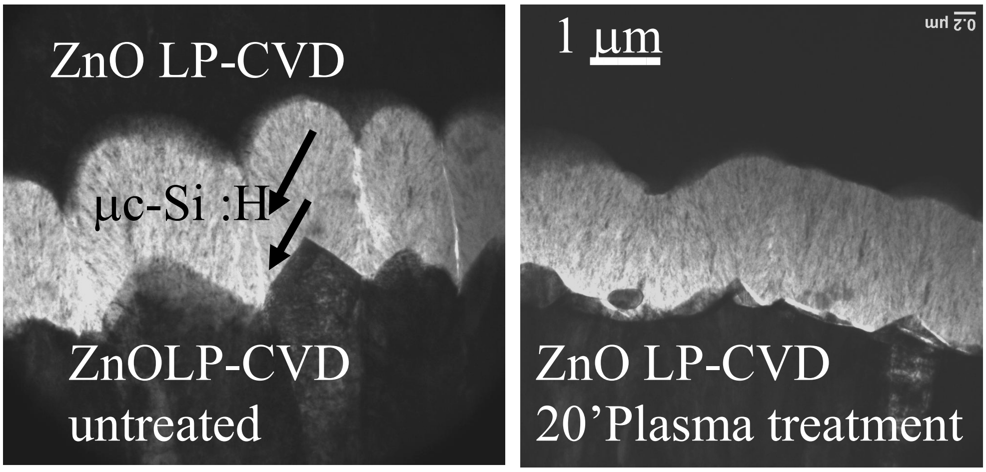

Figure 3-1: TEM cross-section of a n-i-p μc-Si solar cell deposited on an untreated ZnO LP-CVD (left) and 20' surface plasma treatment (right). The cracks and porous areas of the Si are pointed by the black arrows.

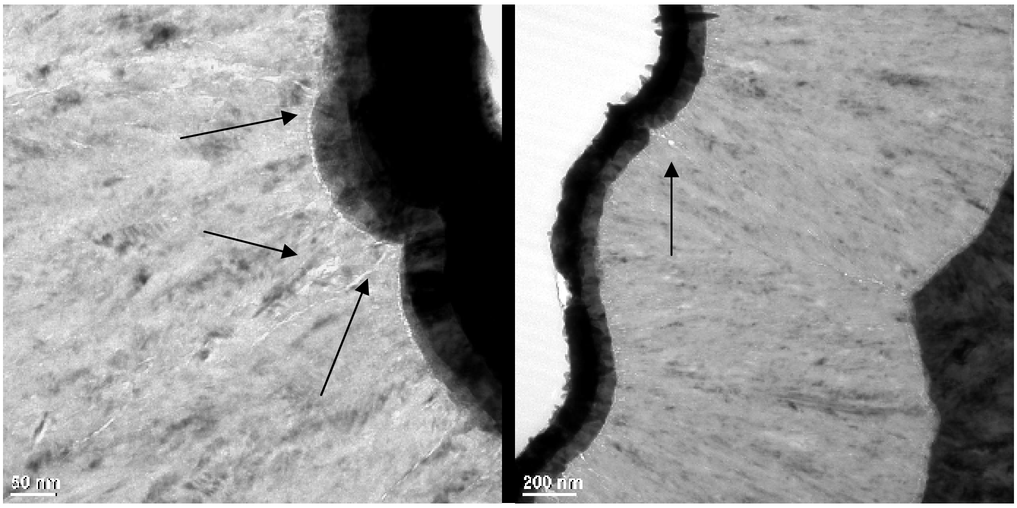

Figure 3-2: TEM cross-section of μc-Si:H solar cell deposited on a texture replicated on plastic substrate.

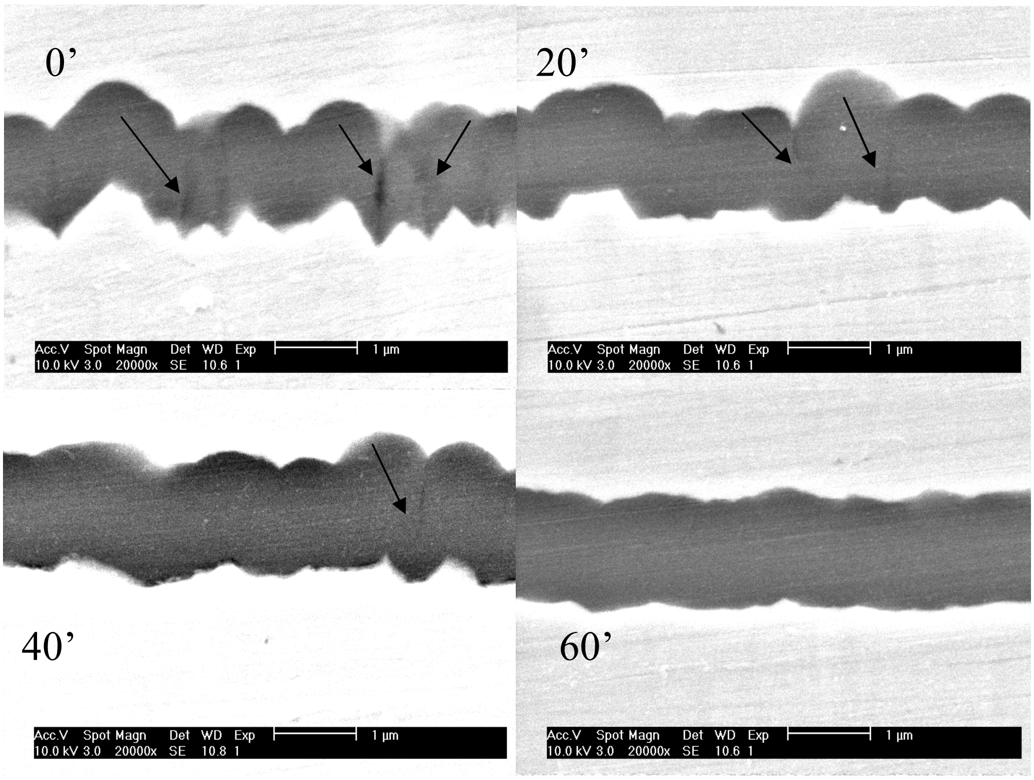

Figure 3-3: SEM micrographs of cross-sectional μc-si:H solar cells. The cells are deposited on LP-CVD ZnO with various treatment times 0’, 20’, 40’ and 60’.

3.2.1.3 Raman crystallinity of the μc-Si:H solar cells

It is established that the Raman crystallinity (C_R) of a μc-Si:H layer can be controlled during the deposition process by the dilution ratio [121] or purely by the depletion ratio of silane during the plasma process [122]. In order to better understand the μc-Si:H growth on different substrate morphologies, we measured C_R profiles throughout the absorber layer on two types of substrate by alternating etching 150 nm of the layer with dry plasma etching (SF_6), and measuring the C_R. These results, shown in Figure 3-4, demonstrate a homogenous material with constant C_R in the bulk region. Towards the interfaces we find slightly higher C_R, which corresponds to the n- and p-doped layers. This is consistent with the aim of having high C_R in the doped layer because doping efficiency is elevated in μc-Si:H compared to amorphous material [123]. The results, described in Figure 3-4, have two particularities: first, the C_R is constant throughout the absorber layer without applying any dilution gradient, and second, for unchanged deposition parameters, C_R is different for the samples prepared on different substrate morphologies. Indeed, it is often reported that dilution profiling [124-126] is required to control the C_R of the μc-Si:H material. The typical gradients are an increased dilution at the beginning of the growth after the first doped layer in order to avoid an amorphous incubation layer, and reduced dilution at the end of the growth in order to avoid excessively high C_R in the material. Here, the films shown in Figure 3-4 are prepared without dilution grading. Nevertheless, their C_R is uniform between the doped layers.

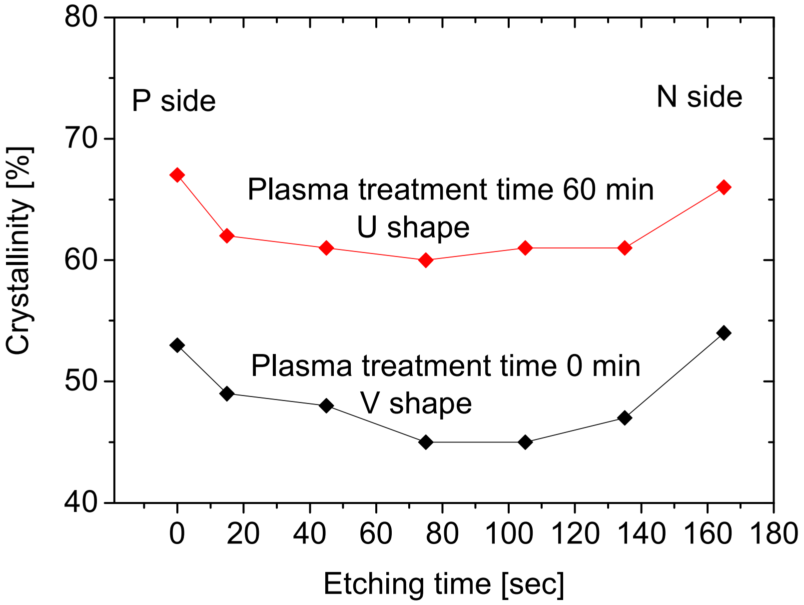

Figure 3-4: Raman Crystallinity fraction of the untreated (V-shape) and strongly treated (U-shape) substrate throughout the entire μc-Si:H solar cell.

3.2.1.4 Light trapping in μc-Si:H solar cells

The J_{sc} decreases with the surface plasma treatment time as shown in Table 3-1. However, the cell deposited on the untreated ZnO has a lower J_{sc} than the cells on the treated ZnO. The reason is that the μc-Si:H absorber material is so defective on the untreated substrate that the defects screen the electric field of the doped layer. Therefore, the lack of charge carrier collection reduces the J_{sc} on untreated substrates. The TEM and SEM micrographs confirm the creation of defective material on untreated substrate. Nevertheless, we think that the as-grown ZnO rough layer is the optimal substrate for light trapping in the μc-Si:H solar cell. This could be inferred from reflection measurements in Figure 3-5. Indeed, the reflection increases with the plasma treatment time; it shows that the optimum substrate, from the light trapping point of view, is the LP-CVD ZnO substrate with no or minimum treatment time.

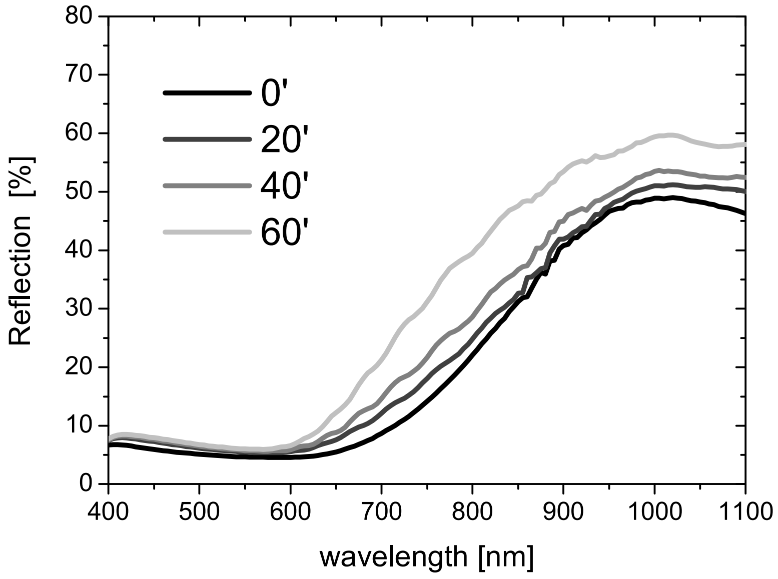

Figure 3-5: Optical reflection as a function of wavelength for μc-Si:H solar cells deposited on LP-CVD ZnO with 0’, 20’, 40’, and 60’ plasma treatment times.

In the following section and until the end of section 3.2.3, we focus on two types of plasma treatment; a mild 20 minute treatment (20’), which preserves the V-shape, and a 40 minute treatment (40’), resulting in a U-shape. The μc-Si:H solar cells show an increase of 20 mV in the V_{oc} and a strong increase of FF from 60.6% to 70.0% for the 40’ case compared to the 20’ case. The diminished J_{sc} clearly shows the reduced light trapping capabilities of the substrate. Between 20’ and 40’ plasma treatment, J_{sc} typically decreases by 1 to 1.5 mA/cm^2. The EQE curves in Figure 3-6 show that the changes occur predominantly in the red part of the spectrum. This has significant consequences for its application in micromorph solar cells because of a high current density in this portion of the spectrum [113, 114].

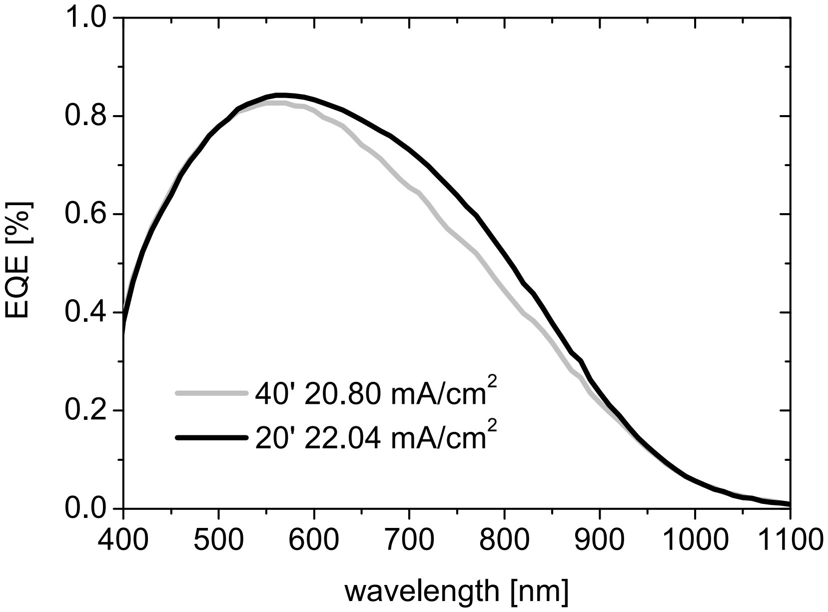

Figure 3-6: EQE as a function of wavelength for μc-Si:H on LP-CVD ZnO substrate with 20’ and 40’ surface plasma treatment times.

3.2.1.5 SIMS measurements

The oxygen content is a key parameter in the μc-Si:H. It is reported by many authors [115-117] that the oxygen concentration is linked to the outgassing of the chamber walls, the purity of the silane, and the growth condition of the layer. In fact, the oxygen acts as an n-dopant [127] in the layers and thus strongly reduces the device performances [128]. Figure 3-7 shows the oxygen profile of a μc-Si:H deposited simultaneously on the LP-CVD ZnO treated for 20’ and 40’. It reveals that the oxygen content is also linked to the substrate morphology. We think that the cracks are paths for post oxidation of the layer for three reasons. First, the presence of cracks correlates with the oxygen content in the layer. Second, we expect constant oxygen through the layer whereas a gradient appears in Figure 3-7 and the gradient is more pronounced for the 20’ substrate than the 40’substrate case. Third, the concentration of oxygen is higher than what is usually reported for device grade material (10^{18}-10^{19} atom/cm^3) and reasonable efficiencies are still made in our system. Therefore, the oxygen should come from post oxidation.

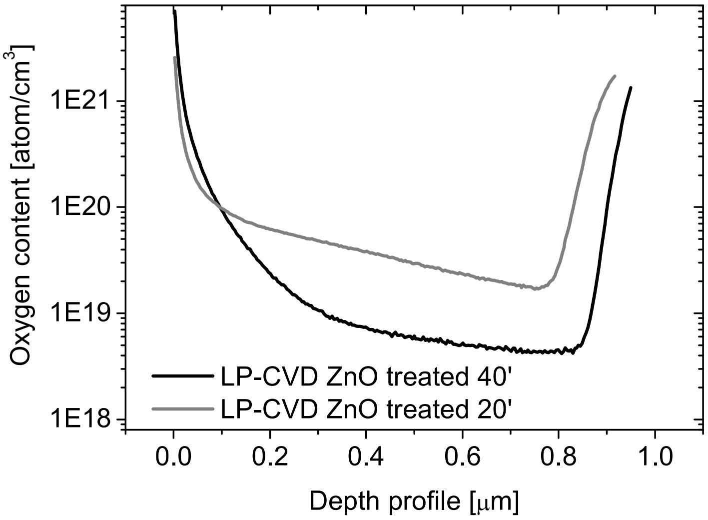

Figure 3-7: SIMS measurement of μc-Si:H solar cells deposited on LP-CVD ZnO substrates treated for 20’ (grey) and 40’ (black).

3.2.1.6 Summary

Our μc-Si:H layers have the following characteristics:

- The crystallinity is constant during the μc-Si:H growth of the absorber layer with constant dilution.
- The crystallinity of μc-Si:H decreases when deposited on V-shape substrate morphologies.
- The V-shape morphologies induce nano-cracks in the μc-Si:H material.
- The cracks deteriorate the μc-Si:H solar cell performances.
- The best efficiency of the μc-Si:H solar cells is obtained on the smooth substratesmorphologies (U-shape with surface plasma treatment).
- The best light trapping scheme is found on the untreated substrates or V-shape morphology.
- The oxygen content in the μc-Si:H layer increases with V-shape morphologies.

Therefore, so far, the best substrate for the solar cells performances is the substrate that has the less favourable light in-coupling in our device. The loss is about 1-1.5 mA/cm^2 which is 5% in relative compared to substrate with V-shape morphology.

3.2.2 Buffer Layer (BL) after the n-layer in µc-Si:H solar cells

3.2.2.1 Raman crystallinty (C_R) and TEM micrographs

In section 3.2.1, we find that the surface plasma treatment applied on the LP-CVD ZnO substrates provides an increase in V_{oc} and FF but a decrease of J_{sc}. Here, we discuss the introduction of a silicon buffer layer (BL) deposited on LP-CVD ZnO substrates treated for 20’ and 40’. The BL dilution is varied from 14.5 to 25 while keeping the same bulk dilution of 17.6 for every cell. The thickness of the BL is chosen arbitrarily to be 200 nm, which is one sixth of the entire i-layer. The influence of the BL is shown in Figure 3-8 where the C_R is measured with laser beam impinging once from the n-side and from the p-side on cells with the different BL dilutions. The C_R is constant in the p-side for every buffer layer dilution. But, the BL strongly influences the C_R close to the n-layer. It varies from 85% to 32% with the decreasing dilution of the BL. This is confirmed in Figure 3-9 which shows a TEM micrograph of a µc-Si:H solar cell with a BL having a low dilution of 14.5. The different contrast clearly reveals that the structure has high C_R at the n-layer, followed by the large amorphous fraction of the 200 nm BL, and then the bulk absorber that has again a higher C_R than the BL.

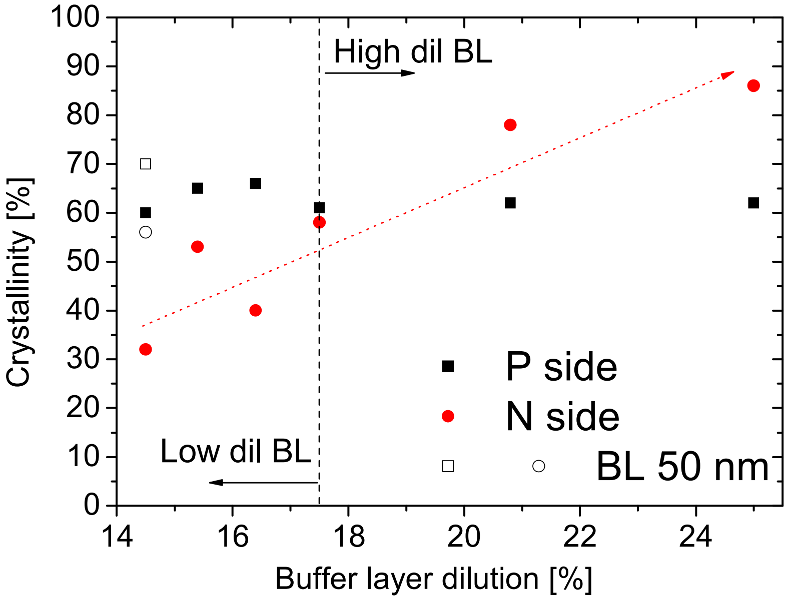

Figure 3-8: Raman crystallinity measurement from the n- and p-side of the µc-Si:H as a function of the BL dilution after the microcrystalline n-layer. The solar cell is deposited on LP-CVD ZnO with 20’ surface treatment time.

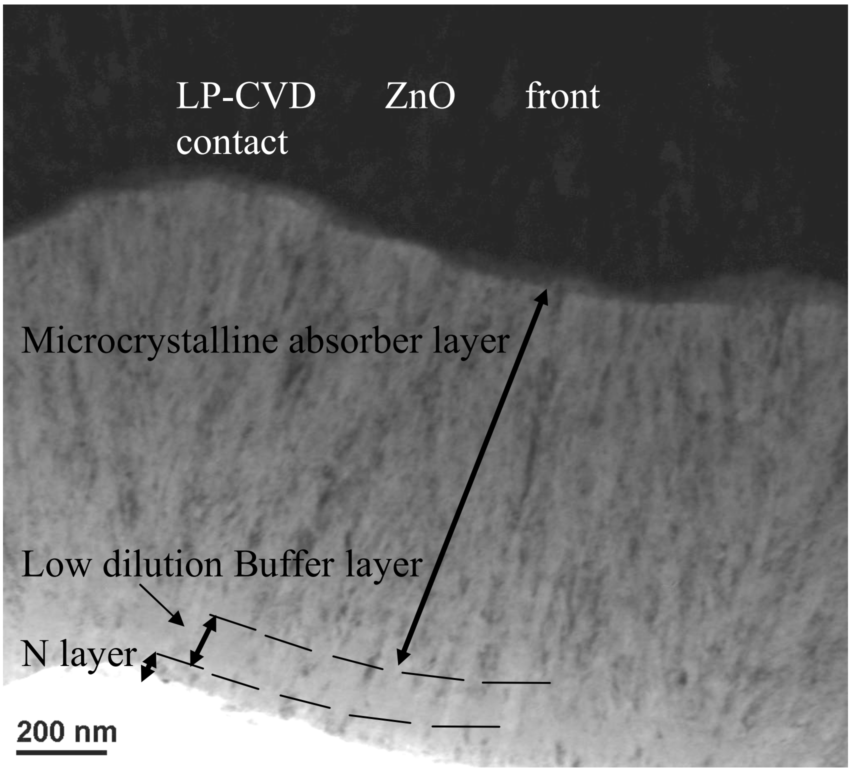

Figure 3-9: TEM cross-sectional micrograph of μc-Si solar cell. Amorphous BL: 200 nm thick, dilution: 14.5%, deposited on LP-CVD ZnO, plasma treatment time: 40’.

3.2.2.2 Solar cell efficiencies

Figure 3-10 shows that the efficiency of the solar cells is increasing while the BL dilution is decreasing from 25 down to 16.4 (the results for the dilution 14.5 and the hot silver substrate will be discussed later). The changes are moderate on the 40’ substrates, but the situation is dramatic for the 20’ substrates, which have a more pronounced V-shape morphology. In fact, the efficiency of the μc-Si:H cells on the substrate treated for 20’ increases by an absolute 2.1%, from 4.6% up to 6.7%, whereas the cells on the substrate treated 40’ increases only by 0.5%, from 7% to 7.5% as shown in Figure 3-10. The different behaviors of the μc-Si:H solar cells exemplifies the relation between the substrate texture and the efficiency. It shows that even though the μc-Si:H cell deposited on 20’ substrate is less efficient, it has a stronger potential because more light is absorbed in the 20’ substrate compared to the 40’ substrate. Hence, the BL is a first step to reduce the deleterious effect of severe V-shape substrates, while maintaining strong light trapping capabilities of the substrate.

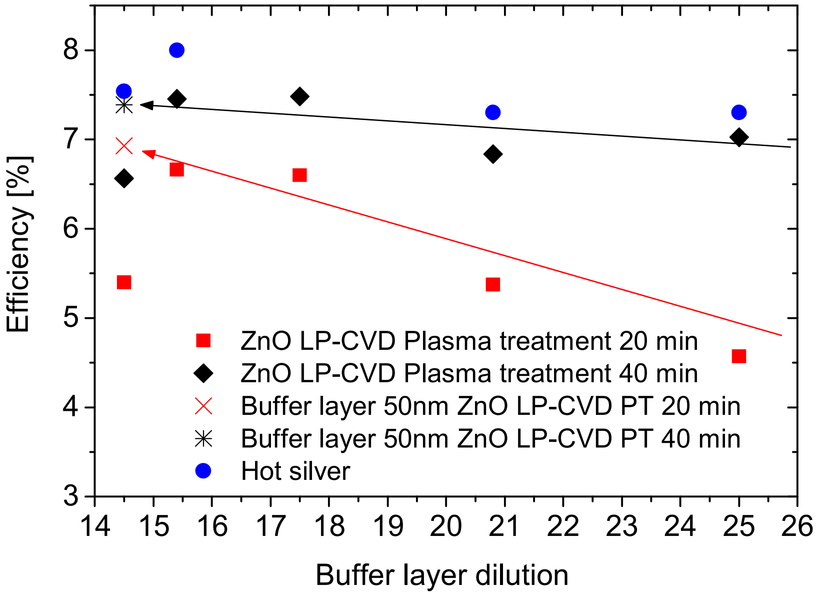

Figure 3-10: Efficiency of a µc-Si:H solar cell on LP-CVD ZnO with 20' and 40' minutes of surface plasma treatment and hot silver substrates as a function of the BL dilution after the microcrystalline n-layer.

3.2.3 Material quality of the µc-Si:H i-layer

3.2.3.1 Solar cell properties and buffer layer

The introduction of this amorphous BL is beneficial for the efficiency of the µc-Si:H solar cells. Figure 3-11 shows, for the case of the 20' treated substrate, that the strongly diluted BL leads to a deteriorated solar cell with low V_{oc} and FF, and that the improvement with the amorphous BL is mostly in FF and V_{oc}. We observe, however, that the amorphous content in the buffer must not exceed a certain limit; reducing the dilution below 15 results in a sharp decrease of FF and J_{sc}.

Therefore, exactly in the dilution range where it is most useful, the BL also entails severe losses in the J_{sc} as shown in Figure 3-11. The reason for the losses in the J_{sc} will be discussed in Section 3.2.3.5. Here, we present a layer with a reduced thickness and low dilution of 14.5. It keeps the V_{oc} and FF properties, while at the same time the losses in the J_{sc} are almost completely suppressed. The open symbols of Figure 3-11 and cross symbols in Figure 3-10 represent solar cells where the dilution of the extra layer is 14.5 but the thickness has been reduced to 50 nm. These thin layers can be more correctly called buffer layers resulting in µc-Si:H solar cells that combine elevated J_{sc}, FF, and V_{oc} on the V-shape substrates.

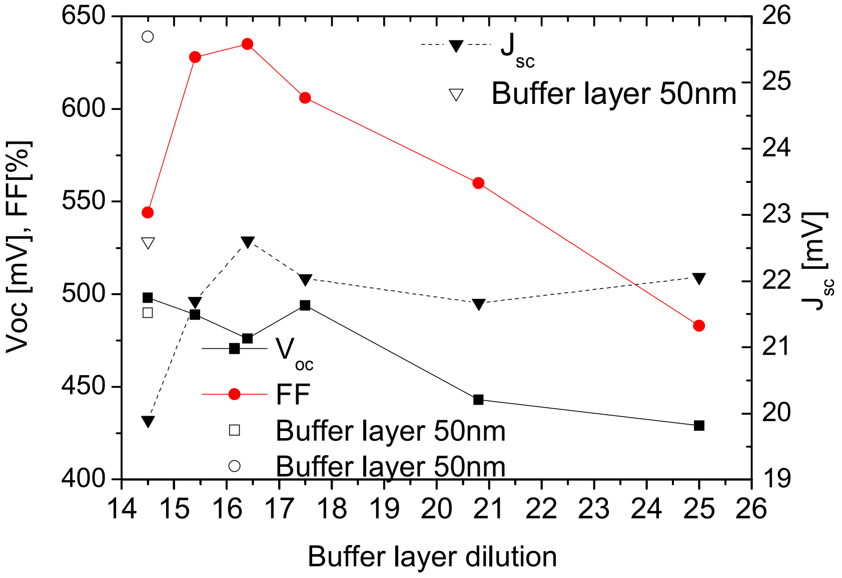

Figure 3-11: V_{oc}, FF, J_{sc} of the µc-Si:H solar cell as a function of the BL dilution ratio on the LP-CVD ZnO substrate with 20' surface plasma treatment. Empty symbols refer to thinner BL (50 nm).

3.2.3.2 Sub band gap absorption of µc-Si:H solar cells (FTPS spectrum)

We have seen that TEM experiments give some idea of the quality of the µc-Si:H material (cracks and porous areas). In this section, we use FTPS to characterize our solar cells. In fact, it has been shown that the absorption coefficient at a photon energy of 0.8 eV ($\alpha_{0.8}$) [110] is proportional to the defect density of the µc-Si:H material. The FTPS measurements in Figure 3-12 show, for the 20' case, the relationship between the absorption at 0.8 eV and the FF of the solar cells. Figure 3-12 shows that the defect density is inversely correlated with the FF of the solar cell. For BL dilutions above the nominal 17.6 dilution, the material is highly crystalline on the n-side (more than 70%), which enhances the defect density in the material due to diminished passivation of the nanocrystal by the amorphous phase in the material [110]. For the dilution below the nominal 17.6, the n-side C_R is decreased down to 32% with the BL dilution 14.5. Note that the value of C_R is an average of the 30 nm highly microcrystalline n-layer and 120 nm of the BL because the Raman measurement has a penetration depth of 150 nm. In other words, the true C_R of the BL is even lower than 30% and thus much lower than the 40% that as suggested for a device quality material by F. Meillaud [42]. We also observe, in Figure 3-12, an increase in $\alpha_{0.8}$ for dilution below 17.6%. In contrast to the low FF and higher FTPS signal for this particular strongly amorphous BL, the V_{oc} is stable or even slightly better with 500 mV compared to higher dilution of the BL as shown in Figure 3-11.

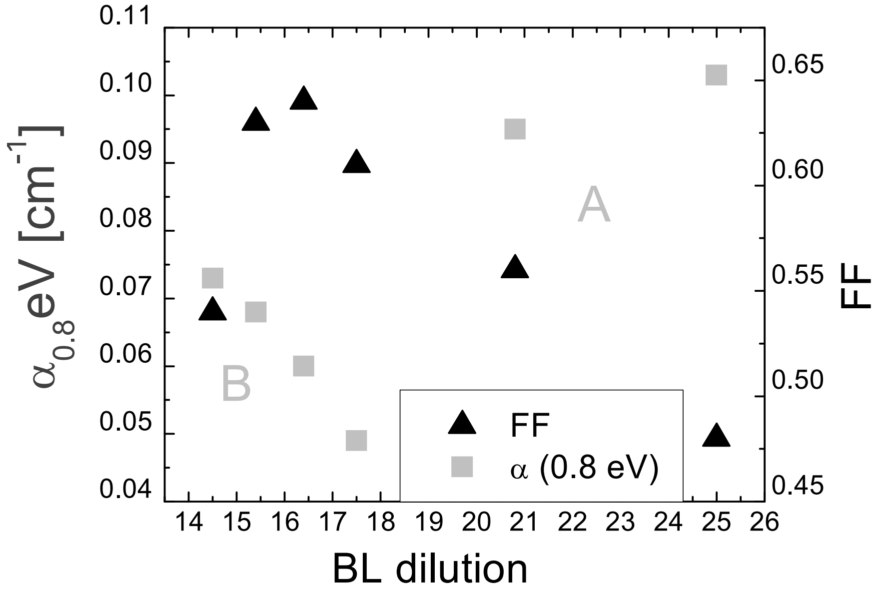

Figure 3-12: Absorption coefficient ($\alpha_{0.8}$ eV) from FTPS measurements and FF of μc-Si:H solar cells as a function of the various BL dilution on the LP-CVD ZnO substrate with 20’ surface plasma treatment.

3.2.3.3 Linear crack density

The nature of the defects in the in μc-Si:H silicon material is difficult to distinguish. Lattice damage can occur inside the nanocrystal, the surface of the nanocrystal are areas for additional defects and the defects can be induced by the a-Si:H phase. Fortunately, the hydrogen and the amorphous material passivate most of the defects at the surface of the nanocrystals and permit device grade material for photovoltaic applications [129]. Kuendig et al. [130] and F. Meillaud [42] irradiate μc-Si:H layers and devices with high energy protons to show that this treatment degrade almost only the μc-Si:H material, whereas the a-Si:H layer is resistant. Therefore, F. Meillaud suggests that this irradiation degrades the surface of the nanocrystal. In addition, the irradiation is reversible by thermal annealing and affects the solar cells, performance in the same way as the light soaking. Nevertheless, (nano-)cracks or porous areas as evidenced from TEM experiments are another class of microstructured defects. As shown by M. Python [35], shadowing effects on rough substrates as well as the low diffusion length of the precursors are responsible for crack formation. These cracks are zones of enhanced recombination for the charge carriers.

M. Python et al. [131] reported a method to count the linear crack density by SEM micrographs. Evaluating about 4000 µm of µc-Si:H material permits a statistically relevant comparison of different deposition processes. In Figure 3-13, the linear density of cracks is calculated for µc-Si:H with and without 50 nm BL with the dilution 14.5. The cracks decrease strongly with the plasma treatment on the LP-CVD ZnO and clearly, for a given treatment, the BL mitigates the apparition of cracks in the material and therefore explains at least partly why the BL is beneficial for the solar cell efficiencies.

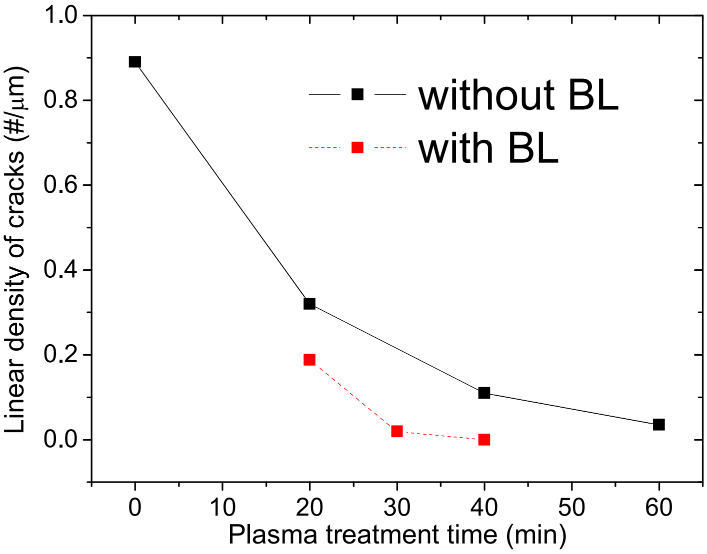

Figure 3-13: Comparison of the linear density of cracks for the µc-Si:H solar cell with BL (round) and without BL (square) as a function of the different plasma treatment times on LP-CVD ZnO substrates.

3.2.3.4 SIMS measurements

The effect of the BL on the oxygen content in the µc-Si:H is shown in Figure 3-14. It shows that the amorphous buffer layer reduces the incorporation of oxygen in the layers. This confirms the idea that the cracks are paths for post contamination of our layers. We have deposited a 50 nm a-Si:H layer on top of the µc-Si:H layer deposited on the 20' substrates. The goal is to protect the µc-Si:H against post contamination. The concentration of oxygen remained higher than that of the 40' substrates and probably suggests that the 50 nm a-Si:H is thin or not dense enough to act as barrier layer. Nevertheless, this result shows that the BL improves the oxygen content on both substrate morphologies. It is assumed that oxygen remains mostly in the crack area.

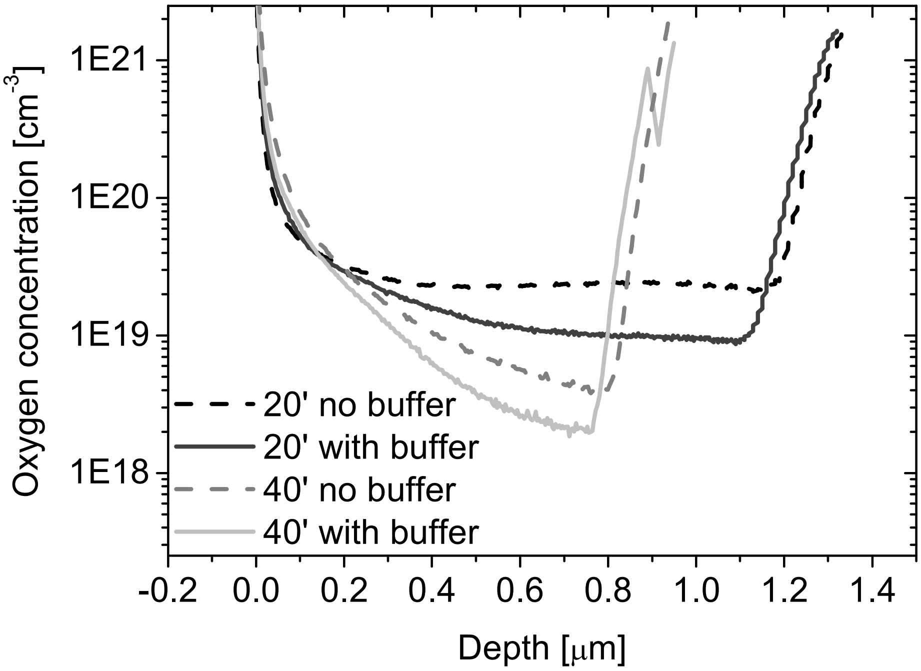

Figure 3-14: SIMS measurement of μc-Si:H layer with (full line) and without buffer layer (dashed line). The layers deposited on the 20’ substrates are thicker and are covered with 50 nm a-Si:H in order to prevent post oxydation.

3.2.3.5 Effect of buffer layer on the photogenerated J_{sc}

Figure 3-11 shows that the FF increases and J_{sc} decreases with increased amorphous content of the BL. The reduction of cracks and oxygen contamination probably improves the FF and the reduction of J_{sc} is mainly due to the apparition of losses in the EQE in the red part of the spectrum, as shown in Figure 3-15. The more amorphous is the BL, the stronger are the losses in the EQE. The difference is partly explained by the lower average crystalline fraction of the cells for the low dilution buffer, which leads to reduced IR absorption, typically by 5-10%. However, it does not explain the “hole-like” features in the 500-700 nm appearing for the more amorphous BL. Figure 3-16 shows the EQE of the same cells but with light illumination from the n-side through the glass/ZnO interface. In this case, the losses appear as absorption in the blue part of the EQE, showing that the absorption is taking place close to the n-layer without extraction of the photogenerated carriers. We think that the amorphous BL region diminishes the diffusion length of the charge carriers and thus increases the recombination in the BL zone, which reduces the J_{sc}. This is confirmed by the fact that when we reduce the buffer layer thicknesses the losses in the EQE is less pronounced as shown by the dashed line in Figure 3-15 and Figure 3-16.

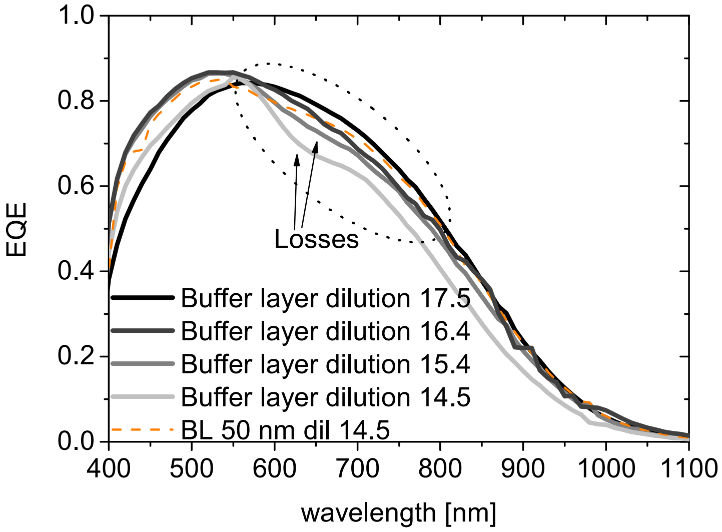

Figure 3-15: EQE of a µc-Si:H solar cell with various BL dilution on the LP-CVD ZnO substrate with 20' treatment time.

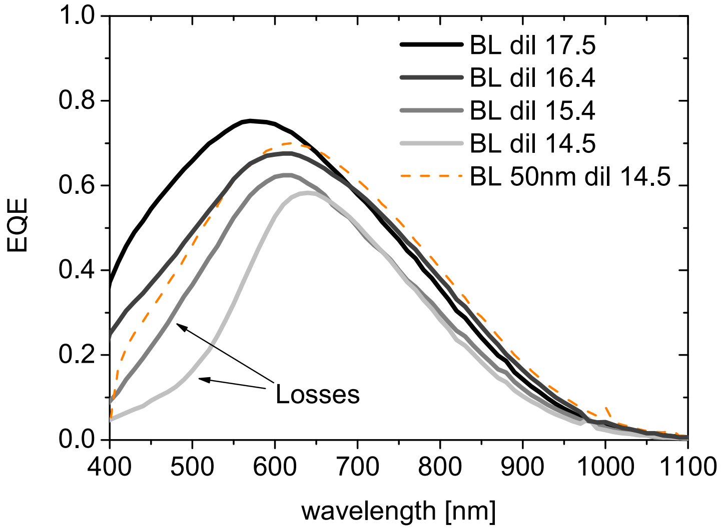

Figure 3-16: EQE of a µc-Si:H solar cell illuminated from the n-side on the LP-CVD ZnO substrate with 20' treatment time.

3.2.3.6 Best μc-Si:H cell on hot silver substrates

We apply the BL strategy to moderately textured “hot silver” substrates. This silver layer is deposited by sputtering at high substrate temperature, which produces a rough texture as described elsewhere [101]. The substrate roughness is adjusted with the temperature and the deposition time. The dimensions of the silver crystals are in the range of 800-1000 nm with a rms roughness of 70 nm. In terms of J_{sc} it corresponds to the LP-CVD ZnO substrate with 30’ treatment time, i.e. the current of hot silver is between the one generated by the TCO treated for 20’ and 40’. In Figure 3-10 the data points for μc-Si:H on hot silver substrates are compared with the LP-CVD ZnO substrates. The trends shown for LP-CVD ZnO are reproduced with the hot silver substrates. In addition, the substrate is well suited for single μc-Si:H solar cell and demonstrates better efficiencies. The best cell of this series has an efficiency of 8 %. We push upwards the efficiency of this μc-Si:H cell by optimizing the doped layers, BL thickness and by annealing the solar cell. By including these developments, an efficiency of 9 % is achieved for an intrinsic layer thickness of only 1.2 μm. The Figure 3-17 shows The IV curve with the following characteristics: V_{oc} = 532 mV, FF = 76 % and J_{sc} = 22.3 mA/cm2. To the knowledge of the authors, this is one of the highest efficiencies reported for such a thin single μc-Si:H solar cell.

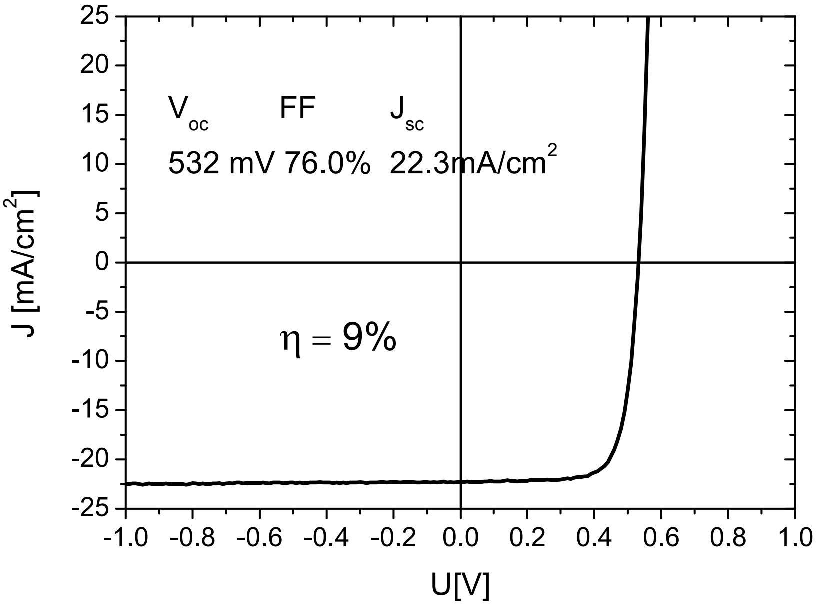

Figure 3-17: JV curve of the best μc-Si:H cell on a hot silver substrate. The cell has a thickness of 1.2 μm.

3.2.3.7 Summary

The BL has the following characteristics:

- It reduces the apparition of cracks.
- It reduces the oxygen content in the µc-Si:H material.
- It increases the efficiency of the µc-Si:H solar cell on textured substrates.
- The record cell has an efficiency of 9 % for a 1.2 µm thick absorber layer deposited on hot silver with BL.

3.2.4 Thick µc-Si:H solar cells

3.2.4.1 µc-Si:H solar cells deposited on the 2D cross grating

The substrate used here is the 2 D cross grating replicated on PEN plastic described in Chapter 2. The efficiency of the best optimized cell after annealing on this substrate is 8.7% for 1.2 µm (512mV, 74%, 23.1 mA/cm^2). The efficiency on the grating is comparable to the efficiency obtained on hot silver substrates for a 1.2 µm thick absorber layer described in the previous section. Nonetheless, the cell is different. Indeed, this substrate is suited for light trapping and higher J_{sc} (+1 mA/cm^2) is obtained compared to hot silver, whereas V_{oc} and FF are lower because the substrate is less suited for the µc-Si:H growth than the hot silver substrate. The TEM micrograph reveals the beginnings of cracks in the middle of the absorber layer similar to the ones reported on LP-CVD ZnO, whereas on hot silver no cracks are present. The damage is limited as the good efficiency of the device.

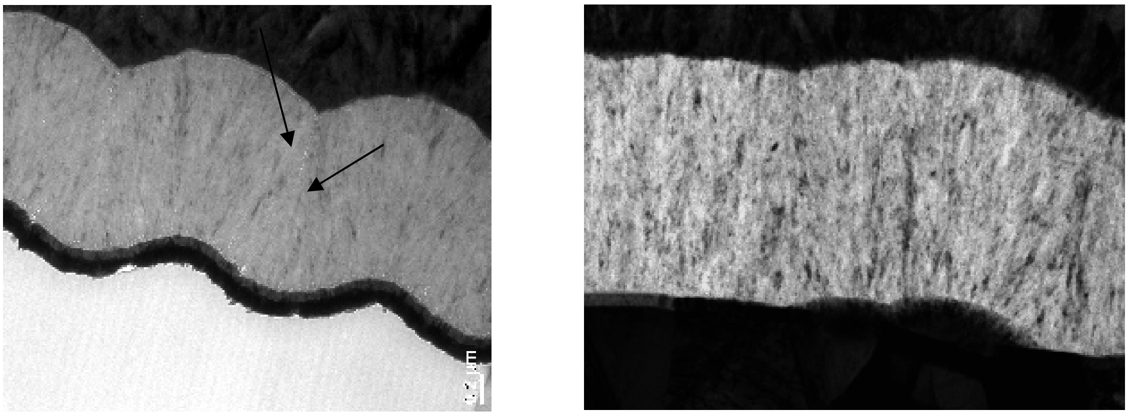

Figure 3-18: TEM micrographs of a µc-Si:H solar cell deposited on the 2D periodic grating (left) and on hot silver substrate (right). The lamella is prepared by FIB.

3.2.4.2 Thickness of the absorber layer

A straightforward way to increase the J_{sc} of the μc-Si:H is to increase the thickness of the cells. Here, we illustrate this effect with a thickness series of μc-Si:H as shown in Table 3-2 and Figure 3-19. The J_{sc} increases from 22.9 mA/cm2 to 25.1 mA/cm^2 with increasing the thickness of the absorber layer from 1 to 3 μm. The dilution of the intrinsic layer is kept constant at 17 for all absorber layers. In fact, only the deposition time increases. The V_{oc} and FF are, here, only moderately reduced by the increase of the thickness to 2.5 μm. Losses appear in the EQE when the thickness increases. These losses are easier to evidence when the cell is thick because “holes” appear in the EQE as shown by arrows in Figure 3-19. In this series an efficiency of 8.8 % on plastic substrates has been obtained. This is one of the best results achieved on flexible substrates with only a 1.5 μm thick absorber layer. Note that with 3 μm thick absorber layer, the J_{sc} is only slightly increased compared to 2.5 μm. In fact, a thickness of the cell over 2.5 μm starts to causes deleterious carrier collection problems as also reported elsewhere [132]. We note this effect for solar cells deposited on hot silver as well.

Table 3-2: Electrical parameters of μc-Si:H solar cells on 2 D cross grating with thicknesses of the absorber layer varying from 1 μm to 2.5 μm. The dilution of the layer is 17.1.

Thickness	V_{oc} [mV]	FF [%]	J_{sc}[mA/cm^2]	Efficiency[%]
1.1	513	69	22.9	8.1
1.5	528	69	24.2	8.8
2	517	67	24.5	8.4
2.5	515	67	25.0	8.6
3	488	60	25.1	7.3

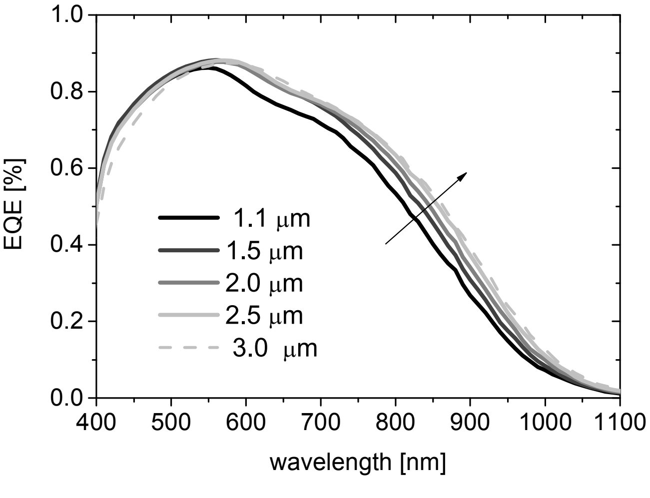

Figure 3-19: EQE of a μc-Si:H solar cell with thickness increasing from 1 μm to 2.5 μm.

3.2.4.3 Substrate morphologies for thick μc-Si:H

We have seen that for a thin absorber layer, the morphology influences the performance of the μc-Si:H solar cells, i.e. sharp V-shape morphology creates cracks that deteriorate the V_{oc} and FF. This effect is attenuated with our BL for thin cells. For thick solar cells, the situation is more dramatic as shown in Figure 3-20. Indeed, the EQE of a 2.5 μm thick μc-Si:H solar cell on severe substrates (LP-CVD ZnO with 20' treatment times) presents losses from 450 nm to 800 nm and no gain in the light trapping (800 nm – 1100 nm). Hence, we think that the losses come from poor carrier collection. In addition, the gains in light trapping are of course less effective for thicker solar cells.

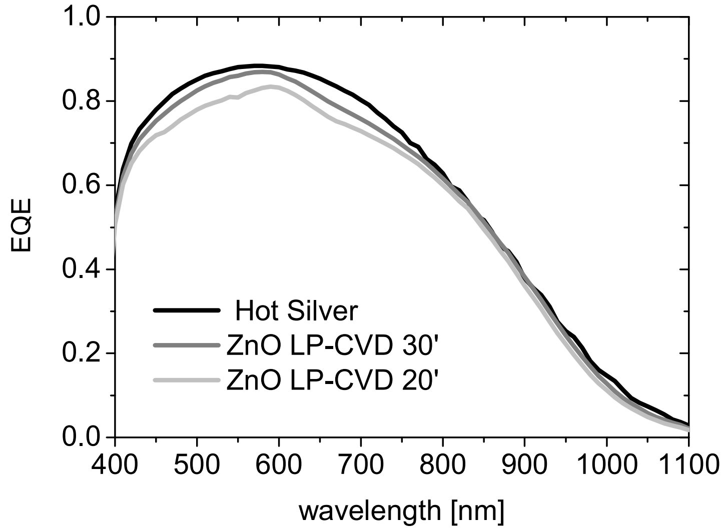

Figure 3-20: EQE of 2.5 μm thick μc-Si:H solar cells on a substrate covered with hot silver, LP-CVD ZnO treated for 20' and 30'.

Figure 3-21 shows IV parameters of a set of thick μc-Si:H solar cells deposited on LP-CVD ZnO treated for 20' and 30', and on a hot silver substrate. The dilution profile include our amorphous BL (50 nm) and 1.7 μm absorber layer with dilution 17.6, which is identical for all cells. The dilution of the remaining 0.8 μm is varied from 14.4 to 25. It shows that the C_R, measured from the p-side, is strongly increased from 51% to 85% on the last layer. Hence, the V_{oc} and FF decreased due to the excessively elevated C_R close to the p-layer. The V_{oc} is rather low, which is often observed for thick μc-Si:H solar cells. The V_{oc} is more sensitive to the C_R than to substrate morphology whereas the FF is much lower on the LP-CVD ZnO than on hot silver. In fact, the J_{sc} is really the limiting factor. Indeed, a similar J_{sc} is obtained on every substrate for low dilution but it is much higher on hot silver for dilution higher than 14.6. The main conclusion from this series is that high J_{sc} cannot be made on a substrate with strong light trapping properties such as LP-

CVD ZnO with little treatment time but only on substrates adapted to µc-Si:H growth, such as hot silver or the 2D periodic grating.

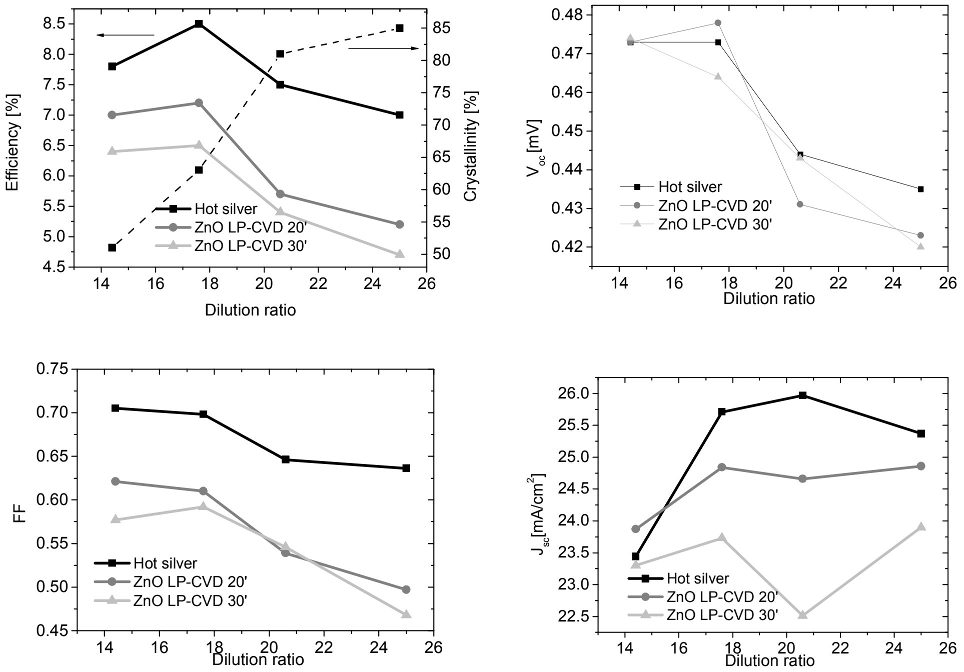

Figure 3-21: Electrical parameters of a µc-Si-H solar cell on three different substrates: hot silver, LP-CVD ZnO treated for 30’ and 20’. The cells are grown with 1.7 µm thick absorber with a single dilution of 17.6. Then the dilution is varied for the remaining 0.8 µm of absorber layer.

Therefore from these results, we continue our experiments for thick cells either on hot silver or on the 2D periodic grating. Figure 3-21 shows that, in that case, the best µc-Si:H is achieved with a single dilution (17.6) process as the first thick absorber layer (1.7 µm) is also deposited at 17.6. However in Figure 3-22, the EQEs of the µc-Si:H solar cells show that the J_{sc} increased for the long wavelength if the dilution is decreased or the C_R increased. The gain is only marginal and does not compensate the V_{oc} and FF losses. Hence, the single dilution process and substrates compatible with thick µc-Si:H is used for the high efficiency tandem development in Chapter 6.

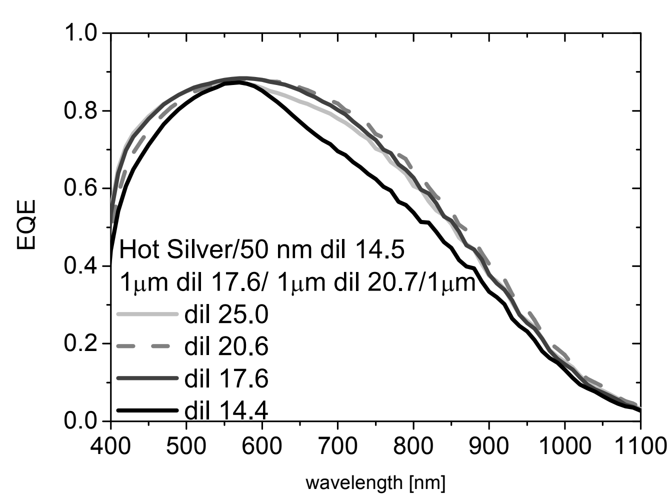

Figure 3-22: EQE of 2.5 μm thick μc-Si:H solar cells with the profile dilution of the last 800 nm varying from 14.4 to 25. The substrate used is hot silver.

3.2.5 Degradation of μc-Si:H solar cell

Here, we present the results of the μc-Si:H cell exposed to light soaking conditions. J. Meier [133] reported that the μc-Si:H solar cells can be made stable when exposed to light soaking. In fact, this is not completely true. F. Meilllaud [42] found that the cell does degrade from 0-10% depending on the C_R. In fact, our n-i-p μc-Si:H cell ndergoes light-induced degradation. The first example is a 1.2 μm thick μc-Si:H cell deposited on LP-CVD ZnO treated for 40', the C_R measured from the p-side and from the n-side are both 50 %. The cell is light soaked during 1000 h and then annealed at 180° for 1h 30min. As shown in Table 3-3, the cell degrades relatively by 11% after 1000h of light soaking and fully recovered the initial value after the annealing. All parameters are reduced after the light soaking, including J_{sc}. Figure 3-23 shows that the J_{sc} is mostly reduced in the blue wavelengths region (400-500 nm) of the solar cell.

Table 3-3: Electrical parameters of 1.2μm thick μc-Si:H solar cell in the initial state, after 1000h light soaking (LS) and after annealing.

	Voc[mV]	FF[%]	Jsc[mA/cm2]	Efficiency[%]
Initial	523	68	20.7	7.2
1000h LS	508	63	20.0	6.4
After anneal	525	67	20.4	7.2

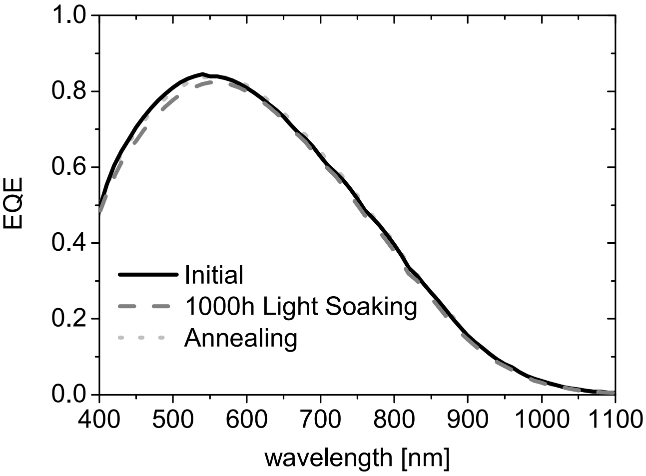

Figure 3-23: EQE of 1.2µm thick µc-Si:H cell in the initial state, after 1000h light soaking and after an annealing step.

The same light soaking experiment is conducted with 2.5 µm thick µc-Si:H solar cell and results are shown in Table 3-4 and Figure 3-24. The results are similar to the case of thin absorber layer above. Nonetheless, the light soaking induces a degradation of J_{sc} on the thick solar cell a on the full spectrum and not only on the p-side.

Table 3-4: Electrical parameters of a 2.5µm thick µc-Si:H solar cell in the initial state, after 1000h light soaking (LS) and after annealing.

	V^{oc}[mV]	FF[%]	J_{sc}[mA/cm2]	Efficiency[%]
Initial	492	68	25.1	8.4
1000h LS	477	67	24.2	7.7
After anneal	503	70	24.8	8.7

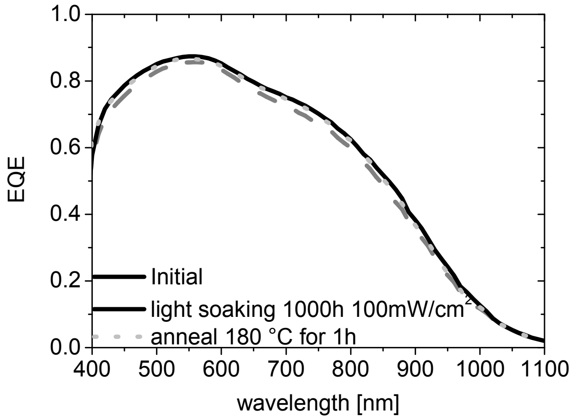

Figure 3-24: EQE of 2.5 µm thick µc-Si:H cell in the initial state, after 1000h light soaking and after an annealing step.

The µc-Si:H is always implemented into tandem micromorph cells because the efficiency of the tandem module is always higher than the single µc-Si:H for equivalent thicknesses. Therefore, the top cell acts as a filter for the bottom cells. We simulate an a-Si:H filter of the tandem cell by covering the cell with a glass covered with an a-Si:H layer. The light soaking results with an a-Si:H filter are shown in Figure 3-25 and Table 3-5. No significant light-induced degradation is observed with an a-Si:H filter.

Table 3-5: Electrical parameters of a 1.2 µm thick µc-Si:H solar cell deposited on a Al/ZnO back contact in the initial state and after 1000h light soaking (LS).

	V_{oc} [mV]	FF[%]	J_{sc}[mA/cm2]	Efficiency[%]
Initial	514	67	20.6	7.1
1000h LS	504	68	20.5	7.1

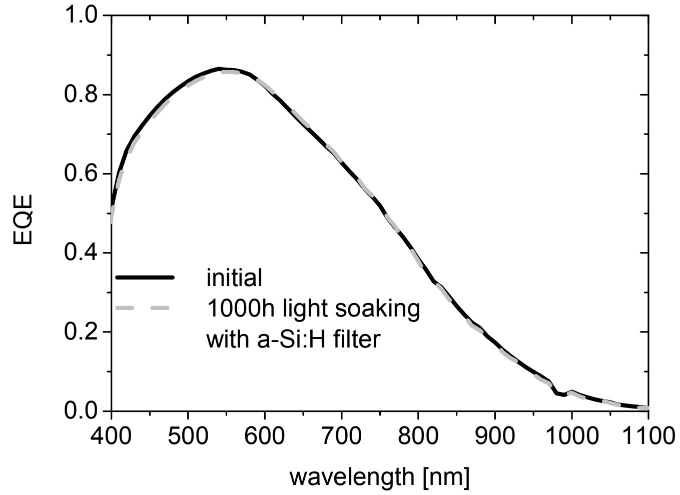

Figure 3-25: EQE of a 1.2 µm thick µc-Si:H cell deposited on a Al/ZnO back contact in the initial state and after 1000h light soaking.

3.3 Discussion

3.3.1 Thin µc-Si:H solar cell

3.3.1.1 Influence of the substrate on the Raman crystallinity

We have shown that the substrate morphologies strongly influence the growth conditions of the µc-Si:H material. From the strong crystallinity difference between the two substrate morphologies, whereas the plasma parameters were identical, we conclude that in our deposition regime, the morphology of the substrate is a parameter that can influence the crystallinity in the bulk of the absorber layer. Its effect is pronounced for every layer, i.e. n doped, intrinsic and p doped layers. This influence was already pointed out by E. Vallat-Sauvain et al. [134] who showed that the substrate topography has an impact on the spatial distribution of the amorphous and microcrystalline phases. Here, we show that the C_R can decrease by 10 % in absolute values by varying the morphology from V-shape to U-shape. It is an important difference when we compare the J_{sc} density between two substrates with different morphologies. Indeed, the differences of C_R also influences the resulting currents because a higher C_R means that the ratio between the crystalline part and the amorphous part is increased. The effective absorption thickness is increased for wavelengths above 800 nm. Hence, the difference of J_{sc} between the cells deposited on the 20' treated substrate and the 40' treated substrate is, in fact, underestimated. The lower C_R for the 20' case indicates that the difference in J_{sc} would be even higher than 1.5 mA/cm^2 if we would compare cells with similar level of C_R. This reinforces the elevated light trapping capabilities of the LP-CVD ZnO with low treatment times.

3.3.1.2 Influence of deposition condition on the Raman crystallinity

In the next part of the discussion, we consider the C_R of μc-Si:H layers on the same substrate morphologies, i.e. LP-CVD ZnO treated for 20'. The C_R is mostly influenced by the SiH_4 dilution in the plasma during the deposition of bulk of the absorber layer [111, 121], the substrate texture (as already discussed), and the chemical nature of the substrate material [134]. A highly diluted seed layer is usually required during the beginning of the growth to remove the first incubation amorphous layer [135, 136]. This incubation layer has two origins [134, 137, 138]. First, it can be the chemical nature of the substrate, which can influence the growth of the μc-Si layer. In our case, the C_R at the p-side of the solar cell does not depend on the BL dilution whatsoever and recovers the value it has without the buffer. This suggests that the bulk C_R close to the p-layer is not influenced by the C_R of the material close to the n-doped layer. Secondly, this incubation layer can be partly attributed to back diffusion of SiH_4 from the vacuum chamber to the plasma as shown by M.N. van der Donker et al. [139]. However, they show that for the case of high dilution (which is our case with dilution of 17.6), these effects are not dominant. Nevertheless, for high dilution close to our condition they also report that a tailored initial SiH_4 flux is beneficial because it provides a constant SiH_4 density in the plasma directly after the ignition. This has two main effects. First, it removes the amorphous incubation layer. Second, it provides a more stable C_R throughout the layer compared to the standard deposition. Here, the standard means that the C_R increases with the growth of the layer. These results have been obtained with deposition frequencies of 13.6 MHz. In our case, the frequency is 70 MHz. At higher frequencies the decomposition of SiH_4 in the plasma is more efficient and thus the plasma equilibrium is reached sooner [52, 140]. To conclude, in our deposition condition, the C_R of the μc-Si:H template has no or little impact on the growth condition of the absorber material and a uniform C_R is achieved through the μc-Si:H layer. This reveals that our deposition conditions rapidly reach equilibrium SiH_4 densities in the plasma thanks to the VHF and high dilution regime of SiH_4 in H_2.

3.3 Discussion

3.3.1.3 Cracks and buffer layer

Our results show that the coalescence of the grain boundaries in μc-Si:H material is strongly affected when the substrate morphology has a V-shape structure, resulting in reduced cell performance. Indeed, we think that these voids or porous areas act as diffusion path for dopants or contaminants into the absorber layer. We have seen that the amorphous BL or low dilution BL itself is not beneficial to the solar cell performance because the cells exhibit low FF and losses appear in the EQE. The apparition of cracks is clearly linked with the substrate morphology as shown in Figure 3-13, and the BL clearly reduces their apparition in the μc-Si:H material. In fact, our BL acts as "surgical tape" for the cracks. This explains why the increase of efficiency with the BL is higher on severely V-shaped substrate rather than on U-shape substrate. In fact, the BL improves the μc-Si:H cells by preventing the apparition of cracks and voids through the layer thanks to its higher content of amorphous phase. In addition, the BL is also beneficial to U-shape substrate, which does not have cracks. The oxygen content is also reduced for the crack free layers. Hence, we think that the BL can also prevent the diffusion of contaminant by creating a barrier with a denser amorphous material between the doped layer and the intrinsic layer.

3.3.1.4 Summary

We need to point out that the BL layers achieve only part of the desired result because the cells with a 40' treatment time are still better in terms of absolute efficiency compared to the solar cell deposited on the 20' treated substrate. Although, our BL clearly reduces the efficiency gap between these substrates, the electrical parameters of the solar cell are still better on U-shape substrates and even higher on hot silver. However, the layers introduced in this work represent a first step towards higher efficiency μc-Si:H solar cells and further great improvements are expected if we can tame severe substrate morphologies further, i.e. such as obtained with low treatment time of the LP-CVD ZnO substrates. There are interesting results from M. Python [35] who shows that increasing the deposition temperature (250°C) reduced the number of cracks or from Y. Nasuno et al. [141] who shows that decreasing the temperature to 140 °C suppresses the activation of the oxygen donor by hydrogen passivation.

3.3.2 Thick μc-Si:H solar cell

For the fabrication of high efficiency micromorph, which is the final goal of this thesis (Chapter 6), high J_{sc} is needed. The easy way to further increase the J_{sc} is to increase the absorber layer thickness. Our results show that, so far, it is only possible on moderately textured substrates for the μc-Si:H growth, i.e. on hot silver or the 2D periodic grating. Difficulties remain even on these gentle substrates. When the thickness increases over 2.5 μm, the V_{oc} and FF decrease. We assume that the limitation of the J_{sc} comes from the contamination of our absorber layer during the μc-Si:H growth due to wall degassing . Decreases in the wall temperature or increases in the deposition rate could reduce the incorporation of nitrogen or oxygen in the layer [142] and therefore increase the performance of thick μc-Si.H solar cells.

3.3.3 Light-induced degradation

The light-induced degradation of μc-Si:H silicon has been studied by different authors. J Meier reported that no significant light-induced degradation occurs in the entire solar cells [133]. F. Meillaud reported that the degradation depends on the crystallinity of the layer [42]. The cells that are closer to the amorphous phase have a higher degradation. Yue et al. [143] reported that the degradation occurs mostly in the amorphous phase of the μc-Si:H cells and therefore only the high energy photons are responsible for the light-induced degradation because the a-Si:H phase is transparent to the light wavelength above 750 nm. Our results also show that the light-induced degradation is suppressed for the cells protected from high energy photons, whereas significant degradation is observed when the μc-Si:H is exposed to the full spectrum. However, it remains unclear if the light-induced degradation creates defects in the a-Si:H phase or at the interface between the nanocrystal and the a-Si:H material.

3.4 Conclusion

N-i-p μc-Si:H cells require careful management of the incoming light. The ultimate goal is to achieve complete light trapping in order to benefit from all incoming photons. Two strategies are tested for harvesting the photons. First, we work on thin μc-Si:H absorber layers compatible with production requirements and thick absorber layer for high J_{sc}. So far, each strategy require a different approach.

The current work focuses on optimizing the thin μc-Si:H solar cell design in terms of V_{oc} and FF on severely structured substrates like moderately treated V-shape LP-CVD ZnO, which yields superior light trapping. In this chapter, we discuss the introduction of an amorphous buffer layer that is capable of limiting the losses of V_{oc} and FF that are observed in μc-Si:H solar cells on strongly textured substrates. The gain in efficiency is clearly linked with the diminution of crack density in the μc-Si material. Eventually, it shows that with combined suitable substrate and processing, high efficiency thin microcrystalline cells can be fabricated (9% is made on glass substrate and 8.8% on plastic foil).

The strategy for the thick absorber layer is tested and J_{sc} is increased to 25 mA/cm^2 for a 2.5 μm thick absorber layer. Nonetheless, thick μc-Si:H solar cells on moderately textured substrates are the only choice. Indeed, the influence of the severe substrate texture could not yet be compensated with dilution profiling.

Chapter 4: Amorphous Si

Single junction a-Si:H solar cells

4.1 Introduction

This chapter discusses the optimization of amorphous silicon thin film (a-Si:H) solar cells. The first challenge is to introduce textured substrates that enhance the light trapping in thin cells. This is a compulsory technique because the absorber thickness has to be below 500 nm in order to limit the light induced degradation while the penetration depth of the light at 750 nm is over 1 µm. It was already shown by Bailat et al. [66] that the current density (J_{sc}) can be increased on textured plastic substrates, but this increase was accompanied by a reduction of open-circuit voltage (V_{oc}) and fill factor (FF) compared to cells deposited on flat substrates. Indeed, the interaction between substrate morphology and PECVD growth of thin films is critical for most a-Si:H. It was shown by Sakai et al. [144] that the substrate morphology has dramatic consequences on the absorber layer growth and on the cell performances. Thus, the optimum structure for n-i-p solar cells, taking into account the needs for a strong light trapping and suitable growth of the n-i-p a-Si:H devices is not yet known.

The first part of this chapter focuses on the relationship between the surface morphology of the substrate and the J_{sc} in the a-Si:H n-i-p cells. For this study, we develop textured zinc oxide (ZnO) back reflectors where the roughness (feature size) and the morphology (feature shape) can be adjusted independently via the deposition time [145] and a plasma surface treatment [119], respectively. This was described in Chapter 2 and applied to the µc-Si:H case in Chapter 3 and, here, it is applied in the a-Si:H case.

In the second part of the chapter, the study concentrates on the cell design required in order to increase open circuit voltage (V_{oc}) and fill factor (FF) on textured substrate. In the n-i-p configuration, the n-layer is the first layer deposited and therefore influences the growth of the subsequent layers. A microcrystalline n-layer (n-µc) is a good candidate, because the layer can be doped efficiently and it has a lower absorption coefficient than the a-Si:H layer. Nevertheless, its growth is strongly influenced by the chemistry of the substrate material [137]. In addition, we investigate on the dependence of the n-doped microcrystalline layer (n-µc) on the substrate morphologies and look for more robust layers. In p-i-n solar cells, N. Pellaton-Vaucher [146] suggest that an amorphous n-layer is robust, in other words the deposition parameters have only small influences on the electrical characteristics of the layer. Here, we apply this concept to the n-i-p configuration by introducing an amorphous carbide layer (n-SiC), which is robust with respect to the deposition parameters and to the substrate morphologies. Furthermore, the addition of carbon increases the gap and gives higher V_{oc} than amorphous Si [147] and microcrystalline Si layers without carbon. Furthermore, we describe how the benefits of the n-SiC layer can be used fully in the solar cell. We propose a surface treatment to enhance the TCO/n-SiC contact and the introduction of a buffer layer to reduce the band discontinuities between the intrinsic and the n-SiC layer.

In the third part, the study provides experimental results of light-induced degradation of the n-i-p a-Si:H solar cells deposited with aprocess temperature compatible with low T_g substrates. The degradation varies with the thickness of the intrinsic layer from 15% to 30% for thicknesses varying from 140 nm to 400 nm.

Finally, by applying the benefits of our findings, we show that a flexible a-Si:H solar cell on a PEN substrate with an initial efficiency of 8.8% can be achieved. The stable efficiency after 1000h of light soaking is 7% with 20% degradation for a 270 nm absorber thickness.

4.2 Results

4.2.1 Substrates

We investigate the effect of the surface structure on the a-Si:H n-i-p solar cell properties. We work on LP-CVD ZnO substrates that allow independent variation of the dimensions and the shapes of the surface texture as described in Chapter 2. Therefore, two degrees of freedom are available to investigate light trapping in the a-Si:H solar cells. For this development, the design of the solar cell is kept as simple as possible. The structure as shown in Figure 4-1 consists of Glass / Cr / Ag / LPCVD ZnO / µc n-layer / a-Si:H / µc p-layer / LPCVD ZnO.

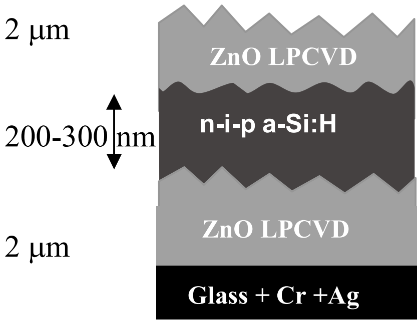

Figure 4-1: Structure of the n-i-p solar cell on substrate coated with silver and LP-CVD ZnO.

Figure 4-3 shows the EQE of a-Si:H solar cells deposited from the same LP-CVD ZnO substrate, but with different surface plasma treatment times. Note that EQE is measured at reverse bias voltage (-1V) in order to assess the light trapping without the influence of the collection efficiency. The Si cell thickness is below 300 nm and here the dilution

([H_2]/[SiH_4]) of the intrinsic layer is 6. The size of the ZnO pyramids (feature size of 300 nm - 400 nm) is reduced compared to the one used in Chapter 3 (feature size of 1 μm) in order to be adapted to the needs of a-Si:H cells. The surface plasma treatment changes the substrates from a V-shape to a U-shape morphology of the ZnO pyramids as described in Chapter 2 and illustrated in Figure 4-2.

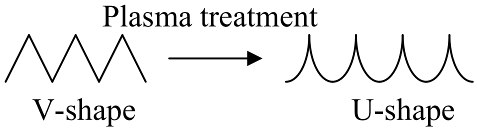

Figure 4-2: The surface plasma treatment transforms the valleys of the LP-CVD ZnO from V-shape to U-shape morphology.

In this series of surface plasma treatment times, the collected current density is reduced from 13.9 mA/cm2 to 12.6 mA/cm2. The current density loss is due to reduced absorption in the wavelength range from 550 to 800 nm, which depends on the light scattering properties of the substrate. Table 4-1 summarizes the solar cell parameters V_{oc}, FF, J_{sc} and the efficiencies of this series versus the plasma treatment time. It shows that the treatment slightly reduces the rms roughness from 69 nm to 59 nm. This small difference suggests that for a given size of the ZnO texture, the treatment modifies the morphology of the substrate rather than the height of the pyramids. The treatment reduces also the light trapping in the a-Si:H solar cells as shown in Figure 4-3. Of course this is an undesired effect because it reduces the J_{sc} of the cells. However, we find that the treatment dramatically improves V_{oc} and FF, resulting in improved efficiencies of the a-Si:H solar cells as shown in Figure 4-4. In fact, the difference in V_{oc} between cells on the standard flat substrate and on non-treated substrate is almost 200 mV. These results show that the shape of the substrate can lead, similarly to the case of the μc-Si:H cells in Chapter 3, to dramatic changes in the cell electrical characteristics. In addition, the optimum substrate is found to be the most treated one because the improvement of V_{oc} and FF overcompensate the losses in J_{sc}. Note that even though the absorption in the cells is higher for low treated substrates, the collection losses $|J(-1V) - J_{sc}|$ are also reduced for treated substrates and reinforce the advantage of the treated substrates.

Table 4-1: Solar cell parameters for different back reflector morphologies.

Plasma treatment time [min]	0’	15’	30’	45’	flat
V_{oc} [mV]	710	772	821	846	888
J_{sc} [mA/cm^2]	13.0	13.0	12.6	12.3	11.0
J_{-1V} [mA/cm^2]	13.9	13.7	13.1	12.6	11.1
FF [%]	59	66	69	69	67
Efficiency [%]	5.4	6.6	7.1	7.2	6.6
RMS [nm]	69	64	61	59	-

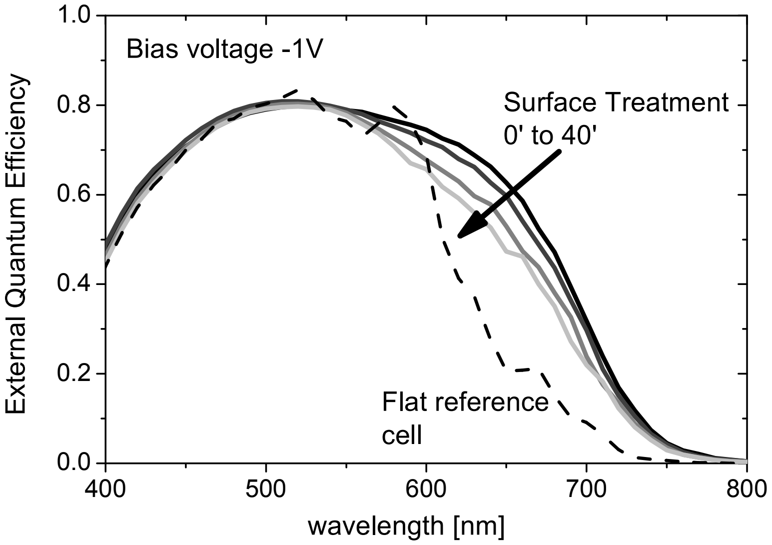

Figure 4-3: External Quantum Efficiency at -1 V for back reflector structures after different times of surface treatment (solid line, black to light grey for increasing treatment time) of the ZnO LP-CVD and a flat reference (dashed line).

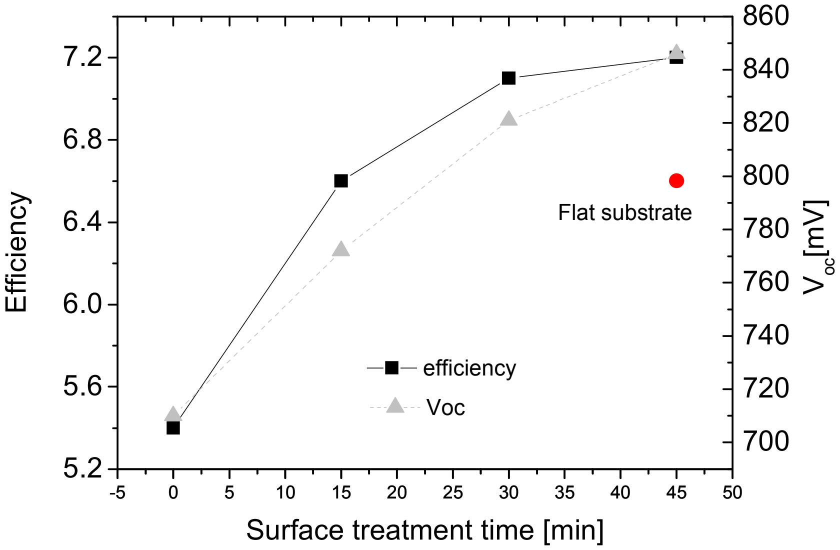

Figure 4-4: Efficiency and V_{oc} of the solar cells deposited at various surface plasma treatment times.

Figure 4-6 shows the results of a series where the feature size of the substrate is varied as shown in Figure 4-5. In Figure 4-6, the current density of the n-i-p cells is plotted at a reverse bias of -1V for wavelengths between 550 nm and 800 nm as a function of the rms roughness of the different substrates. Choosing this particular wavelength range better emphasizes the light scattering effect in the solar cell. It demonstrates that the light trapping in a-Si:H is more affected by a change of morphology (shape) than the size of the pyramids. In fact, a long treatment time (45 min) of the substrate still has a relatively high rms but only a small current density gain is observed compared to flat substrates.

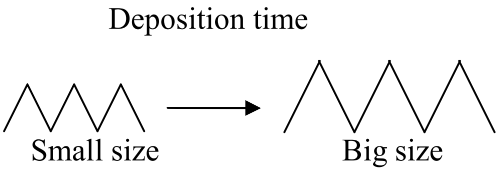

Figure 4-5: The size of the ZnO LP-CVDpyramids increases with deposition time, i.e. the thickness of the layer.

Also shown in Figure 4-6 are simulation results obtained with the Sunshine software developed by the University of Ljubljana [148, 149]. The software implements a semi-empirical model based on the scalar scattering theory and allows the simulation of a multilayer system with various roughnesses and scattering capabilities of each interface. The simulation suggests a strong increase of J_{sc} for increasing rms between 0 and 60 nm, for even higher rms the current density tends to saturate. The rms range that is accessible experimentally reproduces the saturation behavior, but we note that the current density degrades once the roughness exceeds 100 nm. In fact, the optimum for the light scattering is around rms equal to 70-80 nm (corresponding to the lateral dimension of 400 nm), but the simulation does not reproduce this result. We think that the simple linear increase in haze with rms in Eq. 2.6 of the semi-empirical theory overestimates the amount of light scattering in this case. In fact the angular distribution of scattered light is also modified as the size of the pyramids increase. This can be modified in the simulation program with the angular distribution function (ADF). For the standard simulation we use an ellipsis ADF with the ratio b/a = 0.5. We note during our simulation experiments that the ADF2T, which is the ADF of the already scattered and transmitted light, has the most important impact on the J_{sc} of the solar cell. Therefore, we vary only the ellipsis ratio b/a of ADF2T between 0.3 and 0.8. Figure 4-6 shows that for the simulated results the difference in J_{sc} due to the ADF variation is important, even more important than the rms. This is also the case for the ADF in air of the LP-CVD ZnO substrate as shown by D. Dominé [19] and for the J_{sc} in the solar cells as shown in Figure 4-3.

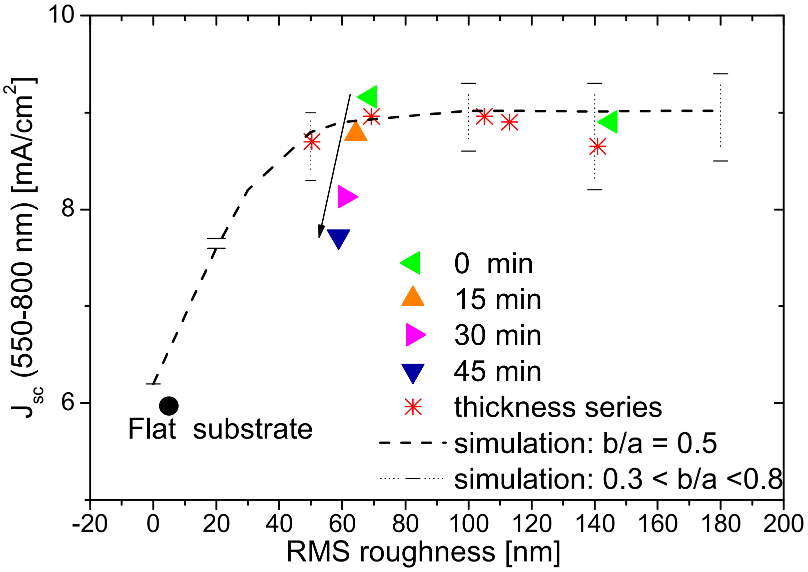

Figure 4-6: Current density (-1V) between 550-800 nm of the n-i-p a-Si:H solar cell on LP-CVD ZnO/flat Ag substrates with different surface feature shapes and sizes. The stars indicate substrates with different ZnO grain sizes and with a standard plasma treatment of 20 min. The left-oriented triangle is an untreated substrate and the up, right, and down triangles are treated for 15, 30 and 45 minutes, respectively. A point for a flat substrate is added for reference (circle) and the dashed line represents simulations (Sunshine) with ADF2T with b/a = 0.5. The dotted lines with the bars are also simulations by varying ADF2T from b/a = 0.3 to b/a = 0.8.

4.2.2 n-layers

4.2.2.1 Influence of the substrate morphology on the n-μc

So far, we have shown that the morphology of the substrate strongly influences the a-Si:H solar cell performance. Here, we evaluate the influence of the first deposited silicon layer (n-layer) on the V_{oc}. State of the art n-i-p solar cells deposited on flat substrates are usually prepared with a microcrystalline n-layer (n-μc) deposited directly onto the substrate, as is the case for the cells presented in Section 4.2.1. The design gives good results on flat substrates thanks to the high doping efficiency of microcrystalline layers and lower absorption of microcrystalline material compared to a-Si:H layer. However, we observe that the n-μc layers can have different properties depending both on the substrate texture and on the material. This effect is shown in Figure 4-7. The activation energy of the same deposited n-μc layers is measured on various textured plastic substrates. The textures used here are replications of various textures in the plastic (LP-CVD ZnO, hot silver and a 2D sinusoidal cross grating). It shows that the microcrystalline layer properties are influenced by the substrate morphology. In addition, it is well established that microcrystalline layers are influenced by the materials chemistry (e.g. a-Si:H, SiO_2, ZnO, SnO_2, PEN, etc.) [137].

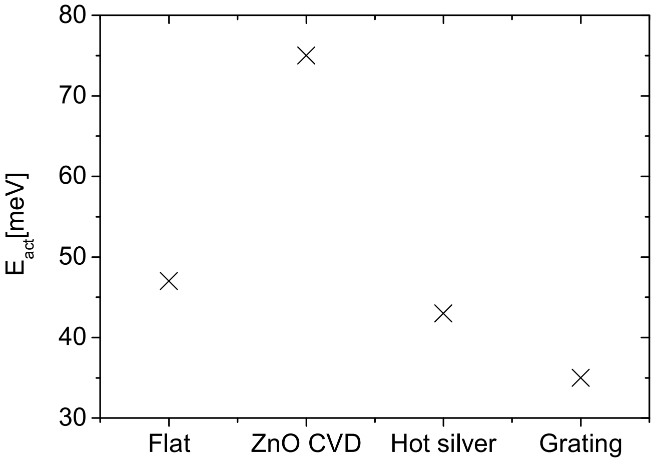

Figure 4-7: Activation energy of n-µc deposited directly on PEN substrates containing different replications of textures. The grating has moderate morphology whereas the LP-CVD ZnO has the sharpest texture (angles) morphology.

The TEM micrographs in Figure 4-8 and Figure 4-9 also show that the texture of the substrate influences the growth of the silicon layers. The cells in Figure 4-8 and Figure 4-9 left are made of cells with n-µc layers. Figure 4-9 right is a tandem a-Si:H cells with an amorphous n-layer in the bottom cell and microcrystalline p-layer. The almost flat substrate micrograph (strongly treated LP-CVD ZnO), Figure 4-8 (left), shows a uniform and homogenous deposition of n, i and p-layers. The textured substrates of Figure 4.5 (right) and Figure 4-9, which contain n-µc, reveal the appearance of voids and nano-cracks in the layers. Two effects are visible, the first is the porosity of the n-µc and the second is the apparition of voids and nano-cracks in the a-Si:H. Figure 4-8 shows the appearance of cracks in the beginning of the valley of the LP-CVD ZnO and propagating through the entire intrinsic layer. In Figure 4-9, the micrograph shows in more detail the n/i interface in a µc-Si:H solar cell on a textured substrate. We already see the appearance of voids in the n-doped layer. The valley of the pyramids is also a start of the defective region in the microcrystalline material. The Figure 4-9 (right) shows the cross section of an a-Si:H tandem cell with n-SiC layers and a p-µc layer for both the top and bottom cells. The bottom cell is homogenous whereas cracks start in the valley of the top cells. They are marked in the micrographs with black arrows. It suggests that the µc-layer in the recombination junction initiates the cracks whereas the amorphous n-SiC prevents the crack formation. Another possibility that might explain the crack formation is the pinches that often appear after the bottom cell deposition. This creates a valley with even higher surface angles than the as-grown LP-CVD ZnO.

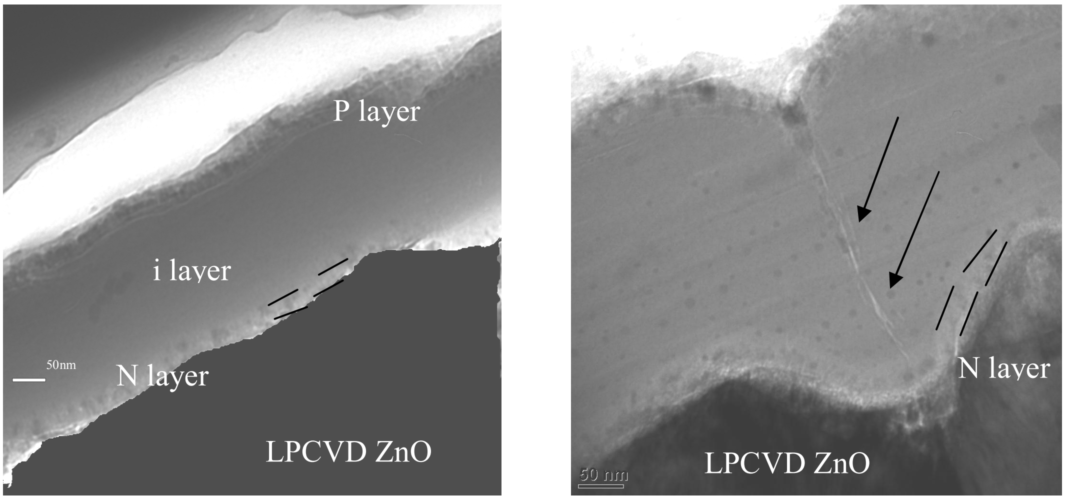

Figure 4-8: TEM micrograph of a-Si:H solar cell on strongly treated substrate (almost flat) and on rough LP-CVD ZnO.

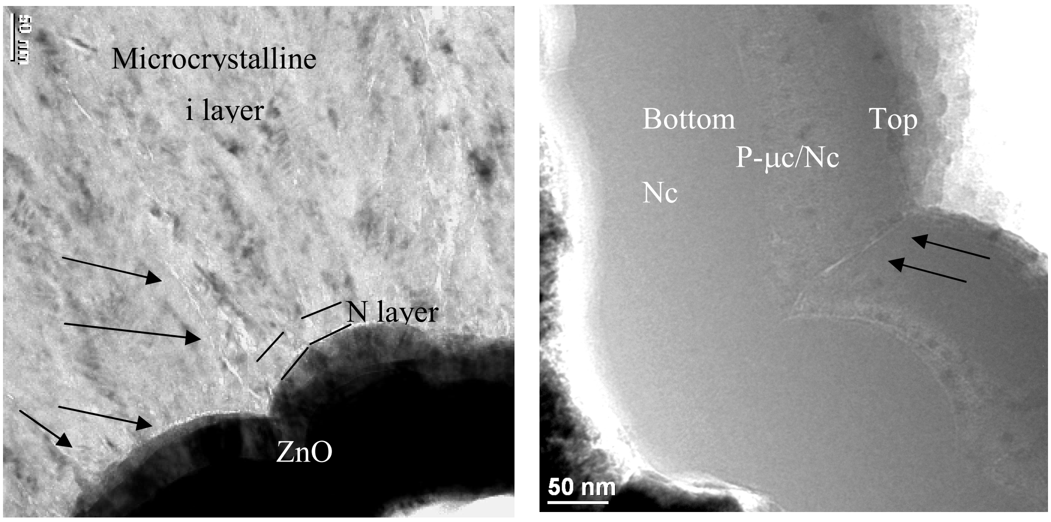

Figure 4-9: TEM micrograph of μc-Si:H on textured substrate coated with silver and with 80 nm of sputtered ZnO (left) and an a-Si/a-Si tandem (right) deposited on LP-CVD ZnO.

4.2.2.2 Influence of the n-layer on the V_{oc}

In order to ameliorate the problems related to the defective material in the n-µc layer, we develop an amorphous n-layer with the addition of methane (CH_4) resulting in n-doped silicon carbide or n-SiC, which prevent the apparition of cracks as shown in the previous section. Figure 4-10 compares the Voc of n-i-p solar cells with n-µc and n-SiC deposited on the rough LP-CVD ZnOs, with all the other parameters kept constant. The trend lines show that the decrease in Voc from strongly treated to untreated substrate is less pronounced for the carbide n-layers (solid lines) than for microcrystalline n-layers (dashed line). The increase in V_{oc} with the n-SiC layer is more than 170 mV (710 mV to 882 mV) for the untreated substrate. Even for the strongly treated substrate (which is close to the flat case), the n-SiC layer gives a better V_{oc} (900 mV) than the n-µc layer (878 mV).

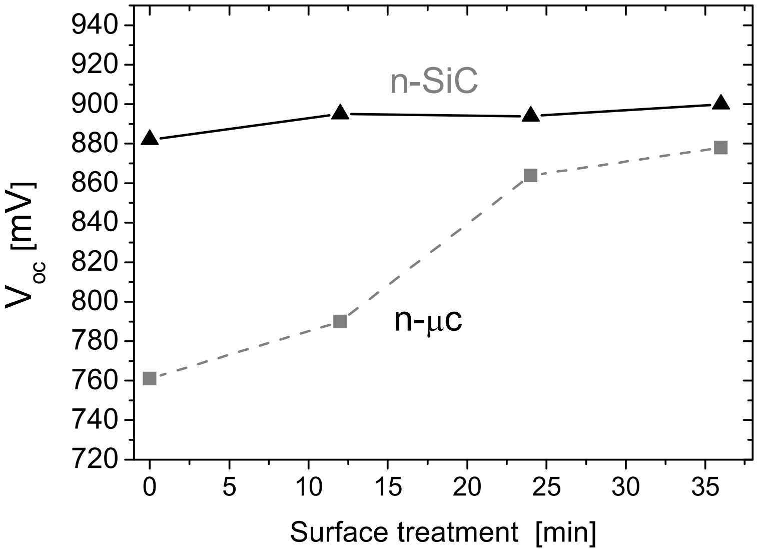

Figure 4-10: Open circuit voltage (V_{oc}) comparison of n-i-p cells with a microcrystalline n-mc (dashed line) and an amorphous n-SiC layer (solid line). The substrate is a rough LP-CVD ZnO/Flat Ag deposited on glass, with different surface treatment times.

4.2.2.3 Carbide n-layer

The amorphous n-layer is sufficient to stabilize the V_{oc} on rough substrates but the addition of CH4 is also beneficial for the a-Si:H solar cells. Indeed, it was shown by Y. Hamakawa and Y. Tawada [147, 150] that the carbon in the n and p-layers increase the V_{oc} and thus the efficiency of the a-Si:H solar cells. The literature is rather limited on the n-layer whereas the carbide p-layer has been studied extensively, since a window layer is crucial for the front side of the solar cells. The Figure 4-11 shows that the adjunction of

CH_4 slightly enhances the V_{oc} (10 mV) but strongly enhances the FF from 63 % to 68 %. Nevertheless, the methane concentration in the plasma must not exceed a certain level before it starts deteriorating the FF. The optimum CH4 concentration is with a low CH4 flux of 0.3 sccm compared to 1.5 sccm of SiH_4.

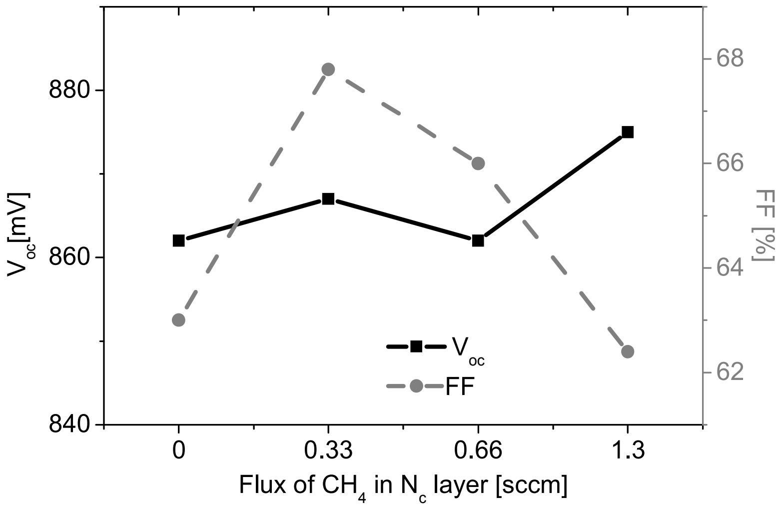

Figure 4-11: Electrical parameters of a-Si:H solar cells deposited on LP-CVD ZnO substrates. The flux of methane is varied from 0 to 1.3 sccm (SiH_4 is constant at 1.5 sccm).

The next developments are made with a non-optimal carbide flux (0.66 sccm instead of 0.33 sccm) because the last experiment was only performed recently. Thus, the standard n-SiC has a high optical band gap of 1.84 eV (determined by ellipsometry with a Tauc-Lorentz model). At room temperature, the dark conductivity of the n-SiC layer is 2*10-5 Scm^{-1}. The activation energy is Ea = 388 meV. Note that the typical activation of a n-µc is between 20 and 50 meV and for an a-Si:H n-layer it is between 150 meV and 300 meV [22]. It is reported in the literature that the carbide layer has higher energy band gap and activation energy than amorphous layer without carbon [150, 151]. Therefore, the elevated activation energy suggests that the layer is amorphous and moreover that it is a carbide compound.

The optoelectrical properties of the a-Si:H layers change with doping or alloying. Indeed, Figure 4-12 shows the gap (E_g), the refractive index (n @ 600nm) and the extinction coefficient (k @ 600nm) of the intrinsic a-Si:H (open symbol) and n-doped a-Si:H (full symbols). It shows that the gap of the material decreases by 0.13 eV when adding dopant in the layer even though the doped layer is made at higher dilution. This decrease is also reported in the literature for both p and n-doped layers [140, 142] and it is due to the increase of defect density caused by the doping [22]. We observe a reduction of the refractive index and an increase of the extinction coefficient as shown in Figure 4-12. The increased of k is undesired because the photogeneration in the doped layers is lost for the J_{sc}. The reduction of k can be made by alloying the a-Si:H with carbon as shown in

Figure 4-12. In fact, the C increases the gap from 1.6 to 2 eV, diminishes n from 4 to 3, and k from 0.12 to 0, while increasing the CH_4 from 0 to 2.4 sccm (SiH4 flux is constant at 1.5 sccm).

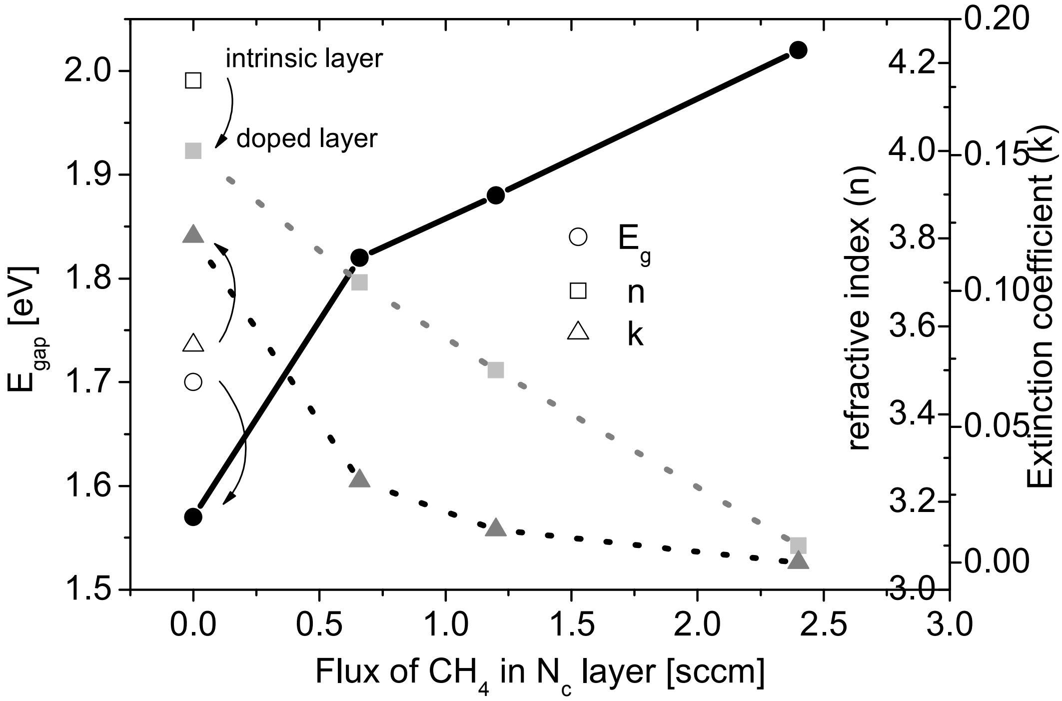

Figure 4-12: Undoped a-Si:H (open symbols), n-doped a-Si:H (solid symbols) layers with addition of CH4. The gap (E_g, rounds), n (squares) and k (triangles) are determined by ellipsometry from a Tauc-Lorentz model. The n and k are shown for light wave of 600 nm.

4.2.2.4 Microcrystalline interface treatment

The improvement in V_{oc} on textured substrates and in FF of the n-SiC is now clear but the potential of that doped layer is only fulfilled with a good contact between the ZnO and the n-SiC. Figure 4-13 shows the J(V) curve of the cell with the n-SiC (dashed black line); a strong serial resistance lowers the FF to 59%. To overcome the contact resistance problem, we introduce an interface treatment between the ZnO substrate and the n-SiC. The treatment is made in the microcrystalline regime with high dilution of H_2. In Figure 4-13, the J(V) curves of cells with and without the interface treatment are compared. The absolute 6% gain in FF demonstrates the improved contact resistance between ZnO and n-SiC layer. This procedure is capable of improving the contact resistance, either by applying it for a short time, which is effectively a treatment, or by applying it for an extended time, which actually results in the growth a microcrystalline layer without amorphous nucleation phase. The treatment is preferred because it limits the optical losses. Note that, the efficiency of the treatment is particularly useful for a n-SiC layer with high band gap, i.e. high carbon flux such as $CH_4 > 1$ sccm.

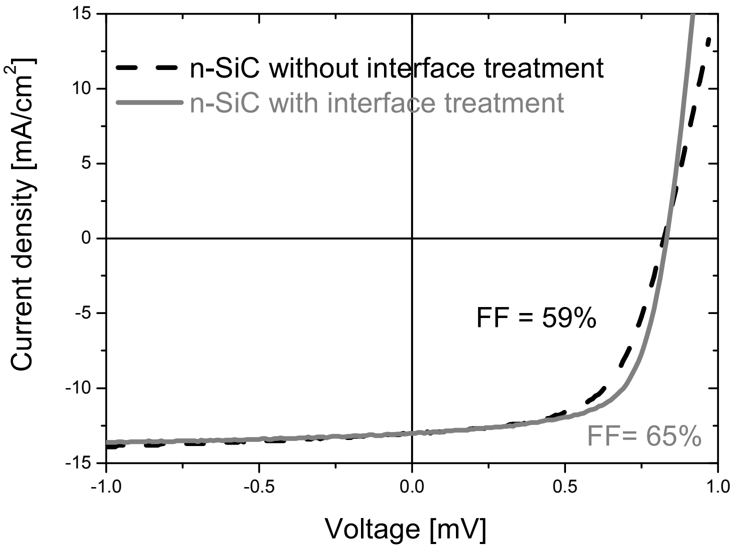

Figure 4-13: Comparison of the J(V) curve of a-Si:H solar cell with (plain curve) and without (dashed curve) interface treatment at the ZnO/n-SiC interface

4.2.2.5 Buffer layer at n/i interface

Each interface of our devices is important. Here, we focus on the interface between n-SiC and the intrinsic layer. For that, we introduce a 20 nm buffer layer in order to improve the interface between the n-SiC and the intrinsic layers of the solar cell. The buffer layer is deposited with a dilution ratio of 9, which has two effects: it increases the band gap of a-Si:H, which acts as a graded interface between the i-layer and the n-SiC layer, and it reduces the density of defects at the n/i interface [152] [136, 153]. Figure 4-14 shows the efficiency of the cell with and without a buffer layer for different surface plasma treatment times on the LP-CVD ZnO. Table 4-2 gives the solar cell characteristics for a 12 minute surface treatment applied to the substrate. The gain due to the buffer layer is mostly in FF (63.4% => 67.6%) and slightly in Voc, (885mV => 895mV). The buffer layer at the n/i interface increases the relative efficiency of the cell by 9% (8.0% => 8.7%).

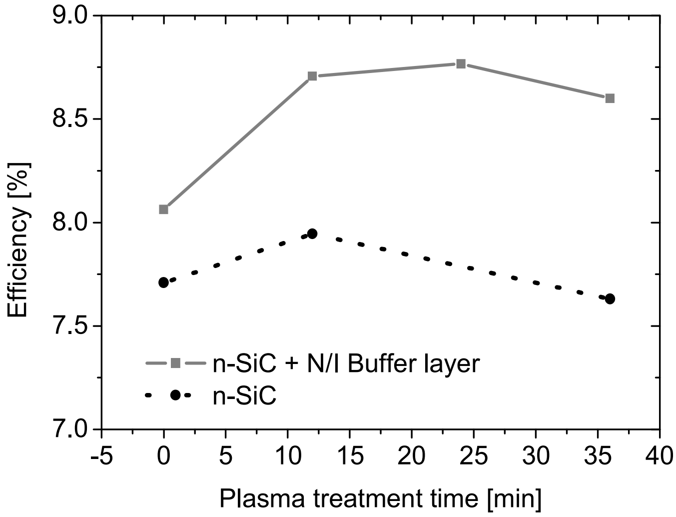

Figure 4-14: Efficiency of a-Si:H solar cell with and without buffer layer at the n/i interface

Table 4-2: Solar cell parameters with and without buffer layer at n/i interface for a 12' surface treatment applied to the substrate

Buffer layer	Yes	No
Efficiency [%]	8.7	8.0
V_{oc} [mV]	895	885
FF [%]	67.6	63.4
J_{sc} [mA/cm^2]	14.4	14.2

The I(V) curve in Figure 4-15 does not resolve the question as to whether the gain in FF is a collection improvement close to the maximum power point, or a reduction of shunts or series resistance. The distinction between these effects is possible with the variable illumination measurements (VIM) [154]. Table 4-3 indicates that the difference in FF loss between the cells is mainly due to series resistance. In fact, the impact on the FF due to shunt resistance (R_{sh}) is negligible for both cells because R_{sh} has an impact on the FF only if R_{sh} < 10 kohm*cm^2, as reported by F. Meillaud [42]. Since both cells have R_{sh} higher than 100 kohm*cm^2, no reduction on the FF is expected. The collection voltage (V_{coll}) is similar for both cells (12.5 compared to 13) and thus has the same FF impact. The series resistance (Rs) differs significantly, 5.3 ohm*cm^2 for cells with the buffer layer compared to 7.8 ohm*cm^2 for the cells without buffer layer. The evaluation then implies a FF reduction of 8.0% and 11.7% compared to ideal case of 75 %, respectively. The difference of 3.7% (11.7 – 8%) almost completely explains the experimental observed value of 4.2% (67.6% - 63.4%) deviation between the two solar cells in Table 4-3.

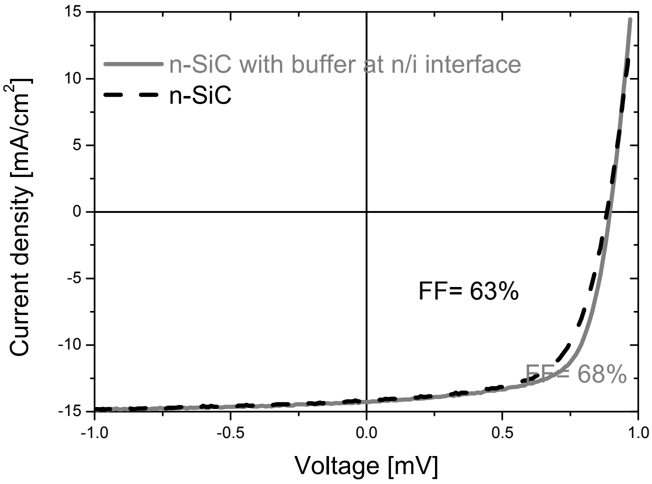

Figure 4-15: IV curve of a-Si:H solar cell with (plain curve) and without (dashed curve) the buffer layer at the n/i interface

Table 4-3: Parameters determined from the variable illumination measurements on cells without and with buffer layer.

Buffer layer	Yes	No
Vcoll [V]	12.5	13.0
Rsh [kΩcm2]	170	1580
Rs [Ωcm2]	5.3	7.8

4.2.2.6 Carbide buffer layer

We also investigate the addition of C to the buffer layer. This is made by adding methane (CH_4) in the plasma during deposition of the layer. Figure 4-16 shows the variation of V_{oc} and FF with increasing the CH_4 flux in the buffer layer on a-Si.H deposited on LP-CVD substrate. The CH_4 increases the FF by a relative value of 1.5, but high fluxes of CH_4 have the opposite effect. Above 3 sccm, the efficiency of the cells is lower than the cell without buffer layer.

Figure 4-17 shows that the collection efficiency of the solar cells is also improving with a carbide buffer layer. The cells are illuminated from the n-side during the EQE measurement in order to assess the effectiveness of the n/i buffer layer. Again deterioration is shown for the higher flux (4 sccm of CH_4). Since the gain in efficiency is less than 2 % with the carbide buffer layer in the initial state, we choose to continue our development with carbon free buffer layer. Indeed, the inclusion of carbon in the i layer or as buffer layer increases the defect density and decreases the solar cell performance by 3 to 5% compared to the cells without carbon, as reported for p-i-n solar cell by R. Platz [151].

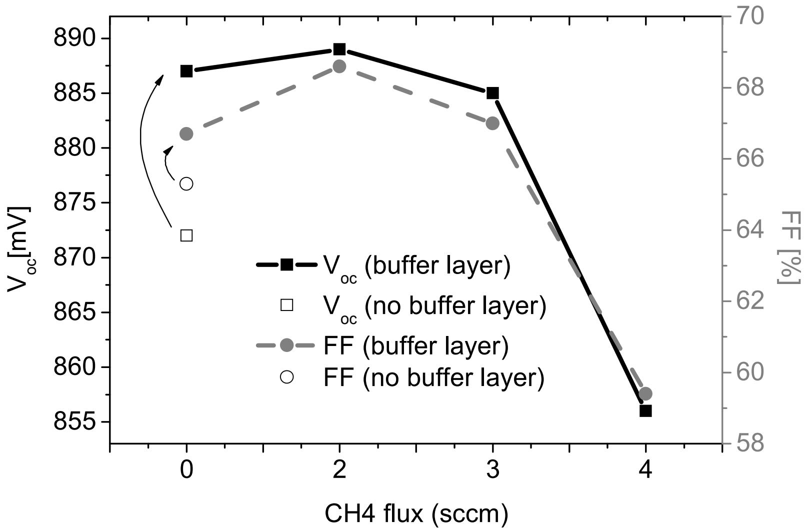

Figure 4-16: Electrical parameters of a-Si:H solar cells deposited on LP-CVD ZnO substrates. The cells are compared with various buffer layers with various levels of CH4 addition (solid symbol). The cell without buffer layer is added for reference (open symbol).

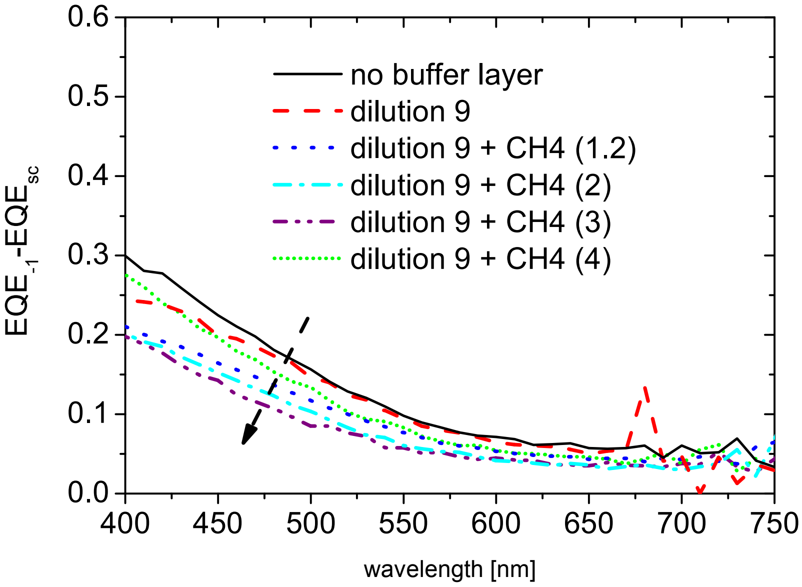

Figure 4-17: Comparison of the collection efficiency from the n-side of an a-Si:H solar cells deposited on LP-CVD ZnO substrates. The methane concentration is varied from 0 to 4 sccm.

4.2.3 Applications

4.2.3.1 Best single a-Si:H solar cells on flexible plastic substrates

Here, we apply the findings of the previous sections to flexible solar cells where the glass substrate is replaced by PEN. We compare a flat PEN + silver + 70 nm ZnO and a flat PEN + silver + textured LP-CVD ZnO as back reflectors, see Figure 4-18. The EQEs are shown in Figure 4-19 where a glass Hot Silver + 70 nm sputtered ZnO is added for reference. The results of Table 4-4 show a relative increase of 20% to 25% in efficiency on the rough substrates compared to the flat substrate. An initial 8.8% efficiency for an a-Si:H on plastic substrates is obtained, compared to 9.2% on glass substrates.

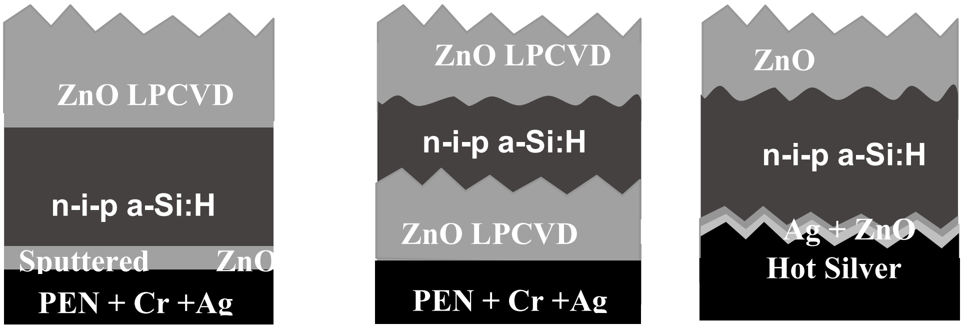

Figure 4-18: Structure of the n-i-p solar cell on plastic with a flat (left) and rough (right) back reflector.

Table 4-4: n-i-p a-Si:H solar cell parameters for different back reflectors: LP-CVD ZnO deposited on plastic coated with thin 80nm Ag/ZnO, LP-CVD ZnO deposited on glass with white paint at the back of the glass, flat PEN and a glass hot silver with LP-CVD ZnO front TCO.

Back refl. Substrates	LP-CVD PEN	LP-CVD Glass	Flat PEN	Hot Silver Glass
J_{sc} [mA/cm^2]	14.3	14.8	12.3	14.2
V_{oc} [mV]	888	889	895	915
FF [%]	70	70	66	69
Efficiency [%]	8.8	9.2	7.3	9.0

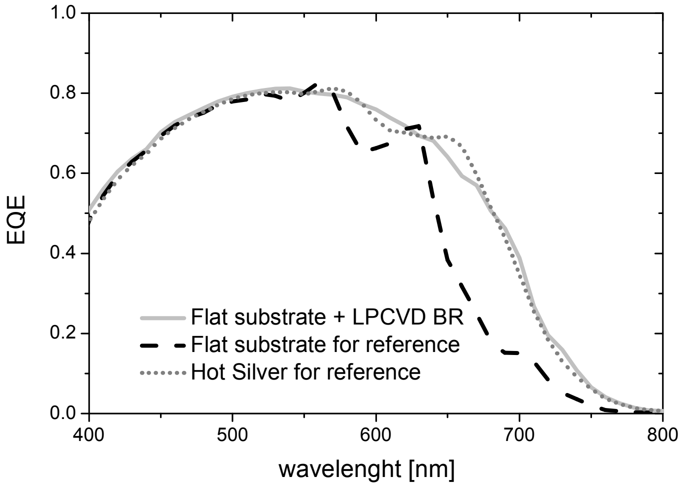

Figure 4-19: EQE of the a-Si:H on flat plastic substrate with LP-CVD ZnO (solid, light grey curve) back reflector and LP-CVD ZnO front contact. The dashed black curve is a flat substrate and the dotted grey curve is the hot silver on glass substrate.

4.2.3.2 Tandem a-Si:H solar cells

An amorphous tandem solar cell is composed of a stack of two a-Si:H cells. The two cells are connected in series. Therefore, the voltage of the subcells is added and the current density is divided between the two subcells. In fact at equivalent total thicknesses, no or minimum gain in the initial solar cell efficiency is expected in the initial state by going to a tandem structure compared to a single junction solar cell because the absorbed light quantity is still limited by the energy band gap. The energy band gap can be increased by adding hydrogen to the plasma [152], by alloying the a-Si:H material (C or O) [151] or by decreasing the deposition temperature [65]. But it is also reported that alloying a-Si:H or reducing temperature deposition increases the defect density and therefore increases the light-induced degradation [29, 65, 151, 155]. Nevertheless, even with identical band gaps, there are advantages in the stable state [156] and at the module level. Indeed, a thicker total absorber layer can be used compared to a single junction solar cell because the electric field is generated twice (once in the top cell and once in the bottom cell). In addition, the tandem structure is advantageous for the efficiency of the modules because it diminishes losses in the TCO. Table 4-5 and Figure 4-20 compare our typical parameter for single and tandem solar cell. The intrinsic layer of the two subcells is identical to the single cell. The initial efficiency is almost identical with 8.8% and 8.7 % with identical structure (white paint/glass/ZnO LP-CVD/Si layers/LP-CVD). If we divide the V_{oc} of the tandem by two and compare it to the single cell, we observe a loss of V_{oc} around 60 mV per cell. Part of the loss is explained by the fact that illumination of each cell is divided by two and the simple diode equation predicts a V_{oc} loss around 20 mV. The remaining losses are attributed to shunts of the top cell because of its thin absorber layer (only 60 nm) and possibly growth induced cracks and losses in the recombination junction. The total J_{sc} of the tandem cell is increased by 1 mA/cm^2 compared to the single cell. This is due to an increase of the total thickness of the absorber from 200 nm for the single cell to 260 for the tandem cell (200 nm for the bottom and 60 nm for the top cell) and a better charge carrier collection thanks to an increase of electrical field in the top cell of the tandem compared to the single junction solar cells.

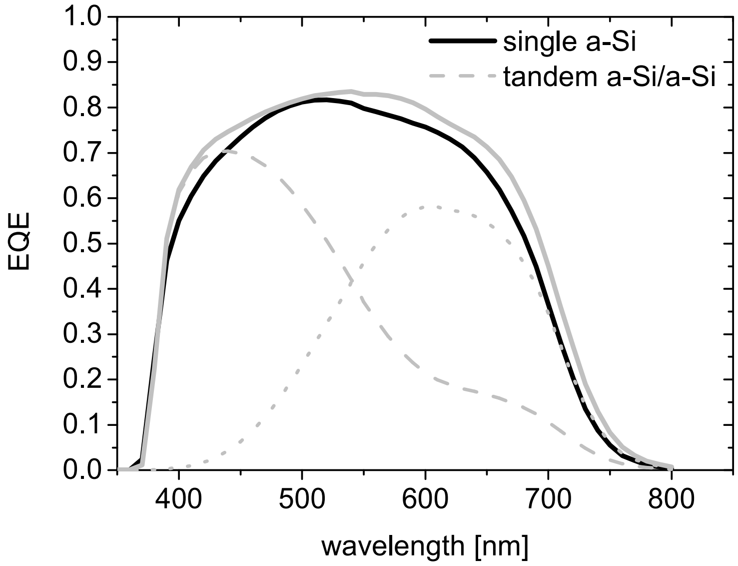

Figure 4-20: EQE of single a-Si:H with absorber layer of 200 nm and tandem a-Si-H/a-Si:H with 200 nm thick bottom cell and 60 nm thick top cell. The back reflector is ZnO LP-CVD on glass.

Table 4-5: Comparison between single a-Si:H with absorber layer of 200 nm and tandem a-Si:H solar cells with 200 nm bottom cell and 60 nm top cell thickness. The value in parenthesis is the J_{sc} of the subcells.

	Single a-Si:H	Tandem a-Si:H
J_{sc} [mA/cm2]	14.4	15.4 (7.6,7.8)
V_{oc} [mV]	899	1660
FF [%]	68	69
Efficiency [%]	8.8	8.7

4.2.4 Degradation of a-Si:H solar cells

In Chapter 1, we have mentioned, the light-induced degradation of amorphous material and its reversible behavior with thermal annealing. This was first evidenced by Staebler and Wronski in 1977 [10]. Furthermore, Yang et al. [157] and Hata et al. [158] reported that the long term stability is governed by the competition between light induced degradation and thermal annealing. Hence, a steady state can be reached. The stabilization procedure considered below exposes the solar cells to 1000h light soaking at 50°C , 50mW/cm^2 and V_{oc} condition.

In a-Si:H silicon solar cells, the degradation depends mostly on the thickness of the absorber layer [159, 160]. In fact, a thinner cell has a higher electric field, hence a higher collection efficiency of the charged carriers. Therefore, the recombination process is limited to the absorber layer. It was reported by S. Benagli et al. [14, 160, 161] that the degradation depends on absorber thickness, buffer layer (close to the p-side) thickness and the substrate morphology for p-i-n a-Si:H solar cells. In Figure 4-21 the effect of the absorber layer thickness is shown in our n-i-p a-Si:H solar cell. Note that in our series, the solar cells do not have any buffer layer close to the p-side nor on the n-side. The degradation of the n-i-p a-Si:H is decreased from 27% to 10% when the absorber thickness is decreased from 400 nm to 140 nm. The optimum cell thickness is around 200 nm in the stable state. The cell with a 140 nm thick layer looses in V_{oc} and this is mostly due to the appearance of shunts in the device, possibly growth-induced cracks on severely textured LP-CVD ZnO substrates. Note that in our cells, the J_{sc} and FF are the parameters that degrade the most significantly. This is not the case for every device made in different laboratories. Indeed, the p-i-n solar cell reported by S. Benagli et al. [160] degrade in V_{oc} whereas our cells have almost no degradation in V_{oc}. In fact, the doping layer can also be influenced by the illumination. For a-Si:H, the doping efficiency is increased when exposed to light soaking which could increase the V_{oc} of the solar cell [22, 162, 163]. Furthermore, Ishikawa et al. [61] shows that the degradation of the solar cell in the V_{oc} can be related to the dilution of the absorber layer. They report that for high dilution (15 to 25) V_{oc} is almost stable or even increases, whereas for low dilution (5-10) V_{oc} decreases. Theses results are not directly comparable to ours because they are obtained at low temperature (110°C) deposition. But, different degradation behavior is observed depending on the deposition condition of the layers. In our case, the cells degrade mostly in J_{sc} by 1 mA/cm2 and in FF by 10 %.

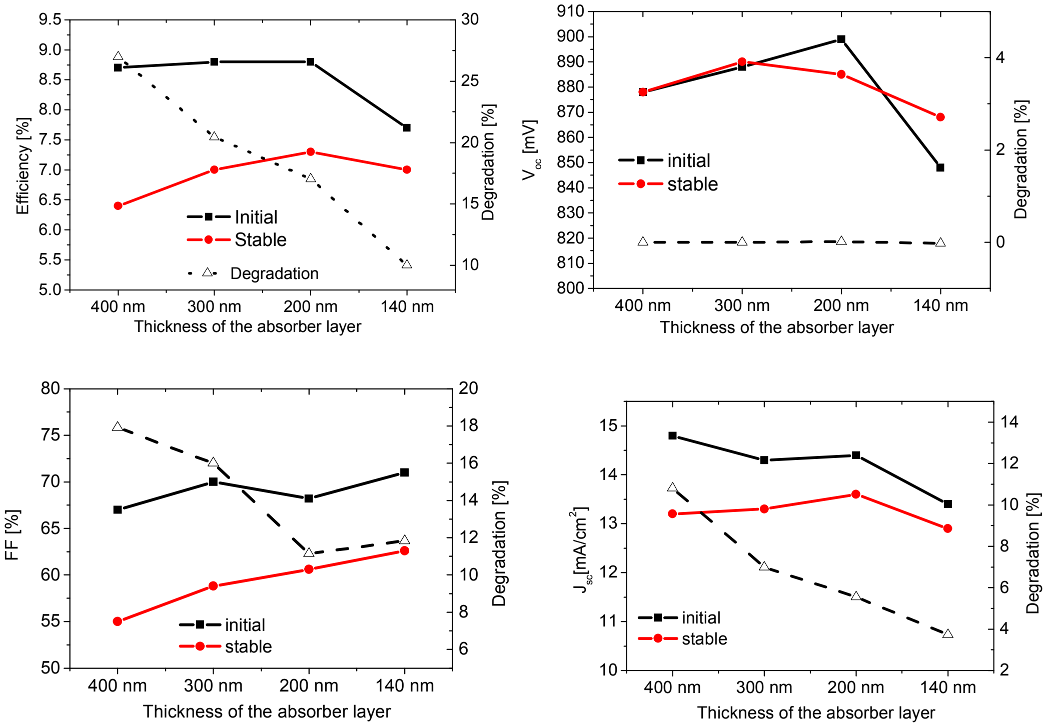

Figure 4-21: Initial (square) and stable (round) parameters for various thickness of a-Si:H absorber layer. The cells are deposited on glass coated with LP-CVD ZnO and treated for 6 minutes. The triangle shows the relative degradation of the cell on the right axis.

Figure 4-22 presents the initial and stable values for single a-Si:H cells deposited on flat substrates, and two textured substrates (hot silver and LP-CVD ZnO). The cells have a thickness of 270 nm (same deposition time) and do not include any buffer layers. In addition we add the results for a tandem cell to a 300 nm bottom cell and a 80 nm top cell deposited on LP-CVD ZnO. For single junction solar cells, the substrate texture tends to limit the degradation. Indeed, the degradation is 25% for a flat substrate and only 20% on the highly textured ZnO LP-CVD. On the hot silver substrate, the light-induced degradation is also 25%, as same the flat substrate case. In fact, the effective thickness of the absorber layer is thinner on a highly textured substrate, justifying the lower degradation. Hence, the effect of the texture is reinforced in the stabilized state.

The next step in reducing the degradation of the a-Si:H solar cells is to choose tandem devices. The results in Figure 4-22 show that the degradation is reduced to 15% for a cell with a total absorber thickness of almost 400 nm, whereas the degradation for a single solar cell of 400 nm is 27% as shown in Figure 4-21. This confirms the advantages of the a-Si:H tandem cell in the stabilized state.

Our best stabilized efficiencies after 1000h of light soaking are 7.3%, and 7 % for single a-Si:H on glass and on plastic substrates, respectively, and 8% for tandem cells on glass substrates.

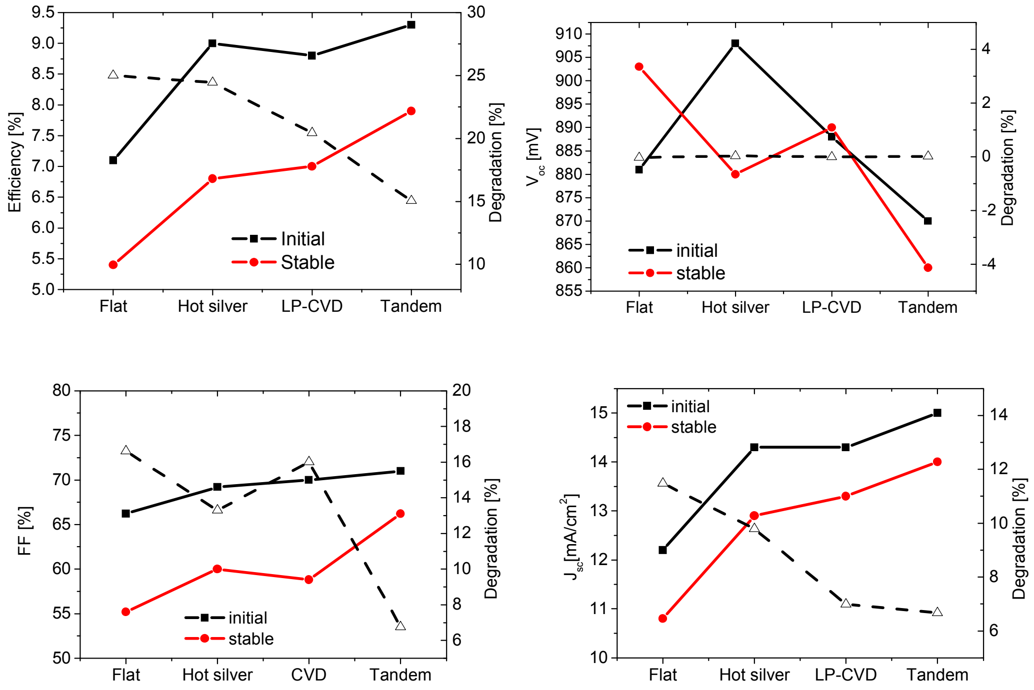

Figure 4-22: Initial (square) and stable (round) parameters of a-Si:H solar deposited on flat, hot silver, PEN/ZnO LP-CVD. The single a-Si:H cells have a thickness of 270 nm. The tandem a-Si:H has 300 nm bottom cell and 80 nm in the top cell, and was prepared by O. Cubero and presented in [164].

4.3 Discussion

Our results show that, even for simple single-junction a-Si:H devices, a complex interplay between substrate morphology, chemistry and subsequent n-layer takes place. It has been shown in the past that a-Si:H cell is sensitive to the substrates morphology [144] and that thin microcrystalline layers are sensitive to the substrate chemistry [137]. We show, that by using systematic variation of the substrate geometry that it is also sensitive to the morphology of the substrate. We think that the sensitivity of the n-μc layer comes from growth competition between adjacent grains. The valley of the sharp V-shape texture of LP-CVD ZnO results in a defective material, which increases the defect density at the n/i interface and results in the formation of voids and cracks in the amorphous material as shown in the TEM micrographs and reported elsewhere [101, 165, 166]. For p-i-n μc-Si:h cells, M. Python et al. [167] describe in detail how these defective regions affect the performance of the solar cell. Presumably, the density of electric defects is enhanced, and they may act as contamination routes and shunting paths. In contrast, we see that on flat or smooth substrates a high V_{oc} of 890 mV can be achieved, and the micrograph on the flat substrate shows a uniform deposition without voids of the µc-n and of the subsequent layers. Thus, a n-µc can be an efficient doped layer for flat substrates but not for textured substrates because strong V_{oc} reduction is observed.

Our solution to avoid V_{oc} losses on textured substrates is to utilize an amorphous n-SiC layer, which is less sensitive to the substrate morphology and material. Furthermore, the n-SiC layer achieves very good results on textured substrates. We demonstrate that high V_{oc} (over 900 mV) can be achieved with a low dilution intrinsic layer ($[H_2]/[SiH_4] = 2$). By simulation of a p-i-n device, Y. Poissant has compared n-µc and amorphous n-layers in single junction a-Si:H solar cells [123]. They reported that they are equivalent in the solar cell even though the activation energy of n-µc layers can be strongly reduced down to 0.03 eV. Here, we show experimentally that the n-SiC layer can have advantages compared to amorphous and microcrystalline doped layers. Indeed, the higher gap diminishes the optical losses in the doped layer and the band alignment can be favorable for the V_{oc}. Figure 4-23 illustrates the band alignment for n-µc and n-SiC layers. The gap of the microcrystalline material is assumed to be 1.1 eV and it has low activation energy of about 0.02 eV. On the other hand the carbide n-layer has a larger gap (1.9 eV) and a higher activation energy of 0.4 eV, which is extracted from our optical and electrical measurements. We assume for n-µc as reported in [123] similar band discontinuities with a-Si:H absorber layer. For the n-SiC, we assume that they are distributed between the valence and the conduction band, but it is so far not possible to distinguish to what extent. This might create a barrier for the holes and the electrons in the valance and conduction bands, respectively. We suggest that the blocking barrier in the valence band could repel the holes from the defective interface area and reduce retrodiffusion of the holes in the doped n-layer and thus enhance the collection of the charge carriers. A similar thinking applies to the simple n-aSi layer, which has a reduced bang gap compared to the absorber layer as shown by the ellipsometry data in Figure 4-12.

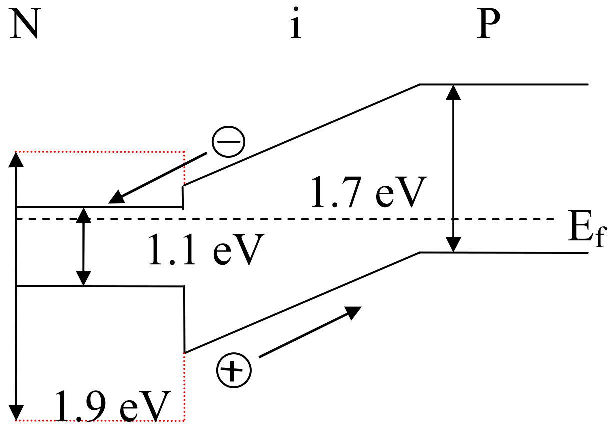

Figure 4-23: Band diagram of a n-i-p solar cell with n-SiC (dashed lines) and microcrystalline n-layer or a-Si:H n-layer (solid lines).

The limitation of high quality thin film silicon solar cells is often dominated by the quality and structure of its interfaces. Here, the efficiency of the n-i-p solar cell is enhanced by a buffer layer at the n/i interface, from 7.9% to 8.8%. The buffer layer is highly diluted with H_2, which promotes the growth of material with a better quality and a higher band gap [136, 152, 153]. The buffer layer slightly improving the V_{oc} and mainly reduces the series resistance of the a-Si:H solar cell, and thus improves the FF of the a-Si:H solar cell. We assume that the higher energy band gap of the buffer layer reduces the band discontinuity in the conduction band previously mentioned, and thus enhances the collection of the electrons close to the n/i interface. In Figure 4-24, we represent the band diagram of the n-i-p stack with n-SiC layer. We include (dashed line) the effect of the buffer layer with a higher band gap, the effect is exaggerated for the sake of clarity. Based on previous work on the p/i interfaces [168-170], we assume that the increased buffer band gap is reported in the conduction band. The buffer layer reduces the barrier for the electrons and thus reduces the series resistance of the cell which is observed experimentally in section 4.2.2.5. A similar buffer layer at the n/i interface has been studied in the pin case by Sakai et al. [168] but without significant improvements. The discrepancy between their observations and ours could be explained because they use a carbon free amorphous n-layer and thus no barrier was created at the n/i interface.

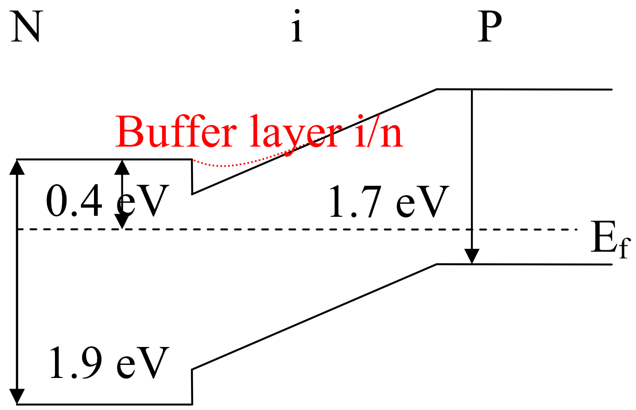

Figure 4-24: Band diagram of a n-i-p solar cell before (solid lines) and after the introduction of a highly diluted buffer layer (dashed line)

The contact between the carbide n-SiC layer and the ZnO potentially introduces a high series resistance in the solar cell. A solution already exists for the p-i-n case [171] where the best contact with the ZnO/TCO is accomplished with a microcrystalline n-doped layer. We show that microcrystalline n treatment provides a good contact in the n-i-p configuration. The drawback of this double n-layer (n-μc + n-SiC) is the optical loss due to the increase thicknesses of the total doped layer. This has only minor consequences. First of all because the n-μc layer is thin, the deposition time is being kept shorter than or close to incubation time. Secondly, the absorption coefficient of a microcrystalline layer is small for the light that reaches the n-layer, at a wavelengths between 550-800nm. In addition, the higher energy gap of the n-SiC layer limits the losses in the second doped layer. In fact, the absorption losses will be, in a simple n-aSi, 3 to 4 times higher compared to the n-SiC. Indeed from the extinction coefficient of Figure 4-12 (k = 0.12 for n-aSi and k = 0.03 for standard n-SiC at a wavelength of 600 nm), the absorption calculated with the Lambert-Beer law that is 8 % for two straight passes in the n-aSi, whereas only 2 % is absorbed with an n-SiC (assuming a 15 nm thick n-layer).

This development on glass substrates is transferred on plastic with a novel possibility of back reflector structure where the roughness is obtained by the LP-CVD ZnO (PEN/Ag/LP-CVD/n-i-p/TCO). This development gives valuable insight into the effect of the substrate texture on optical and electrical properties of n-i-p solar cells. In addition, it reduces the texture mediated plasmon absorption [101, 104, 172] in the metallic back reflector and thus diminishes the optical losses. However, thanks to the LP-CVD ZnO, it supplies a sufficient amount of roughness for an efficient light in-coupling in the absorber. Similarly, it has been reported in a p-i-n solar cell [70] that the configuration with a smoothed metallic back reflector has optical advantages compared to a rough back reflector. Nevertheless, for an industrial application the goal would be to have a texture embossed in the PEN and then deposited silver and a thin 70 nm ZnO as the back reflector. Our preliminary results show that these structures can provide sufficient light trapping. We achieve initial efficiency of 8.1% with 14.5mA/cm^2, 871mV and 64% of FF but further development is needed in order to incorporate the correct morphology found here directly in the plastic without introducing shunts in the a-Si:H solar cells.

The degradation of the a-Si:H cell is a complex issue and a complete picture of these effects is not yet established. Here, the results show that when material and interfaces are controlled and for our temperature constraint, the cell thickness is the parameter that can limit the degradation. Therefore, the texture of the substrate, which allows for a effective thickness reduction, is key for improving the stabilized efficiency in a-Si:H single junction solar cells.

4.4 Conclusion

This chapter reports on the achievement of simultaneously high J_{sc} and V_{oc} on textured substrates and the optimization of a n-i-p a-Si:H solar cell on flexible substrate. We develop substrate morphology for light trapping and a cell design that simultaneously maintains high V_{oc} and FF. We show that for optimum light trapping the morphology of the substrate is more important than the feature size or rms. Physically, it means, according to the scalar scattering theory, that the angular distribution of the scattered light is more important than the rms for the light trapping. In addition, the benefits of an amorphous carbide n-layer are fully implemented in the a-Si:H solar cell on PEN substrate with the demonstration of an initial 8.8% and stable 7% efficiency, for an intrinsic layer thickness of 270nm. By reducing the thickness of the absorber layer we could increase the stabilized efficiency up to 7.3% and by introducing the tandem design, the stabilized efficiency is increased up to 8.0%.

Chapter 5: Front TCOs and back reflectors

Light in-coupling and optical properties

5.1 Introduction

In this chapter, we discuss the choice of front TCO and back reflectors for n-i-p thin film silicon devices. We have seen in the previous chapters that the first challenge is to increase the J_{sc} of the device by introducing light trapping techniques without changing the other parameters. By doing this, the cell thickness can be reduced leading to a reduction of the light-induced degradation effects and, eventually, to more effective cycle times in production for a-Si:H and µc-Si:H. It is usually assumed that for an efficient light trapping design, the substrate textures should be in the dimension range of the incoming light wavelength. The strategy used in the p-i-n configuration is to deposit a rough front TCO with random [173] or periodic [174] structures, which will scatter the light in the absorber layer and result in an increased light path in the absorber. State-of-the-art light trapping designs are reported without detail by the company Kaneka [175], and more detail is given by the research groups of Jülich [121, 176] and Neuchâtel [177, 178]. They all use random structures and the typical values of J_{sc} are 15 mA/cm^2 for 180 nm a-Si:H absorber and 26 mA/cm^2 for 3 µm microcrystalline absorber as described by D. Dominé et al. [116, 177], May et al. [121] and Saito et al. [79].

In the n-i-p configuration, the strategy relies on the textured back reflector which provides texturation for the next deposited layers as shown on the previous chapters and reported by United Solar [44, 178]. The optimum morphology of the back texture is still not clear and it is not yet confirmed whether the best substrate should have a periodic or random structure. Also, there is a trade off between suitable texture for light scattering and the losses in the back reflector, which come from surface plasmon absorptions in the rough metallic layer [172, 179].

Strong efforts are made in optical modeling with the aim of predicting the light trapping power of optical designs. Given the size of typical light trapping structures, the optical system is at the frontier between geometrical and nano optics, and usually when modeling the random structures semi-empirical theories are applied such as “scalar scattering theory” [115]. This approach has been implemented in different simulation programs, e.g. by Krc et al. [148, 149], Zeman et al. [106] and Springer et al. [180]. Another approach is to use periodic structures where exact solutions of the Maxwell’s equations have been performed by Heine and Morf [69]. In addition, numerical solutions of the Maxwell’s equations have been performed with success by Stiebig and Haase on periodic and quasi periodic substrates [181, 182] and random substrates have been studied by Rockstuhl et al. [183]. However, typical devices with roughness structures and thicknesses of the layers in the range of the incoming light wavelength still remain complicated to analyze either because of over simplified assumptions or because of the difficulties of performing exact numerical simulations for complex systems. Thus, the predictive power of these models is still limited.

Our experimental investigations of this chapter address the interaction between back contact structures and textured or nominally flat front contacts, including the effect of the thin film silicon absorber layer that is sandwiched between the two. We compare two transparent conductive oxides (TCOs) as a front contact; the first one is a flat thin ITO layer and the second one is a rough thick LP-CVD ZnO. The TCOs are applied to various devices and substrate structures: in particular we consider the case of thin a-Si:H and thick μc-Si:H devices. We find that the optimum dimension of the substrate texture is different for the two types of cell, not only because the light trapping region is increased toward the near IR part of the spectrum for the μc-Si:H, but also because the optical couplings in a system with a thin a-Si:H (250 nm) absorber and a thick (2 μm) microcrystalline μc-Si:H are completely different. Thus, the combination of front contact and substrate structure is studied and interpreted for a-Si:H and μc-Si:H.

5.2 Experimental

The study is carried out with two different substrates. The first is a 2D periodic grating on poly-ethylene-naphtalate (PEN) covered with Ag/ZnO, as described in Chapter 2 which is well suited for micromorph or μc-Si:H cells as shown in Chapter 3. The structure has a root mean square (rms) roughness of 70 nm and lateral dimension of 1.2 μm, cf. Figure 5-1 (A and B). The second substrate consists of a random pyramidal structure that is made of LP-CVD ZnO and which provides high current for single a-Si:H junction solar cells, cf. Figure 5-1 (C and D). The feature size of the LP-CVD ZnO can also be adapted for the light trapping in μc-Si:H or multiple-junction cells by increasing the grain size. In this work, typical rms and lateral dimension are 70 nm and 360 nm for a-Si:H solar cells and 140 nm and 1 μm for μc-Si:H solar cells, respectively. The back reflector on glass substrate is a white paint applied at the back of the 0.7 mm thick (Schott AF45) glass.

The transparent front electrodes are zinc oxide (ZnO) deposited by low pressure chemical vapor deposition (LP-CVD) [145] (Figure 5-1(A and C)) or indium tin oxide (ITO) deposited by DC sputtering at room temperature (Figure 5-1(B and D)). The ZnO is doped with boron and its deposition conditions result in a textured surface with rms roughness of about 70 nm for standard 2 μm thick layers. The ITO is deposited nominally flat, and it has a thickness of 70 nm in order to achieve an antireflection condition with the Si absorber centered at $\lambda_0 = 550$ nm. The total transmission (T), diffuse transmission (DT), and total reflection are measured with a photo-spectrometer (Perkin Elmer lambda 900) with integration-sphere within a spectral range of 350 nm to 2000 nm. The absorbance (A) is calculated from T and R with A=1-T-R. The measured samples are

TCO/glass with the light first entering through the TCO. For the rough ZnO, the measurement is also performed with a thin film of index matching liquid di-iodomethane (CH_2I_2). It removes the effect of the rough interfaces during transmission and reflectance measurements as described by J. Steinhauser et al. [184].

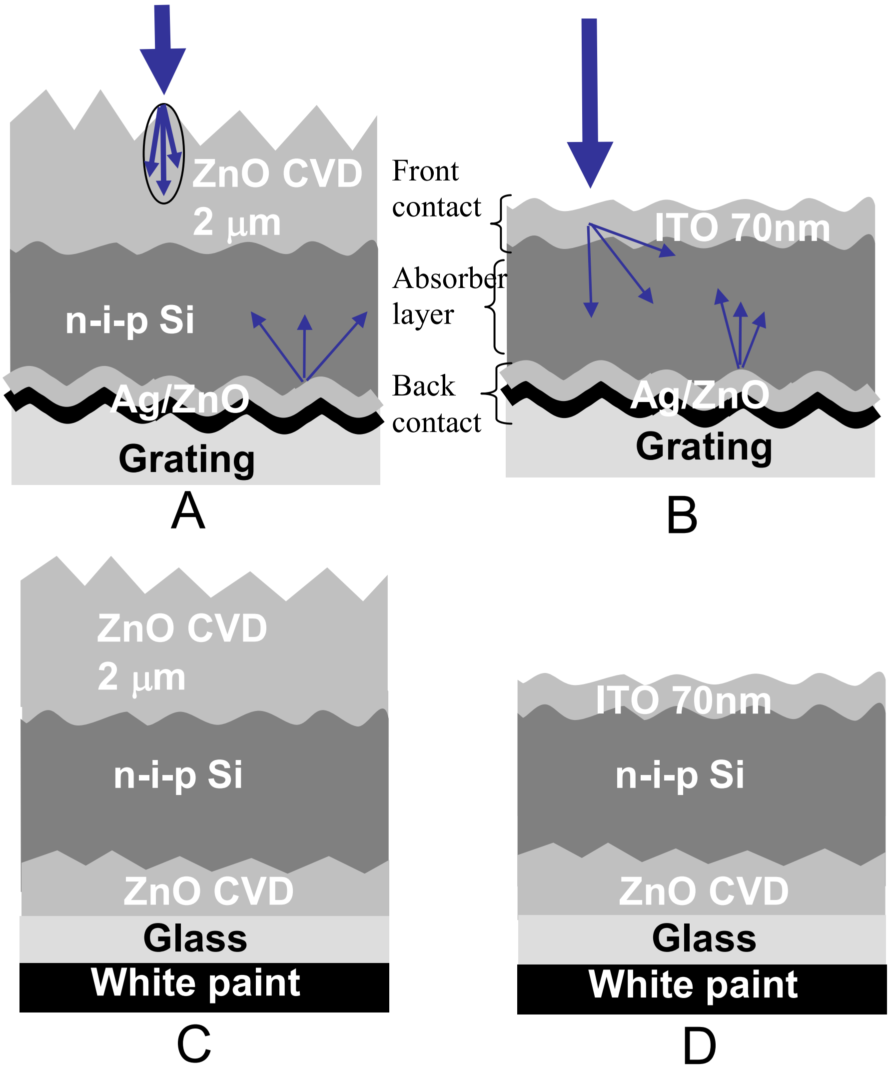

Figure 5-1: Schematic illustration of the four different designs used in this paper. Two substrates used and two front contacts are in a-Si H and μc-Si:H solar cells. A and B are plastic substrates with a periodic texture: 2D cross grating covered with 100 nm of silver and 60 nm sputtered ZnO. C and D are glass substrates covered with random texture: rough LP-CVD ZnO and white paint is used as back reflector. A thin 70 nm ITO front contact is used for B and D and 2 μm thick LP-CVD ZnO for A and C.

5.3 Results

5.3.1 Textured ZnO and flat ITO on glass

Figure 5-2 shows the T, R and A curves of the ITO and LP-CVD ZnO with CH_2I_2 on glass. The absorbance of the ZnO film with CH_2I_2 and of the layer of ITO is below 3% for all the wavelengths between 400 to 1100 nm. The difference in T and R is due to the different optical systems: 2 µm thick ZnO and thin 80 nm ITO films. Hence in Figure 5-2 interferences appear for the thin flat ITO. The Figure 5-3 shows that, when no matching liquid and cover glass is used, the textured ZnO provides diffuse transmittance, which is negligible in the case of ITO and of ZnO measured with CH_2I_2. The rough interface of the ZnO leads to an increase in the absorbance and in the reflection between 400 to 600 nm as shown in Figure 5-3. Enhanced absorption is attributed to light trapping in the 2 µm thick ZnO due to scattering of the light at the air/ZnO interface and internal reflection between the glass/air and the ZnO/air interface. It enhances the path of the light in the ZnO and increases absorption due to residual optical defects and mostly free carrier absorption, whereas the reflectance is increased because incident angle of the light on the flat ZnO/glass interface is increased [185]. This TCO/glass structure does not give direct information on the optical behavior in the solar cell (TCO/Si) because light trapping due to total internal reflection will only moderately take place for the TCO/Si interface ($n_{Si} > n_{TCO}$, which is different from $n_{TCO} > n_{glass}$ at the TCO/glass interface).

Note, that the haze (DT/T) in air of the textured ZnO is 85% at 400 nm and only 12% at 800 nm. The scattering power of the LP-CVD ZnO is famous for having exceptional light scattering properties [20] at the Si/TCO interfaces but the textured ZnO is, in air, limited for the infra-red part of the spectrum, which is crucial for elevated light trapping in thin film silicon solar cells. In fact, the effective wavelength of the light λ_0 is higher in air (λ_0) than in Si (λ_{Si}). The relation between the two effective wavelengths is given by the difference in refractive index where λ_{Si} is approximately four times smaller than λ_0 and two times smaller than λ_{ZnO}. In the scalar scattering theory, the haze (eq 2.6) depends exponentially on the refractive index difference of two media and inversely to the effective wavelength. Therefore, a high haze is obtained with low effective wavelength and high refractive index contrast. This is not the case for the ZnO in air but this is really the case in Si because the haze is over 60% for the full spectrum needed (400 – 1100 nm) as shown by D. Dominé [19, 116].

Therefore, the roughness of the top contact should be less important in n-i-p solar cells than for p-i-n solar cells. The measurements confirm this idea in the next sections.

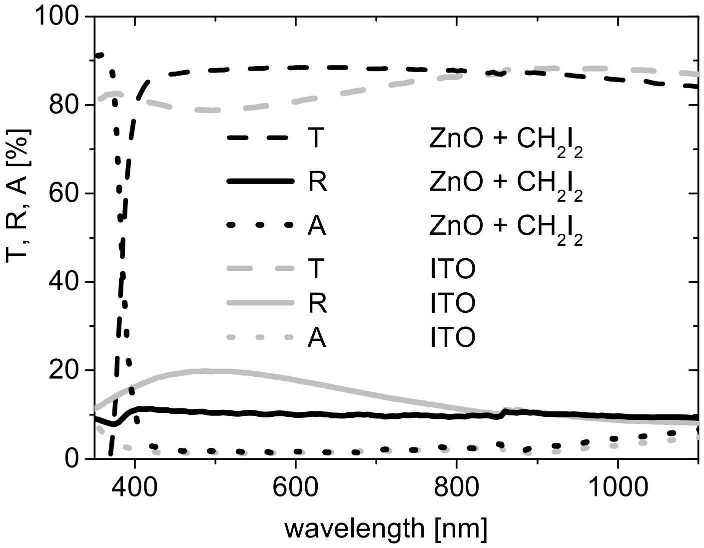

Figure 5-2: T, R and A of a flat 80 nm ITO on glass, 2 µm thick ZnO LP-CVD on glass measured with CH2I2 index matching liquid.

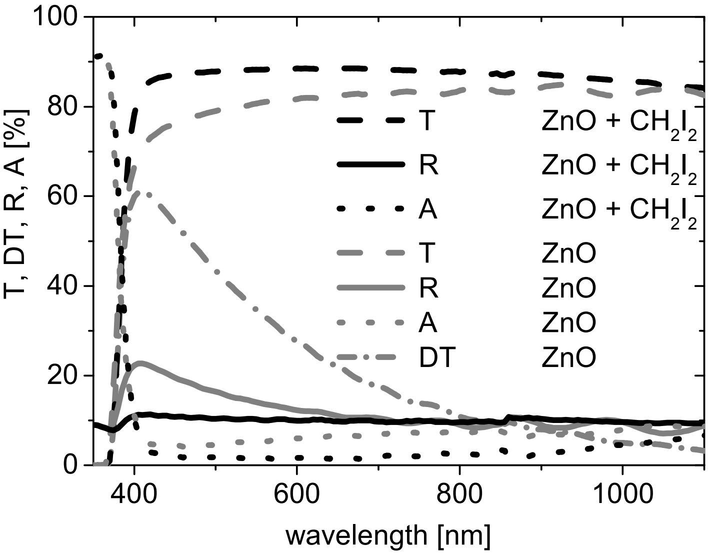

Figure 5-3: T, DT, R and A for 2 µm rough ZnO LP-CVD layer on glass and for LP-CVD ZnO on glass with CH_2I_2 index matching liquid.

5.3.2 ZnO and ITO as front contacts in thin absorber cells

In Figure 5-4, we compare the EQE of an a-Si:H solar cell with a 250 nm thick absorber and two different front TCOs (a rough thick front ZnO and a thin flat ITO) deposited on flat substrates for reference and on the 2D periodic substrate (70 nm rms). The J_{sc} on flat substrates for both front TCOs is almost unchanged with 12.2 and 12.3 mA/cm^2 for ITO and ZnO, respectively. However, the EQE of the cell with ZnO is higher at wavelengths above 600 nm, whereas the EQE with ITO is higher between 450-550 nm thanks to its antireflection effect with silicon. On the periodically textured substrate, we observe a current enhancement of 9 % with ITO and 17 % with LP-CVD ZnO, compared to the flat substrate. Compared to the thin ITO front contact, the enhancement with the textured ZnO front contact is mostly obtained for the red part of the spectrum (over 600 nm) as shown in Figure 5-4. The IQEs of the cells deposited on the periodic grating are equal, indicating identical properties of the absorber layer and no additional absorption effects in the inactive device layers. Hence, the rough front ZnO yields true enhancement of light trapping in the infra red part of the spectrum compared to the thin flat ITO.

In Figure 5-5, we compare the same flat ITO and the 2 μm thick LP-CVD ZnO as a front TCO, but with LP-CVD ZnO back contact deposited on glass substrate with a feature size of 0.36 μm optimized for a-Si:H. In this case, The results show that there is an advantage in using a flat front ITO with 3% relative increase of J_{sc}. Figure 5-5 shows that the antireflection effect of 70 nm of ITO at 550 nm increases the response compared to the case of thick front ZnO, whereas the EQEs in the light trapping region (600-800 nm) are similar. The IQEs are completely matched and confirm that the difference between the two TCOs is mostly due to reduced primary reflection losses at the antireflection condition of the ITO (500-550 nm).

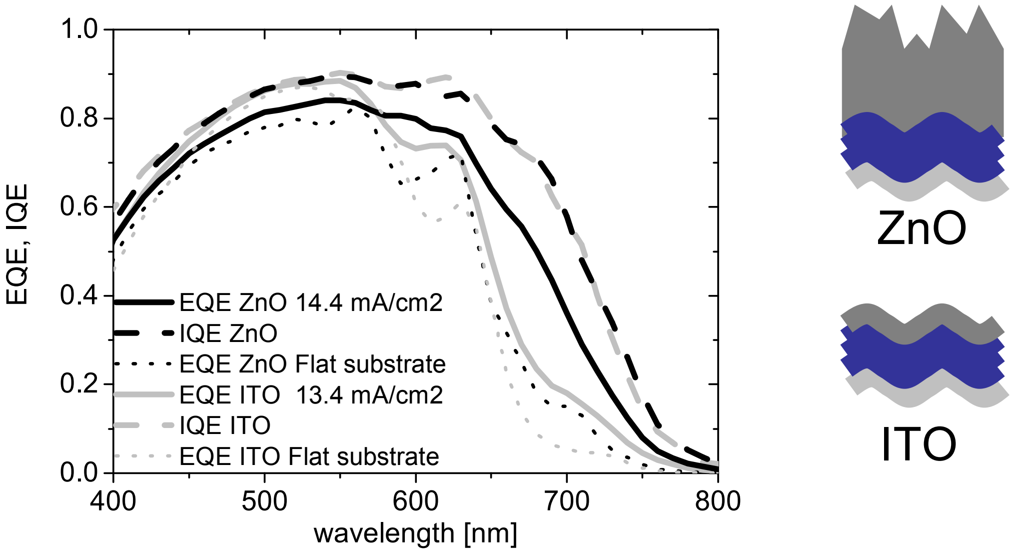

Figure 5-4: Comparison between flat ITO and rough LP-CVD ZnO front contacts with a-Si:H solar cell deposited on a 2D grid substrate and flat substrates for reference.

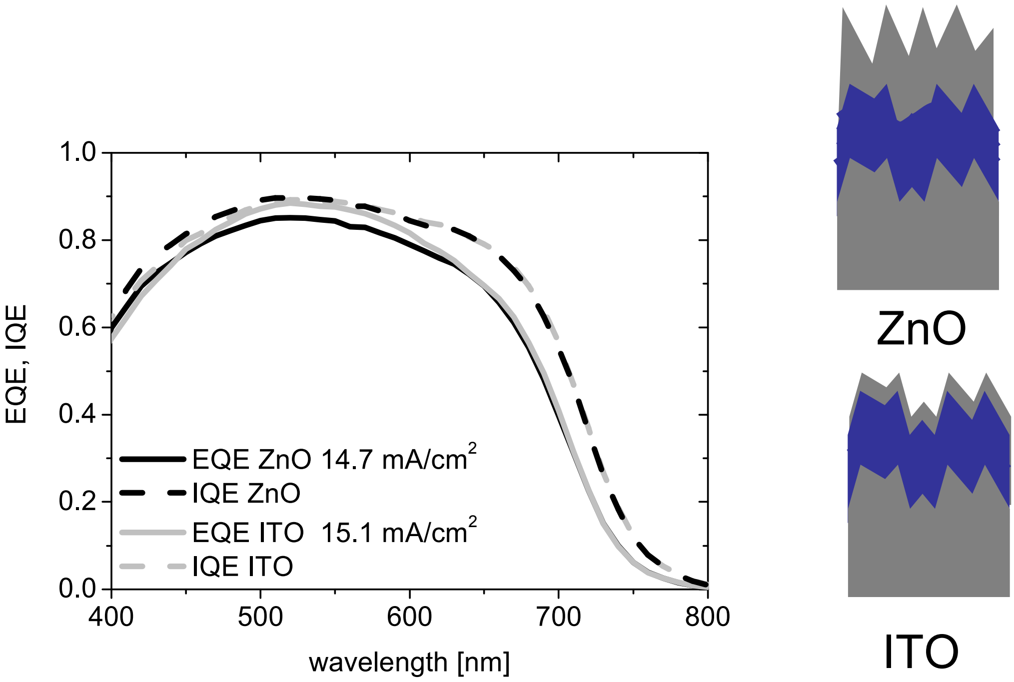

Figure 5-5: Comparison between flat ITO and rough LP-CVD ZnO front contacts with a-Si:H solar cell on LP-CVD ZnO substrates.

5.3.3 ZnO and ITO on thick absorbers

In Figure 5-6, we compare flat thin ITO and rough thick ZnO on top of a 1.6 μm thick μc-Si:H single junction solar cell. The substrate is the 2D periodic grid, which provides high J_{sc} in μc-Si:H solar cells and is identical to the one used in section 5.3.2 or in [186]. Note that, in contrast to the amorphous case of section 5.3.2, the features of the ZnO pyramid substrates are adapted to the μc-Si:H cell; their typical lateral size is now 1 μm and the rms roughness is 140 nm. Compared to the rough LP-CVD ZnO front contact, the ITO provides higher current (4% relative increase). The antireflection effect of the 80 nm ITO at 600 nm increases the spectral response in a wavelength with high photon flux under AM 1.5g illumination. In the IR part of the spectrum, the response is similar for both TCOs and this suggests a different optical behavior from the a-Si:H case on the 2 D periodic substrate. The shape of this EQE for rough front ZnO is linked to interference effects. In the IQE these effects should disappear, but, as the EQE and the reflection measurements are performed with two different setups, apparent interferences still remain in the IQE, though strictly speaking they are artifacts. In Figure 5-6, a flat substrate with a ZnO LP-CVD front contact is added for reference. The gain with the periodic substrate compared to the flat is almost a 30% relative increase, mostly in the infra red part of the spectrum. Note that the difference in the blue part is due to different p layer thicknesses.

We observe the same results for single junction μc-Si:H solar cells deposited on LP-CVD ZnO substrate on glass [187], i.e. the ITO front contact provides a relative gain of 4 % compared to the LP-CVD ZnO front contact. We also evaluate the TCOs on a triple junction a-Si:H/a-Si:H/SOIR/μc-Si:H with 80 nm, 300 nm for the a-Si:H cells and 1.2 μm thick μc-Si:H silicon solar cells, respectively. Additionally, the triple cell structure includes a 80 nm thick SiO_x intermediate reflector (SOIR) [188] between the middle and bottom cells. Compared to the rough LP-CVD ZnO front contact, the ITO provides higher current, just as in the μc-Si:H case and we see from Figure 5-7 that most of the gain is in the a-Si:H middle cell. The increase in J_{sc} is around 5 % (5.7 to 6.0 mA/cm^2). This effect is important in triple junction cells with two purely amorphous Si cells since the J_{sc} is limited by the absorption coefficient of the amorphous Si material. Figure 5-7 illustrates clearly the difficulties of matching the current of the three solar cells. The amorphous cells have 6 mA/cm^2 each and the μc-Si:H has 9 mA/cm^2. Table 5-1 summarizes the J_{sc} of all cell structures shown.

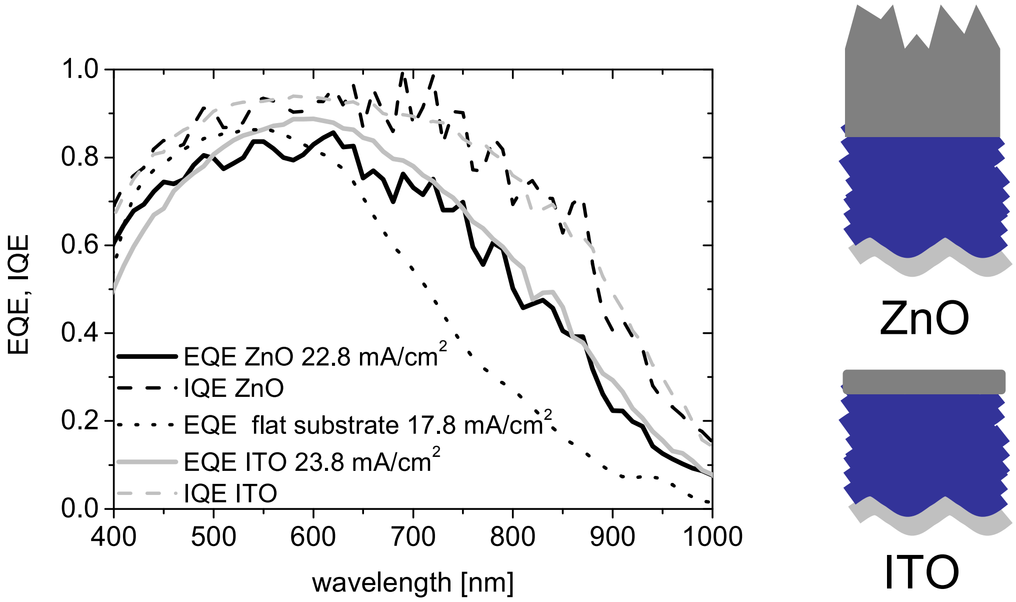

Figure 5-6: Comparison between flat ITO and rough LP-CVD ZnO front contacts with μc-Si:H solar cell on 2D periodic grid and flat substrates for reference.

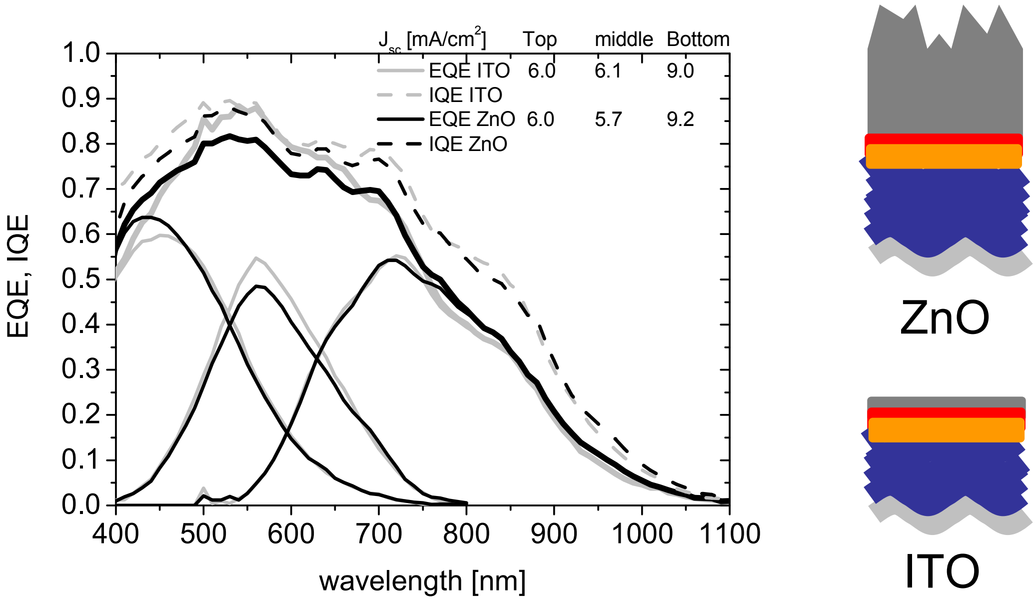

Figure 5-7: Comparison between flat ITO and rough LP-CVD ZnO front contacts with triple junction a-Si:H/a-SiH/μc-Si/H solar cell on LP-CVD ZnO substrate.

Table 5-1: Summary of J_{sc} for the a-Si:H and μc-Si:H cells deposited on the periodic grating and the random LP-CVD ZnO. The front contact is either a thin flat ITO or a thick textured ZnO LP-CVD. The grating and flat substrate are coated with 100 nm Ag and 60 nm ZnO as back contact. Cells on LP-CVD ZnO back contact are measured with white paint added at the back of the glass as a back reflector.

Structure Figure 5-1	Substrate texture	Feature size [µm] / roughness [nm]	Absorber thickness [µm]	Front TCO	J_{sc} total [mA/cm^2]
A	Grating	1.2/70	a-Si:H/0.27	ZnO	14.4
B	Grating	1.2/70	a-Si:H/0.27	ITO	13.4
C	ZnO	0.36 / 70	a-Si:H/0.27	ZnO	14.7
D	ZnO	0.36 / 70	a-Si:H/0.27	ITO	15.1
Flat	-	-	a-Si:H/0.27	ZnO	12.3
Flat	-	-	a-Si:H/0.27	ITO	12.2
A	Grating	1.2 / 70	µc-Si:H/1.6	ZnO	22.8
B	Grating	1.2 / 70	µc-Si:H/1.6	ITO	23.8
C	ZnO	1.0 / 140	Triple/1.1	ZnO	20.9
D	ZnO	1.0 / 140	Triple/1.1	ITO	21.1
Flat	-	-	µc-Si:H/1.6	ZnO	17.8

5.3.4 Electrical comparison between ITO and ZnO layers

The ITO has a sheet resistance of 30 Ω_{sq} and the thick LP-CVD ZnO has a sheet resistance below 10 ohmsq, for thicknesses of 70 nm and 2 µm, respectively. At the module level it means that silver fingers or reduction of the width of the solar cell between the interconnection can be necessary for ITO, depending on the current density of the cells as discussed by Brecl et al. [189]. In Table 5-2, we report typical electrical parameters for amorphous cells and triple junction solar cells with thick ZnO front contacts and thin ITO front contacts, corresponding to the case of Figure 5-1, C and D, respectively. The effect of the different sheet resistances is not reflected in the FF because the cell area is kept small. The difference in FF in the triple junction solar cell is attributed to different current mismatch of the three cells. Indeed, the measurement of such a cell is certainly a difficult issue because of the current matching of the three cells, and hence the FF is strongly sensitive to deviations of the solar simulator spectrum from the AM1.5g spectrum. Furthermore, a V_{oc} reduction between 20 to 30 mV is observed for the flat ITO for single and triple junction solar cells. This is attributed to the non optimized p/ITO interface, which needs further optimization as reported elsewhere [165]. In addition, we also cannot exclude that during the deposition of ITO, the sputtering does not damage the thin p layer.

Table 5-2: Solar cell parameters of a-Si:H and triple solar cells a-Si/a-Si/µc-Si with thin ITO and thick LP-CVD ZnO front contact. The cells are deposited on LP-CVD ZnO back contact with the feature size adapted for a-Si:H (360 nm, first two lines) and µc-Si:H (1 µm, last two lines).

	V_{oc} [mV]	FF [%]	J_{sc} [mA/cm^2]	Efficiency [%]	
ZnO Single a-Si:H	864	66	14.7	8.4	Fig 1 C
ITO Single a-Si:H	835	66	15.1	8.3	Fig 1 D
ITO Triple	2126	67	6.0	8.5	Fig 1 D
ZnO Triple	2157	64	5.7	7.9	Fig 1 C

5.3.5 Index matching layer of the back reflector: ZnO

A thin ZnO layer is often used between the metal and silicon layer [46]. The purpose of this layer is two-fold. It is a barrier layer that protects the silicon layer from diffusion of the metallic atoms into the silicon layer and it acts as an optical matching layer between silicon and the metallic layer [190]. The results in Figure 5-8 and Table 5-3 show a μc-Si:H solar cell deposited on hot silver covered with various thicknesses of ZnO. It shows that the thicker the ZnO layer, the higher the J_{sc} of the solar cells. This corroborates well with plasmonic absorption effects reported by Haug et al. [179]. In fact, they show that the ZnO layer is capable of shifting the plasmonic interaction into a range of wavelengths where this effect is less problematic for the J_{sc} of the μc-Si:H solar cell.

Table 5-3: Electrical parameters of μc-Si:H solar cells deposited on hot silver with various thicknesses of ZnO (from 20 nm to 80 nm).

ZnO thickness [nm]	V_{oc} [mV]	FF [%]	J_{sc} [mA/cm^2]	Eff. [%]
20	509	72	22.1	8.1
40	509	72	22.4	8.2
60	502	70	22.4	7.9
80	503	71	22.9	8.2

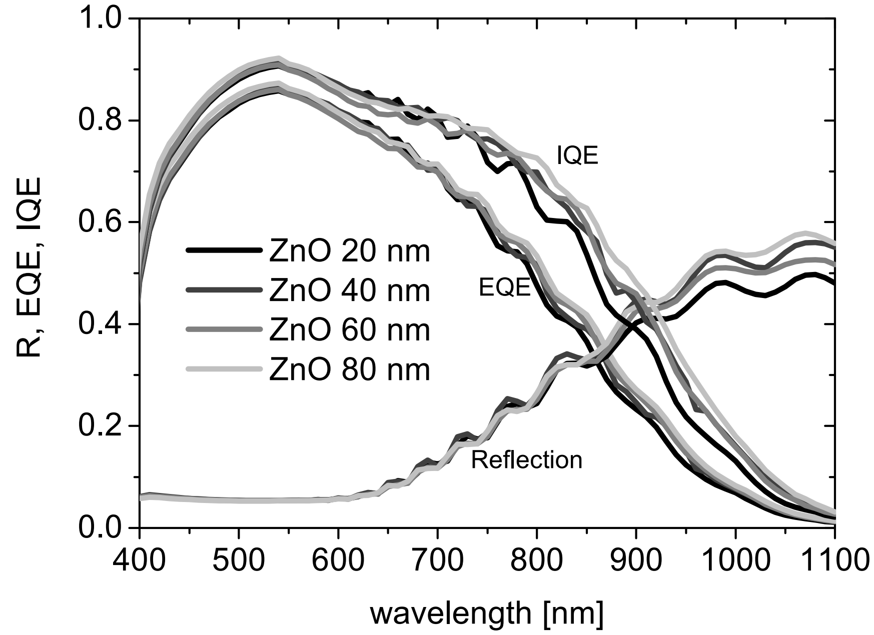

Figure 5-8: EQE and R of a µc-Si:H solar cell deposited on hot silver with various thicknesses of ZnO (from 20 nm to 80 nm).

5.3.6 Silver or aluminum back contact

We have found that for thin absorber layers (a-Si:H) both, random and periodic substrates can be used with high J_{sc} and that for thick absorber layers (µc-Si:H) the periodic substrate is preferable so far. Here, we compare two metals, silver (Ag) and aluminum (Al), for the back contact deposited on the rough substrates. It is of course an important topic for production because Al is more abundant than Ag (10^6 time more abundant on the earth crust), available at low cost and provides a better adhesion to other layers. However, as predicted by the Fresnel coefficient, the reflection of light is about 10 % lower on Al than on Ag. This difference is increased to 20% or even 30% when the reflection occurs at the ZnO/metal or Si/metal as shown in Figure 5-9.With Al, stronger losses also occurs between 750 nm and 900 nm and therefore also predict that the losses are more critical for µc-Si:H than a-Si:H solar cells.

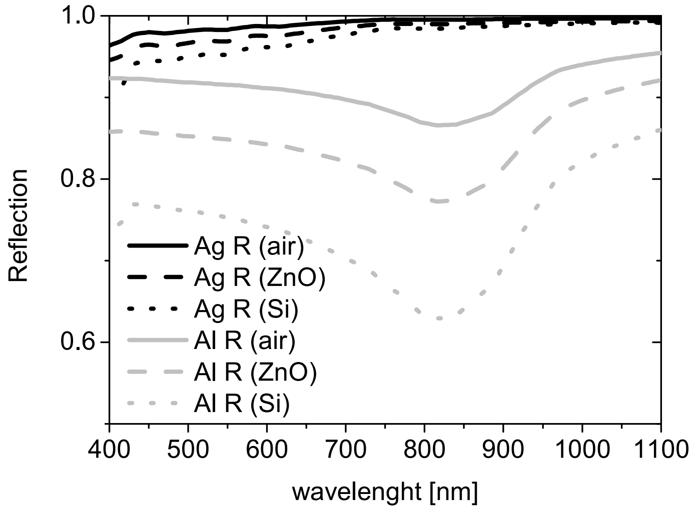

Figure 5-9: Reflection of Al (grey) and Ag (black) calculated from the Fresnel coefficients. The reflections are calculated for air/metal (solid line), ZnO/metal (dashed line) and Si/metal (dotted line) assuming that the materials are semi-infinite.

Figure 5-10 shows the results of an a-Si:H solar cell deposited on Ag and Al back contact covered with a thin 80 nm ZnO index matching layer. On the flat substrates, no significant difference between Ag and Al is found in the J_{sc}. However, the situation is different on the textured substrates. Indeed, the solar cell deposited on Al loses almost 2 mA/cm^2 compared to the cell deposited on Ag. This confirms that the Ag back contact provides more J_{sc} than Al for a-Si:H solar cells [191]. Nevertheless, this loss on Al can be mitigated by adding a thin ZnO index matching layer as also used here [192]. In addition, the Al back contact is used for textured p-i-n cells with reasonable J_{sc} and Bailat et al. have shown that J_{sc} up to 14.4 mA/cm^2 is possible with Al back contact [66]. Therefore, further optimization of the ZnO and the Si layers is needed for a high efficiency a-Si:H solar cells deposited on the Al back contact. Indeed, the losses, in thick cell (800 nm) deposited on the Al compared to Ag back reflectors, can be almost canceled by using a flat Al coupled with a thick rough LP-CVD ZnO deposited on top of the metallic layer as shown in Figure 5-11. In that case, the losses are reduced because the thick layer reduces the number of reflections on the metallic layer compared to thin absorber layers and the thickness (2µm) of the ZnO reduce the sensibility of the Al layer on the Si.

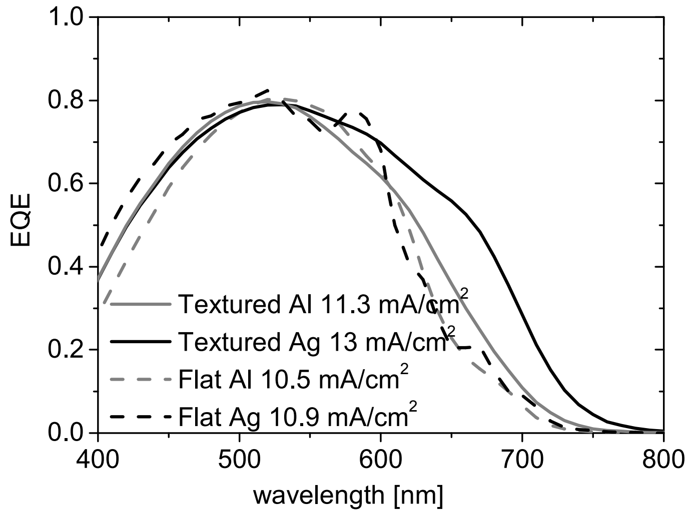

Figure 5-10: EQE of a-Si:H solar cell deposited on flat and textured (replication of LP-CVD ZnO) substrates coated with Ag and Al covered with a thin 80 nm ZnO.

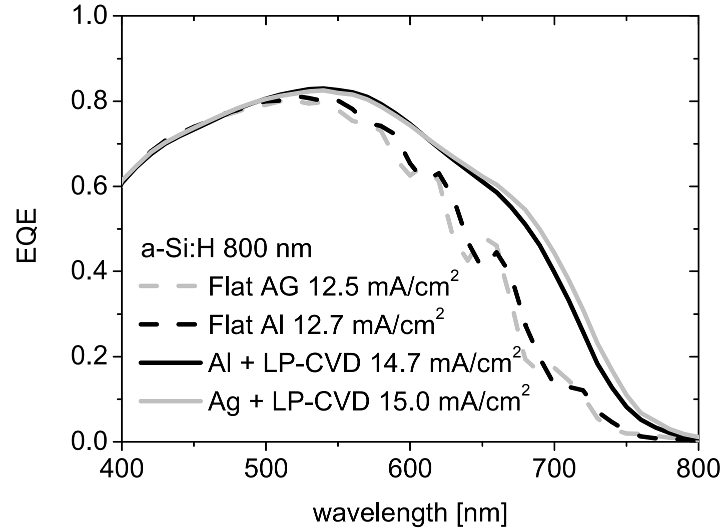

Figure 5-11: EQE of thick a-Si:H solar cells (800 nm) deposited on flat and LP-CVD ZnO substrates. The substrates are coated with Ag and Al and a thin ZnO (60 nm) for the flat case and a 2 µm thick LP-CVD ZnO for the textured case is added on top of the metallic back contacts. The cells are deposited on the large area KAI reactor by C. Denizot.

The results with thick µc-Si:H absorber layers are shown in Figure 5-12 where the loss of J_{sc} is up to 3 mA/cm^2 with an Al back contact compared to an Ag. This confirms the results obtained by Springer et al. [70] for Al back contacts. It shows that Ag back reflector deposited on rough substrates is a must for both the a-Si:H and µc-Si:H. Indeed, part of the benefits of the texture (light scattering and light trapping) is lost with the Al back reflector. The drop of J_{sc} can be intuitively understood as the results of the multiple reflections on Al, which has a stronger absorption compared to Ag.

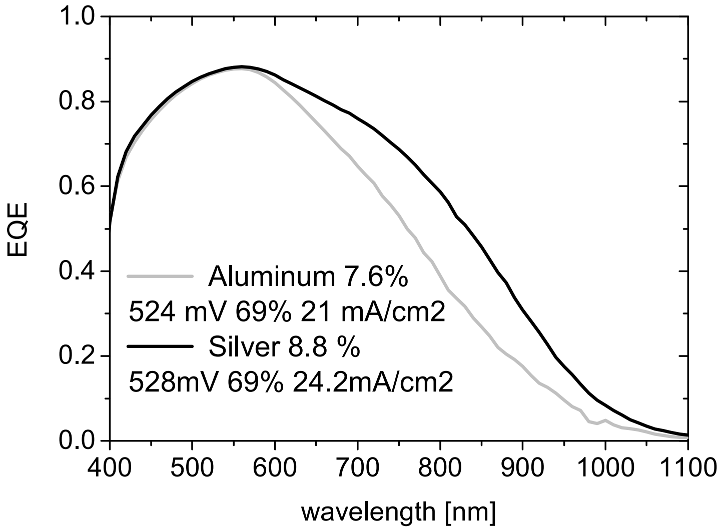

Figure 5-12: EQE of µc-Si:H solar cell deposited on the 2D cross grating substrates coated with Ag and Al covered with a thin 80 nm ZnO.

5.4 Discussion on light trapping and interfaces effect

In this section, the different observations made throughout this chapter are discussed and an attempt to explain the difference between thin and thick layers is provided. Thin layers are deposited conformally and thick layers tend to flatten the initial substrate texture. Then, we relate our observations to the solar cells result obtained on the grating substrate for thin (a-Si:H) and thick absorber layers (µc-Si:H).

5.4.1 Interface roughness and light coupling

Figure 5-13 shows a SEM micrograph of a µc-Si:H solar cell cross section prepared by focused ion beam (FIB). The cell has an absorber layer thickness of 1 µm on the 2 D periodic grating (periodicity 1.2 µm). The back contact structure consists of a double layer of 80 nm of silver and 70 nm of ZnO. Such thin layers guarantee an elevated degree of conformality at each interface, and they closely reproduce the grating characteristics.

However, considerable flattening of the structure is observed throughout the 1 µm thick µc-Si:H layer. Finally, after the deposition of 3 µm of LP-CVD ZnO, the shape of the grating has completely disappeared, and is now replaced by the intrinsic texture of the ZnO.

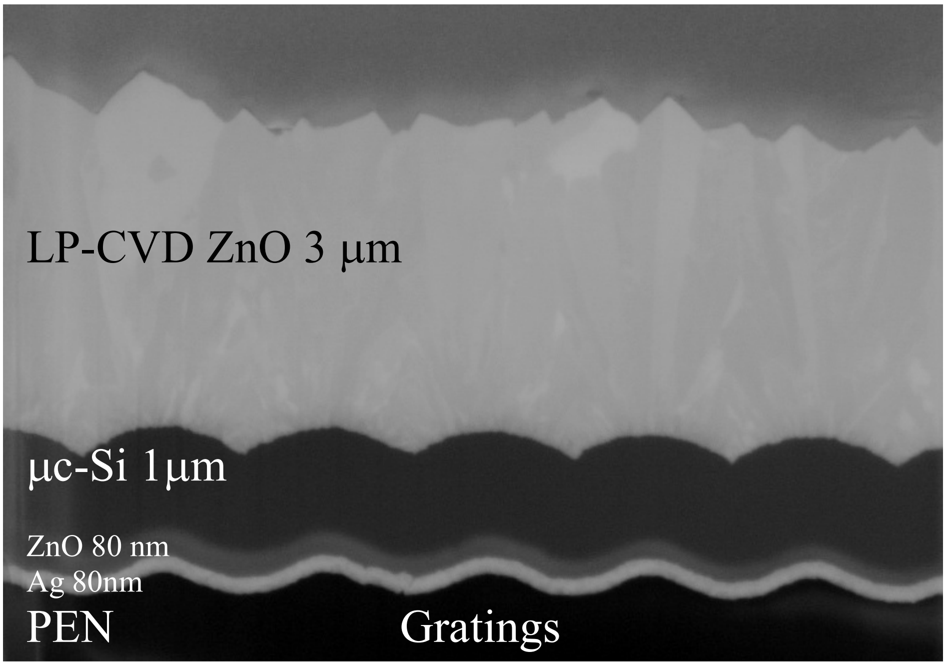

Figure 5-13: SEM micrograph of µc-Si solar cell with a ZnO LP-CVD front contact deposited on the 2 D sinusoidal cross gratings.

The a-Si:H and µc-Si:H solar cells deposited on the grating substrate in the previous section have two different behaviors. The thick textured LP-CVD ZnO increases the light trapping in the thin a-Si:H compared to the flat ITO whereas nothing is observed with a thick µc-Si:H layer. We consider two effects to tentatively explain the observed behavior. First, the effectiveness of light scattering at the diffractive grating structures is seriously influenced by the changes of the interface morphology. Indeed, we distinguish the case of thin layers (< 500 nm), which reproduce the surface morphology at both the back and the front interface of the absorber layer, and the case of thick absorber layers (> 1 µm), which flatten the surface texture of the substrate. For a description of the diffraction at the periodically structured interfaces we have to keep in mind that diffraction is a far field phenomenon. We make use of the well known grating equation for assessing the light propagation in those layers where the layer thickness exceeds the effective wavelength $\lambda_{eff} = \lambda_0/n$ (λ_0: wavelength in vacuum, n: refractive index):

$$n_1 \sin(\theta_1) - n_2 \sin(\theta_2) = \frac{m \cdot \lambda}{D}, \text{ m} = 0, \pm 1, \pm 2, \pm 3, \ldots \qquad (5\text{-}1)$$

Here, $\theta_{1,2}$ denote the incident and diffracted angles. The wavelength and periodicity of the grating are denoted by λ and D, respectively, and the diffraction order is given by the integer m. For solar cell applications, it is important to know the diffracted intensities into each order. For the case of a sinusoidal grating, an exact solution exists which predicts that the intensity diffracted into m-th order is proportional to the square of the m-th order Bessel function, where the argument of the Bessel function contains the wavelength and the grating amplitude [115]. In its simplest form, the validity of this prediction is only valid for small diffracted angles, whereas we are mostly interested in elevated diffracted angles in our device. An extended range of validity was reported with a "non-paraxial correction" where the intensity of a particular mode is normalized by the sum over the intensities of all propagating modes, as proposed by Harvey et al. [193].

A second observation addresses the condition of total internal reflection; for the case of flat interfaces, transmission into a medium with lower refractive index is prohibited when the incident angle exceeds the Brewster angle because the angle of the refracted beam would exceed 90°. However, when the surface is periodically textured, diffraction may occur into angles below 90°, and these orders are still allowed to propagate. Thus, a grating at the front interface can relax the condition of total internal reflection by introducing escape modes for the light!

5.4.2 Thick absorber (μc-Si:H)

Our results show the optical advantage of flat thin ITO front contacts compared to the rough LP-CVD ZnO for multijunction structures that have thick absorber layers (above 1 μm). Indeed, the antireflection of the ITO is ideal with no reflected light from the solar cell at 550 nm. First, the thick layer (between 1 μm to 3 μm) of microcrystalline material flattened the TCO/Si interface and thus also the air/TCO interface as discussed in Section 5.4.1. In this case the light would see a flat or flattened interface at the front of the solar cell and light trapping would be achieved by diffraction at the back reflector, as shown in case B of Figure 5-14. Note that even if the front Si/TCO interface is not completely flat, the depth of the grating is decreased, and according to the grating theory this leads to decreased diffraction intensities.

We consider that the wavelength of interest for light trapping is typically about 900 nm for multijunction structures. The diffraction angles and intensities at the Si/ZnO/Ag interface of the back reflector can be calculated using Equation 5-1 the "non-paraxial correction" and perpendicular incidence ($\theta_1 = 0$). In fact, this grating is well suited for this optical situation because our calculation shows that 65% of the light is reflected at the silicon/ZnO/Ag with angles higher than 16°. Note that 16° is the angle of internal reflection at the front Si/TCO/air interface if we consider this interface as flat, further assuming refractive indexes of 4 for silicon, 2 for the TCOs (ITO or ZnO), and 1 for air. Note that the angle of total internal reflection (TIR) of the system Si/TCO/air is equal to the TIR of the Si/air system, independently of the refractive index of the TCO.

This situation corresponds to our experimental results. Indeed, this substrate achieves strong increase of J_{sc} in the red part of the spectrum compared to the flat substrate case as shown in Figure 5-6. We think that, in our structure, the flattening of the front Si/TCO interface will result in an increase in reflection at the first Si/TCO interface. Hence, a thin ITO becomes extremely important to reduce the reflection at this interface and enhances the in-coupling of the light in the thick absorber layer as shown in Figure 5-6. In addition, the rough ZnO/air interface does not add any extra light trapping in the device. This is linked to the low scattering power of the LP-CVD ZnO in air for the infra red light as shown in Section 5.3.1. Similar results are found by simulation but applied to CIGS solar cells by Campa et al. [194].

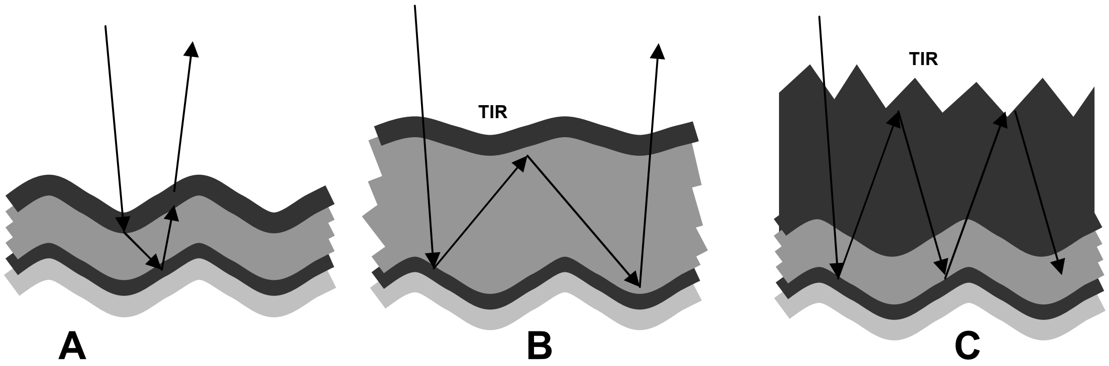

Figure 5-14: Schematic illustration of the light path in thin (A) and thick (B) absorber layers. A grating on the front surface allows out-coupling of light even at angles above the condition of total internal reflection. When the front interface is flattened due to the growth of a thicker absorber layer, the condition of total internal reflection is more and more restored, allowing at least two more passes through the structure (B). Note that the antireflection condition of the ITO layer is also valid for the light that is coupled out of the device. When the periodicity at the front interface is lost due to the growth of a thicker TCO layer, the condition of total internal reflection is partly restored at the TCO/air interface, allowing more passes through the structure (C).

5.4.3 Thin absorber (a-Si:H)

In the case of a thin absorber layer (a-Si:H) the optical properties and the role of the rough LP-CVD ZnO are different, as shown in Figure 5-4. Here, the grating properties are reproduced at each interface of the solar cell and the light wavelengths for the light trapping are reduced to 500–750 nm because a-Si:H is transparent for larger wavelengths. Therefore, our considerations focus on the behavior of light with a wavelength of 700 nm, which represents the light trapping region in the a-Si:H cells. In this thin device, we assume that two diffractions take place, one at the front TCO/Si interface of the solar cell and one at the back reflector of the solar cell (Si/ZnO/Ag interface). This is because the grating properties are reproduced at the front of the layers. Using the assumptions, the periodicity of the grating (1.2 μm), the refractive indexes ($n_{Si} = 4$ and $n_{ZnO} = n_{ITO} = 2$), and perpendicular incidence ($\theta_1 = 0$), the result of the Equation 5-1 for the front TCO/Si interface gives 6 orders of diffractions with 57% of the intensity having angles higher than 50°. This should create good conditions for light trapping but this is not observed in the solar cells (Figure 5-4). These assumptions simplify the physics of the device by splitting the interaction between the light and the layer in two parts. In fact, the interaction is, in reality, of course not uncoupled and therefore, a more exact calculation should consider the device as whole.

One possible explanation for the poor performance of the thin a-Si:H cell with the flat ITO on the grating is the next diffraction at the back contact and at the front contact as shown in Figure 5-15. Indeed, the diffraction at the ITO/Si or at the Si/ZnO is symmetric and therefore the light is reflected at the back contact with angle close to normal incidence, which is favorable for light out-coupling as shown Figure 5-15 (2b). In addition, even if the light has an incident angle at the front Si/TCO interface, the light is not trapped because the grating properties relax the condition of total internal reflection, and out-coupling of the light from the device becomes possible. Additionally, the thin ITO layer acts also as an antireflection layer in this direction, which reinforces the out-coupling of light. However, when the thick LP-CVD ZnO front contact is used, the out-coupling of the light at the ZnO/Si interface takes place but the grating properties are lost at the ZnO/air interface. Hence, the internal reflection at the ZnO/air interface is restored (at least partly) and light trapping is enhanced as described in Figure 5-14 (C).

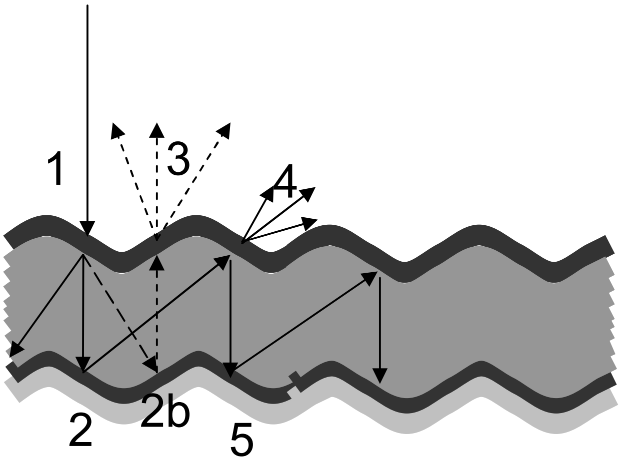

Figure 5-15: Schematic illustration of the light path in thin a-Si:H solar cells deposited on a grating with a thin ITO layer as a front contact. The light is first diffracted at the TCO/Si interface (1). At 700 nm, the majority of the light has large diffractive angles (57 % have angles higher than 50°C) but the symmetry of the diffraction at the back reflector reflects the light normally to the substrates (2b). At 700 nm 7 % the light is not diffracted at (1) and is then diffracted at (2). This moderate part of the light is trapped in the devices or out coupled because the grating relaxes the total internal reflection in (4).

In order to assure that it is not the roughness of the LP-CVD ZnO which enhances the scattering of the light in our device, we “switched off” the roughness by an optically thick film of index matching CH_2I_2. Figure 5-16 compares EQEs of a cell with a rough LP-CVD ZnO surface and the same cell measured through the index matching fluid, which yields a flat surface. Note that CH_2I_2 absorbs below 450 nm, but in the light trapping region between 650 and 800 nm the EQEs are essentially unchanged. This confirms that the roughness of the front surface does not play a significant role in the light trapping of this device. This is in accordance with Figure 5-3, which shows that the haze in air of the LP-CVD ZnO for wavelengths above 700 nm is relatively low, i.e. below 25 %. However at shorter wavelengths (400-500 nm), we still expect advantages for the textured front surface because of reduced primary reflection at the TCO/air interface. Indeed, the substrate roughness provides an index grading with the air, which diminishes the reflection.

In the case of the LP-CVD ZnO substrate, the sharp and random morphology provides rough interfaces at both the back and the front of the cell. This efficiently scatters light into the absorber by multiple scatterings of the light at every interface of the device, and no dominant diffraction occurs. Thus, the antireflection effect of a flat thin ITO is a better choice. This effect would even be reinforced after encapsulation thanks to the enhanced index matching in the three layer system air/encapsulant/ITO.

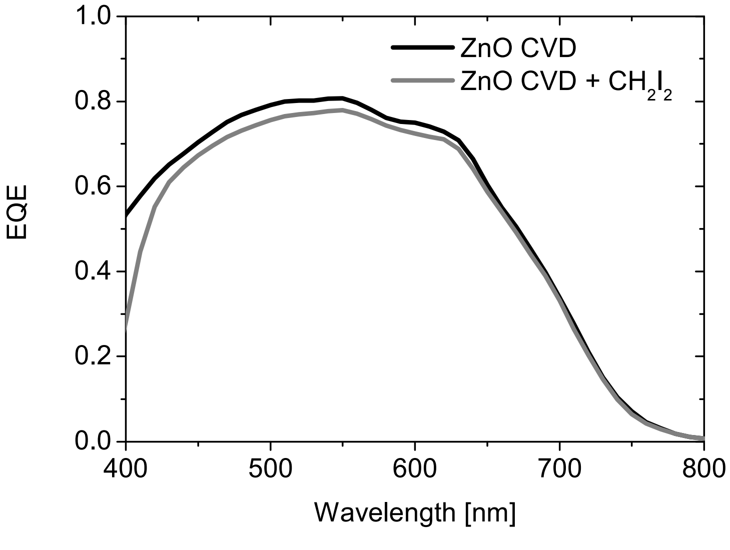

Figure 5-16: Comparison of a-Si:H EQE with LP-CVD ZnO front contact and with a drop of CH_2I_2 on top of the LP-CVD ZnO. This proves that the increased in J_{sc} in this device is not due to the rough front interface.

5.4.4 Light trapping and device performances

The light trapping properties in a-Si:H n-i-p solar cells on a variety of substrates have previously been reported by V. Terrazzoni-Daudrix et al. [15, 65]. Using textured LP-CVD ZnO front contacts, the authors reported current enhancements up to 16 % with respect to cells on flat substrate. J. Bailat et al. reported relative gain in J_{sc} up to 15% on an Al back contact. Summarizing our results on light trapping for a-Si:H, we find J_{sc} enhancements between 8 % and 23 %, depending on the combination of back contact texture and the choice of front contact. The performance of periodic and randomly textured substrates is comparable when a thick LP-CVD ZnO front contact is used. However, on randomly textured substrates a superior performance is observed for a thin ITO front contact because of the additional anti-reflection effect between ITO and Si.

For μc-Si:H solar cells Haase et al. performed an analysis of the light trapping properties by numerically solving Maxwell's equations [182]. For a substrate consisting of an array of regular pyramids they predict a current density of 21 mA/cm^2 for 1 μm thick absorber layers. Heine and Morf [69] suggest blazed gratings as ideal substrate because the reduced symmetry of the system prevents out-coupling into a zero order beam. In section 5.3.3, we studied the performance of μc-Si:H solar cells on a simple sinusoidal grating. In cells with a 1.6 μm thick absorber layer, we find 22.8 mA/cm^2 which represents a current density enhancement of 28 % compared to the flat reference cell of the same absorber thickness. This J_{sc} compares well to state-of-the-art μc-Si:H devices on random structures for equivalent thicknesses [72, 195]. We think that more refined grating structures, e.g. the implementation of blazing, still leaves some room for improvement.

Our investigations show that ITO represents a favorable choice of TCO for n-i-p cells with thick absorber structures like micromorph tandem or triple cells. In fact, ITO is used as front contacts by several companies [13, 196]. Specifically for triple junction solar cells, V_{oc} and sheet resistance are less of a concern because the voltage of the cell is higher (over 2 V) and the J_{sc} is relatively low (6 mA/cm^2, see Table 5-1). Noticeably, one of the advantages of ITO is also its good resistance to a humid environment.

5.5 Conclusion

Our study reveals that the interaction between the front and back surface structure is not trivial. It gives clear guidelines for substrate and TCO optimization taking into account different substrate textures and absorber thicknesses. For thick absorbers (μc-Si:H) it is essential to provide a suitably scattering back contact because loss of conformity due to the thick layer will reduce the scattering properties of the front interfaces. We have demonstrated that on textured substrate, a textured front TCO does not enhance the J_{sc} by scattering the light in the device compared to a flat ITO. Hence, ITO is a better choice for the front contact thanks to the efficient antireflection effect between air and silicon. In addition, the antireflection effect can be tuned to be especially favorable in the green region which is adapted for triple junction solar cells. For thin absorbers, a thick textured front contact can be advantageous in combination with a periodic substrate structure because it switches off the periodicity of the grating at the front interface. Indeed, on the plastic substrate, with periodic structure, we achieve a short circuit current of 14.4 mA/cm^2 with a LP-CVD ZnO front contact, which is a 7% relative increase compared to the standard ITO front contact.

Chapter 6: Multi-junction thin film silicon solar cells

Strategies for a dual optical system

6.1 Introduction

The micromorph tandem solar cell, composed of an amorphous (a-Si:H) top cell and a microcrystalline (μc-Si:H) bottom cell, is one of the promising multijunction candidates for high stabilized efficiency thin film silicon solar cells [49]. Indeed, the combination of the high a-Si:H band gap (1.7 eV) and the low μc-Si:H band gap (1.1 eV) creates an almost ideal tandem device. The advantage of this device is that the two absorber layers can be deposited by PECVD in the same reactor chamber and with a similar deposition process.

The challenge of this device is to achieve ideal J_{sc} matching between the two sub cells. Indeed in multi-junction solar cells, the J_{sc} is limited by the lowest J_{sc} of the sub cells. In micromorph tandem cells, the light passes through the top cell only once and the light induced degradation forbids the use of thick a-Si:H solar cells. Therefore, the limitation in J_{sc} comes usually from the top cell. In this case, the cell is said to be top limited.

One widely used solution in the superstrate configuration (p-i-n) is to introduce a thin intermediate reflector (IR) [197] which enhances the J_{sc} of the top cell without the need of increasing its absorber layer thickness. The IR is usually a material with a lower refractive index than silicon (typically $1.5 < n_{IR} < 3$ compared $n_{Si} = 4$) in order to have an index contrast that increases the reflection of the light at the Si/IR interface. Therefore, it enhances the J_{sc} of the top cell without increasing its thickness. The IR is usually a thin layer, between 50 and 150 nm, deposited in-situ [12, 188] or ex situ [198]. In situ Silicon Oxide Intermediate Reflector (SOIR) [116], Silicon Nitride [199] or ex situ Zinc Oxide Intermediate Reflector (ZIR) [177] have been reported to be very effective and are already implemented in complete products [200]. However in the substrate configuration (n-i-p), the problem of obtaining high efficiency micromorph tandems with elevated J_{sc} in the top cell was not yet solved. So far, the alternative to avoid to solve the problem is to implement triple junction solar cells which split the J_{sc} into the three sub cells and therefore allow the use of thin a-Si:H top cells [13]. Nonetheless, this strategy demands the implementation of a more complex process, e.g. one more cell and profiling [201, 202] of Ge in the a-Si:Ge solar middle cells.

In this chapter, we first present the limitation of increasing J_{sc} with a standard micromorph tandem cell without the IR shown in Figure 6-1 (left) while keeping a thin top absorber in order to limit the light induced degradation of the a-Si:H top cell. Then we discuss the implementation of a symmetric intermediate reflector (SIR) [197] which is very effective in the p-i-n solar cells. This SIR, shown in Figure 6-1 (middle), reproduces the morphology of its substrate which is often not adapted to create a strong light in-coupling into the next deposited cell. In fact, the difficulty comes from the large spectrum of absorption of the tandem solar cell and the different light trapping region of the two subcells. The top a-Si:H cell absorbs until 750 nm whereas the bottom μc-Si:H cell absorbs up to 1100 nm. In addition, the ideal structure for the μc-Si:H solar cell has a texture with soft or U shape morphology and feature size above 1 μm as shown in Chapter 3. The top cell is usually less sensitive to the substrate morphology and requires a feature size around 300 nm as shown in Chapter 4. Therefore, in the third part of this chapter, we focus on a new n-i-p design that can perfectly accommodate these two requirements, i.e. a design that yields ideal structure size and morphology for both the μc-Si:H and a-Si:H cells. This original concept proposes the use of an asymmetric intermediate reflector (AIR) which separates the light in-coupling between the two sub cells of n-i-p micromorph tandem solar cells as shown in Figure 6-1 (right) and allows the achievement of high efficiency stable devices.

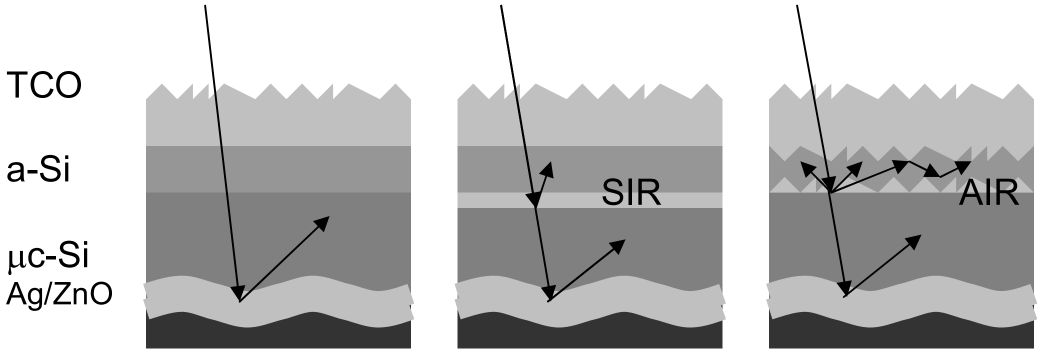

Figure 6-1 : Schematic design for standard micromorph without any intermediate reflector (left), with SIR (middle) and with AIR (right).

6.2 Results

6.2.1 Micromoph n-i-p tandem cells without intermediate reflectors

In the first part, we present the results of micromoph tandem cells without an intermediate reflector between the top and bottom cells. The substrate is the 2 D periodic grating on plastic foil coated with Ag/ZnO or the hot silver deposited on glass as described in Chapter 2. Then, the μc-Si:H cell is deposited. The surface of the μc-Si:H cell acts as textured “substrate” for the a-Si:H top cell. In order to study the morphology of the different interfaces on textured substrates, we prepared a cross sectional sample of a micromorph tandem cell for TEM analysis, as shown in Figure 6-2. The micrographs reveal that for the 2D grating the periodicity of the substrates is maintained through the Si layers but the shape (height) is strongly decreased. Therefore, the surface is flattened as already discussed in Chapter 5. Nevertheless, the zoom of Figure 6-2 (right) shows that the μc-Si:H substrate created pinches for the a-Si:H top cell on the valleys of the grating. This could be a disadvantage for the V_{oc} and FF of the top cell, and, therefore, for the efficiency of the micromorph tandem cell.

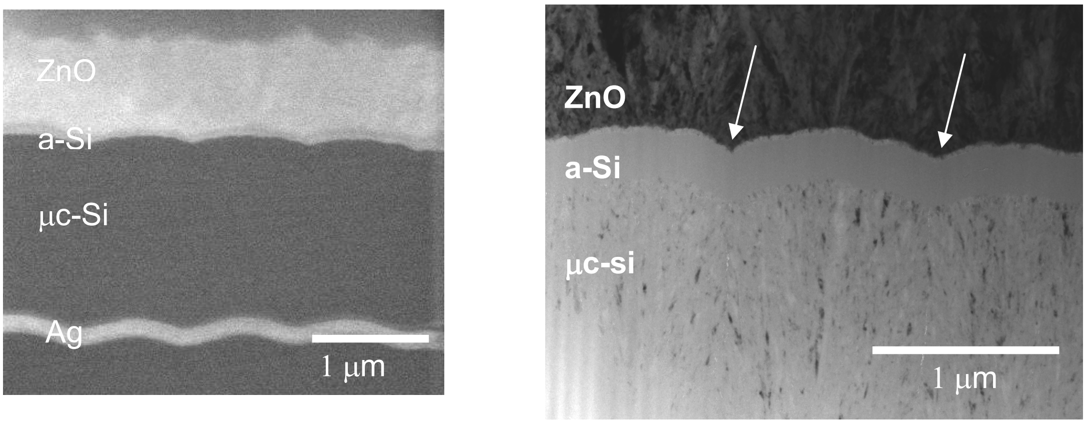

Figure 6-2: Left, cross section of a micromorph tandem solar cell after preparation by focused ion beam (FIB). Right, TEM cross section through the upper part of a micromorph tandem solar cell. In the middle is the amorphous i-layer, the upper dark part represents the ZnO front contact.

The light induced degradation of a micromorph tandem is mainly driven by the increase in defect density in the a-Si:H material because the light-induced degradation of μc-Si:H is limited when an a-Si:H filters the blue light as shown in Chapter 3. Therefore as described in Chapter 4 for single a-Si:H solar cells, the simple rule is also valid for the a-Si:H solar cell in the tandem device; the thicker the a-Si:H absorber, the lower the electric field in the absorber and the higher the recombination, which is the source of the defect creation in a-Si:H material. Hence for micromorph tandem cells, there is an optimum between the reduction of the top cell thickness and the light-induced degradation of the tandem, which partly is driven by the decrease of J_{sc} of the a-Si:H cell. But, the J_{sc} of the tandem is usually lower than the J_{sc} of a single junction solar cell because only one light pass is possible. Therefore, the optimum thickness of the a-Si:H top cell in the tandem might be shifted compared to the optimum thickness (200 nm) found for single junction a-Si:H cells in Chapter 4.

Figure 6-3 shows the variation of top cell current densities with increasing thickness of the a-Si:H top cell. It shows that the J_{sc} of the a-Si:H top cell increases almost linearly with the thickness and saturates at 12 mA/cm^2 for thicknesses above 400 nm. Table 6-1 shows the initial and stabilized parameters of micromorph tandem solar cells with different thicknesses of the a-Si:H top cell. It shows, as expected, that the thicker the a-Si:H absorber, the higher the degradation of the micromorph cells; it is almost 20% for a 400 nm thick a-Si:H absorber and only 13% for 160 nm. In Chapter 4, we have shown that the light-induced degradation of single junction a-Si:H solar cell is linked mostly to the degradation of the J_{sc} and the FF. Note, that the cells have different bottom cell thicknesses, which induces different FF of the tandem cell. This is due to different J_{sc} mismatch between the bottom and top cells; as rule of thumb [19, 203], the stronger the mismatch, the better the FF of the tandem cell. This is illustrated by the elevated FF of 77% for the strongly mismatched cell of Table 6-1. Therefore, we choose in the following to focus on the comparison of the top cell J_{sc} in order to switch off the mismatch effect included in the FF.

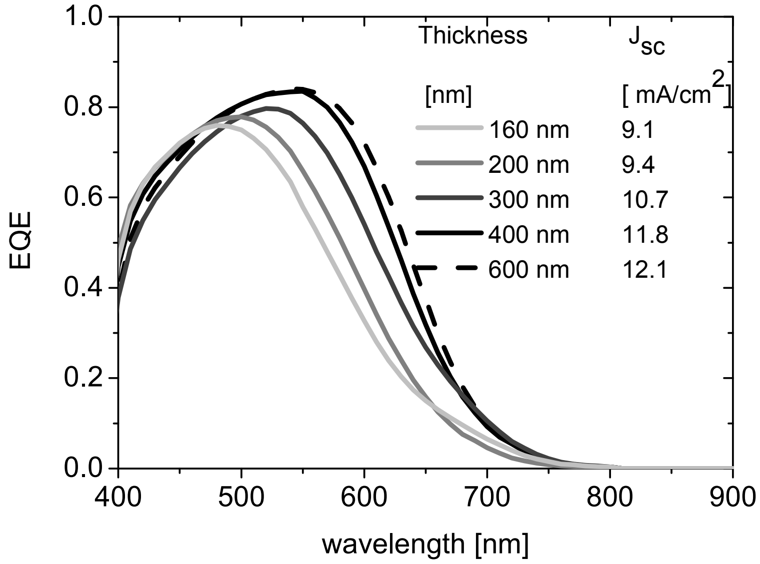

Figure 6-3 : EQE of n-i-p micromorph with various thicknesses of the a-Si:H absorber top cell.

Table 6-1 : Initial and stable (in parentheses) parameters of the n-i-p micromorph tandem solar cells with various thicknesses of the a-Si:H top cell. The dilution of the intrinsic layer is 2 except for the 600 nm where it is 3. The stable parameters are obtained after 1000h at 50°C and 50 mW/cm^2. The substrates for this micromorph are hot silver except for the solar cells in grey (270 nm), which are the 2D periodic grating.

a-Si :H [nm]	V_{oc} [V]	FF [FF]	J_{top} [mA/cm^2]	J_{bottom} [mA/cm^2]	Eff. [%]	Deg. [%]
160	1.36 (1.36)	77(70)	9.1 (8.7)	12.9(12.5)	9.6 (8.3)	13
200	1.30	71	9.4	14.2	8.7	
220	1.27(1.25)	74(66)	9.5 (8.9)	14.9(14.6)	8.9 (7.4)	16
270	1.37(1.33)	67(61)	11.3(11.0)	12.1(11.7)	10.4(8.9)	15
270	1.33(1.31)	71(62)	11.0(10.4)	11.9(11.4)	10.3(8.4)	18
300	1.35(1.34)	73 (62)	10.7(10.3)	11.5(11.2)	10.5(8.6)	18
400	1.33 (1.32)	65 (59)	11.8(10.6)	13.8(13.3)	10.2(8.3)	19
600	1.25	58	12.1 (9.9)	11.3	8.2	

Figure 6-4 shows the initial and stablized J_{sc} versus the a-Si:H top cell thicknesses of tandem micromorph deposited on hot silver substrates. The initial J_{sc} saturate at 12 mA/cm^2 whereas the stable J_{sc} saturate at about 10.5 mA/cm^2. We see that for a tandem cell, the optimum top cell thickness is between 250 to 300 nm. This thickness is thicker than the optimum thickness (200 nm) found for single junction solar cells in Chapter 4.

The main difference between the tandem structure and the single cell comes from the multiple light passes in the single cell whereas only one light pass is possible in the a-Si:H top cell. The situation of the top cell is equivalent to a flat cell with an absorbing back reflector like chromium. In this situation, the J_{sc} of the cell is small and any gain in J_{sc} with a thicker absorber compensates the losses in FF which occurs by increasing the a-Si:H cell thicknesses. The situation is therefore far from optimal because a 300 nm thick solar cell has to be used in the tandem and the FF suffers from higher light-induced degradation than in the ideal 200 nm case. Nevertheless, the best micromorph tandem cell achieved on plastic foils without an intermediate reflector has initial and stable conversion efficiencies of 10.4% and 8.9%, respectively, with a degradation of 15%. Note that this cell has an exceptional stability in J_{sc} compared to the other ones and this result was not reproduced.

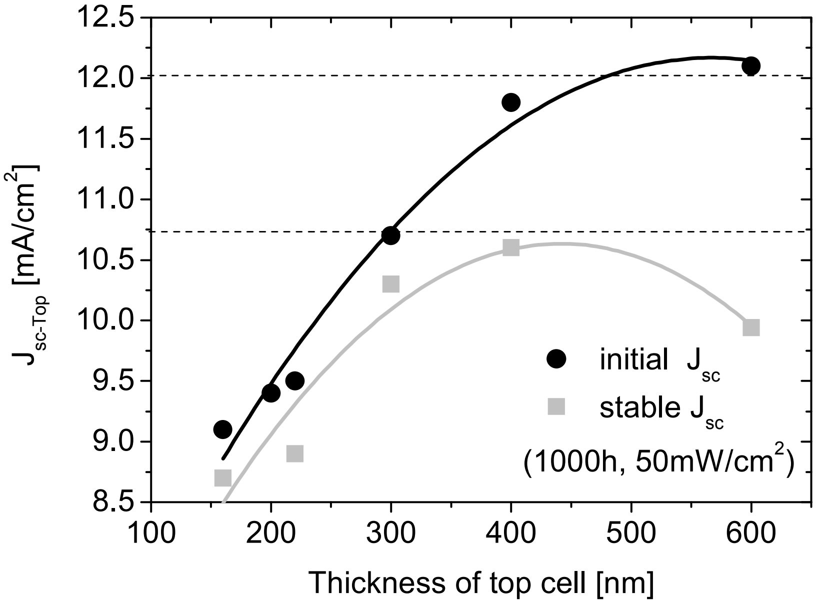

Figure 6-4: Initial and stable top cell J_{sc} for various a-Si:H top cell absorber thicknesses deposited on hot silver substrates. The solid line are guide for the eye.

6.2.2 Micromorph n-i-p with symmetric intermediate reflectors (SIR)

So far, the stable J_{sc} of the top cell is limited to 10.5 mA/cm^2 whereas as shown in Chapter 3, the thickness of the μc-Si:H can be increased to 2.5 μm with a total J_{sc} of 25 mA/cm^2. The higher current density is not useful though, as the added absorption in the near infra red cannot contribute to the solar cell efficiency since the J_{sc} is limited by the top cell as shown in Figure 6-5. Therefore, one solution proposed in the p-i-n solar cell configuration [188, 197] to the problem of moderate J_{sc} in the a-Si:H top cell is to include a thin IR or symmetric intermediate reflector (SIR) between the top and bottom cell. In principle, the IR has a lower refractive index than silicon, preferably $n < 2$ for $\lambda_0 = 600$ nm and should selectively reflect the blue-green light (550-750 nm) in the top cell while transmitting the red part of the spectrum in the bottom cell as described in Figure 6-6. In the p-i-n configuration, this was intensively studied by D. Dominé [19, 116]. He showed that the IR increases the total reflection of the micromorph tandem cell compared to tandem cell without IR and that the losses are between 0.5 to 1 mA/cm^2 for a total J_{sc} of 28 mA/cm^2. Yamamoto et al. have reported that the IR can even increase the total J_{sc} of the micrmoprh tandem cells thanks to internal light trapping between the IR and the back electrode [200]. The IR is crucial for achieving high J_{top} and efficiency micromorph tandem cells. D. Dominé achieved an initial conversion efficiency up to 13.3% [204] and Yamamoto et al. achieved an initial conversion efficiency of 14.7% [200]. Here, we also use a SIR composed of silicon oxide in the n-i-p configuration, equivalent to the thin IR used by Dominé et al. [204].

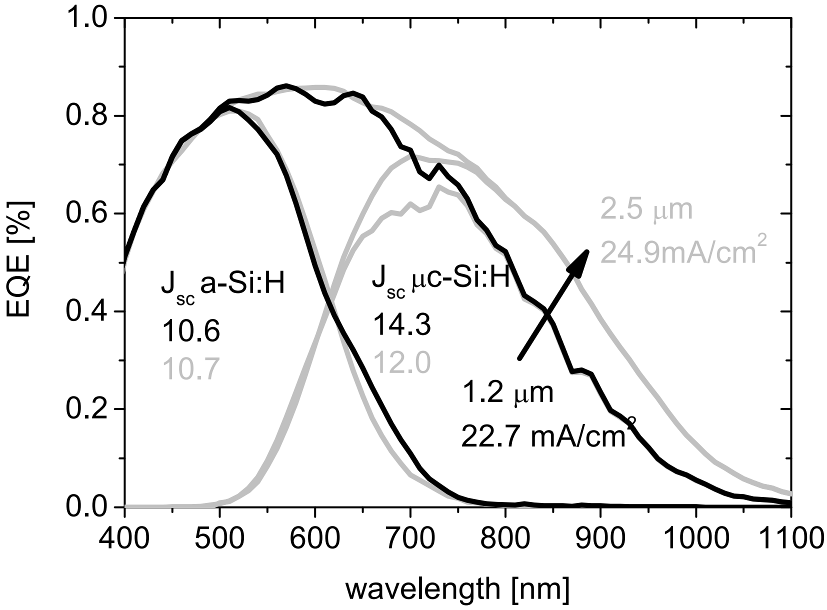

Figure 6-5 : EQE of n-i-p micromorph on LP-CVD ZnO substrates and LP-CVD ZnO front contact with varying μc-Si:H thicknesses from 1.2 μm to 2.5 μm.

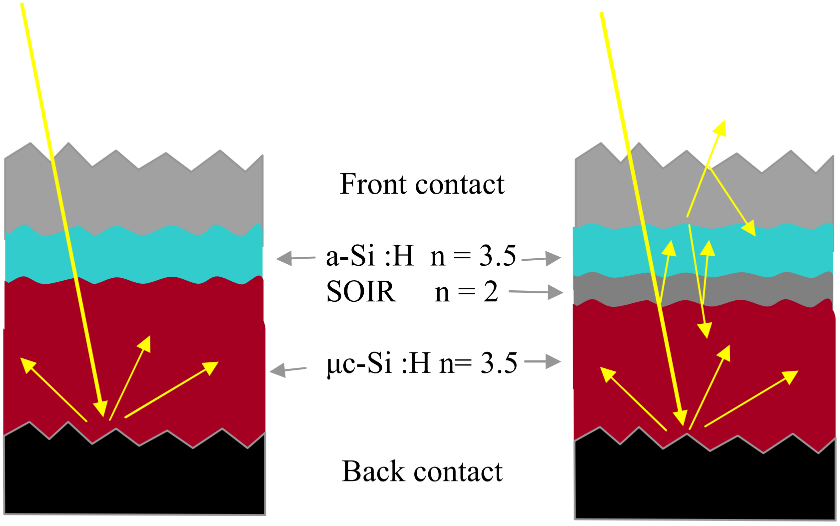

Figure 6-6 : Structure of a n-i-p micromorph tandem cell with (right) and without (left) SOIR.

6.2.2.1 Silicon Oxide Intermediate Reflector (SOIR)

The Silicon Oxide Intermediate Reflector (SOIR) is deposited by adding CO_2 to the plasma and n doped with PH_3. Further details about the deposition conditions and applications in p-i-n solar cells are reported by P. Buhlemann et al. [188], D. Dominé et al. [116] and D. Chandan et al. [205]. The conductivity is between 10^{-8}-10^{-10} S/cm in order to secure charge transport through the recombination junction. Figure 6-7 shows that the conductivity drops suddenly when the ratio of CO_2/SiH_4 increases whereas the refractive index varies almost linearly. Since the goal is to introduce an IR with a refractive index as low as possible in micromorph tandem cells, we tested many SOIR directly in the devices. Even if the conductivity does not vary much in the 10^{-8} S/cm range, the SOIR can block the device (S shape in the J(V) curve). The optimization of the SOIR leads us to the one with 2 sccm of CO_2 used for all cells shown below. Note that two techniques are used for the determination of the refractive index: ellipsometry and transmission reflection (TR) curves. For the TR, the interference of the curves is fitted with a simple layer model where the thickness of the film is given as an input parameter (profilometer measurement). The fit is more complex with the ellipsometry, in which a multilayer model with bulk and roughness is implemented in the program DeltaPsi2 [206]. Therefore, the discrepancy in the value obtained from the two techniques comes from the two different models applied.

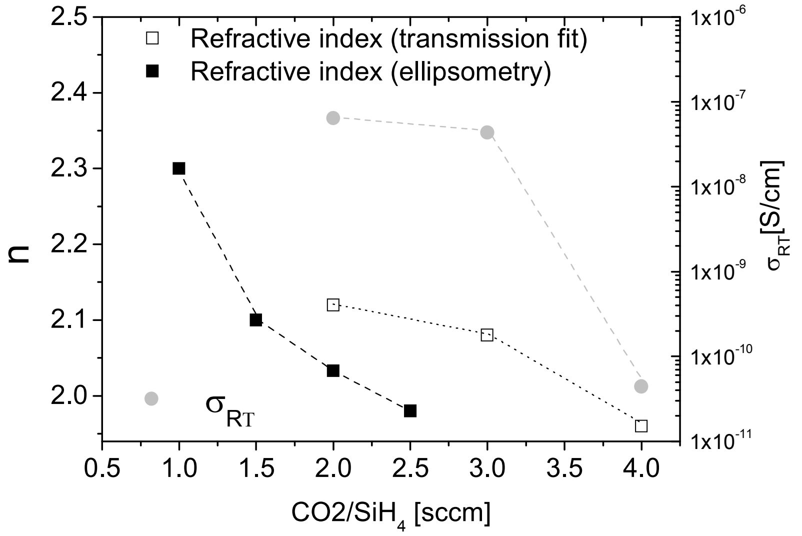

Figure 6-7 : Refractive index and conductivity of SOIR with varying CO_2/SiH_4 ratios in the plasma. The refractive index is calculated from a Tauc-Lorentz model for the ellipsometry measurement and the refractive index is calculated from the interference fringes of the transmittance of the SOIR deposited on glass (assuming the thickness measured by a profilometer for the other measurement).

6.2.2.2 SOIR in the tandem cells

The effect of the SOIR (100 nm) in the tandem cell is shown in Figure 6-8. The SOIR reflects the blue-green light in the a-Si:H top cell as presented in Figure 6-6. The J_{sc} of the top cell is increased by 1 mA/cm^2 and the J_{sc} of the bottom cell is decreased by 2.4 mA/cm^2. The initial solar cell efficiency is 9.6% (1.29 V, 64%, 11.7mA/cm^2). Table 6-2 shows two examples of micromorph tandem cells with and without SOIR having similar effects. Table 6-3 summarizes the results of tandem cells with SOIR having different thicknesses of a-Si:H top cells. The gain in J_{top} is promising with a relative increase of 10%. However, the gain is not yet shown in the efficiency of the tandem device for two reasons: the reflection loss is increased and the recombination junction is not completely optimized.

There is a total J_{sc} reduction (1-2 mA/cm^2) by implementing the SOIR in the tandem cells. The losses are due to reflection, parasitic absorption in the SOIR and absorption in the doped layers, which sandwich the SOIR. It should be possible to limit this effect by optimizing the thickness of the doped layer, improving the transparency of the SOIR, and by using the spectral selectivity of the SOIR (thickness and refractive index).

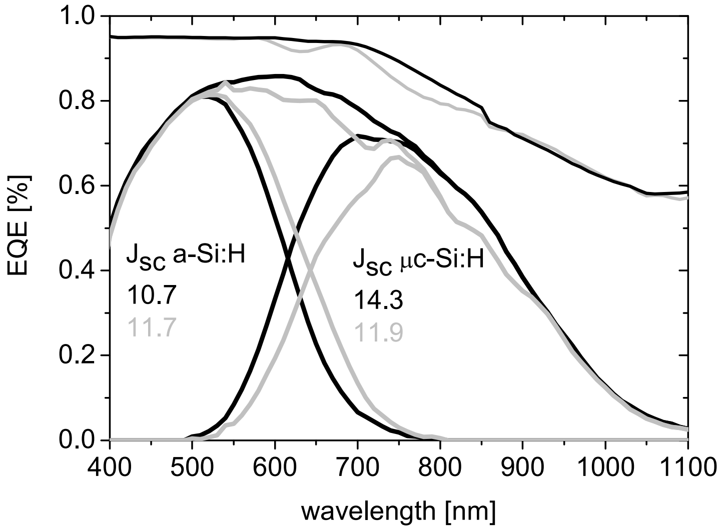

Figure 6-8 : EQE and 1-R of micromorph solar cells with (grey) and without (black) SOIR. The back and front contacts are LP-CVD ZnO.

Table 6-2: Initial and stable (in parentheses) parameters of the micromorph tandem solar cells with and without SOIR.

Thickness a-Si	V_{oc} [V]	FF [%]	J_{top} [mA/cm^2	J_{bottom} [mA/cm^2]	Efficiency [%]
220nm	1.27 (1.28)	70 (65)	10.2 (9.4)	13.1 (12.9)	9.1 (7.9)
Without IR	1.27 (1.25)	74 (70)	9.5 (8.9)	14.9 (14.6)	9.0 (7.4)
270 nm	1.36 (1.28)	68 (64)	12.1 (11.5)	10.5 (10.5)	9.7 (8.6)
Without IR	1.37 (1.33)	67 (61)	11.3 (11.0)	12.5 (11.7)	10.4 (8.9)

Table 6-3 : Initial and stable (in parentheses) parameters of the micromorph tandem solar cells with various thicknesses of the a-Si:H top cell with SOIR.

Thickness a-Si	V_{oc} [V]	FF [%]	J_{top} [mA/cm^2	J_{bottom} [mA/cm^2]	Efficiency [%]
220 nm	1.32 (1.3)	69 (60)	11.0 (10.0)	10.3 (10.0)	10 (7.8)
220nm	1.27 (1.28)	70 (65)	10.2 (9.4)	13.1 (12.9)	9.1 (7.9)
270 nm	1.36 (1.28)	68 (64)	12.1 (11.5)	10.5 (10.5)	9.7 (8.6)
300 nm	1.29 (1.33)	64 (57)	11.7 (10.5)	11.9 (11.6)	9.6 (8.0)
400 nm	1.31	55	12.6 (11.2)	12.3 (12.1)	8.9

The SOIR is made between the top and bottom cells. Therefore, the SOIR is close to the recombination junction, making the conductivity of the layer and also the interface between the SOIR and the cell very important. Indeed, if we only insert the SOIR at the junction or after the junction (e.g. between two amorphous doped layers) we obtain low

FF (37%) with an “S” shape IV curve as shown in Table 6-4. This problem is partly solved by introducing a microcrystalline n layer between the p doped layer and the SOIR. The FF is increased from 37% to 64%. However, the FF obtained with the SOIR is still below the one found without SOIR. This layer works well in p-i-n devices [188]. Therefore, we should be able to improve the efficiency of the micromorph tandem cells by further optimizing the doped layer in contact with the SOIR.

Table 6-4: Micromorph tandem cells parameters with microcrystalline or amorphous n layer at the junction before the SOIR. The cells are deposited on LP-CVD ZnO and treated with surface plasma for 30’. The cell from system B has SOIR made by P. Buehlman identical to the one used in [188].

Junction	V_{oc} [V]	FF [FF]	J_{top} [mA/cm^2]	J_{bottom} [mA/cm^2]	Eff. [%]
p-µc/n-aSi/SOIR/n-aSi	1.07	37	11.8	11.9	4.7
p-µc/n-µc/SOIR/n-aSi	1.28	64	11.7	11.9	9.6
p-µc-(n-µc-SOIR)$_{system B}$- n-aSi	1.3	60	11.8	11.8	9.2

6.2.3 Micromorph tandems with Asymmetric Intermediate Reflector (AIR)

So far, the SIR for the n-i-p substrate is promising but now we decided to concentrate more effort, on an even more promising concept, which is presented in this section. In fact, the J_{top} gain can be strongly enhanced with an asymmetric intermediate reflector (AIR), which reflects but also scatters the blue and green light in the top cell as shown in Figure 6-9 (right). With this AIR, we obtain a more efficient light in-coupling in the top cell between the AIR and the front contact. In fact, the light is scattered both at the front and back interface of the a-Si:H top cell. The light trapping effect is even reinforced by the texturation of the front interfaces since the Fresnel coefficient predicts higher reflection for light reaching an interface with an angle of incidence. Therefore, instead of having a conformal IR, we introduce a thick textured ZnO intermediate reflector deposited by LP-CVD as AIR.

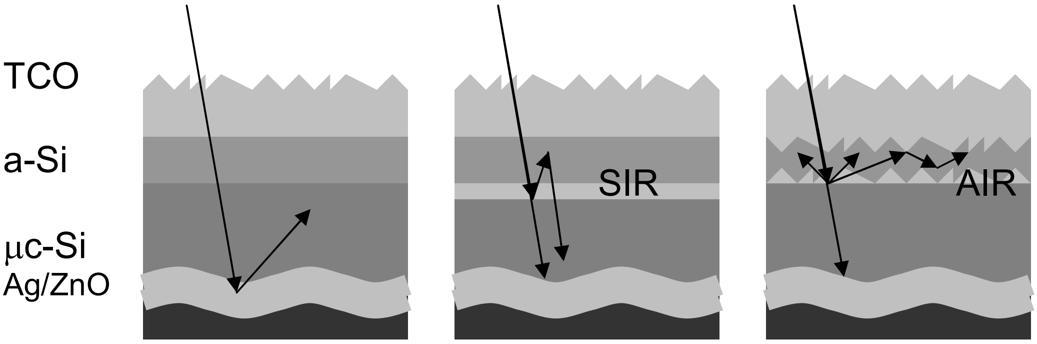

Figure 6-9: Schematic of n-i-p micromorph without IR (left), with SIM (middle) and with AIR (right).

Figure 6-10 presents a TEM cross section view of the structure of the device with AIR. First the 2 D cross grating is replicated on PEN foils. Then the texture is covered with a thin Ag/ZnO, which is used as a back contact and a back reflector. Then, 2.8 µm of µc-Si:H is deposited as a bottom cell, 1.5 µm of LP-CVD ZnO as AIR, 180 nm of a-Si:H as a top cell and finally 4 µm of ZnO LP-CVD as a front contact. The structure is designed with the aim of having soft or U-shape morphology texture, which preserves the quality of the µc-Si:H material and still has elevated scattering of the red light, between 800 – 1000 nm. This is the reason why the feature size is kept large (1.2 µm) and the shape of the morphology is soft, i.e. no incised valleys. Then, the AIR serves as optimum AIR with sharp textured morphology and feature sizes of 300 nm, which scatter efficiently the blue-green light in the a-Si:H top cell.

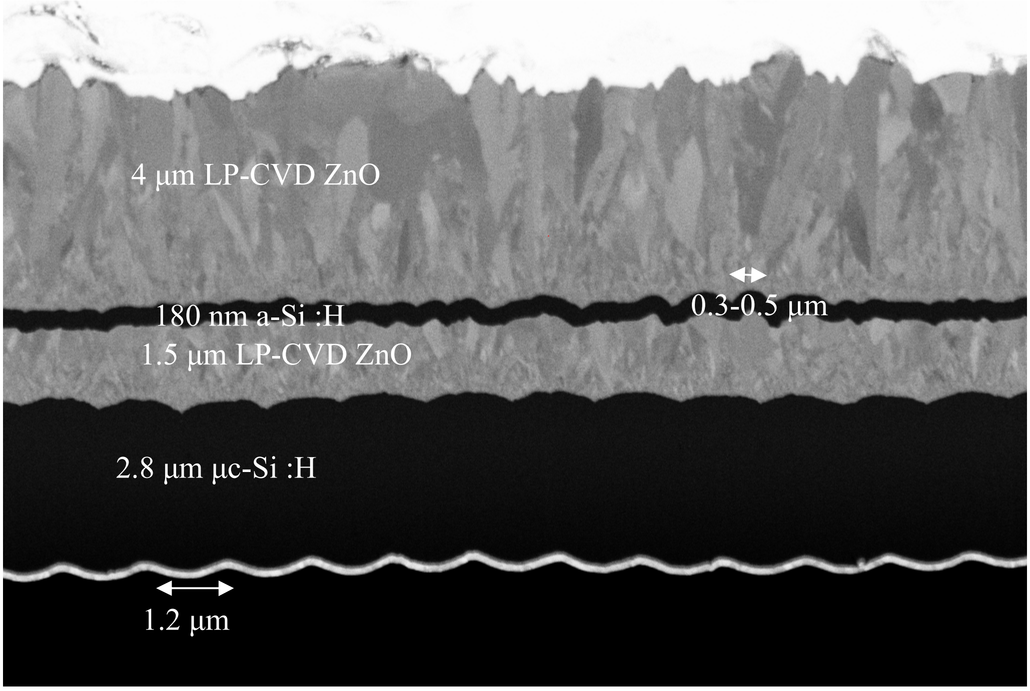

Figure 6-10: SEM micrographs of a cross-section of a n-i-p micromorph with AIR deposited on plastic foils.

The effect of the AIR is shown in Figure 6-11, where the EQE of three top a-Si:H cells of n-i-p micromorph tandem solar cells, without IR, with 100 nm SOIR with (n_{soir} = 2) and with AIR of 1.5 µm OF LP-CVD (n_{AIR} = 1.8) are compared. All a-Si:H top cells have equal absorber thicknesses of 200 nm. The J_{sc} of the top cell increases with the introduction of the IR. In Figure 6-11, the SOIR increases the J_{sc} by an absolute 0.7 mA/cm^2 whereas the AIR increases the J_{sc} by 3 mA/cm^2. At 650 nm, the relative gain in the EQE is 60% for the SOIR and 220% for the AIR. The strong efficiency of the AIR is mainly due to the texture of the AIR. Indeed, the µc-Si:H layer smoothes the initial substrate texture but the AIR restores a roughness and a length scale (300 nm), which creates ideal light scattering for the top cell. Therefore, the light is both scattered and reflected by the AIR which induces light trapping in the a-Si:H top cell, sandwiched between the top front contact and the IR.

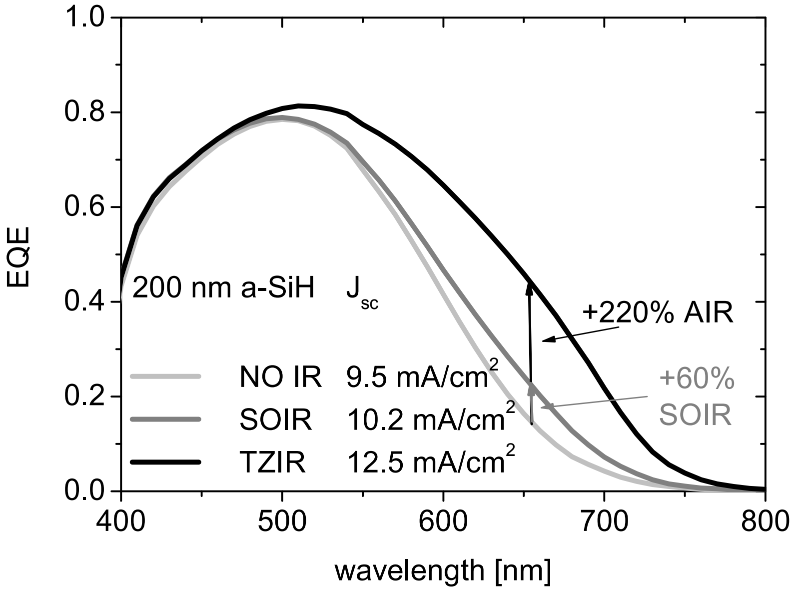

Figure 6-11 : EQE of 200 nm top a-Si:H in n-i-p micromorph solar cell without IR, with a SOIR, with AIR.

6.2.3.1 Size and morphology of the AIR

The power of the AIR is that the LP-CVD ZnO pyramids can be adapted in both size and morphology as shown in Chapter 2. Indeed, we make an equivalent experiment to the one conducted in Chapter 4 for the single a-Si:H solar cell. The results of the LP-CVD ZnO with different pyramid sizes and surface plasma treatment times are presented in Figure 6-12. It shows that if we aim at maximizing the J_{sc} of the top cell, then the morphology is more important than the size of the pyramids. This result is equivalent to what is found for single a-Si:H solar cell in Chapter 4. Furthermore, Figure 6-13 shows that the J_{sc} behavior of the a-Si:H top cell in a tandem cell with the LP-CVD ZnO is equivalent to the result obtained in a single junction solar cell (glass/ZnO/n-i-p/ZnO) without white paint at the back of the glass substrate. Therefore, the optimization of top cell of the tandem can be done in the single junction solar cells deposited on the LP-CVD ZnO without a back reflector.

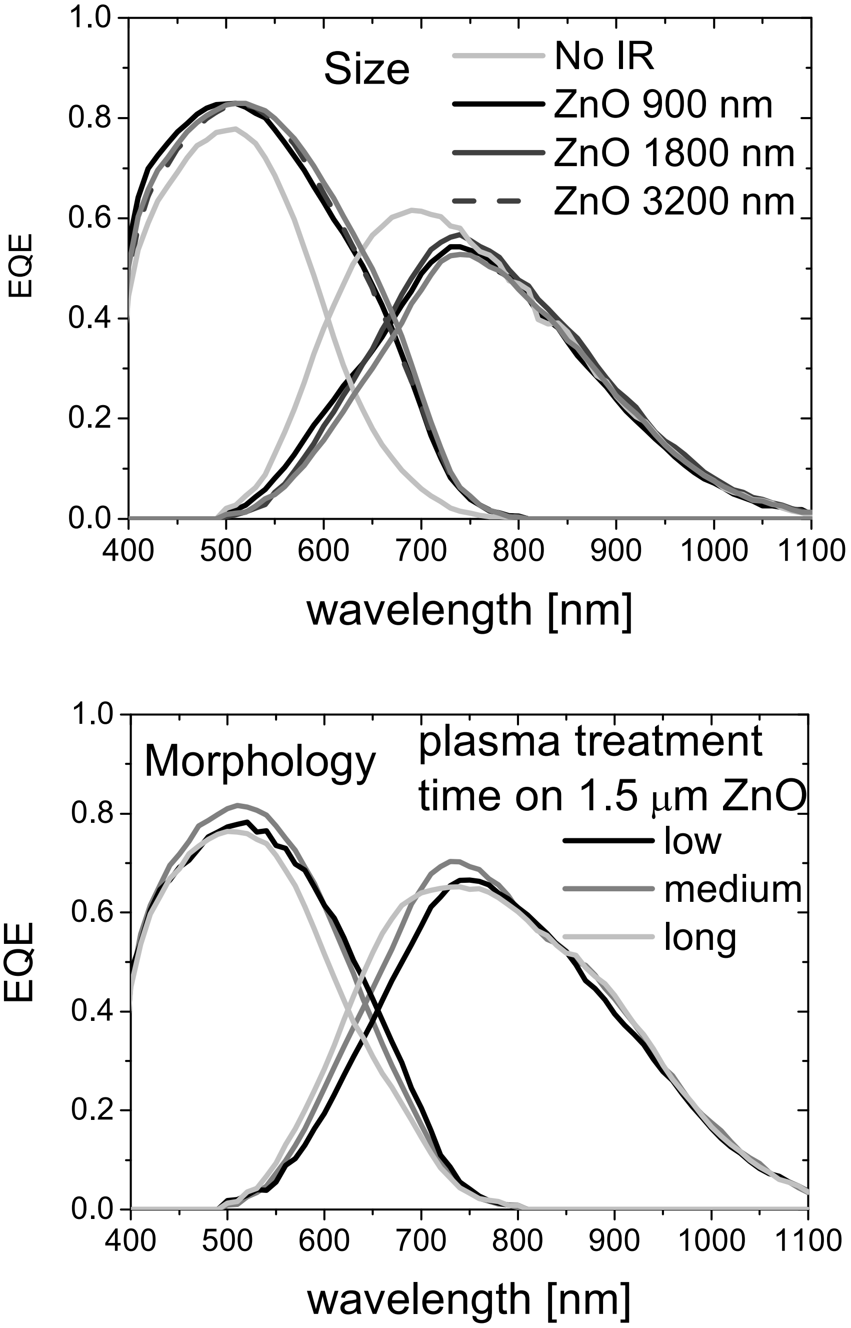

Figure 6-12: Variation of size (up) and morphology (down) of the LP-CVD ZnO in the micromorph tandem cell.

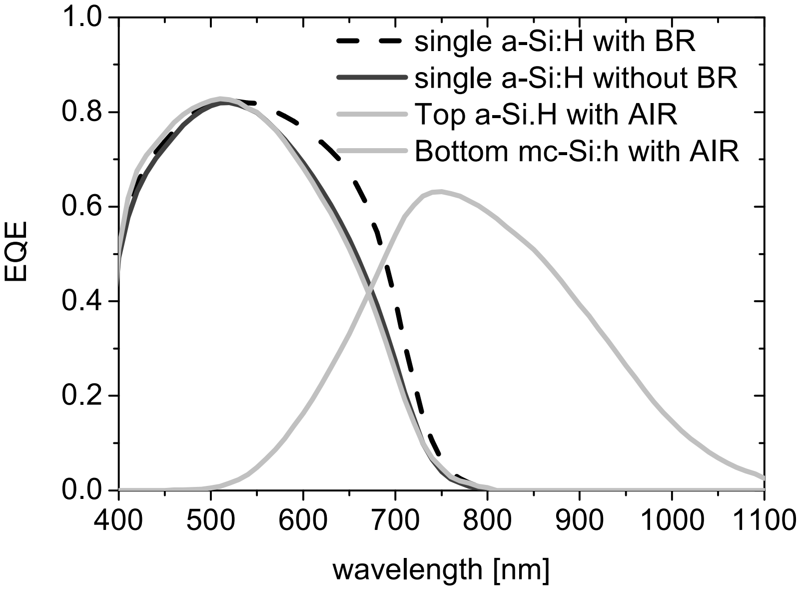

Figure 6-13: Comparison of EQE between single junction a-Si:H (glass/ZnO/n-i-p/ZnO) with and without back reflector (BR) (white paint at the back of the glass) and top cell a-Si:H combined with AIR.

6.2.3.2 Shunts and processes

In the previous section, we mentioned the shunting problem in the micromorph tandem cells prepared with LP-CVD ZnO as AIR. In fact, shunting is a common issue in thin silicon solar cells because every dust particle basically can create a shunt. The shunts of our device are illustrated with the thermography measurement in Figure 6-14. It shows that the shunts are located both on the border and on the center of the cells.

For a micromorph cell, we use several deposition systems, which increases the possibility of incorporating dust particles on our layers as shown in the right micrographs of Figure 6-16. The process with the AIR increases the number of air breaks by two compared to standard micromorph solar cells; one ZnO deposition and a surface plasma treatment on the LP-CVD ZnO. Therefore with such processes, it is advisable to work in a clean room environment, which is not the case for the systems used here. Once the cell is made, we usually isolate the cell for measurement. For a cell with a ZnO IR, we need two steps of wet etching (HNO_3) of the ZnO and two steps of dry etching ($SF_6/0_2$) for Si layers. For dry etching the cell is protected with a plastic film (P70). Nevertheless, this process creates exotic features at the border of the solar cells as shown in Figure 6-15 and Figure 6-16. We also try to use two lift-off processes for isolation of the solar cells [94]. One lift-off is made after the AIR deposition and a second one after the front TCO deposition. The borders of the cell are cleaner as shown in Figure 6-17 (left). Nevertheless, small ZnO particles are found on all layers as shown in Figure 6-17 (right) and can be shunt sources. It is not clear what the dominant shunting mechanisms are but many of them are playing a role.

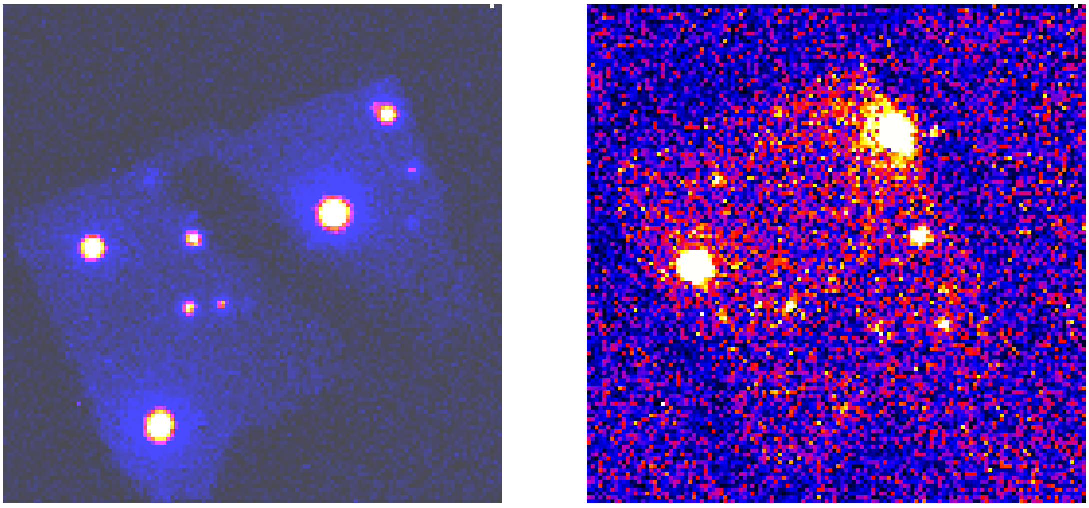

Figure 6-14 : Thermography measurement on n-i-p micromorph solar cells with AIR. The blue pixels are colder spot, whereas red and white spot are warmer due to thermal heating of the shunts.

The next three figures are SEM micrographs of a micromorph solar cell deposited on hot silver with ZnO LP-CVD as AIR.

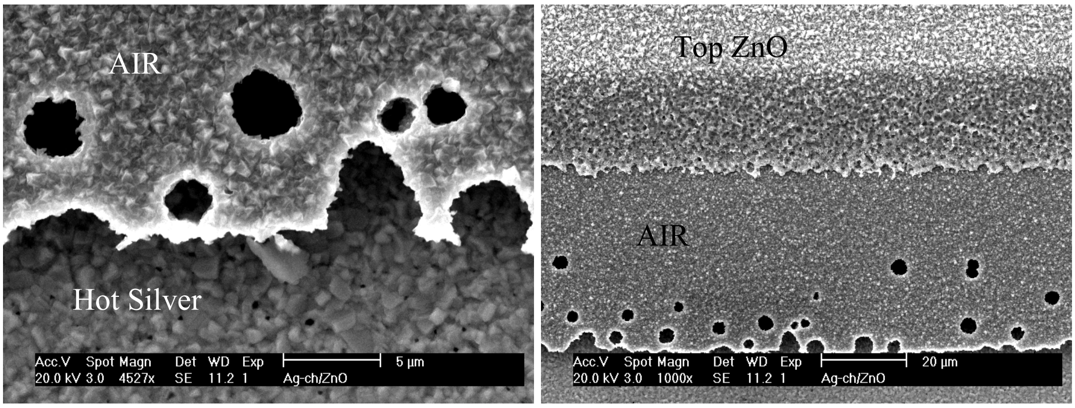

Figure 6-15: The left micrograph shows a zoom of holes in AIR deposited on hot silver. The right micrograph is an overview of the border of the cells with the hot silver at the bottom of the micrograph, and the AIR with the holes and the top contact above.

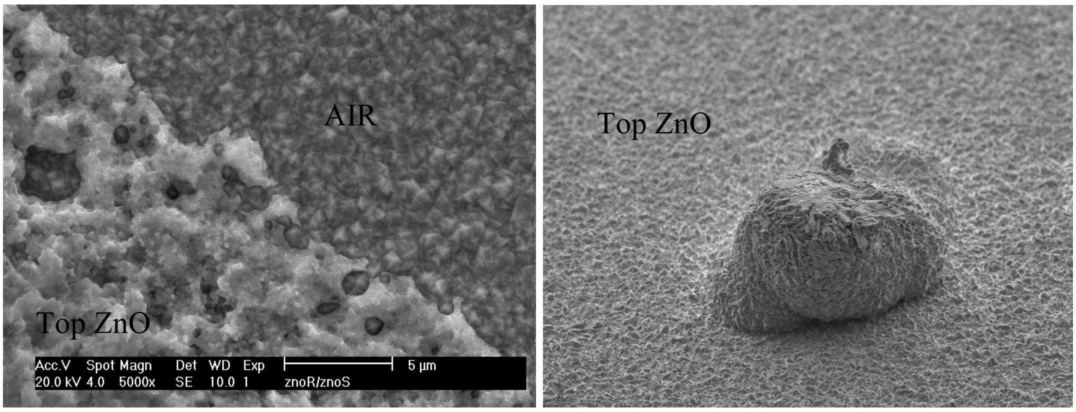

Figure 6-16: The left micrograph shows the border of the solar cell, which is isolated by two lift-off processes. The right micrograph shows an example of a dust particle on which the top ZnO contact is deposited.

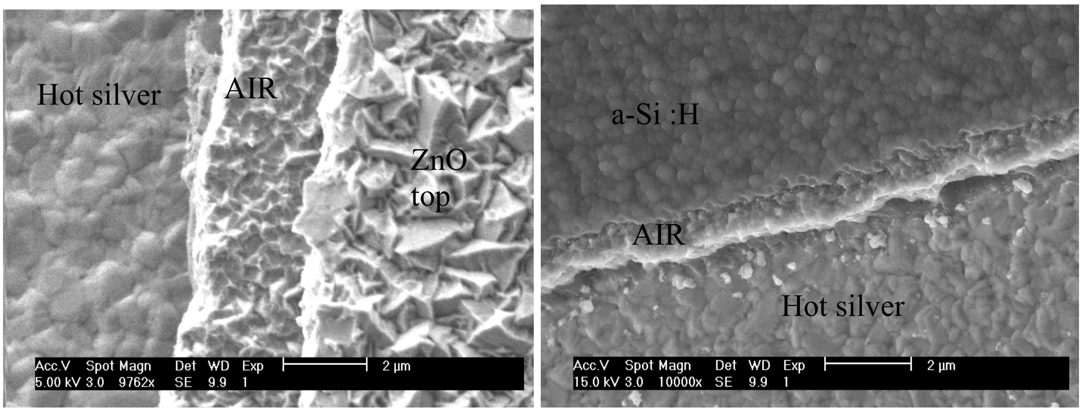

Figure 6-17: The left micrograph show the border of the solar cell, which is isolated by two lift-off processes. The right micrograph shows the border between hot silver, AIR, and a-Si:H cells. Dust ZnO particles lie on the hot silver back contact.

6.2.3.3 Reflection losses due to the AIR

The AIR enhances the J_{sc} of the top cell but part of the weakly absorbed light is also out-coupled from the solar cell due to reflection on the IR. Figure 6-18 (left) shows the EQE comparison of micromorph cell with a 600 nm a-Si:H top cell and a 200 nm a-Si:H top cell combined with an AIR. For both cells, the bottom cells have equal thicknesses. The J_{sc} of the a-Si:H are equal (12.1 and 12.2 A/cm^2) even though the cell without AIR is three times thicker. Furthermore, for light wavelengths between 600 nm and 750 nm, the EQE of the cell with AIR is higher and thus the effective thickness is in fact higher than three. The photogeneration distribution is different between the two structures. In fact, the cell without IR has higher EQE between 500 nm and 600 nm, whereas the EQE is higher from 600-750 nm for the cell with the AIR. The efficiency of the AIR is wavelength dependent and thus the wavelengths below 600 nm are only weakly back scattered by the AIR. The reflection from the micromorph tandem cell increases between 550 and 900 nm for the cell with AIR. By integrating the differences in reflection, we estimated the losses around 0.5 mA/cm^2. The difference in EQE in the μc-Si:H cell between 700 and 900 nm is attributed to shunts in the device and not to reflection or absorption losses. Indeed, in Figure 6-18 (right) we compare the total J_{sc} of a micromorph cell with a 3 μm μc-Si:H and the J_{sc} of a single μc-Si:H with a3 μm thick absorber layer. It shows that both J_{sc} are equal and that the losses can be minimized almost completely.

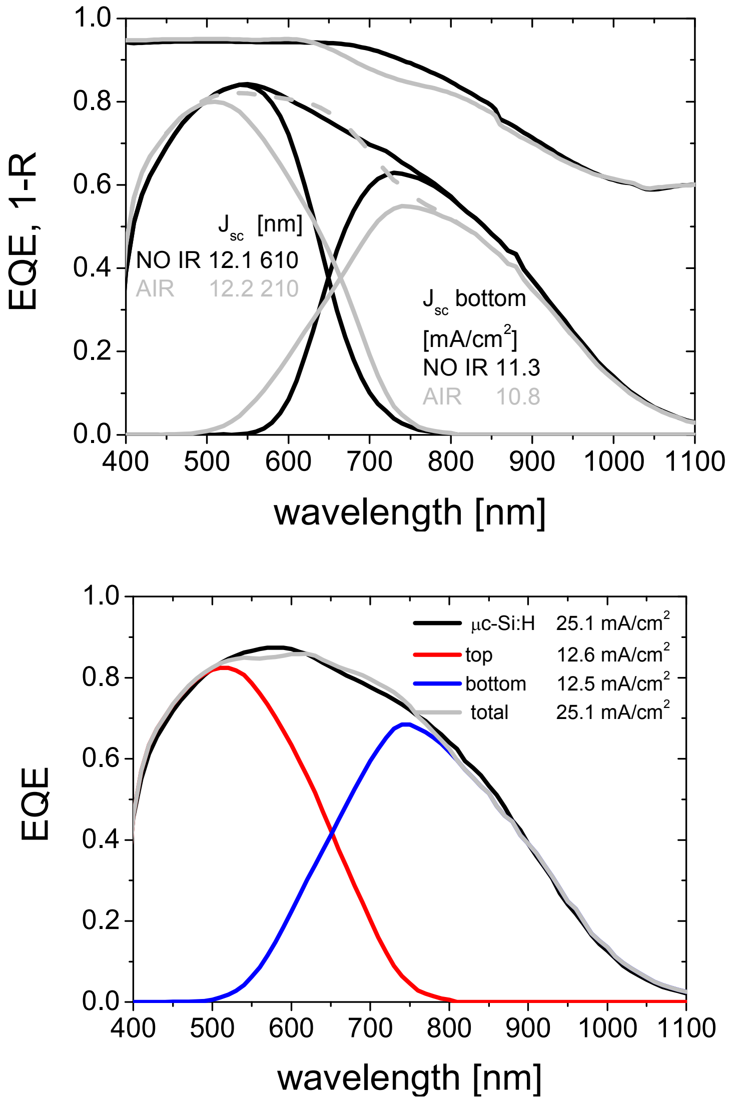

Figure 6-18: Up, EQE and 1-R of micromorph with 600 nm top cell without IR (black curve) and 200 nm top cell with AIR (grey curve). Down, EQE of μc-Si:H cell with 3μm thick absorber layer and EQE of micromorph with a total thickness of 3 μm deposited on the 2D cross grating.

Figure 6-19 shows the typical total reflection curves obtained with and without IR. The reflection curve of the cell with a SOIR has interference that comes from the flat or almost flat interfaces after the μc-Si:H deposition. For the AIR case, the interference disappears due to the scattering and the reflection is higher than with the SOIR between 650 and 830 nm. The roughness of the AIR decreases the reflection between 400 nm and 600 nm thanks to the higher roughness at the Si/TCO interface, which provides a refractive index gradient, slightly reducing the reflection at the front Si/TCO interface. From 830 to 950, the reflection is higher with the SOIR compared to the AIR. The interference effect of the SOIR can be tuned to be varied in wavelength, whereas with the AIR the effect is more constant. We think that the antireflection effect linked to the roughness is decreased after 830 nm because the scattering is decreased for long wavelengths.

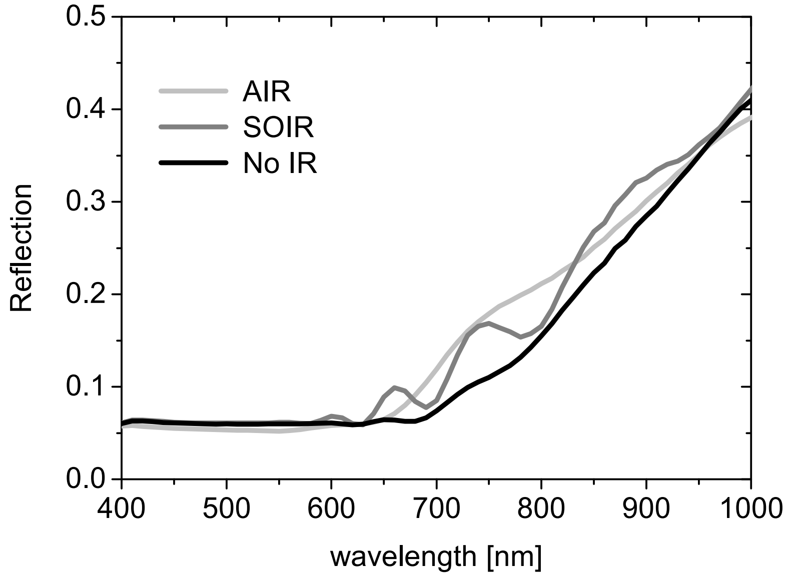

Figure 6-19: Reflection curves of micromorph tandem cells without IR (light grey), with SOIR (grey) and with AIR (black)

6.2.3.4 Solar cell efficiency and degradation with AIR

The AIR increases the effective thicknesses of the a-Si:H layer, which is crucial for the light-induced degradation of the a-Si:H cell and thus the micromorph tandem cell. In Table 6-5, we compare the typical degradation for micromorph cells without IR and with AIR. The degradation is between 15-20% for a top cell of 300 nm without IR whereas the degradation is limited to 5-10% for the cell with 140 nm and AIR. The results shown in Table 6-5 and Table 6-6 are obtained on glass covered with hot silver and a LP-CVD ZnO front contact. The results obtained with AIR in Table 6-5 have a stable efficiency of 9.6% with thin 1.4 μm μc-Si:H cells and 10.1% with 3 μm thick bottom cells. The optimum efficiency is obtained for top cell thicknesses just below 200 nm. There are two reasons that explain why we can not use thicker layers. First we showed in Chapter 4 that the optimum thickness for the a-Si:H top cell is 200 nm and that going into thicker cell results in lower stable efficiencies. Second, for matching condition we need also to use a thicker μc-Si:H solar cell which (as shown in Chapter 3) leads to lower V_{oc} and FF performances. Therefore the J_{sc} gain should compensate these losses, it has to be truly beneficial for thick tandem micromorph solar cells.

Table 6-5: Performance parameters of the micromorph tandem solar cells deposited on hot silver without IR and with AIR (stabilized parameters are given in brackets).

Thickness a-Si/μm-Si [μm]	V_{oc} [mV]	FF [%]	J_{top} [mA/cm2]	J_{bottom} [mA/cm2]	Efficiency [%]	Deg. [%]
0.3/1.2 No IR	1.35 (1.34)	73 (62)	10.7 (10.3)	11.5 (11.2)	10.5 (8.6)	18
0.14/1.4 AIR	1.32 (1.34)	74 (70)	11.4 (10.3)	10.6 (10.2)	10.4 (9.6)	8
0.18/3 AIR	1.32 (1.35)	66 (65)	12.4 (11.7)	11.9 (11.5)	10.3 (10.1)	3

Table 6-6: Performance parameters of the micromorph tandem solar cells deposited on hot silver with AIR (stabilized parameters are given in brackets).

Thickness a-Si [nm]	V_{oc} [V]	FF [%]	J_{top} [mA/cm^2]	J_{bottom} [mA/cm^2]	Efficiency [%]	Deg. [%]
140	1.32 (1.34)	74 (70)	11.4 (10.3)	10.6 (10.2)	10.4 (9.6)	8
140	1.32 (1.35)	70 (68)	11.5 (10.9)	10.4 (10)	9.6 (9.1)	5
140	1.32 (1.34)	74 (70)	11.4 (10.3)	10.6 (10.2)	10.4 (9.5)	9
160	1.32 (1.33)	71 (66)	11.7 (11.3)	10.2 (9.8)	9.5 (8.6)	10
180	1.32 (1.35)	66 (65)	12.4 (11.7)	11.9 (11.5)	10.3 (10.1)	3
200	1.31 (1.34)	71 (66)	12.9 (11.8)	11.5 (10.9)	10.7 (9.6)	11
220	1.30 (1.35)	71 (65)	12.9 (11.7)	11.5 (11)	10.5 (9.6)	8
200	1.29 (1.28)	71 (67)	11.9 (10.7)	11.1 (10.8)	10.2 (9.1)	11
200	1.31 (1.34)	71 (71)	12.8 (11.7)	9.8 (9.4)	9.1 (8.9)	3
200	1.29 (1.33)	73 (72)	13.2 (12.1)	9.1 (8.3)	8.4 (8.2)	2
200	1.26 (1.32)	72 (69)	12.9 (12.3)	9.6 (9.1)	8.3 (8.6)	-3
240	1.28 (1.28)	68 (63)	13.3 (12.3)	11.7 (11.3)	10.2 (9.1)	10
240	1.28 (1.3)	68 (66)	13 (12.0)	11.6 (11.2)	10.1 (9.6)	5
300	1.29	64	13.9	11.1	9	
300	1.29 (1.31)	65 (59)	13.7(12.0)	11.5 (11)	9.6 (8.5)	11

The micromorph cells presented in Table 6-6 also have different matching conditions and as already discussed, this creates difficulties for FF and efficiency comparisons. Therefore, we again focus on the degradation in J_{sc} of the top cell. Figure 6-20 compares the J_{sc} of micromorph tandems cells with and without AIR. It shows that in the initial state, the AIR can provide J_{sc} up to 14 mA/cm^2 for a 300 nm thick a-Si:H top cell, whereas a cell without IR can hardly reach more than 12 mA/cm^2. In the stable state, the situation is even more critical because the J_{sc} with the AIR attains more than 12 mA/cm^2 with only 200 nm whereas only 10.5 mA/cm^2 is achieved without IR. The relative efficiency gain is close to 15% thanks to the J_{sc} and we also expect a gain in FF which is also linked to the thickness of the a-Si:H top cell as shown in Chapter 4. Our experimental results confirm this efficiency gain since the best stable efficiency on hot silver substrate is 10.1 % with an AIR and 8.6% without IR, which is an increase of efficiency close to 17 %.

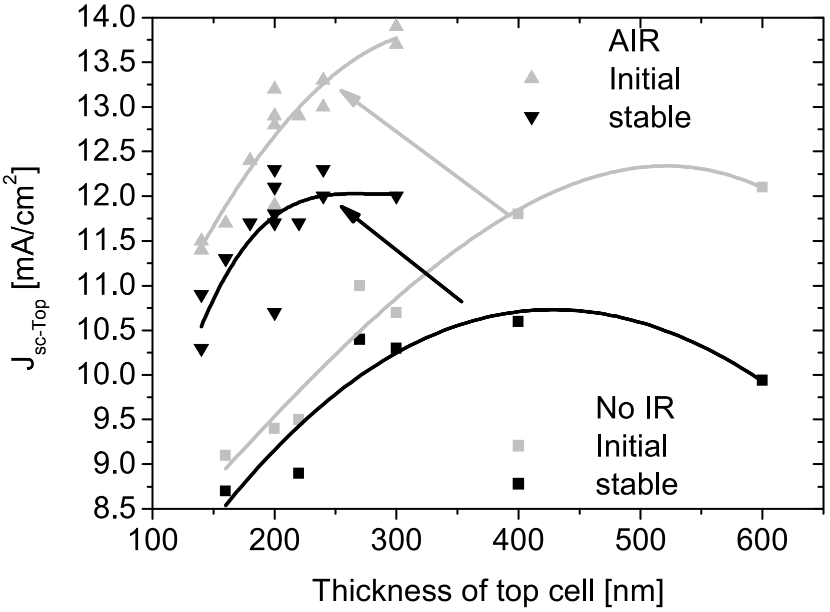

Figure 6-20: J_{sc} of initial and stable (1000h, 50°C and 50 mW/cm^2) micromorph tandem cells with and without AIR.

6.2.3.5 Best micromorph on plastic substrate

The title of this thesis suggests that the power of the n-i-p configuration is the applicability to flexible substrates. Therefore, our last result shows an n-i-p micromorph tandem cell on flexible plastic (PEN) foils. We transfer the glass processes onto PEN with the 2D cross grating. The thickness of the μc-Si:H is increased to 2.8 μm in order to increase the total J_{sc} of the tandem cell and thus fully benefits from the potential of our AIR. Our best result is a micromorph n-i-p solar cell with initial efficiency of 11.2% (1.34 V, 68%, 12.3 mA/cm2) and stable efficiency of 9.8% (1.35 V, 64%, 11.9 mA/cm^2). This cell is light soaked during 1000h at 50°C and 100 mW/cm^2. Note that the light intensity is double compared to all the previous light soaking tests of this thesis. The structure of the cell is PEN/2D grating/100 nm Ag/ 60 nm ZnO/2.5 µm µc-Si:H/1.5µm LP-CVD ZnO/180 nm, a-Si:H top cell and an LP-CVD ZnO front contact. The initial and stable EQE value is shown in Figure 6-21 (left) and the J(V) in Figure 6-21 (right). The potential for further improvement is still high because our a-Si:H is far from optimal (only 9% initial and 7.3% stable efficiency) whereas we should be able to achieve 10% with a proper p window layer. Furthermore, an ITO front TCO contact would give 4% more J_{sc} than our LP-CVD ZnO as shown in Chapter 5.

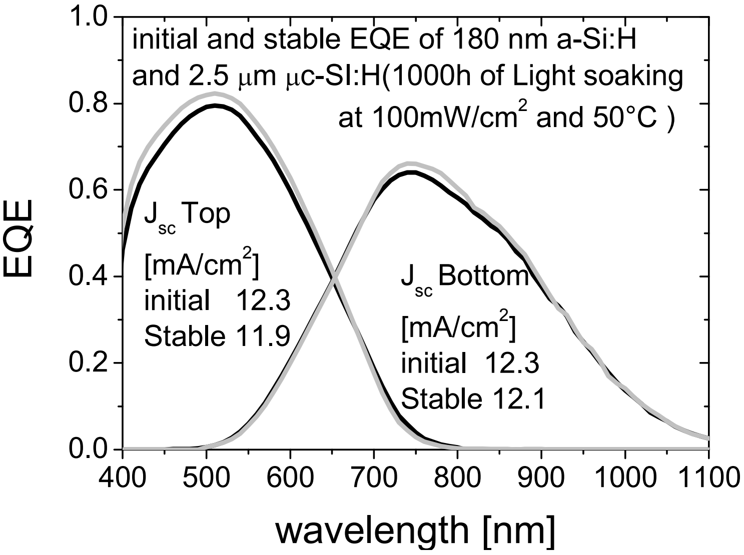

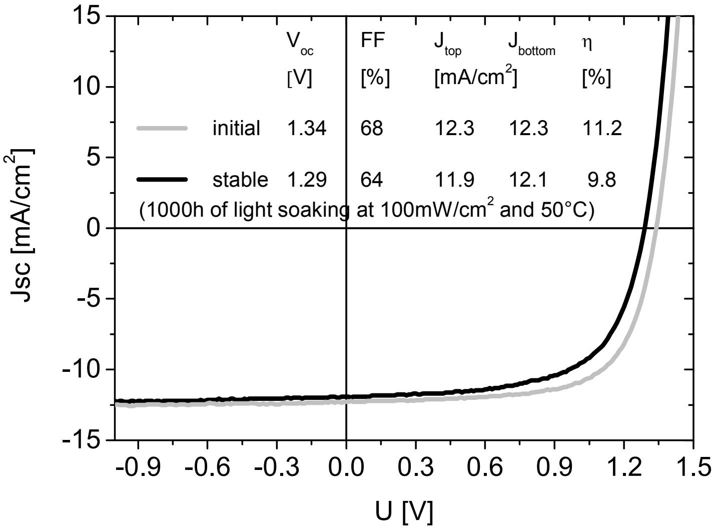

Figure 6-21 : Initial and stabilized EQE (up) and IV (down) of a micromorph tandem cell with an AIR deposited on PEN plastic substrates.

Table 6-7: Initial and stable efficiencies of n-i-p micromorph tandem cells with an AIR deposited on PEN plastic substrates. The stable parameters are obtained after 1000h of light soaking in standard conditions (1 sun, 100 mW/cm^2 and 50°C).

	V_{oc} [V]	FF [%]	J_{top} [mA/cm2]	J_{bottom} [mA/cm2]	Efficiency [%]
initial	1.34	68	12.3	12.3	11.2
stable	1.29	64	11.9	12.1	9.8

6.2.3.6 Triple junction solar cell

The AIR is also an efficient tool for triple junction structures with two purely amorphous top cells. A triple junction device with two a-Si:H cells does not offer further efficiency possibilities than a micromorph tandem cell since there is no increase of light absorption. In fact, we reduce the potential of absorption in the µc-Si:H solar cell since the limiting J_{sc} is half the possible limited J_{sc} of the micromorph case assuming that the limiting J_{sc} is proportional to the absorption in the a-Si:H material. Nonetheless, there are several advantages of making triple junction solar cells and modules. The voltage is higher than in micromorph cells and this should limit losses in the TCO, the light-induced degradation should be reduced as it is the case for tandem a-Si:H cells compared to single junction a-Si:H cells. Since the J_{sc} potential is lower, a lower µc-Si:H thickness is required. Therefore, for module and production costs, the triple junction solar cell is an interesting concept.

In Table 6-8, we report the initial and stable efficiency of a triple junction a-Si:H/a-Si:H/LP-CVD ZnO/µc-Si:H solar cell with thicknesses of 60 nm, 300 nm, 1.5 µm, and 1.4 µm for respectively top, middle, AIR and bottom cells. The back reflector is hot silver. The bottom cell EQE is not measurable. This happens with the AIR when the cell isolation is not ideal, i.e. there are probably also shunts. From our experience, we expect a bottom cell J_{sc} of 9 mA/cm^2, which will not be limiting. Therefore, the initial efficiency is 10.4% and is close to the best efficiency obtained with micromorph cells (11%) but this cell has a large light induced degradation of 18 %, which is a priori not expected. It is not yet clear why we observe such a high degradation but we suspect strong influences of the matching condition in the FF in such a triple junction device [151]. This is a first trial and therefore further work is needed. In fact this structure has the potential to achieve more than 10 % stable efficiency with less than 1 µm thick µc-Si:H bottom cells, assuming 6.5 mA/cm2, 2.3 V, and 70% of FF.

Table 6-8: Initial and stable performance parameters of a triple junction a-Si.H/a-Si:H/μc-Si:H solar cell. The μc-Si:H is 1.4 μm thick. The J_{sc} of the μc-Si:H cannot be determined by EQE measurements.

	V_{oc} [V]	FF [%]	J_{top} [mA/cm2]	J_{middle} [mA/cm2]	Efficiency [%]
initial	2.18	72	6.6	6.7	10.4
stable	2.17	63	6.4	6.2	8.5

6.3 Discussion

The single junction solar cells of Chapter 3 and 4 have initial efficiency close to 9 % for both a-Si:H and μc-Si:H solar cells. This Chapter shows that going to the tandem micromorph structure improves the initial efficiency to 11%. Clearly, the increase of light absorption with the combination of two different band gaps is the key to this improvement. Nonetheless, the best devices in the n-i-p configuration are made with a triple junction structure incorporating one or two a-Si:Ge cells [51]. So what are the benefits of SiGe cells compared to tandem micromorph devices?

In fact, there is no gain in light absorption because the band gap of a-Si:Ge is rarely below 1.1 eV. There is no real gain in conversion efficiency since in triple junction devices the gain in efficiency (voltage) due to the increased absorption of light in the middle cell instead of the bottom cell is compensated by the loss in efficiency (voltage) due to the absorption of light in the middle cell instead of the top cell. This is shown in Table 6-9 where we assume that the FF is constant (70%) for single and multi-junction structures. We assume typical V_{oc} and J_{sc} for a-Si:H and μc-Si:H. For an optimum middle cell, the band gap of the a-Si:Ge should be between the band gap of the a-Si:H and μc-Si.H. Therefore, we assume that the V_{oc} and J_{sc} of the middle cell to be the average between the a-Si:H and μc-Si:H (0.7 V and 21 mA/cm^2) which is close to reported data [207] . Assuming these values, we find that the efficiency of both tandem and triple junction solar cells are potentially equal according to the calculation, with 13.7% conversion efficiency.

6.3 Discussion

Table 6-9: Simulation of parameters for single junction, tandem micromorph and triple a-Si:H/a-Si:Ge/μc-Si:H.

	V_{oc} [mV]	FF [%]	J_{top} [mA/cm2]	J_{middle} [mA/cm2]	J_{bottom} [mA/cm2]	Eff. [%]
Single a-Si:H	0.9	70	16			10.0
Single μc-Si:H	0.5	70	28			9.8
Single a-Si:Ge	0.7	70	21			10.3
Micromorph	1.4	70	14		14	13.7
Triple junction	2.1	70	9.3	9.3	9.3	13.7

Therefore, choosing for a triple junction solar cell does not improve the initial efficiency of the solar cell. Nevertheless, the company Unisolar give solar cell efficiency of up to 15% and the main advantage is in the total J_{sc} with 28 mA/cm^2. Figure 6-22 shows the difference of EQE between their triple junction solar cell [13] and our micromorph. The difference is around 3 mA/cm^2(1 mA/cm^2 400-550 nm, 1mA/cm^2 550-750, 1mA/cm^2 750-1100nm):

- 1mA/cm^2 is explained by their ITO front contact as discussed in Chapter 5.
- 1 mA/cm^2 is explained by their p window layer.
- 0.5 mA/cm2 is due to our excess of reflection with our AIR as already discussed.
- 0.5 mA/cm2 is due to an increase of absorption in the red

Therefore, by using an ITO front contact and by working on the p layer of the amorphous cell, we should be able to reach a similar level of efficiency. One advantage of the triple junction structure is the reduced degradation of the top cell since it can be made thinner than in a high efficiency tandem cell. In fact the AIR concept is an alternative solution to make high efficiency tandem cells by using neither the triple junction devices nor Ge. The drawback of the micromorph concept compared to the triple junction are reflection losses which as shown can be minimized, and it is in compensation for the strong degradation problem arising from the inclusion of Ge in the a-Si:H layers. The best triple junction devices with Ge degrade by only 10% [208], which is comparable to degradation obtained in Table 6-7 with the AIR.

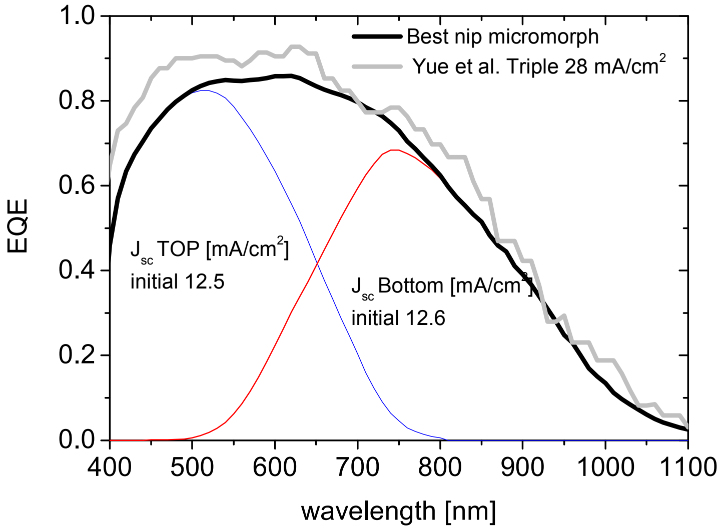

Figure 6-22: EQE of triple junction solar cell from Unisolar [13] and EQE of our best matched micromorph.

In summary, we have fully implemented an AIR that selectively scatters the blue-green light into the top cell whereas the scattering of the red light into the bottom cell is achieved by the back reflector structure which is applied to the substrate. Such a structure can reach matched J_{sc} up to almost 12 mA/cm^2 in the stabilized state, which is a necessary starting point for realizing 12% stable efficiencies in micromorph tandem cells on plastic substrates (assuming, e.g. a V_{oc} of 1.4 V and a FF of 71%). Stable J_{sc} of 12 mA/cm^2 correspond to state-of-the-art micromorph tandem cells reported by Unisolar [208] and Kaneka [11] (assuming 4 segments in ref. [11]). The idea of having a double structure with a diffractive interlayer (DIR) was proposed by numerical calculation in the p-i-n by Obermeyer et al. [209]. Nevertheless, the technological tools are not yet available for this complex p-i-n design. Our AIR in the n-i-p configuration overcomes the technological challenges that is limiting the p-i-n devices, and offers an alternative to the complex triple junction devices.

6.4 Conclusion

The combination of the high gap 1.7eV a-Si:H and 1.1 eV µc-Si:H in the micromoprh tandem cell is almost ideal. Nonetheless, many technical constraints have to be taken into account to achieve high conversion efficiency cells and this is especially true for n-i-p solar cells. Indeed, we showed that the degradation of the a-Si:H solar cell requires the implementation of the IR concept. Furthermore, the µc-Si:H deposition flattens the surface for the top cell deposition, which results in reduction of light scattering in the top a-Si:H solar cell. Therefore, the AIR is one solution to restore the ideal texture for a-Si:H solar cell. By including this tool in our device, we were able to fabricate a micromorph tandem cell with close to 10% stabilized efficiency on PEN plastic substrate.

Chapter 7: Final conclusion

Summary and perspectives

The aim of this work was to develop high efficiency thin film silicon devices, but taking into account two constraints: one was to keep the compatibility with low T_g substrates, and the second was to concentrate on the thin film silicon materials a-Si:H and μc-Si:H without the addition of Ge. Thereby, the accessible range of deposition temperatures between 150 and 180°C is not ideal for the deposition of high quality silicon material, and the accessible band gaps restrict the spectral management of the light inside the devices. All devices considered here are grown in the n-i-p configuration for which less experience was available in the laboratory compared to the standard p-i-n structures on glass. In the following section, we summarize the major results and insights provided by this work and show that, even taking into account the mentioned constraints, we achieve efficiencies well within the range of state-of-the-art devices.

The light trapping scheme in a variety of configurations has been tested and the interaction between front TCO and back contact could be clarified. Indeed, we demonstrate that high J_{sc} can be achieved on random and on periodic substrates for both a-Si:H and μc-Si:H. The conventional ZnO/Ag back contact deposited on a texture can be replaced by a rough LP-CVD ZnO, which provides the template for the light trapping, coupled with flat silver or white paint placed below the LP-CVD ZnO as back reflector. This structure reduces the parasitic plasmonic absorptions observed for rough metallic layers. We confirm the J_{sc} gain in using Ag instead of Al for textured substrate and the importance of the ZnO layer in the back reflector. For a-Si:H, the morphology of the substrate's nanotexture is found more critical compared to the size of theses structures for efficient light trapping inside the device. Indeed, the J_{sc} of a-Si:H cell is increased relatively by 11% on a V-shape structure compared to a U-shape structure, whereas almost no variation is observed when the feature size is varied from 250 nm to 1 μm. We show that a rough LP-CVD ZnO front contact improves for the light trapping compared to flat ITO, but only when a thin a-Si:H cell is deposited on periodic substrates. In this case, the relative gain in J_{sc} is 7 % for the LP-CVD ZnO. For thick μc-Si absorber layers, the ITO front contact is better and provides 4 % more J_{sc} compared to LP-CVD ZnO.

The influence of the texture morphology on the device electrical parameters could be quantified by the variation of the shape of the LP-CVD ZnO pyramids. V_{oc} and FF losses are correlated with nano-cracks observed by TEM and these effects seem universal for both a-Si:H and μc-Si:H solar cells deposited on V-shape morphology (ideal for light trapping). However, these effects can be mitigated by implementing additional layers and processes. An amorphous n-SiC layer with a highly diluted buffer layer suppresses these nano-cracks and therefore the V_{oc} and FF losses. Hence, the efficiency of single junction a-Si:H solar cells can be really increased by more than 20 % on textured substrate compared to the flat case. For μc-Si:H solar cells, we show that an amorphous buffer layer increases the efficiency of the cell by decreasing the numbers of cracks in the absorber material and decreasing the oxygen content in the layer. A μc-Si:H solar cell with efficiency of an 9% is made for an only 1.2 μm thick absorber layer.

The light trapping, V_{oc} and FF issues are simultaneously addressed for micromorph tandem cells. For that, we compare tandem cells without an intermediate reflector, with a symmetric intermediate reflector (SIR) and with asymmetric intermediate reflector (AIR). In particular, the innovative AIR solution allows the uncoupling of the light trapping and the growth of the layers in the top a-Si:H and bottom μc-Si:H solar cells. With that, we achieved stabilized micromorph tandem solar cells deposited on low T_g flexible plastic substrate with a 9.8 % efficiency.

The first results with triple junction a-Si/a-Si/μc-Si solar cells with AIR between the two top and the bottom cell are promising. Indeed, 10.4 % initial efficiency is attained with only 1 μm thick μc-Si:H bottom cells.

In this thesis, we have focused on specific parts of the devices (emphasis on n-i interface, light trapping, and role of substrate morphology). We therefore expect further improvement when other aspects of the devices and interfaces are studied in more detail. This concerns, especially the p-side of the device where better p-i interface, window layers and improved ITO/p contact should be implemented to reach higher device performances. We expect that by implementing better window- and p-layers in the a-Si:H top cell that the stabilized efficiency on plastic substrates can be increased to up to 8.5 % efficiency for single junction a-Si:H cells and above 12 % efficiency for micromorph tandem cells, which would be higher than the currently best certified stabilized efficiency reported on glass substrates (11.7%). As most of our findings are applicable to low T_g plastic, some of them could hopefully be implemented in production lines at some point, thereby contributing to the target of lower productions costs.

Acknowledgements

The work was supported by the University of Neuchâtel, the European project Flexcellence (019948) and the OFEN (101191).

I sincerely thank Prof. Christophe Ballif for giving me the opportunity to discover the photovoltaic world. His enthusiasm, scientific skills and his will to go beyond traditional ideas guide this work.

I appreciate greatly the acceptance of the referees (Dr. Diego Fischer, Dr. Wim Soppe and Prof. Helen Stoeckli-Evans) to devote time to reading and improving this manuscript.

The results shown in this work are shared with my PV-LAB colleagues. Indeed, the solar cell development is a multi-dimension problem that can only be solved with the group of competencies in Neuchâtel. In particular I would like to thank my closest colleagues: Dr. Franz-Joseph Haug, Dr. Vanessa Terrazzoni and Xavier Niquille. They all add value to this thesis through their expertise. Franz devotes his scientific knowledge and his talent to explain me the physics of the devices. Vanessa supports this work with her clear mind, pragmatic and structured vision. Xavier brings his instinct for microcrystalline solar cell developments.

I also thank S. Perregaux for the SEM micrographs, Dr. M. Python and M. Charrière for the TEM micrographs used in this work. I thank S. Sweetnam and K. Verrechia for the reading and correcting the English.

I appreciate the enthusiasm and the great discussions I have shared with Julien, Didier, Peter, Jérome, Andrea, Fanny, Gregory, Stefan, Nicolas, Gaetano, Adrien, Sara, Benjamin, Céline, Richard, Yann, Alo, Reto, Cédric, Sylvie, Nuno, Fabrice, Sylvain, Luc, Ségolène, Marylène, Marlène, who helped to improve the device performances and my understanding. I thank Brigitte, Hassan and Joelle for the administrative, IT and friendly support.

My last word goes to my girlfriend Ana Cudell who continuously supports me and my ideas.

List of publications and patent

1) **T. Söderström**, F.-J. Haug, V. Terrazzoni-Daudrix, X. Niquille and C. Ballif
Asymmetric Intermediate Reflector for Micromorph Thin Film Silicon Solar Cells
Applied Physics Letters, 94, 063501, 2009

2) **T. Söderström**, F.-J. Haug, X. Niquille, C. Ballif
TCOs for nip thin film silicon solar cells
Progress in Photovoltaics: Research and Applications, p. 165-176, 2009

3) **T. Söderström**, F.-J. Haug, X. Niquille
Dispositif Photoelectrique à Jonction Multiple et son Procédé de Réalisation
Patent EP08169423.4, 2008

4) F.-J. Haug, **T. Söderström**, M. Python, V. Terrazzoni-Daudrix, X. Niquille, C. Ballif
Development of micromorph tandem solar cells on flexible low-cost plastic substrates
Solar Energy Material and Solar cells, 2008

5) **T. Söderström**, F.-J. Haug, V. Terrazzoni-Daudrix, X. Niquille, M. Python and C. Ballif
N/I buffer layer for substrate microcrystalline thin film silicon solar cell
Journal of Applied Physics, 104, p.104505, 2008

6) O. Cubero, **T. Söderström**, F.-J. Haug, V. Terrazzoni-Daudrix, X. Niquille, S. Perregaux, M. Raeis-Barneoud and C. Ballif
Latest Results on Stabilized Flexible Thin Film Silicon Solar Cells
Proceedings of the 23th EU-PVSEC, Valencia, p. 2101, 2008

7) L. H. Slooff, S. Böhme, W. Eerenstein, S. C. Veenstra, W. Verhees, J. M. Kroon, **T. Söderström**
Fabrication and characterisation of polymer based solar cells
Proceedings of the SPIE Organic Photovoltaics IX, Vol. 7052, 2008

8) F.-J. Haug, **T. Söderström**, O. Cubero, V. Terrazzoni-Daudrix, C. Ballif
Plasmonic absorption in textured silver back reflectors of thin film solar cells
Journal of Applied Physics, Vol. 104, p. 064509, 2008

9) **T. Söderström**, F.-J. Haug, V. Terrazzoni-Daudrix, and C. Ballif
Optimization of amorphous silicon thin film solar cells for flexible photovoltaics
Journal of Applied Physics, 103, p. 114509, 2008

10) **T. Soderstrom**, F.-J. Haug, X. Niquille, O. Cubero, S. Perregaux, and C. Ballif
Optical developments for silicon thin film solar cells in the substrate configuration
Proceedings of the MRS Spring Meeting, San Francisco, 1101-KK04-05, 2008

11) F.-J. Haug, **T. Söderström**, O. Cubero, V. Terrazzoni-Daudrix, X. Niquille, S. Perregeaux, and C. Ballif
Periodic textures for enhanced current in thin film silicon solar cells
Proc. of the MRS Spring Meeting, San Francisco, p. 1101-KK13-01, 2008

12) K. Brecl, F.-J. Haug, **T. Söderström**, M. Topic
Electrical losses in substrate and superstrate micromorph modules
Proceedings of the 22nd EU-PVSC Conference, Milan, p. 2157, 2007

13) F.-J. Haug, V. Terrazzoni-Daudrix, **T. Söderström**, X. Niquille, and C. Ballif
Development of micromorph tandem solar cells on flexible low cost plastic substrates
Technical digest of the 17th International Photovoltaic Solar Energy Conference, Fukuoka, p. 335, 2007

14) J. Bailat, D. Dominé, P. Buehlmann, **T. Söderström**, F. J. Haug, V. Daudrix-Terrazzoni, N. Wyrsch, J. Steinhauser, S. Fay and C. Ballif
Thin Film Silicon Solar Cells: Latest Developments in Europe
Technical digest of the 17th International Photovoltaic Solar Energy Conference, Fukuoka, p. 33, 2007

15) **T. Söderström**, F.-J. Haug, V. Terrazzoni-Daudrix X. Niquille, S. Perregaux, M. Fahland and C. Ballif
Open-circuit voltage optimisation of amorphous silicon thin film solar cells for flexible photovoltaics
Proceedings of the 22nd EU-PVSC Conference, Milan, p. 1819, 2007

16) F.-J. Haug, V. Terrazzoni-Daudrix, **T. Söderström**, X. Niquille, J. Bailat, C. Ballif
Flexible microcrystalline silicon solar cells on periodically textured plastic substrates
Proceedings Of the 21st EU PVSEC, Dresden, p. 1661, 2006

17) F. Meillaud, A. Shah, J. Bailat, E. Vallat-Sauvain, T. Roschek, B. Rech, D. Didier, **T. Söderström**, M. Python, C. Ballif
Microcrystalline silicon solar cells: Theory and diagnostic tools
Proc. of the 4th WCPEC Conference, Hawaii, p. 1572, 2006

References

[1] OFEN, Office Fédéral de l'Energie http://www.bfe.admin.ch

[2] A. E. Becuerel, Comptes Rendus de l'Académie des Sciences 9 (1839) 561.

[3] N. S. Lewis and D. G. Nocera, Proc. of National Academy of Science USA 103 (2006) 15729.

[4] K. Kurokawa, K. Komoto, P. Van Der Vleuten, and D. Faiman, Earthscan, IEA PVPS Task 8, http://www.iea-pvps.org/products/download/rep8_02s.pdf (2006)

[5] Swissolar, http://www.swissolar.ch/fileadmin/x_lib/download/SWIS_Photovoltaik_2007_fr.pdf (2007)

[6] A. Jäger-Waldau, Office for Official Publications of the European Communities (2008)

[7] D. Sarti and R. Einhaus, Solar Energy Materials and Solar Cells 72 (2002) 27.

[8] S. Guha and J. Yang, Technical Digest of the International PVSEC-18, Kolkata, India, 2009 (2009)

[9] Worldwatch, Earth Policy Institute, http://www.earth-policy.org

[10] D. L. Staebler and C. R. Wronski, Applied Physics Letters 31 (1977) 292.

[11] M. Green, K. Emery, D. King, Y. Hisikawa, and W. Warta, Progress in Photovoltaics: Research and Applications 14 (2006) 45.

[12] K. Yamamoto, A. Nakajima, M. Yoshimi, T. Sawada, S. Fukuda, T. Suezaki, M. Ichikawa, Y. Koi, M. Goto, and T. Meguro, Progress in Photovoltaics 13 (2005) 489.

[13] J. Yang, A. Banerjee, and S. Guha, Applied Physics Letters 70 (1997) 2975.

[14] S. Benagli, U. Kroll, J. Meier, D. Borrello, J. Spitznagel, G. Androutsopoulos, G. Monteduro, D. Zimin, O. Kluth, T. Roschek, C. Ellert, W. Stein, G. Buechel, A. Buechel, and D. Koch-Ospelt, Proceedings of the 21st EUPVSEC, Dresden, Germany (2006) 1719.

[15] V. T. Daudrix, J. Guillet, F. Freitas, A. Shah, C. Ballif, P. Winkler, M. Ferreloc, S. Benagli, X. Niquille, and D. Fischer, Progress in Photovoltaics: Research and Applications 14 (2006) 485.

[16] J. Bailat, L. Castens, S. Benagli, D. Borello, J. Spitznagel, Y. Djeridane, P.-A. Madliger, B. Dehbozorgi, G. Monteduro, J. Steinhauser, M. Marmelo, J. Hoetzl, E. Vallat-Sauvain, U. Kroll, and J. Meier, Technical Digest of the International PVSEC-18, Kolkata, India, 2009 (2009)

[17] B. Rech, T. Repmann, S. Wieder, M. Ruske, and U. Stephan, Thin Solid Films 502 (2006) 300.

[18] C. Das, A. Lambertz, J. Huepkes, W. Reetz, and F. Finger, Applied Physics Letters 92 (2008) 053509.

[19] D. Domine, PhD Thesis, Neuchâtel (2009)

[20] J. Meier, U. Kroll, E. Vallat-Sauvain, J. Spitznagel, U. Graf, and A. Shah, Solar Energy 77 (2004) 983.

[21] C. Kittel, "Introduction to solid state physics", Wiley (1986)

[22] R. A. Street, "Hydrogenated amorphous silicon", Cambridge Solid State Science Series (1991)

[23] P. W. Anderson, Physical Review 109 (1958) 1492.

[24] R. A. Street, Physical Review Letters 49 (1982) 1187.

[25] G. A. Swartz, Applied Physics Letters 44 (1984) 697.

[26] H. Dersch, J. Stuke, and J. Beichler, Applied Physics Letters 38 (1981) 456.

[27] H. R. Park, J. Z. Liu, P. R. i. Cabarrocas, A. Maruyama, M. Isomura, S. Wagner, J. R. Abelson, and F. Finger, Applied Physics Letters 57 (1990) 1440.

[28] H. R. Park, J. Z. Liu, and S. Wagner, Applied Physics Letters 55 (1989) 2658.

[29] C. Hof, Y. Ziegler, R. Platz, N. Wyrsch, and A. Shah, Journal of Non-Crystalline Solids 227-230 (1998) 287.

[30] R. A. Street, Physical Review B 43 (1991) 2454.

[31] M. Stutzmann, W. B. Jackson, and C. C. Tsai, Physical Review B 32 (1985) 23.

[32] D. K. Biegelsen and M. Stutzmann, Physical Review B 33 (1986) 3006.

[33] E. Sauvain, PhD Thesis, Neuchâtel (1992)

[34] C. Droz, PhD Thesis, Neuchâtel (2003)

[35] M. Python, PhD Thesis, Neuchâtel (2009)

[36] B. Strahm, A. A. Howling, L. Sansonnens, C. Hollenstein, U. Kroll, J. Meier, C. Ellert, L. Feitknecht, and C. Ballif, Solar Energy Materials and Solar Cells 91 (2007) 495.

[37] M. N. Van Den Donker, B. Rech, F. Finger, L. Houben, W. M. M. Kessels, and M. C. M. Van De Sanden, Progress in photovoltaics 15 (2007) 291.

[38] M. Katiyar and J. R. Abelson, Materials Science & Engineering A 304 (2001) 349.

[39] N. Layadi, P. Roca i Cabarrocas, B. Drévillon, and I. Solomon, Physical Review B 52 (1995) 5136.

[40] K. Nakamura, K. Yoshida, S. Takeoka, and I. Shimizu, Japanese Journal of Applied Physics 34 (1995) 442.

[41] S. Sriraman, S. Agarwal, E. S. Aydil, and D. Maroudas, Nature 418 (2002) 62.

[42] F. Meillaud, PhD Thesis, Neuchâtel (2006)

[43] T. Dylla, Phd Thesis, Jülich (2004)

[44] R. W. Collins, A. S. Ferlauto, G. M. Ferreira, C. Chen, J. Koh, R. J. Koval, Y. Lee, J. M. Pearce, and C. R. Wronski, Solar Energy Materials and Solar Cells 78 (2003) 143.

[45] J. Bailat, PhD Thesis, Neuchâtel (2004)

[46] A. Banerjee and S. Guha, Journal of Applied Physics 69 (1991) 1030.

[47] I. Tobías and A. Luque, Progress in Photovoltaics: Research and Applications 10 (2002) 323.

[48] W. Shockley and H. Queisser, Journal of Applied Physics 32 (1961) 510.

[49] J. Meier, S. Dubail, S. Golay, U. Kroll, S. Fay, E. Vallat-Sauvain, L. Feitknecht, J. Dubail, and A. Shah, Solar Energy Materials and Solar Cells 74 (2002) 457.

[50] K. Saito, M. Sano, K. Matuda, T. Kondo, T. Nishimoto, K. Ogawa, and I. Kajita, Proc. 2nd World Conf. Vienna (1998) 351.

[51] B. Yan, G. Yue, J. M. Owens, J. Yang, and S. Guha, Conference Record of the 2006 IEEE 4th World Conference on Photovoltaic Energy Conversion (IEEE Cat. No. 06CH37747) (2006) 4 pp.

[52] U. Kroll, A. Shah, H. Keppner, J. Meier, P. Torres, and D. Fischer, Solar Energy Materials and Solar Cells 48 (1997) 343.

[53] X. Xu, B. Yan, D. Beglau, Y. Li, G. DeMaggio, G. Yue, A. Banerjee, J. Yang, S. Guha, P. Hugger, and J. Cohen, MRS Proceedings 1066 (2008) A14.

[54] M. Shimosawa, S. Kawano, T. Ischikawa, T. Nakamura, Y. Sakakibara, S. Kiyofuji, H. Enomoto, H. Nishiara, T. Kamoschita, M. Miyagi, J. Saito, and A. Takano, MRS Proceedings, Symposium A 1066-A14-01 (2008)

[55] W. J. Soppe, C. Devilee, M. Geusebroek, J. Löffler, and H. J. Muffler, Thin Solid Films 515 (2007) 7490.

[56] W. J. Soppe, H. J. Muffler, A. C. Biebericher, C. Devilee, A. R. Burgers, A. Poruba, L. Hodakova, and M. Vanecek, Proc. 20th European PVSEC (2005) p. 3DV.3.21.

[57] R. E. I. Schropp, Technical Digest of the International PVSEC-18, Kolkata, India, 2009 (2009)

[58] A. Matsuda, Journal of Non-Crystalline Solids 338-340 (2004) 1.

[59] H. Mase, M. Kondo, and A. Matsuda, Solar Energy Materials and Solar Cells 74 (2002) 547.

[60] C. Koch, M. Ito, M. Schubert, and J. Werner, Proc. of the MRS 557 (1999)

[61] Y. Ishikawa and M. B. Schubert, Japanese Journal of Applied Physics 45 (2006) 6812.

[62] K. Katsuma, S. Hayakawa, A. Masuda, T. Matsui, and M. Kondo, Proc. of the 22th EU PVSEC (2007)

[63] J. K. Rath, Technical Digest of the International PVSEC-18, Kolkata, India, 2009 (2009)

[64] P. Pernet, R. Felder, M. Goetz, H. Keppner, D. Fischer, and A. Shah, Proceedings of the 14th EC Photovoltaic Solar Energy Conference (1997) 2339.

[65] V. Terrazzoni-Daudrix, Phd Thesis, Neuchâtel (2004)

[66] J. Bailat, V. Terrazzoni-Daudrix, J. Guillet, F. Freitas, X. Niquille, A. Shah, C. Ballif, T. Scharf, R. Morf, A. Hansen, D. Fischer, Y. Ziegler, and A. Closset, Proc. of the 20th European PVSEC (2005) 1529.

[67] M. Hirasaka, K. Suzuki, K. Nakatani, M. Asano, M. Yano, and H. Okaniwa, Solar Energy Materials 20 (1990) 99.

[68] H. Sai, H. Fujiwara, M. Kondo, and Y. Kanamori, Applied Physics Letters 93 (2008) 143501.

[69] C. Heine and R. H. Morf, Applied Optics 34 (1995) 2476.

[70] J. Springer, B. Rech, W. Reetz, J. Muller, and M. Vanecek, Solar Energy Materials and Solar Cells 85 (2005) 1.

[71] Y. Nasuno, M. Kondo, and A. Matsuda, Jpn. J. Appl. Phys., Part 40 (2001) L303.

[72] J. Bailat, D. Domine, R. Schluchter, J. Steinhauser, S. Fay, F. Freitas, C. Bucher, L. Feitknecht, X. Niquille, T. Tscharner, A. Shah, and C. Ballif, Proc. of the 4th World WCPEC (2006) 4

[73] M. Python, E. Vallat-Sauvain, J. Bailat, D. Dominé, L. Fesquet, A. Shah, and C. Ballif, Journal of Non-Crystalline Solids 354 (2008) 2258.

[74] H. B. T. Li, R. H. Franken, J. K. Rath, and R. E. I. Schropp, Solar Energy Materials and Solar Cells 93 (2009) 338.

[75] M. Lill and B. Schroder, Applied Physics Letters 74 (1999) 1284.

[76] A. Vijh, X. Yang, W. Du, and X. Deng, Solar Energy Materials and Solar Cells 90 (2006) 2657.

[77] Y. Ichikawa, S. Fujikake, H. Ohta, T. Sasaki, and H. Sakai, Photovoltaic Specialists Conference, 1991., Conference Record of the Twenty Second IEEE (1991) 1296.
[78] R. E. I. Schropp, H. Li, R. H. Franken, J. K. Rath, C. H. M. van der Werf, J. W. A. Schüttauf, and R. L. Stolk, Thin Solid Films 516 (2008) 6818.
[79] K. Saito, M. Sano, S. Okabe, S. Sugiyama, and K. Ogawa, Solar Energy Materials and Solar Cells 86 (2005) 565.
[80] F. R. Jeffrey, D. P. Grimmer, S. Brayman, B. Scandrett, M. Thomas, S. A. Martens, W. Chen, and M. Noak, Vol. 394 (C. E. Witt, A.-J. Mowafak, and M. G. James, eds.), AIP, 1997, p. 451.
[81] Y. Liu, J. K. Rath, and R. E. I. Schropp, Surface and Coatings Technology 201 (2007) 9330.
[82] B. Vet, M. Zeman, A. Borreman, E. A. G. Hamers, and R. Schlatsmann, Proc. 23rd European PVSEC (Valencia) (2008)
[83] http://www.semiconductor-sanyo.com/amorton/solar_battery/amorton_film.htm,
[84] S. Guha, J. Yang, P. Nath, and M. Hack, Applied Physics Letters 49 (1986) 218.
[85] G. Yue, B. Yan, G. Ganguly, J. Yang, S. Guha, C. W. Teplin, and D. L. Williamson, in Proc. of the 4th World IEEE Conference, Vol. 2, 2006, p. 1588.
[86] W. Du, X. Liao, X. Yang, H. Povolny, X. Xiang, X. Deng, and K. Sun, Solar Energy Materials and Solar Cells 90 (2006) 1098.
[87] X. Deng, R. W. Collins, X. Cao, C. Das, W. Du, L. Edwards, Y. Ishikawa, T. Kahle, N. Podraza, H. S. S. Povolny, D. Sainju, J. Stoke, X. Yang, and A. Vijh, DOE Solar Program Review, Denver (2005)
[88] M. Yano, K. Suzuki, K. Nakatani, and H. Okaniwa, Thin Solid Films 146 (1987) 75.
[89] T. Söderström, F. J. Haug, X. Niquille, and C. Ballif, Progress in Photovoltaics (2009)
[90] T. Söderström, F. J. Haug, V. Terrazzoni-Daudrix, and C. Ballif, Journal of Applied Physics 103 (2008) 114509.
[91] T. Söderström, F.-J. Haug, V. Terrazzoni-Daudrix, X. Niquille, S. Perregeaux, M. Fahland, and C. Ballif, Proc. 22nd European PVSEC (2007)
[92] T. Soderstrom, F. J. Haug, V. Terrazzoni-Daudrix, X. Niquille, M. Python, and C. Ballif, Journal of Applied Physics 104 (2008) 104505.
[93] T. Soderstrom, F.-J. Haug, X. Niquille, V. Terrazzoni, and C. Ballif, Applied Physics Letters 94 (2009) 063501.
[94] U. Graf, Phd thesis University of Neuchâtel (2005)
[95] R. C. Chittick, J. H. Alexander, and H. F. Sterling, Journal of The Electrochemical Society 116 (1969) 77.
[96] M. Tanda, M. Kondo, and A. Matsuda, Thin Solid Films 427 (2003) 33.
[97] Y. Takeuchi, H. Mashima, M. Murata, S. Uchino, and Y. Kawai, Jpn. J. Appl. Phys. 40 (2001) 3405.
[98] M. Fahland, V. Kirchhoff, C. Charton, and P. Karlsson, Proc. of the 43rd Technical Conference of the Society of Vacuum Coaters (2000) 357.
[99] L. Feitknecht, O. Kluth, Y. Ziegler, X. Niquille, P. Torres, J. Meier, N. Wyrsch, and A. Shah, Proceeding PVSEC11, Sapporo, Japan (1999)
[100] J. Steinhauser, Phd thesis University of Neuchâtel (2008)

[101] R. H. Franken, R. L. Stolk, H. Li, C. H. M. v. d. Werf, J. K. Rath, and R. E. I. Schropp, Journal of Applied Physics 102 (2007) 014503.

[102] M. Worgull, J. F. Hétu, K. K. Kabanemi, and M. Heckele, Microsystem Technologies 12 (2006) 947.

[103] C. Elsner, J. Dienelt, and D. Hirsch, Microelectronic Engineering 65 (2003) 163.

[104] F.-J. Haug, V. Terrazzoni-Daudrix, T. Söderström, X. Niquille, J. Bailat, and C. Ballif, Proc. of the 21st European PVSEC (2006) 1651.

[105] K. Taretto, U. Rau, and J. H. Werner, Applied Physics A: Materials Science & Processing 77 (2003) 865.

[106] M. Zeman, J. A. Willemen, G. Tao, and J. W. Metselaar, Applied Solar Energy 31 (1995) 30.

[107] J. Merten, J. M. Asensi, C. Voz, A. V. Shah, R. Platz, and J. Andreu, IEEE Transactions on Electron Devices 45 (1998) 423.

[108] M. Vanecek, J. Kocka, J. Stuchlík, and A. Tríska, Solid State Communications 39 (1981) 1199.

[109] A. C. Boccara, D. Fournier, and J. Badoz, Applied Physics Letters 36 (1980) 130.

[110] A. Poruba, M. Vanecek, J. Meier, and A. Shah, Journal of Non-Crystalline Solids 299-302 (2002) 536.

[111] C. Droz, E. Vallat-Sauvain, J. Bailat, L. Feitknecht, J. Meier, and A. Shah, Solar Energy Materials and Solar Cells 81 (2004) 61.

[112] M. S. Bennett, J. l. Newton, and K. Rajan, Proc. of the 2nd PVSEC (1987)

[113] M. Stutzmann and R. A. Street, Physical Review Letters 54 (1985) 1836.

[114] J. Benedict, R. Anderson, and S. J. Klepeis, Proc. of the MRS 254 (1992) 121.

[115] P. Beckman and A. Spizzichno, Pergamon Press, Oxford Chapter 5 (1963)

[116] D. Dominé, P. Buehlmann, J. Bailat, A. Billet , A. Feltrin, and C. Ballif, Physica Status Solidi (RRL) - Rapid Research Letters 2 (2008) 163.

[117] J. Woerdenweber, T. Merdzhanova, R. Schmitz, A. Muck, U. Zastrow, L. Niessen, A. Gordijn, R. Carius, W. Beyer, H. Stiebig, and U. Rau, Journal of Applied Physics 104 (2008) 094507.

[118] M. Losurdo, R. Rizzoli, C. Summonte, G. Cicala, P. Capezzuto, and G. Bruno, Journal of Applied Physics 88 (2000) 2408.

[119] J. Bailat, D. Domine, R. Schluchter, J. Steinhauser, S. Fay, F. Freitas, C. Bucher, L. Feitknecht, X. Niquille, T. Tscharner, A. Shah, and C. Ballif, Conference Record of the 2006 IEEE 4th World Conference on Photovoltaic Energy Conversion (IEEE Cat. No. 06CH37747) (2006) 4 pp.

[120] R. B. Bergmann and J. H. Werner, Thin Solid Films 403-404 (2002) 162.

[121] Y. Mai, S. Klein, R. Carius, J. Wolff, A. Lambertz, F. Finger, and X. Geng, Journal of Applied Physics 97 (2005) 114913.

[122] B. Strahm, A. A. Howling, L. Sansonnens, and C. Hollenstein, Plasma Sources Science and Technology 16 (2007) 80.

[123] Y. Poissant, P. Chatterjee, and P. R. I. Cabarrocas, Journal of Applied Physics 93 (2003) 170.

[124] B. Yan, G. Yue, J. Yang, S. Guha, D. L. Williamson, D. Han, and C.-S. Jiang, Applied Physics Letters 85 (2004) 1955.

[125] A. Gordijn, J. Francke, L. Hodakova, J. K. Rath, and R. E. I. Schropp, MRS Proceedings 862 (2005) 87.

[126] C. Niikura, M. Kondo, and A. Matsuda, 19th European PVSEC (2004) 1637.

[127] P. Torres, J. Meier, R. Fluckiger, U. Kroll, J. A. A. Selvan, H. Keppner, A. Shah, S. D. Littelwood, I. E. Kelly, and P. Giannoules, Applied Physics Letters 69 (1996) 1373.

[128] T. Kilper, M. N. M.N. van den Donker, D. Grunsky, A. Mück, R. Schmitz, U. Zastrow, B. Rech, G. Bräuer, S. Klein, and T. Repmann, Proc. 21st European PVSEC (Dresden) (2006) 1738.

[129] A. Shah, E. Vallat-Sauvain, P. Torres, J. Meier, U. Kroll, C. Hof, C. Droz, M. Goerlitzer, N. Wyrsch, and M. Vanecek, Materials Science and Engineering B 69-70 (2000) 219.

[130] J. Kuendig, M. Goetz, A. Shah, L. Gerlach, and E. Fernandez, Solar Energy Materials and Solar Cells 79 (2003) 425.

[131] M. Python, E. Vallat-Sauvain, T. Söderström, and C. Ballif, To be submitted in APL (2008)

[132] B. Schroeder, Thin Solid Films 430 (2003) 1.

[133] J. Meier, R. Fluckiger, H. Keppner, and A. Shah, Applied Physics Letters 65 (1994) 860.

[134] E. Vallat-Sauvain, J. Bailat, J. Meier, X. Niquille, U. Kroll, and A. Shah, Thin Solid Films 485 (2005) 77.

[135] J.-H. Zhou, K. Ikuta, T. Yasuda, T. Umeda, S. Yamasaki, and K. Tanaka, Applied Physics Letters 71 (1997) 1534.

[136] J. Koh, A. S. Ferlauto, P. I. Rovira, C. R. Wronski, and R. W. Collins, Applied Physics Letters 75 (1999) 2286.

[137] P. R. i. Cabarrocas, N. Layadi, T. Heitz, B. Drevillon, and I. Solomon, Applied Physics Letters 66 (1995) 3609.

[138] M. Kondo, Y. Toyoshima, A. Matsuda, and K. Ikuta, Journal of Applied Physics 80 (1996) 6061.

[139] M. N. van den Donker, S. Klein, B. Rech, F. Finger, W. M. M. Kessels, and M. C. M. van de Sanden, Applied Physics Letters 90 (2007) 183504.

[140] L. Sansonnens, A. A. Howling, and C. Hollenstein, Plasma Sources Science and Technology 7 (1998) 114.

[141] Y. Nasuno, M. Kondo, and A. Matsuda, Applied Physics Letters 78 (2001) 2330.

[142] U. Kroll, J. Meier, H. Keppner, S. D. Littlewood, I. E. Kelly, P. Giannoules, and A. Shah, Materials Research Society, 1995.

[143] G. Z. Yue, B. J. Yan, G. Ganguly, J. Yang, S. Guha, and C. W. Teplin, Applied Physics Letters 88 (2006)

[144] H. Sakai, T. Yoshida, T. Hama, and Y. Ichikawa, Japanese Journal of Applied Physics 29 (1990) 630.

[145] S. Fay, U. Kroll, C. Bucher, E. Vallat-Sauvain, and A. Shah, Solar Energy Materials and Solar Cells 86 (2005) 385.

[146] N. P. Vaucher, B. Rech, D. Fischer, S. Dubail, M. Goetz, H. Keppner, N. Wyrsch, C. Beneking, O. Hadjadj, V. Shklover, and A. Shah, Solar Energy Materials and Solar Cells 49 (1997) 27.

[147] Y. Hamakawa and Y. Tawada, US Patent 4385199 (1983)

[148] J. Krc, F. Smole, and M. Topic, Progress in Photovoltaics: Research and Applications 11 (2003) 15.

[149] J. Krc, Phd Thesis, University of Ljubljana (2002)

[150] Y. Tawada, M. Kondo, H. Okamoto, and Y. Hamakawa, Solar Energy Materials 6 (1982) 299.

[151] R. Platz, Phd Thesis, Neuchâtel (1999)

[152] B. J. Yan, J. Yang, and S. Guha, Applied Physics Letters 83 (2003) 782.

[153] J. H. Koh, Y. H. Lee, H. Fujiwara, C. R. Wronski, and R. W. Collins, Applied Physics Letters 73 (1998) 1526.

[154] F. Meillaud, Phd thesis University of Neuchâtel (2006)

[155] C. Hof, (1999)

[156] M. S. Bennett and K. Rajan, Photovoltaic Specialists Conference, Conference Record of the Twentieth IEEE (1988) 67.

[157] L. Yang, L. Chen, and A. Catalano, Applied Physics Letters 59 (1991) 840.

[158] N. Hata and S. Wagner, Journal of Applied Physics 72 (1992) 2857.

[159] M. S. Bennett, J. L. Newton, and K. Rajan, 7th EPVSEC (1986) p. 544.

[160] S. Benagli, U. Kroll, J. Meier, D. Borrello, and J. Spitznagel, Proc. of the 23rd EUPVSEC, Milan, Italy (2007)

[161] S. Benagli, J. Hoetzel, D. Borrello, J. Spitznagel, U. Kroll, J. Meier, E. Vallat-Sauvain, J. Bailat, L. Castens, P. Madliger, B. Dehbozorgi, G. Monteduro, M. Marmelo, and Y. Djeridane, Proceedings of the 24th EUPVSEC, Valencia, Spain (2008)

[162] M. Stutzmann, D. K. Biegelsen, and R. A. Street, Physical Review B 35 (1987) 5666.

[163] R. A. Street and K. Winer, Physical Review B 40 (1989) 6236.

[164] O. Cubero, T. Soderstrom, F.-J. Haug, X. Niquille, V. Terrazzoni, and C. Ballif, Proc. 23rd European PVSEC (Spain) (2008)

[165] J. Loffler, A. Gordijn, R. L. Stolk, H. Li, J. K. Rath, and R. E. I. Schropp, Solar Energy Materials and Solar Cells 87 (2005) 251.

[166] J. Bailat, E. Vallat-Sauvain, L. Feitknecht, C. Droz, and A. Shah, Journal of Non-Crystalline Solids 299 (2002) 1219.

[167] F. Meillaud, A. Shah, J. Bailat, E. Vallat-Sauvain, T. Roschek, B. Rech, D. Didier, T. Söderström, M. Python, and C. Ballif, Photovoltaic Energy Conversion, Conference Record of the 2006 IEEE 4th World Conference on 2 (2006)

[168] H. Sakai, T. Yoshida, S. Fujikake, T. Hama, and Y. Ichikawa, Journal of Applied Physics 67 (1990) 3494.

[169] R. R. Arya, A. Catalano, and R. S. Oswald, Applied Physics Letters 49 (1986) 1089.

[170] C. H. Lee, J. W. Jeon, and K. S. Lim, Journal of Applied Physics 87 (2000) 8778.

[171] S. R. Sheng, H. Y. Hao, H. W. Diao, X. B. Zeng, Y. Xu, X. B. Liao, and T. L. Monchesky, Applied Surface Science 253 (2006) 1677.

[172] J. Springer, A. Poruba, L. Mullerova, M. Vanecek, O. Kluth, and B. Rech, Journal of Applied Physics 95 (2004) 1427.

[173] J. Meier, J. Spitznagel, S. Faÿ, C. Bucher, U. Graf, U. Kroll, S. Dubail, and A. Shah, Proc. of the 29th IEEE PVSC (2002) 1118.

[174] C. Eisele, C. E. Nebel, and M. Stutzmann, Journal of Applied Physics 89 (2001) 7722.

[175] K. Yamamoto, M. Yoshimi, T. Suzuki, T. Nakata, T. Sawada, A. Nakajima, and K. Hayashi, Proc. of the 28th IEEE PVSC (2000) 1428.

[176] O. Kluth, B. Rech, L. Houben, S. Wieder, G. Schöpe, C. Beneking, H. Wagner, A. Löffl, and H. W. Schock, Thin Solid Films 351 (1999) 247.

[177] D. Dominé, J. Bailat, J. Steinhauser, A. Shah, and C. Ballif, Proc. of the 4th World WCPEC (2006) 1465.

[178] J. Meier, J. Spitznagel, U. Kroll, C. Bucher, S. Fay, T. Moriarty, and A. Shah, Proc. of the 3rd World WCPEC 3 (2003) 2801.

[179] F. J. Haug, T. Söderström, O. Cubero, V. Terrazzoni-Daudrix, and C. Ballif, Journal of Applied Physics 104 (2008) 064509.

[180] J. Springer, A. Poruba, M. Vanecek, S. Fay, L. Feitknecht, N. Wyrsch, J. Meier, A. Shah, T. Repmann, and O. Kluth, Proc. of the 17th PVSEC (2001) 2830.

[181] H. Stiebig, C. Haase, C. Zahren, B. Rech, and N. Senoussaoui, Journal of Non-Crystalline Solids 352 (2006) 1949.

[182] C. Haase and H. Stiebig, Applied Physics Letters 91 (2007) 061116.

[183] C. Rockstuhl, F. Lederer, K. Bittkau, and R. Carius, Applied Physics Letters 91 (2007) 171104.

[184] J. Steinhauser, L. Feitknecht, S. Faÿ, R. Schlüchter, A. Shah, C. Ballif, J. Springer, L. Mullerova-Hodakova, A. Purkrt, A. Poruba, and M. Vanecek, Proc.of the 20th European PVSEC (2005) 1608.

[185] J. Steinhauser, Phd Thesis, Neuchâtel (2008)

[186] F.-J. Haug, T. Söderström, X. Niquille, and C. Ballif, Accepted in Solar Energy Material (2008)

[187] T. Söderström, F.-J. Haug, O. Cubero, X. Niquille, and C. Ballif, Mater. Res. Soc. Symp. Proc. 1101E (2008) KK04.

[188] P. Buehlmann, J. Bailat, D. Domine, A. Billet, F. Meillaud, A. Feltrin, and C. Ballif, Applied Physics Letters 91 (2007) 143505.

[189] K. Brecl and M. Topic, Progress in Photovoltaics: Research and Applications 16 (2008) 479.

[190] R. Ross, R. Mohr, J. Fournier, and J. Yang, Proc. IEEE Photovoltaic Specialists Conference (1987) A88.

[191] J. Morris, R. R. Arya, J. G. O'Dowd, and S. Wiedeman, Journal of Applied Physics 67 (1990) 1079.

[192] C. Kothandaraman, T. Tonon, C. Huang, and A.-E. Delahoy, Mater. Res. Soc, Proc 219 (1991) 475.

[193] J. E. Harvey and A. Krywonos, Proc. of the SPIE Am100-26, Denver (2004)

[194] A. Campa, J. Krc, J. Malmström, M. Edoff, F. Smole, and M. Topic, Thin Solid Films 515 (2007) 5968.

[195] K. Yamamoto, M. Yoshimi, Y. Tawada, Y. Okamoto, A. Nakajima, and S. Igari, Applied Physics A: Materials Science & Processing 69 (1999) 179.

[196] K. Saito, M. Sano, H. Otoshi, A. Sakai, S. Okabe, and K. Ogawa, Proc. of the 3rd World WCPEC (2003) S2O.

[197] D. Fischer, S. Dubail, J. A. A. Selvan, N. P. Vaucher, R. Platz, C. Hof, U. Kroll, J. Meier, P. Torres, H. Keppner, N. Wyrsch, M. Goetz, A. Shah, and K.-D. Ufert, in 25 IEEE PVSC, Washington D. C., 1996, p. 1053.

[198] D. Domine, J. Bailat, J. Steinhauser, A. Shah, and C. Ballif, Conference Record of the 2006 IEEE 4th World Conference on Photovoltaic Energy Conversion (IEEE Cat. No. 06CH37747) (2006) 4 pp.

[199] P. Vineri, L. Mercaldo, I. Usatii, P. Ciani, and C. Privato, Proc. 23rd European PVSEC (2008)

[200] K. Yamamoto, A. Nakajima, M. Yoshimi, T. Sawada, S. Fukuda, T. Suezaki, M. Ichikawa, Y. Koi, M. Goto, T. Meguro, T. Matsuda, M. Kondo, T. Sasaki, and Y. Tawada, Solar Energy 77 (2004) 939.

[201] J. Zimmer, H. Stiebig, and H. Wagner, Journal of Applied Physics 84 (1998) 611.

[202] S. Guha, J. Yang, A. Pawlikiewicz, T. Glatfelter, R. Ross, and S. R. Ovshinsky, Applied Physics Letters 54 (1989) 2330.

[203] A. Nakajima, M. Ichikawa, T. Sawada, M. Yoshimi, S. Fukuda, Y. Tawada, T. Meguro, H. Takata, T. Suezaki, and M. Goto, Proc. of the 3rd World Conference PVSEC (2003) 1915.

[204] D. Domine, P. buehlmann, J. Bailat, A. Billet, A. Feltrin, and C. Ballif, Proc. 23rd European PVSEC (2008)

[205] D. Chandan, L. Andreas, H. Juergen, R. Wilfried, and F. Friedhelm, Applied Physics Letters 92 (2008) 053509.

[206] http://www.jobinyvon.com/DeltaPsi2,

[207] X. Xu, J. Yang, and S. Guha, Applied Physics Letters 62 (1993) 1399.

[208] B. Yan, G. Yue, and S. Guha, Vol. 989, Warrendale, Pa.; Materials Research Society; 1999, 2007, p. 335.

[209] P. Obermeyer, C. Haase, and H. Stiebig, Applied Physics Letters 92 (2008) 181102.